

**Replication and Fabrication of Crafted and Natural  
Artifacts by Reverse Engineering using  
Single Camera Photogrammetry**

**John Kaufman**

A Thesis Submitted for the Degree of PhD

**Lancaster University**

**July 2018**

**Disclaimer**

I hereby declare that this submission is my own work and it contains no material previously published or written by another person, to the best of my knowledge and belief, nor material which has been accepted for the award of any other degree or diploma of the University or other institute of higher learning except where due acknowledgements have been made in the text.

This thesis is submitted in partial fulfilment of the requirements for the degree of  
Doctor of Philosophy

**Author:** ..... **J Kaufman**

**Date:**

## Acknowledgements

The author of this thesis would like to thank the following individuals and organisations for supporting this research activity:

Dr Allan Rennie for his supervision and guidance throughout the period of time I have been studying at Lancaster University as an off campus student. All members of the Lancaster Product Development Unit are thanked for their guidance and for providing many of the fabricated models. I would also like to thank the members of the University Study Skills Unit who provided the author with help and guidance when requested.

This research would not have been possible without the use of the computer software supplied for the duration of the research by Agisoft's *PhotoScan Pro*®, Netfabb's *Studio Pro5*® and AutoDesSys' *form-Z pro*®, for which I am very grateful. Thanks also to Mcor Technologies for the fabrication of two models, the *Eureka Cat* and *Eureka Man*, using their *Iris*® Colour printer and to 3D Systems for the fabrication on their *ProJet 660*® of the *Clay Head*, *Egyptian Bowl* and *Sobekhotep* models.

Thanks is also given to the staff at Kendal Museum, Kendal, Cumbria for their help and collaboration, use of their Egyptian artifacts, and workshop space during the data collection phase.

Finally, thanks to my wife, Sandra, who supported and encouraged my project over many years spending many hours proof reading my manuscript.

## **Abstract**

Photogrammetry has been used for recording objects for well over one hundred and fifty years. Modern photogrammetry, or digital image capture, can be used with the aid of a single medium range Digital Single Lens Reflex (DSLR) camera, to transform two-dimensional (2D) images into three-dimensional (3D) Computer Aided Design (CAD) spatial representations, and together with the use of additive manufacturing (AM) or 3D Printing technology, geometric representations of original cultural, historic and geological artifacts can be fabricated using a process known as Non-invasive Reverse Engineering. Being able to replicate such objects is of great benefit to educationalists and, for example, curators; if the original object cannot be handled because it is fragile, then replicas can give the handler a chance to experience the size, texture and weight of rare objects. Photogrammetry equipment is discussed, the objective being simplicity of execution for eventual realisation of physical products such as the artifacts discussed in this thesis. All the digital photographic data in the research has been captured either with the use of a mid-range DSLR camera or a compact “point and shoot” camera. As the processing power of computers has increased and become more widely available, and with the use of user-friendly software programs it is now possible to digitally combine multi-view photographs, taken from 360° around the object, into 3D CAD representational virtual images, transforming these so they are ready for AM machines to produce replicated models of the originals.

Over 50 objects were used in this research and the results documented: from the reproduction of small modern clay sculptures; 3,500-year-old Egyptian artifacts; household vases, figurines and bottles; fossils, shells and rocks, although not all successfully recreated. A variety of AM technologies have been employed, mostly monochromatic but including colour AM machines, to fabricate the models where good 3D models have been obtained.

A bench-mark test was performed to ascertain the justification for the additional time and computer power required to produce ultra-high resolution digital images for the models to be fabricated on high resolution AM technology, in order to test the best possible limits of artifact reproduction. An in-depth case study on four problematic artifacts was also conducted using amongst other

methods, RAW photographic images as opposed to camera ready Jpeg images; the results were analysed for comparison and conclusions were drawn.

## Table of Contents

<b>Disclaimer</b>	II
<b>Acknowledgements</b>	III
<b>Abstract</b>	IV
<b>Table of Contents</b>	VI
<b>List of Figures</b>	XIV
<b>List of Tables</b>	XXV
<b>List of Abbreviations and Acronyms</b>	XXVII
<b>Appendices Contents see separate booklet</b>	XXX
<b>Outputs</b>	XXXII
<b>Contribution to Knowledge</b>	XXXIII

<b>Chapter 1: Introduction and Background History</b>	<b>1</b>
1.1    Introduction	1
1.2    Overview	1
1.3    Research Objectives	1
1.4    Digital Image Capture	3
1.5    Software programs	3
1.6    Headings and Contents for Main Body of Thesis	4
1.7    Introduction to Background History	6
1.8    Aristotle and Euclid	7
1.9    Camera Obscura	7
1.10    The Next 500 Years	9
1.11    Capturing the Photographic Image – the Early Pioneers	10
1.12    Photographic Cameras	11
1.12.1    Stereoscopic Images	11
1.12.2    Photogrammetry	15
1.12.3    Aerial Photography	15

1.12.4	Le Corbusier	15
1.12.5	Spy in the Sky	17
1.13	Birth of Digital Cameras	17
1.14	The Ruby Red Beam	18
1.15	Laser Scanners	18
1.16	Personal Computers	19
1.17	Development of LS and CAD	19
1.18	Cost of Laser Scanners	22
1.19	Virtual 3D Representational Images	26
1.20	3D Reliefs	27
1.20.1	<i>Bas-relief</i> , Sunken and Raised Relief	27
1.20.2	Image-Based Displacement	29
1.21	Historical Conclusion	30
<b>Chapter 2: Literature Review and Research Objectives</b>		<b>32</b>
2.1	Introduction to Photogrammetry	32
2.2	Overview	33
2.3	Medical	33
2.4	Archaeology	36
2.5	Museums	38
2.6	Cultural Heritage	40
2.7	Aerial Surveillance	44
2.8	Archiving and Storage of Data	45
2.9	Heritage Lost and Gained	46
2.9.1	The Crosby Garrett Helmet	46
2.9.2	Tlingit Community of southeast Alaska, USA	50
2.10	Research Objectives - Development of Simpler Data Capture & Processing	51
2.11	Technology for Computer-literate Operatives	52
2.12	A Cost Effective, Cheaper and Safer System	53
2.13	Systems Utilisation	54
2.13.1	Local Community projects	54
2.13.2	Educational institutions	55
2.13.3	Museum and Gallery Staff	57

2.13.4	Non-invasive Replication of Unique Objects	59
2.14	Product Promotion for Business	59
2.15	Spatial/Tactile Experience by Blind and Visually Impaired	61
2.16	Conclusions	64
2.16.1	Literature Summary and Gaps in Knowledge	64
<b>Chapter 3: Tools of the Trade – Hardware and Software</b>		<b>66</b>
3.1	Photographic Hardware	66
3.2	The Camera	66
3.3	The Lens	67
3.3.1	Close-up Lens	67
3.3.2	Neutral Density Lens	69
3.4	Additional Camera Equipment	70
3.4.1	Compact Camera Support Frame	71
3.4.2	Turntable and other Props	72
3.5	Compact Camera Test – Canon <i>IXUS 100IS</i> ®	74
3.6	Lighting	75
3.6.1	Lighting and the Kelvin Scale	76
3.6.2	Basic Lighting Equipment	78
3.7	White Balance and Grey Scale	79
3.7.1	Accuracy of the Colour requirement	80
3.7.2	Consistency in Colour printing	81
3.7.3	Uniformity of AM printers and inks	82
3.7.4	Auto White Balance camera mode	84
3.8	Light Tents	87
3.8.1	Light Tent Construction	87
3.8.2	“Studio” Lighting Conditions – Spain	89
3.9	Open Room Studio	90
3.10	Alternative “Open Studios”	92
3.11	Software	95
3.11.1	AutoDesk - <i>123 Catch</i> ®	95
3.11.2	Agisoft – <i>PhotoScan Pro4</i> ®	96
3.11.3	Netfabb GmbH – <i>Studio Pro4</i> ®	97

3.11.4	DeskArts <i>3Data Expert</i> <sup>®</sup>	98
3.11.5	Dassault Systèmes - <i>SolidWorks</i> <sup>®</sup>	99
3.12	Software Summary	100
<b>Chapter 4: Methodology for 3D Reconstruction</b>		<b>101</b>
4.1	Method 1	101
4.1.1	Open Room Studio – Setting the Scene	101
4.1.2	Data Capture – <i>123D Catch</i> <sup>®</sup>	103
4.1.3	Computer Data Primary Processing	106
4.2	Case Studies	107
4.2.1	Clay Head	107
4.2.2	Unglazed Ceramic Vase	111
4.2.3	China Figurine Serenity	113
4.3	Data Chart and Image library	116
4.4	Creation of 3D Video	117
4.5	Summary	120
4.6	Method 2	120
4.6.1	“Light Tent” technique	120
4.6.2	Standard Data Capture – using <i>PhotoScan Pro4</i> <sup>®</sup>	122
4.7	Depth of field	123
4.8	Lens Diffraction	126
4.8.1	Histograms	130
4.9	Software control – semi automatic	132
4.10	Pre-Process Masking	134
4.10.1	Alternative uses for Pre-Process Masking	136
4.10.2	Digital Photographs, Point Cloud and Polygon Images	142
4.11	High and Low Resolution Images	147
4.11.2	Print Problems Associated with High Resolution Data	149
4.12	Bench Marking the Model and Adapting to the Limitations of AM Technology	152
4.12.1	AM 3D Printing Machine Envelope Build and Resolution Detail	158

4.13	AM Printer Software	164
4.13.1	AM Printer Drivers	170
4.14	Digital Photographic Information held with the Image	171
4.14.1	Focusing onto the Target	172
4.15	Data Chart and Image Library – with <i>PhotoScan Pro4®</i>	176
4.16	Method 3 - Adapting to Working Environments	177
4.16.1	Using a Backcloth on its Own	177
4.16.2	Hanging on the Wall	181
4.17	Coded and Non-Coded targets	182
4.18	Summary Methodology 2 & 3	185

## **Chapter 5: Secondary Processing** **187**

5.1	Using <i>netfabbPro5®</i>	187
5.2	Reorientation	190
5.3	Measuring the Digital Image	193
5.4	Scaling and Resizing	196
5.4.1	Scaling using <i>PhotoScan Pro4®</i>	197
5.4.2	Scaling using <i>123D Catch®</i>	197
5.4.3	Scaling using <i>netfabbPro5®</i>	198
5.5	Slicing or Free Cutting	202
5.6	Hollowing	204
5.6.1	Shell creation	204
5.6.2	Volume of Material used dictated by Shell Thickness or Artifact attributes	206
5.6.3	Observations on Material Utilisation as used in the Replication of the Artifacts	211
5.7	Boolean Operation	212
5.8	Other useful features	213
5.9	Summary	216

## **Chapter 6: Repair, reconstruction and construction** **218**

6.1	Returned Noisy data Distorted and Incomplete Data	218
6.1.1	Returned Noisy data	218
6.1.2	Incomplete data.	219
6.1.3	Unglazed Ceramic Vase - lesson in sewing	221

6.1.4	Repair using the Mesh	223
6.2	Damaged Digital Images Beyond Repair	225
6.2.1	Figure K.01 - Serenity – Items G.03 and H.32	227
6.2.2	Figure K.02 – Dolphins – Items G.04 and H.33	229
6.2.3	Figure K.03 – Glazed Vase – Item G.06	229
6.2.4	Figure K.04 – Mollusc - Item G.08	229
6.2.5	Figure K.05 – Frosted Bottle - Items G.10 and H.32	231
6.2.6	Figure K.06 – Ceramic Vase - Item G.15	232
6.2.7	Figure K.07 – China Dish - Item H.37	232
6.2.8	Figure K.08 – Batwing Sea Shell - Item H.50	232
6.2.9	Figure K.09 - Lincrusta – Acanthus - Item – G.16	233
	Figure K.10 - Lincrusta – Aphrodite - Item – G.17	233
6.3	Summary of Repaired Data Images	235
6.4	Removing Flare/Glare and Reflection	236
6.4.1	Polarising filters	236
6.4.2	Testing CPL Filters – Artificial Lighting	238
6.4.2	Testing CPL Filters – Natural Lighting	240
6.5.	Digital Negative Editing Software	242
6.5.1	File Format	242
6.5.2	Editing the Data, Post-processing	244
6.6	Overview of other uses and benefits	245
6.7	Repair of broken Photographic Frame	246
6.7.1	The Stair Stepping effect	251
6.8	The Egyptian Bowl	251
6.9	The lost Crown of Horus	254
6.10	Educational use	259
6.10.1	Further use of Horus's Crown	261
6.10.2	Morphing Models	262
6.10.3	A stand for the Amphora	265
6.10.4	Flat Bottom Grain Jar	267
6.10.5	Making Technical Drawings of the Models	267
6.11	Well Protected for the Journey	268

<b>Chapter 7: Compact Camera v DSLR</b>	<b>271</b>
7.1    Compact camera as an alternate option	271
7.2    Basic Trail	272
7.3    The Griffin	275
7.4    Summary	279
<b>Chapter 8: The Finished AM Replicated Models</b>	<b>281</b>
8.1    Introduction to the AM models	281
8.2    Current Diversity	281
8.3    General Observations on Replicated Artifacts	284
8.3.1    Defect or Enhancement	285
8.4    Colour Printing	288
8.4.1    Eureka Cat and Man	288
8.4.2    ‘Greyed out’	294
8.5    Monochrome Models	295
8.5.1    Clay Head	295
8.6    The Egyptians - Ancient	297
8.6.1    Sobekhotep	297
8.6.2    The Bowl	299
8.6.3    The Vase	301
8.7    The Egyptians – Modern	304
8.7.1    Painted Fish Vase	304
8.7.2    Horus	305
8.8    The Dog	307
8.9    The Warrior	310
8.10    Ceramic Vessels	311
8.11    Handled Vessels	314
8.12    Concrete Mix	316
8.13    Items from the Natural World	317
8.13.1    Sea Shell	318
8.13.2    Fossils – Ammonite	319
8.13.3    Fossils – Trilobite	320
8.14    Varnished models	321

8.15	Summary	323
<b>Chapter 9: RAW digital negatives</b>		<b>324</b>
9.1	Historical Background	324
9.2	The Search for Solutions	325
9.3	The Digital Negative	326
9.4	Tiff and Jpeg	326
9.5	Size Matters	327
9.6	Case Studies	328
9.6.1.	Warrior	330
9.6.2.	Serenity	331
9.6.3.	Dolphins	332
9.6.4.	China Dish	333
9.7	RAW v Jpeg - For and Against	335
9.8	Conclusion	337
<b>Chapter 10: Conclusion and Future Research</b>		<b>339</b>
10.1	Introduction	339
10.2	Core Research Questions	340
10.3	Methodological Reconstructions	341
10.4	Empirical Findings	346
10.5	Theoretical Implications in RE using SC Photogrammetry	348
10.6	Limitation of the Study and Challenges	349
10.7	Recommendations for Further Research	351
10.7.2	Colour Fabrication	352
10.7.3	Questionnaires	352
10.8	Conclusion	354
<b>References:</b>		<b>356</b>

## List of Figures

<b>Chapter 1: Introduction and Background History</b>		<b>Page</b>
Figure 1.1	Sequential animation of goat leaping into the air to feed from plant	6
Figure 1.2	Frisius Gemma 's illustration " Eclipse of the Sun 24th January, 1544"	8
Figure 1.3	Johann Zahn, <i>camera obscura portabilis</i> , 1685.	8
Figure 1.4	Fox Talbot's first captured photographic negative image	10
Figure 1.5	Hare's Stereoscopic camera – c1857	12
Figure 1.6	Lenticular's Stereoscope - c1860	12
Figure 1.7	Typical double image for binocular vision	13
Figure 1.8	Kilbourne Stereo Daguerreotype in folding stereoscope – c1860	13
Figure 1.9	Zeiss pocket stereoscopic viewer	14
Figure 1.10	Panasonic State of the art still/ video camera	14
Figure 1.11	Drone or UAV as bought in the local electronics shop with camera	16
Figure 1.12	c1975 Sasson's Digital camera	17
Figure 1.13	Point Cloud 2D enlargement of head section – Front view	20
Figure 1.14	Enlarged head section – side view.	20
Figure 1.15	Full image – 67,063 points	21
Figure 1.16	3D scanned survey of Byland Abbey, North Yorkshire	22
Figure 1.17	Trimble MX2 Dual Head digital laser scanner	23
Figure 1.18	DAVID Structured Light Scanner <i>SLA-2 3D-Scanner</i> ®	24
Figure 1.19	DIY 3D scanner camera Kit	24
Figure 1.20	Examples of 3D virtual textured point cloud data images	26
Figure 1.21	Roman pot shard – bas-Relief	27
Figure 1.22	Egyptian Horus raised-relief	28
Figure 1.23	Full rendered Computer Relief	29
Figure 1.24	Top and Bottom of Block showing surface displacement according to grey scale colour intensity	30

## Chapter 2: Literature Review and Research Objectives

Figure 2.1	X-ray showing deformed arm bone	34
Figure 2.2	Drilling guide for fixing plate attached to model of bone	35
Figure 2.3	POIGO - Bridging the gap between Surgeon and Engineer	36
Figure 2.4	Bronze Copper helmet and mask	47
Figure 2.5	Children look eyeball to eyeball with their cultural history	48
Figure 2.6	Pre cleaned Helmet	48
Figure 2.7	After cleaning – as displayed at Christie's 2010	49
Figure 2.8	The Kéet S'aaxw hat	50
Figure 2.9	<i>Kaagwaantaan</i> clan Sea Monster Hat	51
Figure 2.10	Entry Level Computer - <i>UP!3DPP</i> ®	55
Figure 2.11	Entry Level Computer - <i>RepRap</i> ®	56

Figure 2.12	Entry Level Computer - MakerBot®	57
Figure 2.13	Children handling the Museum replicas	58
Figure 2.14	Children handling replicated models of 3500 year old Egyptian artifacts	58
Figure 2.15	Contemporary Designed Bottle	58
Figure 2.16	Goveshy	60
Figure 2.17	Morling	60
Figure 2.18	Clay Head	61
Figure 2.19	Glazed Clay Bottle	61
Figure 2.20	Mona Lisa by Leonardo De Vinci	62
Figure 2.21	AM <i>Bas-relief</i> of Mona Lisa – shot from above	62
Figure 2.22	AM <i>Bas-relief</i> of Mona Lisa – shot just above horizontal plane	63
Figure 2.23	Original relief painting showing position of X section A/B	63
Figure 2.24	Horizontal cross section of STL virtual image	64

### Chapter 3: Tools of the Trade – Hardware and Software

Figure 3.1	Nikon D3100® DSLR Camera	66
Figure 3.2	AF-S DX Zoom- Nikkor® 18-55mm f/3.5-5.6. - Zoom Lens	66
Figure 3.3	Typical set of Close up lenses	67
Figure 3.4	The Warrior – effect of - f/18 @ 35mm +0	68
Figure 3.5	The Warrior – effect of - f/18 @ 35mm +4	68
Figure 3.6	The Warrior – effect of - f/18 @ 40mm +10	68
Figure 3.7	Models shot at 140mm distance	69
Figure 3.8	Models shot at 140mm distance but with +10 dioptrē lens	69
Figure 3.9	Selection of Neutral Density square and round Filter	70
Figure 3.10	Frame curvature as seen from above.	71
Figure 3.11	Curved pipe supporting 3 compact cameras	71
Figure 3.12	AM support arms and frame	71
Figure 3.13	Close-up of turn table showing degree markings.	72
Figure 3.14	Turn table as in use.	73
Figure 3.15	Use of cord to control radial distance.	73
Figure 3.16	Use of pole to control radial distance	74
Figure 3.17	Colour Temperature – the Kelvin Scale	77
Figure 3.18	bip® fluorescent floodlight	78
Figure 3.19	Single bulb 45W floodlight	78
Figure 3.20	A page from the Nikon Manual	79
Figure 3.21	Small part of the Pantone colour chart	81
Figure 3.22	BSi Fan Deck 475 colours	82
Figure 3.23	Original Photograph	85
Figure 3.24	Screen shot point cloud image	85
Figure 3.25	McOr IRIS® model	85

Figure 3.26	Stratasys <i>PolyJet J750</i> <sup>®</sup> model v1	85
Figure 3.27	Original Sobekhotep model	86
Figure 3.28	Wrl file created in <i>formZ 8 SE</i> <sup>®</sup>	86
Figure 3.29	Model from <i>PolyJet J750</i> <sup>®</sup>	86
Figure 3.30	Re-printed colour model from the <i>PolyJet J750</i> <sup>®</sup> machine v2	87
Figure 3.31	Light tent set up in museum workshop – with poplin cover	88
Figure 3.32	Light tent set up without poplin cover but showing Chroma backdrop	88
Figure 3.33	Spanish walk-in-light tent	89
Figure 3.34	Under grey, dull, northern English, cloudy skies	90
Figure 3.35	Typical artifact – indicated - being photographed in Open Room setup using fluorescent light	91
Figure 3.36	Light Tent under the fluorescent lighting, including ceiling downlights	91
Figure 3.37	Photogrammetry under a Spanish <i>Naya</i> . Backdrop hung on wall	92
Figure 3.38	Backdrop hung from wall but with lighting - Indoors in the UK	93
Figure 3.39	Photographed whilst still hanging on wall	94
Figure 3.40	<i>Infinite-Realities</i> multi camera studio	94
Figure 3.41	Amphora stand	99
Figure 3.42	Arm of compact camera frame	99
Figure 3.43	Final rendering of Horus's Crown	99
Figure 3.44	Un-rendered version of Horus's Crown	99

## Chapter 4: Methodology for 3D Reconstruction

Figure 4.1	Data Capture - Advantageous camera angles	101
Figure 4.2	Data Capture – Supporting model above horizontal plane	102
Figure 4.3	Correlation between camera position and horizontal image deviation	102
Figure 4.4	Four frames from part of the Data set of 75 photographs	103
Figure 4.5	<i>123D Catch</i> <sup>®</sup> Data processing Flow chart	104
Figure 4.6	Close-up screen shot of virtual image waiting to be cleaned	105
Figure 4.7	Clay head identified in blown up image amongst background “noise”	105
Figure 4.8	Original Clay head	107
Figure 4.9	Screen shot of final textured processed digital image	107
Figure 4.10	Digital model - hole under chin	108
Figure 4.11	Distortion on the back of head	109
Figure 4.12	Section of point cloud mesh	110
Figure 4.13	Final Geometric Representation FDM model	110
Figure 4.14	Original digital image of vase	111
Figure 4.15	Initial processed image – Hole in bottom & side	112
Figure 4.16	Hole removed after an extra 15 Images added	113
Figure 4.17	Clean, crisp, sharp image of China figurine	113
Figure 4.18	Textured 3D Mesh image of China figurine	114
Figure 4.19	China figurine - Point cloud 3D mesh	115

Figure 4.20	China figurine - Dark shadows and plumes	115
Figure 4.21	Vertical view of Video Map	118
Figure 4.22	Enlargement of Figure 4.21 showing camera position and projected image of the tracking path produced by the software	118
Figure 4.23	Changes that can be made to video path.	119
Figure 4.24	Turn Table and Green Chroma Key backdrop	121
Figure 4.25	The Egyptian Vase on the turn table	122
Figure 4.26	Results of out of focus images on an SLS fabricated Bowl	123
Figure 4.27	SLS fabricated Bowl using <i>PhotoScan Pro</i> ®	124
Figure 4.28	Bowl - Double point cloud image, caused by initial out of focus data	124
Figure 4.29	Bowl - A texture point cloud “Fur” infill created by computer	125
Figure 4.30	Egyptian Bowl - Stitching of images c/o Agisoft	125
Figure 4.31	Screen shot of completed textured point cloud Egyptian bowl	126
Figure 4.32	Contrasting sharpness between f/stop images	127/128
Figure 4.33	The “Quality” results of the scanned images	129
Figure 4.34	Enlarged images to show difference in sharpness	129/130
Figure 4.35	Histogram - <i>PhotoShop CS6</i> ®	131
Figure 4.36	Histogram - <i>PhotoShop Elements 11</i> ®	131
Figure 4.37	Nikon User Manual explanation of RGB Histogram	132
Figure 4.38	<i>PhotoScan Pro</i> ® Data processing Flow Chart	133
Figure 4.39	Complex Masking line without Chroma Key backdrop	134
Figure 4.40	Simplified masking operation when backdrop is used.	134
Figure 4.41	Non-masked images of the Egyptian Vase – pre-processing	135
Figure 4.42	Masked images of the Egyptian Vase – pre-processing	135
Figure 4.43	Original image – part of image data set of Concrete Mix	136
Figure 4.44	Original image - Sea Shell	137
Figure 4.45	Positive masked over sea shell support	137
Figure 4.46	Negative mask of sea shell	137
Figure 4.47	Final Textured shell	137
Figure 4.48	Positive mask image of Concrete Mix	138
Figure 4.49	Final textured dense cloud image of Concrete Mix	138
Figure 4.50	Sobekhotep seen in centre of light tent	139
Figure 4.51	Screen shots of masked images and view of camera positions	140
Figure 4.52	Photograph of Sobekhotep, son of Nehesy	141
Figure 4.53	Sobekhotep - High resolution point cloud image	141
Figure 4.54	Sobekhotep – Enlarged detail of high resolution image	142
Figure 4.55	Sparse point cloud – 13,639 points	143
Figure 4.56	Medium Build Dense Cloud -1,044,192 points	144
Figure 4.57	A section of “Working Log”	145
Figure 4.58	Medium Build Polygon Mesh - 69,862 polygons	146

Figure 4.59	Three types of mesh – depending on the number of polygons created	147
Figure 4.60	Section of polygon mesh enlarged from Medium resolution image	149
Figure 4.61	Original Ammonite fossil	150
Figure 4.62	Hand painted replica	150
Figure 4.63	Ultra-High resolution <b>Jpeg</b> model	153
Figure 4.64	Ultra-High resolution <b>Tiff</b> model	153
Figure 4.65	High resolution - <b>Jpeg</b> model	153
Figure 4.66	High resolution - <b>Tiff</b> model	153
Figure 4.67	Original photograph of Warrior	153
Figure 4.68	<b>CR</b> Jpeg model	153
Figure 4.69	Original model size 25mm high	153
Figure 4.70	Fabricated model size 25mm high	153
Figure 4.71	Bench mark model heads	154
Figure 4.72	Medium resolution - Jpeg and Tiff models	155
Figure 4.73	Low resolution - Jpeg and Tiff models	155
Figure 4.74	Ultra Low resolution - Jpeg and Tiff models	155
Figure 4.75	Layout of models for printing on the <i>PolyJet J750</i> <sup>®</sup>	156
Figure 4.76	Top view of heads showing grain or layer direction	157
Figure 4.77	Screen shot of the manual build platform layout from <i>GrabCAD</i> <sup>®</sup>	164
Figure 4.78	Screen shot of the Automatic layout from <i>GrabCAD</i> <sup>®</sup>	165
Figure 4.79	Screen shot of the Automatic layout from <i>GrabCAD</i> <sup>®</sup>	165
Figure 4.80	Ultimaker 250µm model	166
Figure 4.81	Without supports	166
Figure 4.82	Model showing outside supports	166
Figure 4.83	Slice level 332 - showing information about the print structure of the model in “Custom” Mode.	168
Figure 4.84	Slice level 1187	169
Figure 4.85	Enlargement of filament layers	169
Figure 4.86	Extra Fine Profile - 0.25mm nozzle	169
Figure 4.87	Fine Profile - 0.4mm nozzle	169
Figure 4.88	Fine Profile - 0.6mm nozzle	170
Figure 4.89	Normal Profile - 0.8mm nozzle	170
Figure 4.90	G code from the instructions as downloaded into a word processor	171
Figure 4.91	Digital information relating to the photographic image. Colour channel histograms shown separately	173
Figure 4.92	Digital information relating to the photographic image. Colour channel histograms seen combined	174
Figure 4.93	Photographing the Trilobite under a Naya with only natural light	178
Figure 4.94	Original Rock	179
Figure 4.95	Screen shot of textured dense cloud rock image	179
Figure 4.96	*.stl image of Rock mounted on a stand. Note holes through body	180

Figure 4.97	Original small rock	180
Figure 4.98	Textured dense cloud image of small rock with wood prop removed	181
Figure 4.99	Relief canvas - Camera positions as seen from above looking down	181
Figure 4.100	Relief canvas - Camera positions as seen from horizontal plane	182
Figure 4.101	Selection from the Photographic sequence from 68 images	182
Figure 4.102	Agisoft non coded targets	184
Figure 4.103	Coded targets	184
Figure 4.104	Quadra1 - underwater target frame	184
Figure 4.105	Selection of target shapes	185

## Chapter 5: Secondary Processing

Figure 5.1	Main data processing functions of StudioPro®	188
Figure 5.2	Original imported image of Botijo	190
Figure 5.3	Reoriented image of Botijo	190
Figure 5.4	Botijo - Front facing - correct orientation	191
Figure 5.5	X,Y,Z Orientation of the three programs	192
Figure 5.6	Imported orientation into <i>netfabbPro5®</i> from <i>PhotoScanPro4®</i>	192
Figure 5.7	Orientation of imported part and rotation table for realignment	193
Figure 5.8	Measuring tools and essential dimensions displayed	195
Figure 5.9	Removal of bulge at bottom of model	196
Figure 5.10	Botijo - Direct Imported dimensions and orientation	198
Figure 5.11	Botijo - Reoriented to correct frontal view	199
Figure 5.12	Botijo - Incorrect ratio used – therefore dimensions are incorrect	200
Figure 5.13	Botijo - Correct ratio obtained from correct alignment of artifact	201
Figure 5.14	Screen shot of new multi-dimensional Automatic Scaling chart	202
Figure 5.15	“Free cutting” tool to slice off the stepped bottom of a Botijo jug.	203
Figure 5.16	Flattening the rounded bottom of the Botijo jug	203
Figure 5.17	Half Ammonite Shell	204
Figure 5.18	Point measurements of wall thickness of Ammonite	205
Figure 5.19	Smooth Hollowed Botijo	206
Figure 5.20	Measuring points of Botijo wall thickness	206
Figure 5.21	Volume of the solid figurine is displayed on chart	209
Figure 5.22	Boolean effect – light subtracted from dark	212
Figure 5.23	Down the drain hole and into the hollowed model	213
Figure 5.24a	Netfabb model information report - Part Analysis	214
Figure 5.24b	Netfabb model information report - Platform Views	215
Figure 5.25	Automatic mesh lines filling in the large hole of the Trilobite.	217

## Chapter 6: Repair, reconstruction and construction

Figure 6.1	Processed digital image ready to be cleaned	218
------------	---	-----

Figure 6.2	Hole under chin – automatic mesh repair	219
Figure 6.3	Distortion on top of head	220
Figure 6.4	Red polygons ready to be removed	220
Figure 6.5	Hole in Vase mesh due to lack of digital data	221
Figure 6.6	Inner Vase mesh now complete	222
Figure 6.7	Identifying and Manually stitching/matching 3 points to integrate additional digital images	223
Figure 6.8	Area needing to be cleaned at mouth of Egyptian Vase	224
Figure 6.9	Working with a large scale mesh – Egyptian Vase	224
Figure 6.10	Figurine – textured point cloud image - rough, spiky surface.	227
Figure 6.11	Figurine - High resolution point cloud image	228
Figure 6.12	Mollusc - High resolution point cloud image	230
Figure 6.13	Enlarged surface texture of original Mollusc – note ridge surface	231
Figure 6.14	Smooth Shell surface of original surface to orange peel effect on image	232
Figure 6.15	Part of a roll of Linrusta – Design “Acanthus”	234
Figure 6.16	Without CPL filter - Focal length 36mm @ f/11 @ 1/1.6s	237
Figure 6.17	With CPL filter - Focal length 36mm @ f/11 @ 1/1.3s	237
Figure 6.18	CPL filter not rotated - fl/48mm @ f/11 @ 2.5sec	234
Figure 6.19	CPL filter rotated - fl/48mm @ f/11 @ 3sec	238
Figure 6.20	No filter - fl/48mm @ f/11 @ 1sec	238
Figure 6.18a	Enlarged image - CPL filter not rotated - fl/48mm @ f/11 @ 2.5sec - artificial lighting	239
Figure 6.19a	Enlarged image - CPL filter rotated - fl/48mm @ f/11 @ 3sec - artificial lighting	239
Figure 6.20a	Enlarged image - No filter - fl/48mm @ f/11 @ 1sec - artificial lighting	239
Figure 6.21	CPL filter not rotated - fl/48mm @ f/11 @ 2.5sec	240
Figure 6.22	CPL filter rotated - fl/48mm @ f/11 @ 3sec	240
Figure 6.23	No filter - fl/48mm @ f/11 @ 1sec	240
Figure 6.21a	Enlarged image - CPL filter not rotated - fl/48mm @ f/11 @ 2.5sec	241
Figure 6.22a	Enlarged image - CPL filter rotated - fl/48mm @ f/11 @ 3sec	241
Figure 6.23a	Enlarged image - No filter - fl/48mm @ f/11 @ 1sec	241
Figure 6.24	Photo frame missing corner	246
Figure 6.25	Damaged corner removed	246
Figure 6.26	Digital image of frame	247
Figure 6.27	Frame Mask	247
Figure 6.28	Mirrored corner of frame	248
Figure 6.29	Small discrepancy on the frame to be rectified	249
Figure 6.30	Reverse of repaired frame	249
Figure 6.31	Repaired Frame	250
Figure 6.32	Copy and original bowl, combined and then off-set to facilitate repair	251
Figure 6.33	Trimming the rim of the repaired bowl	252

Figure 6.34	Underside of bowl	253
Figure 6.35	Inside of new bowl	253
Figure 6.36	Horus minus his crown	254
Figure 6.37	Point cloud image of Horus	254
Figure 6.38	Four styles of crown from large researched range	255
Figure 6.39	FDM printed model - version 1 – no support bar - unpainted	255
Figure 6.40	Crown being constructed within <i>SolidWorks</i> <sup>®</sup>	256
Figure 6.41	<i>SolidWorks</i> <sup>®</sup> screen shot - Crown version 2	257
Figure 6.42	3D printed model - Final version 2 – hand painted	257
Figure 6.43	<i>SolidWorks</i> <sup>®</sup> Screen shot – Horus and unattached crown	257
Figure 6.44	Finished unpainted SLS model of Horus	258
Figure 6.45	Hand painted finished model of Horus	258
Figure 6.46	The SL2 model of <i>XYZRGB</i> <sup>®</sup> structured light scanner	259
Figure 6.47	The first loft of the inner crown	261
Figure 6.48	Second outer crown added	261
Figure 6.49	Top Dome & fillet added to inner crown	261
Figure 6.50	Top of outer crown added and edges smoothed	261
Figure 6.51	Curled front swept extrusion added	262
Figure 6.52	Second support bar added	262
Figure 6.53	<i>RepRap</i> <sup>®</sup> machine as sold on e-Bay for £250.00	263
Figure 6.54	Original Roman jug	263
Figure 6.55	Screen shot of *.stl image	263
Figure 6.56	Screen shots of addition parts made for jug	264
Figure 6.57	The three stages of transformation	264
Figure 6.58	“Dressel” Wine amphora	265
Figure 6.59	Screen shot of amphora *.stl image	265
Figure 6.60	Greco Roman amphora and stand	266
Figure 6.61	<i>SolidWorks</i> <sup>®</sup> amphora stand	266
Figure 6.62	Unpainted white AM fabricated amphora and black stand	266
Figure 6.63	Modern flat bottom jar	267
Figure 6.64	Morphed jar together with original	267
Figure 6.65	2D Drawing of figurine Sobekhotep with information extracted from DeskArtes’ <i>3data Expert</i> <sup>®</sup>	268
Figure 6.66	Five parts of the Boxed Set Transporter	270

## Chapter 7: Compact camera v DSLR

Figure 7.1	Roman Jug – Resolution 4608 x 3072	272
Figure 7.2	Spanish Botijo - Resolution 4608 x 3072	272
Figure 7.3	Dog - Resolution 4608 x 3072	272
Figure 7.4	Roman Jug – Resolution 3264 x 2448	273
Figure 7.5	Spanish Botijo - Resolution 1024 x 768	273

Figure 7.6	Dog – Resolution 640 x 480	274
Figure 7.7	The Griffin	275
Figure 7.8	Dense Cloud image of Griffin	275
Figure 7.9	Section from Shield – from <i>123D Catch</i> <sup>®</sup>	276
Figure 7.10	Section from Shield – from <i>PhotoScan</i> <sup>®</sup>	276
Figure 7.11	Section from Shield – from original photograph	276
Figure 7.12	Original digital image and section used for comparison	276
Figure 7.13	Screen shot from <i>netfabbPro5</i> <sup>®</sup> . Imported from:- Left - <i>123D Catch</i> <sup>®</sup> Right - <i>PhotoScan</i> <sup>®</sup>	278
Figure 7.14	Detail from shield – <i>123D Catch</i> <sup>®</sup>	279
Figure 7.15	Detail from shield – <i>PhotoScan</i> <sup>®</sup>	279

## Chapter 8: The Finished AM Replicated Models

Figure 8.1	Gartner's 3D Printing Hype Cycle 2015	282
Figure 8.2	Gartner's 2017 Trends	283
Figure 8.3	Miniature FDM black dog – 50mm long x 20mm high seen alongside original clay dog	285
Figure 8.4	Enlarged detail of miniature FDM dog	286
Figure 8.5	Dog's head further enlarged to show layer-wise effect	286
Figure 8.6	The back of Dirk Vander Kooij's chair	287
Figure 8.7	Author tries the chair	287
Figure 8.8	Enrico Dini of Monolite UK with <i>Radiolaria</i> - the biggest structure ever built by the D-Shape 3D printer	287
Figure 8.9	Sand blasted enhanced tree ring wood	288
Figure 8.10	Ertel's chair	288
Figure 8.11	Original Eureka Cat	289
Figure 8.12	Unvarnished Mcor Cat	289
Figure 8.13	Enlarged top view of Eureka cat to show vertical paper layers	290
Figure 8.14	Enlarged back hindquarters of Eureka cat show paper contours	290
Figure 8.15	Original Eureka clay man	291
Figure 8.16	Enlarged section of replicated unvarnished Eureka clay man	291
Figure 8.17	Left hand figurine with hair line printed crack visible	292
Figure 8.18	Enlarged image of faded label on back of original cat	292
Figure 8.19	Enlarged image of faded printed label visible amongst contoured paper layers on fabricated cat	292
Figure 8.20	The Eureka Man - Top row – Paper bonded, FDM and SLS. Bottom row - Original	293
Figure 8.21	The Eureka Cats – Top row – SLS and FDM Bottom row – Original and Paper bonded	294
Figure 8.22	The three items in the <i>ProJet 660</i> <sup>®</sup>	295
Figure 8.23	Tinted but not coloured clay head	295
Figure 8.24	The collection of heads. The Original – SLS – Hand painted FDM	296

Figure 8.25	The FDM model head with structure supports	296
Figure 8.26	Unpainted FDM replicated model head	296
Figure 8.27	The Kendal museum replicas with the original Sobekhotep in the centre and greyed coloured models indicated	297
Figure 8.28	Clones of Sobekhotep	298
Figure 8.29	Distorted FDM models – loops and incorrect placement	299
Figure 8.30	of extruded filament	299
Figure 8.31	Full size replicated Egyptian bowl	299
Figure 8.32	Original 3,500 year old bowl	300
Figure 8.33	First attempt – discrepancy between sides of bowl	300
Figure 8.34	The digitally repaired and SLS fabricated Egyptian Bowl	301
Figure 8.35	Original Egyptian Vase	301
Figure 8.36	Four replicas of the Egyptian Vase	302
Figure 8.37	Repaired neck of Vase	303
Figure 8.38	Incomplete FDM model showing detached filaments	303
Figure 8.39	Minor detail of 'chip' in rim replicated across models	304
Figure 8.40	Egyptian Fish Vase – Original and miniature	305
Figure 8.41	Enlarged image of hand painted vase to show detail	305
Figure 8.42	Original Horus and model on left with his alternative Crown	306
Figure 8.43	Family of Dogs – Original – FDM miniature – SLS duplicate	307
Figure 8.44	Enlargement of original Dog's face	308
Figure 8.45	Enlargement of SLS model of Dog's face	308
Figure 8.46	Enhanced features of dog's face due to painting	309
Figure 8.47	Warrior - Original, miniature SLS and FDM model	310
Figure 8.48	Full size SLS with residual powder	311
Figure 8.49	Miniature Urn, Vase and Vase with Silk flowers	312
Figure 8.50	Full size Urn	312
Figure 8.51	Original Vase and Silk flowers	312
Figure 8.52	Repaired FDM model of Vase	312
Figure 8.53	FDM model vase	313
Figure 8.54	Original vase with raised whirls and patterns	313
Figure 8.55	Mesh seen inside from top of vase	314
Figure 8.56	Front view of Roman vase and miniature copy	314
Figure 8.57	Side view of Roman Vase and miniature copy	314
Figure 8.58	Lopsided off set loop handle replicated	315
Figure 8.59	Surface flaws and blemishes replicated	315
Figure 8.60	Topside of concrete mix – Original left - and SLS duplicate - right	316
Figure 8.61	Hollow underside of SLS concrete mix replica	317
Figure 8.62	Sea Shells – side view - Original shell - Copy shell	318
Figure 8.63	Sea Shells – head-on view – Left-hand side – Copy. Right-hand side - Original	318

Figure 8.64	Ammonite fossil family	319
Figure 8.65	Enlarge image of the front of the Ammonite showing the join	320
Figure 8.66	Original Trilobite next to replicated model	321
Figure 8.67	Eureka Cat - Unvarnished – top Varnished - bottom	321
Figure 8.68	Eureka Man - Unvarnished – left Varnished - right	322
Figure 8.69	Concrete Mix - Left – unvarnished – Right - Varnished showing brighter colours	322
Figure 8.70	Concrete Mix – Side view - varnished underside showing bright white base material	322

## Chapter 9: RAW digital negatives

Figure 9.1	Screen shot of application window showing use of Jpeg images	324
Figure 9.2	China Dish	329
Figure 9.3	Serenity	329
Figure 9.4	Dolphins	329
Figure 9.5	Serenity - Original <b>CR Jpeg</b> process to an *.obj file	331
Figure 9.6	Serenity - Processed <b>Jpeg</b> file to an *.obj file	331
Figure 9.7	Serenity - Processed <b>Tiff</b> file to an *.obj file	331
Figure 9.8	Original <b>CR Jpeg</b> process to an *.obj file	332
Figure 9.9	Processed <b>Jpeg</b> file to an *.obj file	332
Figure 9.10	Processed <b>Tiff</b> file to an *.obj file	332
Figure 9.11	Dolphin - Head	333
Figure 9.12	Dolphin - Pupil	333
Figure 9.13	Dolphin - Iris	333
Figure 9.14	Dolphin - Quarter Iris	333
Figure 9.15	Unsuccessful results in processed *.obj files	334
Figure 9.16	UH Tiff file – the best achieved	334
Figure 9.17	Further attempts using coded targets	334
Figure 9.18	Section from Table M.1 showing building time of Point Cloud images	337

## Chapter 10: Conclusions and Future Research

Figure 10.1	Flow Chart of Methodology for Monochromatic Replication	342
Figure 10.2	Schematic diagram of Concerns and Problems	345

## List of Tables

### Chapter 1:

Table 1.1	Details of Popular 3D Scanning Technologies priced up to \$5,250	25
-----------	--	----

### Chapter 4:

Table 4.1	Correlation between camera positions and horizontal image deviation	103
Table 4.2	Camera data – Clay Head	108
Table 4.3	Camera data – Clay Vase	112
Table 4.4	Camera data – China Figurine	114
Table 4.5	24 items processed using <i>123D Catch</i> ®	116
Table 4.6	Ammonite Fossil – wire mesh data	147
Table 4.7	Polygon Mesh count in relation to Kb file size	148
Table 4.8	Third Party Hollowed out Model Costs (August 2014)	151
Table 4.9	Numerical data comparison Hollow Heads - Stl files	158
Table 4.10	AM 3D Printing Machine Envelope Build and Resolution Detail	159 - 163
Table 4.11	Slice data for Warrior model from the Cura v2.6 software	166
Table 4.12	Layers and infill per Profile/Nozzle change	170
Table 4.13	Focusing criterion for ‘Live View’	172
Table 4.14	Copy of ViewNX 2™ table for clarification	175
Table G.1	Data Chart for processed images using <i>123D Catch</i> ®	Appendix G 116
Table G.2	Photographic images, size and material	Appendix G 116
Table G.3	Capture data Log - <i>123D Catch</i> ®	Appendix G 120
Table H.1	Ammonite Data Sheet – Triangles (Polygons) size in relation to Kilobytes size of File”	Appendix H 149
Table H.2	Ammonite Data Resolution Statistics “ <i>Processing 40 images with PhotoScan - Mesh Statistics</i> ”	Appendix H 149
Table J.1	Data Chart and Image Library using <i>PhotoScan Pro4</i> ®	Appendix J 176
Table J.2	Photographic images, size and material	Appendix J 176
Table J.3	Capture data Log – <i>PhotoScanPro4</i> ®	Appendix J 177
Table M.1	Warrior Head – Netfabb Data for Bench Mark Models	Appendix M 154 158

### Chapter 5:

Table 5.1	Dimensions of imported models into <i>netfabbPro5</i> ® from <i>PhotoScan</i> ®	194
Table 5.2	‘Scaled parts’ errors – Spanish Botijo	200
Table 5.3	Botijo wall thickness	206
Table 5.4	Appendix J reference to illustrations	207
Table 5.5	Relationship between shell depth, shape, and percentage volume of materials used	208
Table 5.6	Showing differential volume according to shell wall thickness	210

**Chapter 6:**

Table 6.1	Reference table of original and failed point cloud images	226
Table 6.2	Image Quality Options	244
Table K.1	Capture data Log – Failed Artifacts	Appendix K
Table K.2	Photographic images of Failed Artifacts	Appendix K
		227

**Chapter 7:**

Table 7.1	Basic Camera Data comparison	271
Table 7.2	Dimensional comparison between same digital image data set	278
Table L.1	Compact camera v DSLR Data comparison	272
Table M.1	Warrior Head – Netfabb Data for Bench Mark Models	Appendix M
		274

**Chapter 8:**

Table 8.1	Data comparison chart of 11 artifacts	308
-----------	---------------------------------------	-----

**Chapter 9:**

Table 9.1	Image file size comparison	328
Table 9.2	Number of digital images that can be stored on a card	336
Table M.1	Warrior Head – Netfabb Data for Bench Mark Models	Appendix M
Table N.1	Capture log – RAW & Jpeg – Photographic Image Data	Appendix N
Table N.2	RAW & Jpeg image Processing log – PhotoScan Data processing Information	Appendix N
		328
		337

**Chapter 10:**

Table 10.1	Results of Models Processed and Fabricated	346
------------	--	-----

## List of Abbreviations and Acronyms

2D	2 Dimensional
2.5D	Two-and-a-half dimensional
3D	3 Dimensional
3DP	3D printable
ABS	Acrylonitrile butadiene styrene
AF	Automatic Focus
AFM	Atomic Force Microscopy
AM	Additive Manufacture
AP	Adobe Photoshop
ASME	American Society for Mechanical Engineers
ASPRS	American Society for Photogrammetry and Remote Sensing
ASTM	American Society for Testing and Materials
ATP	Accessible Tactile Pictures
BBC	British Broadcasting Corporation
BCE	Before the Common Era
c	about
CAA	Civil Aviation Authority
CAD	Computer Aided Design
CAM	Computer Aided Manufacturing
CIRP	<i>College International pour la Recherche en Productique</i> The International Academy for Production Engineering
cm	centimetre
CNC	Computer Numerical Control
CO	Camera Obscura
CP	Circular Polarising
CPD	Cloud Point Data
CPL	Circular Polarising Lens (filter)
CPU	Central Processing Units
CR	Camera Ready
CRP	Close Range Photogrammetry
CT	Computerised Tomography
CU	Close Up
DC	Dense Cloud
DIY	Do It Yourself
DLP	Direct Light Projection
DMP	Direct Metal Printing
DSLR	Digital Single Lens Reflex
DVD	Digital Video Disc
DWG	Drawing Database file (as used by AutoDesk)

ESDA	Engineering Systems Design and Analysis
<i>et al</i>	And others
EU	European Union
FDM	Fused Deposition Modelling
G Code	A computer programming language
GB	Gigabyte
gm	grams
GPS	Global Positioning System
H	high
HD	High Definition
HTML	Hypertext Mark-up Language
IBD	Image-Based Displacement
IBM	International Business Machines
ISO	International Organisation of Standardisation
IP	Intellectual Property
IPU	Image processing Unit
IR	Infrared
JISC	Joint International Systems Committee
Jpeg (jpg)	Joint Photographic Experts Group
K	Kelvin scale
k	thousand
Kb	Kilobyte
L	low
LED	Light-Emitting Diodes
LiDAR	Light Detection and Ranging
LS	Laser Scanning
LU	Lancaster University
M	medium
mpg	Megapixels
mm	millimetres
MRI	Magnetic Resonance Imaging
ND	Neutral Density
NEF	Nikon Electronic Format
OBJ (obj)	Object file (Relocatable Object Module Format)
PC	Personal Computer
PCD	Point Cloud Data
PET	Personal Electronic Transactor
PSE	Photoshop Elements
PSD	Photoshop image editing file format
PDF	Portable Document Format

POIGO	Bridging the gap between Surgeon and Engineer
PSG	Patient-Specific Guides
RAM	Random Access Memory
RAW	Unprocessed digital data from camera image sensor
RE	Reverse Engineering
RGB	Red, Green, Blue
ROM	Read only Memory
RNIB	Royal National Institute for the Blind
RP	Rapid Prototype
SC	Single Camera
Sci-Fi	Science Fiction
sec	second
SL	Stereolithography
SLS	Selective Laser Sintering
SLR	Single Lens Reflex
SMEs	Small to Medium sized Enterprises
STL (stl)	Standard Tessellation Language
TIFF (tiff)	Tagged Image File Format
TV	Television
UAV	Unmanned Aerial Vehicles
UH	Ultra-high
UL	Ultra-low
UK	United Kingdom
U3A	University of the 3 <sup>rd</sup> Age
US\$	United States Dollars
USA	United States of America
UV	Ultra Violet
VR	Vibration Reduction
VRML	Virtual Reality Modelling Language (known as *.wri files)
w	watt
WRI (wri)	Windows Write Document file
WebGL	Web standard to support and display 3D graphics
X-ray	Electromagnetic radiation

## Appendices Book - Contents

Appendix A - ASME – J. Computing & Info Science in Engineering – 2014

Appendix B - CIRP – published on line – Sciencedirect.com – 2015

CIRP – Procedia CIRP vol. 36 – 2015

## Media coverage

Appendix C – Ancient Egypt - Vol. 15. No.3 - Dec. 2014

Touching History - The Egyptian collection

Appendix D - Ancient Egypt - Vol. 15. No.5 – April/May 2015

Touching History - The Lost Crown of Horus

Appendix E - American Scholar -Oct 2014 by Josie Glausiusz

Ode on a Grecian Replica

## Data Charts, Photographic Images and Tables

Appendix G -	Table G.1	Data Chart for processed images using <i>123D Catch</i> <sup>®</sup>	Chapter 4.3	page 116
	Table G.2	Photographic images, size and material	Chapter 4.3	page 116
	Table G.3	Capture data Log - <i>123D Catch</i> <sup>®</sup>	Chapter 4.5	page 120
Appendix H -	Table H.1	Ammonite Data Sheet – Triangles (Polygons) Size in relation to Kilobytes size of File”	Chapter 4.11	page 149
	Table H.2	Ammonite Data Resolution Statistics “ <i>Processing 40 images with PhotoScan - Mesh Statistics</i> ”	Chapter 4.11	page 149
Appendix J -	Table J.1	Data Chart and Image Library using <i>PhotoScan Pro4</i> <sup>®</sup>	Chapter 4.15	page 176
	Table J.2	Photographic images, size and material	Chapter 4.15	page 176
	Table J.3	Capture data Log – <i>PhotoScanPro4</i> <sup>®</sup>	Chapter 4.15	page 176
Appendix K -	Table K.1	Capture data Log – Failed Artifacts	Chapter 6.2	page 227
	Table K.2	Photographic images of Failed Artifacts	Chapter 6.2	page 227 - 235
Appendix L -	Table L.1	Compact v DSLR Digital Data comparison	Chapter 7.1	page 272
			Chapter 7.3	page 277
Appendix M -	Table M.1	Warrior Head – Netfabb Data for Bench Mark Models	Chapter 4.12	page 154
			Chapter 4.12	page 158
			Chapter 7.2	page 274
			Chapter 9.4	page 327

Appendix N -	Table N.1	Capture log – RAW & Jpeg – Photographic Image Data	Chapter 9.5	page 328
	Table N.2	RAW & Jpeg Image log – PhotoScan Data processing Information.	Chapter 9.5 Chapter 9.8	page 328 page 337
Appendix P -	Image Sheet 1	Warrior - Pre-processed RAW images v Camera ready Jpeg images	Chapter 9.6.1	page 330
	Image Sheet 2	Serenity - Pre-processed RAW images v Camera ready Jpeg images	Chapter 9.6.2	page 332
	Image Sheet 3	Dolphins - Pre-processed RAW images v Camera ready Jpeg images	Chapter 9.6.3 Chapter 9.7	page 332 page 335

## **Outputs**

ASME – J. Computing & Info Science in Engineering – 2014

Reverse Engineering using Close Range Photogrammetry for Additive Manufactured Reproduction of Egyptian Artifacts and other Objets d'art.  
(ESDA1014-20304)

CIRP – published on line – Sciencedirect.com – 2015 Procedia CIRP vol. 36 – 2015

Single Camera Photogrammetry for Reverse Engineering and Fabrication of Ancient and Modern Artifacts

CIRP 25<sup>th</sup> Design Conference - 2015

Single Camera Photogrammetry for Reverse Engineering and Fabrication of Ancient and Modern Artifacts – PP presentation

## **Media coverage**

Ancient Egypt - Vol. 15. No.3 - Dec. 2014

Touching History - The Egyptian collection

Ancient Egypt - Vol. 15. No.5 – April/May 2015

Touching History - The Lost Crown of Horus

American Scholar -Oct 2014 by Josie Glausiusz

Ode on a Grecian Replica

## Contribution to Knowledge

At the inception of this research, both AM and photogrammetry were well established in their own respective fields. As is shown in the initial chapters covering the historical and literature review aspects of the research, 3D imaging, Laser Scanning (including CT and MRI scanning), as well as digital image capture using a DSLR camera were all being used to produce 3D images, and by converting the imaging format into AM technology readable files, AM fabricated replications were being made.

For the most part, up to this time, 3D imaging was in the domain of specialist software experts and AM machine engineers, who, with a great deal of expertise, could convert 2D images into 3D models. Complex software and expensive hardware was required by those pursuing the subject, which was only available in the commercial sector in certain large organisations with sufficient financial resources. Both technologies were being used in universities or large companies with R&D departments covering many disciplines and industries.

Initially this research undertook to examine the claims of a Beta version of *123D Catch*<sup>®</sup> from AutoDesk, that anybody could “happy snap” with an iPhone, iPad or compact camera, up-load to the internet and produce 3D replicated copies of the original items. The research also undertook to determine whether these claims were indeed achievable with some carefully planned measures using both a mid-range DSLR camera and also a “point and shoot” compact camera. Also, by comparison, it undertook to investigate whether there was commercial software available which was user friendly, to process the digital images and convert the resulting digital files to an AM printable format. It also investigated whether it was possible, without using expensive and complex software and hardware, for a computer literate person to achieve good 3D representations of the original artifact, and whether the research objectives as laid out in Chapter 1 were indeed achievable.

It is proposed that the research as described in this thesis will offer the following contributions to knowledge:

- With the aid of a Compact “point and shoot” camera, establish limits for acceptable image resolution which could be used in the process of converting 2D images into 3D replicated AM objects.
- Contribute to the development of techniques and methods which can be used by computer-literate, but not necessarily expert, computer software operatives.
- Development of a procedure which is more cost effective and cheaper than most 3D scanning systems.
- The development of a system which could potentially be utilised by a variety of users including community projects, educational institutions, and museums and galleries.
- The development of a non-invasive procedure to replicate hand-crafted original artifacts which may be a more economically viable method to be used by small businesses (SME's) for the promotion of their designs.
- Comparison of the use of RAW (NEF) and Jpeg digital image format through the use of bench mark AM models and series of 2D printed image examples, processed within the same software, and evaluation of the benefits of one format over the other, showing that the preconception of the use of RAW images as superior to Jpeg was not always merited.
- Examine the processing of high and ultra-high point cloud digital images and justify their use with AM technology, demonstrating that unless the AM technology output is of a high enough resolution, the artifacts produced will not match the high specification of the digital images. Due to the longer time needed to process high and ultra-high digital images, and the higher more expensive specification of the processing computer hardware required, both time and therefore money would be wasted.



# **Chapter 1: Introduction and Background History**

## **1.1 Introduction**

Since the dawn of man's existence, he has left testimony of his desire to copy and replicate those things around him that he sees and touches in both his physical and metaphysical world. There have been many stages in the development from the first cave drawings and hand-made figurines, to the additive manufactured (AM) artifacts and three-dimensional (3D) images seen today.

## **1.2 Overview**

Over the last decade, Laser Scanning (LS) [1, 2] and Structured Light [3, 4] have been used to digitally replicate objects of all sizes, from large historic buildings to small statues, and have moved to dominant non-invasive method used to digitise smaller objects [5]. In this thesis, an alternative process to the LS method of data capture was researched using a Digital Single Lens Reflex (DSLR) camera, and it was shown, that limited prior "expert" knowledge was required for this alternative digitisation method. Apart from the use of the computer programs selected and without the use of relatively expensive and complicated 3D laser equipment, this objective was achieved. By the use of photogrammetry, high resolution digital images could be manipulated, filtered and processed by specialist software to produce 3D spatial images. In this research, the main primary software used was AutoDes's *123D Catch*<sup>®</sup>, Agisoft's *PhotoScan Pro5*<sup>®</sup> and AutoDesSys' *form-Z pro*<sup>®</sup> [6-8]. The data files created were further processed by additional software, in this case Netfabb's *StudioPro*<sup>®</sup> [9]. The files were made ready for AM machines to replicate the original photographed product into physical models. As such, this technique could contribute to the reproduction, restoration or repair of damaged or broken antiquities by non-invasive methods at modest cost and by computer literate but not necessarily expert computer software operatives.

## **1.3 Research Objectives**

- To develop a simpler, more accessible method of data capture and processing. With the use of AM (or 3D Printing technology), geometric

representations of original cultural, historic and geological artifacts can be fabricated in a process known as Reverse Engineering (RE).

- To investigate how well the software programs used, convert the digital 2D images into AM models, and compare results obtained with the original object.
- That the techniques and methods employed and developed can be used by computer-literate but not necessarily expert computer software operatives.
- With the aid of one medium range DSLR camera, transform two-dimensional images into three-dimensional CAD spatial representations, thereby developing a system which is more cost effective and cheaper than 3D Scanning.
- To experiment with a low budget compact “point and shoot” camera to ascertain the lowest resolution for acceptable images which could be used in the process of converting a 2D image into 3D replicated AM objects.
- To develop a system that could be used by:-
  1. Local Community projects
  2. Educational institutions
  3. Museum and Gallery staff so that the artifacts “behind glass” can be copied and shared with the general public; if the original object cannot be handled because it is too old or delicate, then replicas can give the handler a chance to experience the size, texture and weight of rare objects
  4. Because of the relative low cost of the method, can be developed and used by small businesses (SME's) for the promotion of their products
- To replicate unique objects in a non-invasive way, and by use of this technique, contribute to restoration or repair of damaged or broken antiquities and artifacts.
- To enhance the spatial and tactile experience when “viewing” works of art by the visually impaired.

In this thesis, the whole process was shown, from digital capture of artifacts to their AM replication. This includes entry level AM printers, which are in use by school age students under supervision. Whilst this thesis does not discuss pedagogical aspects of a curriculum, by using moderately priced equipment and

software, as suggested in future chapters, the methods described could be integrated into school curricula to teach both cultural history and 3D modelling technologies [10], at many, if not all, year levels. The term Reverse Engineering is used throughout this thesis and defined as meaning the capture, replication and fabrication of the visible surface of the artifacts that are under discussion. The advantage of this photographic process was that expensive 3D scanners are not required to capture the data necessary to produce 3D CAD images, and experienced technicians were no longer required to operate this equipment. By using a single, relatively modest DSLR camera, good results were shown to be obtainable.

#### **1.4 Digital Image Capture**

This thesis considers how modern photogrammetry, or digital image capture, can be used with the aid of a single medium range DSLR camera, to transform two-dimensional (2D) images into 3D Computer Aided Design (CAD) point cloud images, and together with AM technology, geometric representations of original cultural and historic artifacts can be fabricated. The research has focussed on the use of single DSLR camera photogrammetry, an affordable and accessible technology, as opposed to the more expensive method of 3D scanning.

The basic photogrammetry equipment required is discussed, with the main objective being simplicity of execution for the eventual realisation of physical products. As the processing power of computers has increased and become widely available, at affordable prices, and software programs have improved, it is now possible to digitally combine multi-perspective photographs, taken from 360° around the object, into 3D CAD representational images. This has now led to the possibility of 3D images being created without 3D scanning intervention.

#### **1.5 Software Programs**

Many software programs claim to be able to convert 2D digital photographs into 3D images. On investigation, it has been found that many are still in development and are not necessarily available for use except experimentally. Several commercial computer programs are available with a proven and reliable record to “stitch” multi-view photographs together to produce a 3D image. The primary research task investigates how well two software programs, Agisoft’s *PhotoScan*

*Pro5*<sup>®</sup> and Autodesk's *123D Catch*<sup>®</sup>, convert the digital 2D image into 3D point cloud images and with the use of a third software, Netfabb's *StudioPro4*<sup>®</sup>, converted the data into files that AM machines could read and then fabricate into physical models. Over the course of this research, both Agisoft and Netfabb have upgraded their programs from *PhotoScanPro5*<sup>®</sup> to *Pro7* and from *StudioPro4*<sup>®</sup> to *Pro7* and allowed the author access to the latest version as they became available. For simplicity, the version numbers have been dropped in both cases.

The results obtained – the created models - were then compared with the original photographed artifacts. The research investigates the tactile surfaces of the replicated models and compares them to the original objects; it considers whether those replicated models, when scaled up and down, lose surface detail and whether the AM models created could be substituted for the original or whether they are limited by the capability of the AM technology itself.

During the literature review, the author came across a process about which little has been written; digitally capturing the photographic data of a painting or drawing, into a raised 3D form which is called Image-Based Displacement (IBD). The displacement "tool" used was a software program, AutoDesSys' *form-Z Pro8*<sup>®</sup> [8], which imprints an image onto the surface of a pre-made virtual flat object creating a bas-relief, by manipulating a point cloud mesh. The process is published by AutoDesSys [11], the resulting data files can then be AM replicated. A few examples which were fabricated by the author are included in this thesis. It was felt that this enhanced the overall research into the main theme of simplification of the process of replicating artifacts, which can then be freely handled by the public, enhancing the "viewing" experience by, for instance, a visually impaired person.

## **1.6 Headings and Contents for Main Body of Thesis**

Following on from this section, the next part of Chapter 1, will give the reader an insight into the background and a brief history of some of the important events leading to the developments surrounding this research. A review of existing literature follows in Chapter 2, and the second half of Chapter 2 covers an in-depth look at the objectives for this research, covering the development of a simpler, more accessible method of data capture and processing; a technology that can be used by computer-literate but not necessarily expert computer

software operatives; a more cost effective system than 3D scanning, which can be used by a variety of institutions and SME's, and which can benefit the wider community. The use of hardware and computer software is covered in Chapter 3, followed in Chapter 4, the different methodological techniques used in the experimental processes employed in the thesis.

Two main types of software programs were employed in this thesis, a primary one, which processed the digital images as described in Chapters 4, and a secondary one, described in Chapter 5, which cleaned and finessed the virtual 3D images, and turned them into \*.stl files that could be read by the AM machines to produce the replicated models. Measurement and Scaling up of the models so as to produce accurately sized models and some of the pitfalls that can be encountered are covered.

In Chapter 6, the Repair of Noisy, Distorted and Incomplete Data is examined together with several artifacts that were un-repairable within the remit of this thesis. Several practical uses of the techniques employed are examined, for example how Educational use and Heritage preservation can benefit, and how to repair, renovate and replace lost parts of broken artifacts is shown in later part of this chapter.

As described earlier, one of the prime objectives of this research was to see how simple the process of replication and fabrication of artifacts could be made, using both hardware and software, which could be used by operatives who were camera and computer literate but not experts. The most critical part of the whole operation was the initial data capture of images. Throughout this research, data capture was carried out using a single medium range entry level DSLR Nikon *D3100*® camera. As a comparison, an even simpler and a much lower cost camera was used, an automatic Compact Canon *IXUS 100IS*®, "point and shot". These experiments, comparisons and results are documented in Chapter 7.

The physical detail and comparison of materials used in the fabrication of AM Models is covered in Chapter 8, where the finished AM models are examined and the different methods of manufacture are compared. The use of a more advanced photographic format, the RAW digital image, was discussed in Chapter 9. This RAW format was compared to the simpler Jpeg format which was used throughout this research. The results of the two types of format are examined and evaluated. The final chapter of the thesis contains the results obtained from the

research, a discussion and evaluation of these results and finally conclusions drawn from them, all found in Chapter 10.

### 1.7 Introduction to Background History

This historical section, traces some of the more important aspects of the technology, and attributes the scientific discoveries made, without which this research would not have been possible.

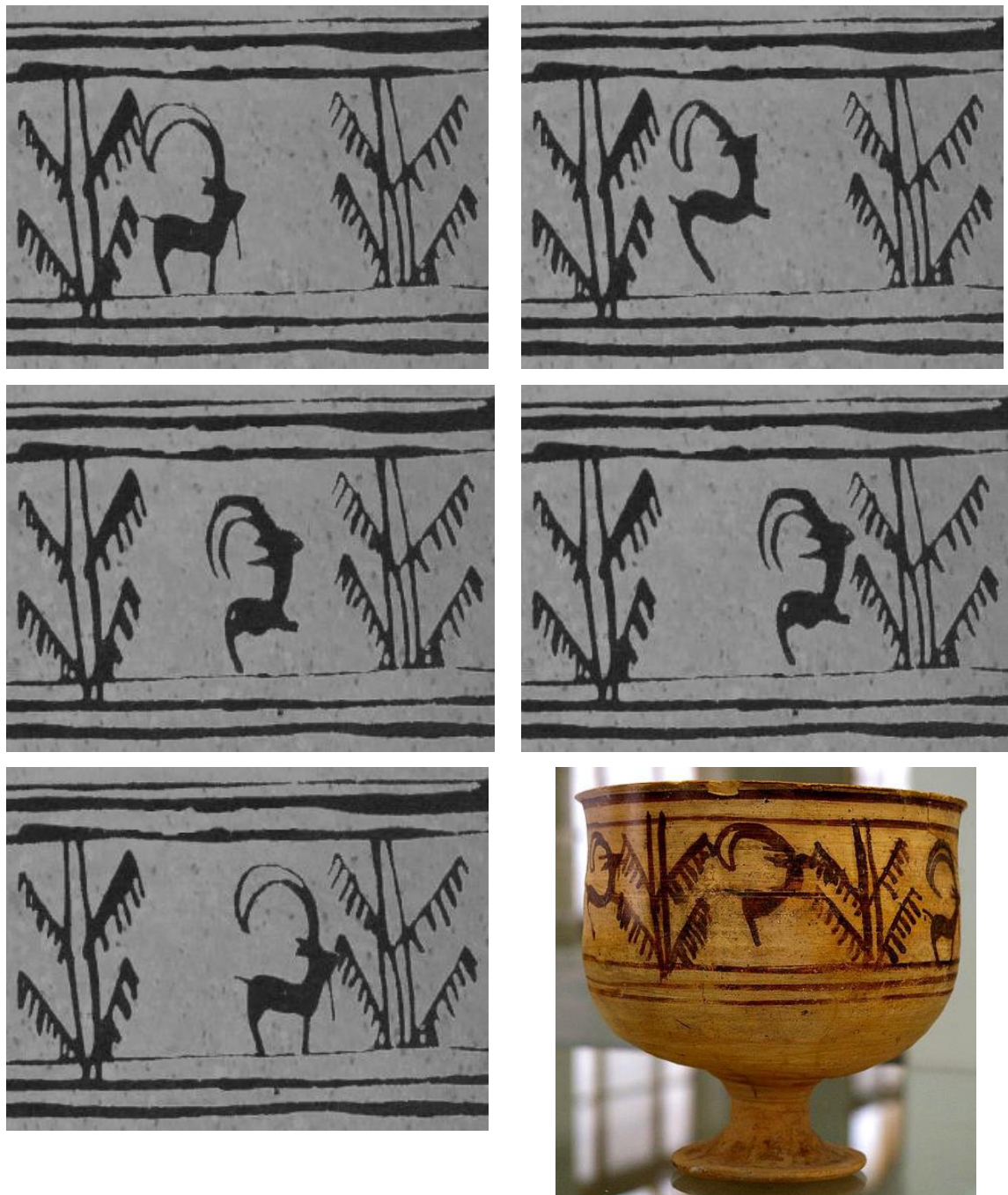


Figure 1.1: Sequential animation of goat leaping into the air to feed from plant.

From the earliest of prehistoric cave paintings, we see the animals man hunted, the pictorial record of enemies defeated, mystical symbols as well as everyday utensils and day to day events. Many palaeontologists and anthropological researchers suggest that the development of the human mind unfolds within these cave drawings, paintings and carvings. Dating from these early periods, 20-35 thousand years ago, archaeologists have found carved limestone, bone or ivory, as well as clay fired figurines, which are among the oldest ceramics known.

An Italian archaeological team working in Iran, in the early 1970's, discovered a 5000 year old, painted ceramic bowl, depicting a goat leaping up at a tree. It was many years later that the leaping goat figures were seen to be sequential. Notice the position of the first goat in the first frame and how the position and movement changed in the succeeding frames. If the bowl was spun round the goat leapt into the air and snatched the leaves from the tree, each animated section is seen in Figure 1.1 whilst the whole bowl can be seen in last image [12]. This is possibly the first recorded example of an animated object.

### **1.8 Aristotle & Euclid**

At about the same time that Aristotle was describing how light images are projected on a wall, in Alexandria, Euclid, one of the most important and prominent mathematicians of the ancient world, was writing the 13 volume mathematical treatise for which he was to become famous:- *The Elements*. Most of the books are a series of Mathematical Definitions and Propositions leading to his three-dimensional geometry [13]. *Optics* was his first work on perspective, which we now know as 3D imaging, based on the proposition that light travels in straight lines [14], as yet unproven until the 10th Century by Ibn al-Haytham (see Chapter 1.10 below).

### **1.9 Camera Obscura**

The desire to replicate and copy to the greatest accuracy is a developing theme through the development of Man. The 'Camera Obscura' (CO) or 'darkened room', coming from the Latin is the first recorded principle of the modern day camera.

Aristotle, of the Ancient Greek era, noted how light passing through a small hole in a wall, into a darkened room, produced an inverted image of the sun on the opposite side wall of the room, during an eclipse of the sun. A plate published in 1544 by Frisius Gemma is thought to be the first illustration of a CO. The plate showed exactly the image of the eclipse of the sun, as described by Aristotle, appearing on the opposite wall of the room (Figure 1.2) [15].

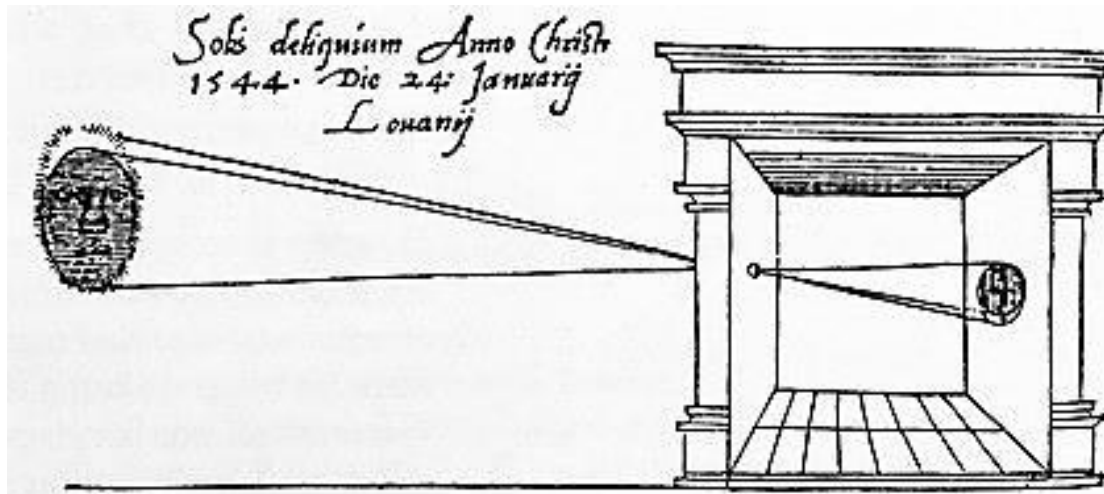


Figure 1.2:

Frissius Gemma's illustration "Eclipse of the Sun 24th January, 1544".

There were many versions made over the following years, both in size and materials. A popular version was a wooden box construction which was both portable and accessible.

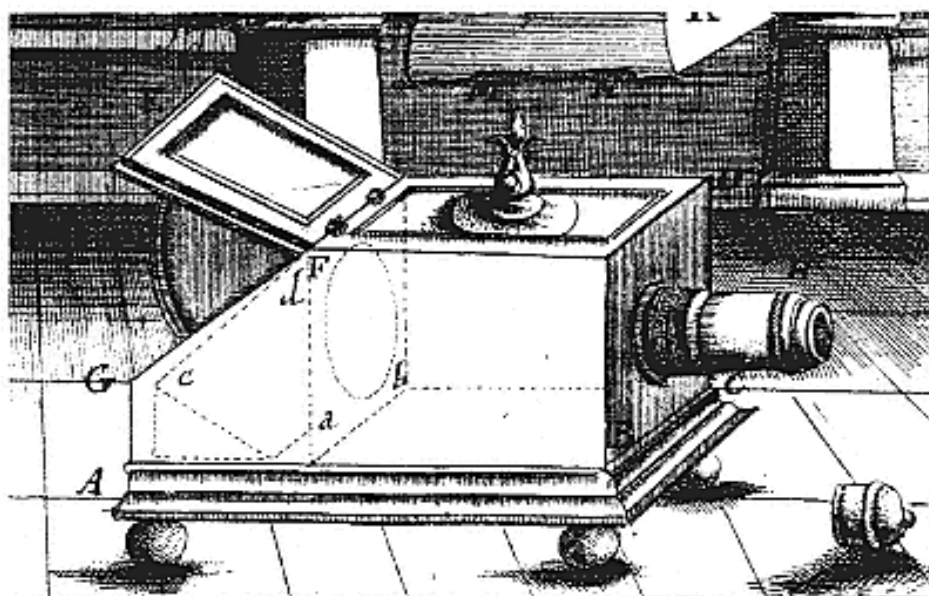


Figure 1.3:

Johann Zahn, *camera obscura portabilis* (reflex box camera obscura), 1685.

In 1685 Johann Zahn, an optician and mathematician, was able to modify the box CO so as to obtain an image the correct way round. He did this by adding a mirror at 45° to reflect the image the right way round (Figure 1.3) [16]. By adding a moveable lens at the front of the box, he was able to focus the object to produce a very clear image, thus creating the Reflex Camera obscura - the forbearer to our modern “*through the lens*” reflex camera, the Single Lens Reflex camera (SLR) which eventually became the Digital SLR (DSLR) as in use today.

### 1.10 The Next 500 Years

The scientific principle behind the CO may have been used even earlier by Stone Age man to produce their cave art, but by the 10<sup>th</sup> Century, the CO was being used for scientific work by Ibn al-Haytham also known as Alhazen, an Arabian scholar, proving Euclid’s proposal, that light travels in straight lines:

*“Light travels in a straight line and when some of the rays reflected from a bright subject pass through a small hole in thin material they do not scatter but cross and reform as an upside down image on a flat surface held parallel to the hole.”* [13]

In the 13<sup>th</sup> Century, the use of the camera obscura was the established way in which astronomers viewed the sun [17]. Three hundred years later it was being used by artists such as the Dutchman Johannes Vermeer as a ‘tool of the trade’, having been developed into “the pin-hole camera”. It became a device by which the complex 3D living world of contrast light and dark, colour and texture, foreground and horizon, could be projected onto a flat wall or table top, creating a 2D image [18]. At the speed of light, this 2D image resolved all the complexity of perspective, which Euclid had postulated, and which the human eye and brain struggled to translate from 3D to 2D.

The projected scene could be preserved only by the hand of an artist or skilled draughtsman. The projected image was still transient, and still subject to the potential error of the human hand to transpose the moving living world into an accurate permanent replication. In the early 15<sup>th</sup> Century, the camera obscura was being used as a “*social media*” event. Darkened tents or booths were set up with the audience inside, viewing live actors performing on the outside, albeit

upside down and seen, at the time, by the audiences as a form of sorcery. But such booths began appearing throughout the western world at carnivals or country fêtes, people paying money to walk in and see on a flat table top, the live action of the moving world outside of the tent. Today many museums around the world still display this simple principle, and the original equipment, of a 2D pictorial display of the outside surrounding scene, which surrounds the building in which the camera obscura is housed.

### 1.11 Capturing the Photographic Image – The Early Pioneers

The Holy Grail of a fixed captured image was finally achieved in 1826 by the French scientist, Joseph Nicéphore Niépce. He placed a bitumen coated plate in his camera obscura, exposing it for several hours. This produced an image of his courtyard as seen from his upstairs window [19]. In 1839 Louis Daguerre, a printmaker and painter, presented the French Académie des Sciences with his images he named *Daguerreotype*, individual images on a sheet of polished silver-plated copper. The two French men, Nicéphore Niépce and Daguerre, had collaborated since the mid 1820's and by the time of Nicéphore Niépce's death in 1833 had produced a light sensitive image which could be fixed permanently by the use of chemistry. But it was not until 1839 that Daguerre felt confident enough to show his invention to the French Académie [20].

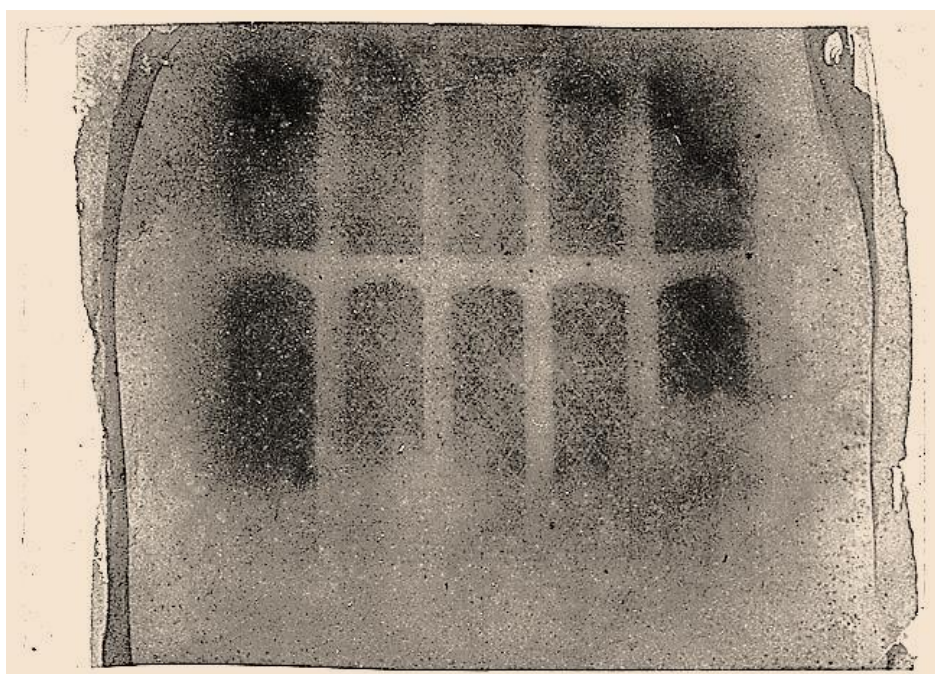


Figure 1.4: Fox Talbot's first captured photographic negative image.

In 1835, William Fox Talbot, an English chemist, working quite independently of the Frenchmen, in his home at Lacock Abbey [21], discovered light sensitive chemicals which when applied to a solid surface, such as glass.

After being subjected to daylight, formed what was to become the first captured photographic negative image (Figure 1.4). This negative image could be chemically stabilised and by repeating the process with the glass negative, form a positive image. This negative glass image could be used several times to make several copies of the original.

It was only when Daguerre proclaimed his invention in 1839 that Talbot came forward with his invention. The race was on for whose method would be declared the '*inventor of photography*'. Daguerre's method was a '*one shot*' picture and could not be replicated whereas Talbot's method of a single negative, which could be copied many times over to produce an infinite number of pictures, ultimately led to the method used by photographers until the birth of digital photography in the 1970/80s.

## 1.12 Photographic Cameras

Within twenty years of Talbot's invention, such was the fast pace of development of this new found technology, the camera as we know it was created, transforming true to life images of 3D objects into the 2D image, the photograph, that we are familiar with today. This was to place the camera obscura into the realms of history. Although still used by artists, it was the automatic, light-sensitive paper that when processed, was transformed into a true representational picture of the captured subject, that caught the imagination. It perhaps could be argued, that this breakthrough, by Messrs Talbot and Daguerre can be classed amongst one of the most important scientific discoveries.

### 1.12.1 Stereoscopic Images

By the mid 1860's the development of the single picture photographic camera had advanced to produce a twin lens camera capable of taking stereoscopic photographic images [22] (Figure 1.5). 3D imaging has been in existence since the invention of Lenticular's Stereoscope [23] in 1860 (Figure 1.6) and there still

exists many of these early stereographic picture sets [24] (Figure 1.7) and viewing apparatus as seen in Figure 1.8.



Figure 1.5 : Hare's Stereoscopic camera – c1857.



Figure 1.6: Lenticular's Stereoscope - c1860.

As with historical documents and especially with photographs, they are able to portray a very vivid picture of part of the social life and reinforcing much of the written word, so described and explained by the New York Public Library on its website “The Stereograminator” [25].

*“Stereoscopic photography recreates the illusion of depth by utilizing the binocularity of human vision. Because our two eyes are set apart,*

*each eye sees the world from a slightly different angle. Our brains combine these two different eye-images into one, a phenomenon that enables us to "see" ever so slightly, around the sides of objects, providing spatial depth and dimension. Stereoscopic views, or stereographs, consist of two nearly twin photographs - one for the left eye, one for the right. Viewing the side-by-side images through a special lens arrangement called a stereoscope helps our brains combine the two flat images and "see" the illusion of objects in spatial depth." [26]*



Figure 1.7: Typical double image for binocular vision.

It will be noted in the examples Figures 1.7 and 1.8 of stereoscopic images, as in all such pairs of photographs, how the right hand image has shifted across the frame.



Figure 1.8: Kilbourne Stereo Daguerreotype in folding stereoscope.

This is the same effect as looking and focusing on an object and closing the lid of each eye in turn; the object will shift in one's vision either to the right or left. The method of using a double image, or binocular vision, created a more *solid* looking image, recreating the human experience of vision, and was a technique that became so popular that camera manufacturers such as Zeiss® were still producing pocket stereoscopic viewers well into the 1950s [27] (Figure 1.9).



Figure 1.9: Zeiss pocket stereoscopic viewer.

Even today, the use of stereoscopic cameras, are in demand more than ever. Modern state of the art still/video stereoscopic cameras such as the Panasonic AG 3DA1 (Figure 1.10) are making “block buster” 3D films for the commercial TV and cinema companies such as the 2009 James Cameron Sci-Fi epic *Avatar* and more recently, Marc Webb’s 2012 film based on the Marvel Comics character Spider-Man, and for the last few years the latest “must have” TV supports high definition and 3D viewing.



Figure 1.10: Panasonic state of the art still/video camera.

### **1.12.2 Photogrammetry**

Photogrammetry, as it is referred to, “*is the practice of determining the geometric properties of objects from photographic images and is as old as modern photography*” [5] dating, as we have seen, from the mid-19th Century. Photography, especially aerial photography and reconnaissance was recognised as a very important source of information/intelligence. The American Society for Photogrammetry and Remote Sensing (ASPRS) was formed in 1934 and defined Photogrammetry as:-

*“the art, science, and technology of obtaining reliable information about physical objects and the environment through processes of recording, measuring and interpreting photographic images and patterns of recorded radiant electromagnetic energy and other phenomena”* [28].

### **1.12.3 Aerial Photography**

It was not long before the camera was taken up into a tethered hot air balloon and in 1858 a photographer named Nader was photographing Paris from the air, patenting his new system of aerostatic photography. Just two years later, the idea of surveying behind the enemy lines by the use of hot air balloon and camera, was used in Boston, during the American Civil War, producing the first documented aerial photos to be used against an enemy. As well as the balloon, the cameras were flown high above the houses and cities by kite, producing photographic records of San Francisco burning in the 1906 fire which destroyed much of the city. So aerial photography was gradually born, but it is not until the aeroplane that the use of this new technology could find its full potential. Used in World War 1 by both sides to survey the enemy lines, it is reported that the airborne division of the German army was surveying 4000 images per day of the battlefields, taken from the air [29].

### **1.12.4 Le Corbusier**

Architects such as Le Corbusier, the Swiss-French architect, designer, painter, urban planner, and one of the pioneers of what is now called modern

architecture, were able to fly over vast areas of land, charting their/his new urban dreams as well as denigrating the industrialisation and city sprawl that had started with the new technologies of the 19<sup>th</sup> century. Le Corbusier's "*Birds eye view*" became the new found phrase for his techniques and visions and those of others who followed him. The view of rivers and coastlines, as seen from the air, became the starting point for the architects and urban planners of the mid 1930s [30]. His ideas and practices still influence many researchers who are using both camera and LS in conjunction with unmanned aerial vehicles (UAV)s to survey and study [31], for example forests [32], crops, valley, river [33] and coastal movements.



Figure 1.11:  
Drone or UAV as available from the local electronics shop equipped with camera.

Now in the second decade of the 21<sup>st</sup> Century, UAVs are everywhere, equipped with state of the art High Definition (HD) cameras or 3D scanners. Drones are still on the front line in war zones surveying the battlefield, or employed in a more genteel way of surveying crop growth, land formation, archaeological sites or used by children playing in the park taking "selfies" from 10 - 20 meters above themselves in the air, in a UAV bought from the local toy or electronics shops (Figure 1.11).

### 1.12.5 Spy in the Sky

In 1960, perhaps the most infamous air photographer/pilot, Francis Gary Powers, was shot down over the Soviet Union in his U2 plane; this had been equipped with a state-of-the-art camera designed to take high-resolution photos of the military installations from the edge of the stratosphere, from approximately 70,000 feet above the earth's surface, showing how far Lenticular's Stereoscope and Nader's tethered balloon had progressed in less than a hundred years. Today the “spy in the sky” has moved onto satellites, although not wholly accepted, is now just a way of life.

### 1.13 Birth of the Digital Camera

Converting the 2D image, displaying it on a television screen and later on computer monitor, was perhaps the next most important step alongside the introduction of mass produced computers of the late 1970's. The first digital camera was invented in 1975 by Steve Sasson, who was an engineer working for *Eastman Kodak*® (Figure 1.12).



Figure 1.12: c1975 Sasson's Digital camera.

It was constructed by using a *Super 8* movie camera lens, plus several dozen digital and analogue circuits wired into circuit boards. The black and white image that was produced took 23 seconds to process, which was then recorded onto a cassette tape. To see the image played back, the data was read from the tape and displayed on a black and white television [34]. This camera has developed from the low resolution 0.01 Megapixels (mpg) early camera to 60 or 80 mpg at the top end of today's professional range Digital Single Lens Reflex cameras, encompassing the digital video cameras on the way.

### **1.14 The Ruby Red Beam**

The origins of the LS can be traced back to the late 1950/60's with the development of the laser. The laser beam's beginnings started in 1960 in the Hughes Research Laboratory in California. The team was led by Theodore Maiman, and at the time researchers referred to the ruby laser beam as "a *solution looking for a problem*" [35]. The story hit the media with front page newspaper reports of a device with "death ray" capability [36]. But the Nobel prize was claimed four years later, after much more research and development by a team at Columbia University in New York, led by Charles Townes [37]. In that same year, 1964, the actor Sean Connery, in the guise of Ian Fleming's James Bond, the infamous secret service character 007, was strapped to a stainless steel gurney, being sliced in two by *Goldfinger*, using a ruby red laser beam [38].

### **1.15 Laser Scanners**

Within the next few years, the ruby red beam was instrumental in solving many a problem and is today found in many everyday items, for example DVD players, supermarket tills, and document printers, as well as scientific equipment such as metal cutting machines and of course laser scanners. In 1968 one of the first prototype scanning devices was built in the Physics department at Cambridge University. A laser beam was moved around by mirrors following lines on photographs of bubble chamber experiments, identifying particles of protons, neutrons, etc., - the building blocks of matter. With financial backing, the Cambridge team started a company called *Laser-Scan*<sup>®</sup>, producing *the Sweepnik* [39]. The machine was improved and over the next few years sold as a commercial product, around the world, to other academic institutions.

## 1.16 Personal Computer

With so much development taking place in the years between the 1950 and late '60's, such technologies as previously discussed might have never got beyond the scientific communities and the multi-national companies as 'interesting research products awaiting future development', but for the event of the personal computer; the portal to mass-communication in the 21<sup>st</sup> century. The arguments as to who invented the first electronic or digital computer may never end but at the end of the 1960's they were large, heavy mainframe structures, and usually run and owned by universities or electronics companies. The mid 1970's saw several companies such as *IBM*<sup>®</sup>, *Texas Instruments*<sup>®</sup>, *Commodore*<sup>®</sup>, *Apple II*<sup>®</sup> and *Radio Shack*<sup>®</sup> bringing together circuit boards, processors, numeric key pads and monitors and looking to the business communities to market their new "computers". At the 1977 *Consumer Electronics Show* in Chicago, *Commodore*<sup>®</sup> introduced the *PET*, and is acknowledged as the first fully functional out of the box, desktop computer. By 1983 computers had entered into the domestic market selling for about \$200. *Commodore 64* (6510, 64KB RAM, 20KB ROM with *Microsoft BASIC*<sup>®</sup>, custom sound, and colour graphics), selling an estimated 17/22 million units. The personal computer (PC) had arrived and was here to stay [40]. In a report in 2014 from the Office for National Statistics [41], the number of computers per UK household with internet access had risen from under 10% in 1998 to just under 85% by 2014, with 18% of households owning on average more than 3 computers.

## 1.17 Development of LS & CAD

The two most recent significant events were the development of computer software that could read the point cloud data (PCD) [42] from the output of LS, and the development of CAD.

A point cloud data set can be created by LS, in a three dimensional space, where each point is defined by X, Y, and Z co-ordinates. These points are reference points collected from the object that the laser is scanning. These points could be created by computer software, which had identified hundreds, or millions of matching points on artifacts, landscapes, or buildings etc., which had been captured on two dimensional digital or scanned photographs.



Figure 1.13: Point Cloud 2D enlargement of head section – Front view.



Figure 1.14: Enlarged head section – side view.

These point clouds, however created, are reconstructed to form a 3D surface skin of the original object. The point cloud file can then be saved, depending on the converting software, to a variety of formats. The point cloud 3D model can then be exported to an editing software program for further development or enhancement. Figures 1.13 to 1.15, show the point density of the whole image as 67,063 points. The 2D screen shot of the enlarged front view of the head of the Warrior (Figure 1.13) is somewhat confusing as it appears less dense because of the enlargement and therefore transparent, showing the back of the head and shoulders, through to the front. The side view seen shown in

Figure 1.14 is less complicated to comprehend although exactly the same size and from the same 3D image data.



Figure 1.15: Full image – 67,063 points.

It was these developments, over the next twenty years, that brought LS to the attention of architects, surveyors and engineers. Many technology companies were founded or started to develop both software and scanners in this era, and bring them to the market place [43]. By the late 1970s, market leaders emerged such as *Trimble<sup>®</sup> Navigation Limited* with its' range of 3D scanners closely followed by academic papers on first experiences with these new machines [44]. Later, how accurate the scanners performed, information regarding data acquisition, registration, geo-referencing and typical tasks that they were being used for [45] and by 2010 there was plenty of detailed literature on the use and practise of scanning of buildings and monuments as well as many other artifacts. A typical example of this is the English Heritage's commissioning of a survey of Byland Abbey by a third party specialising in 3D scanning surveying [46] (Figure 1.16).

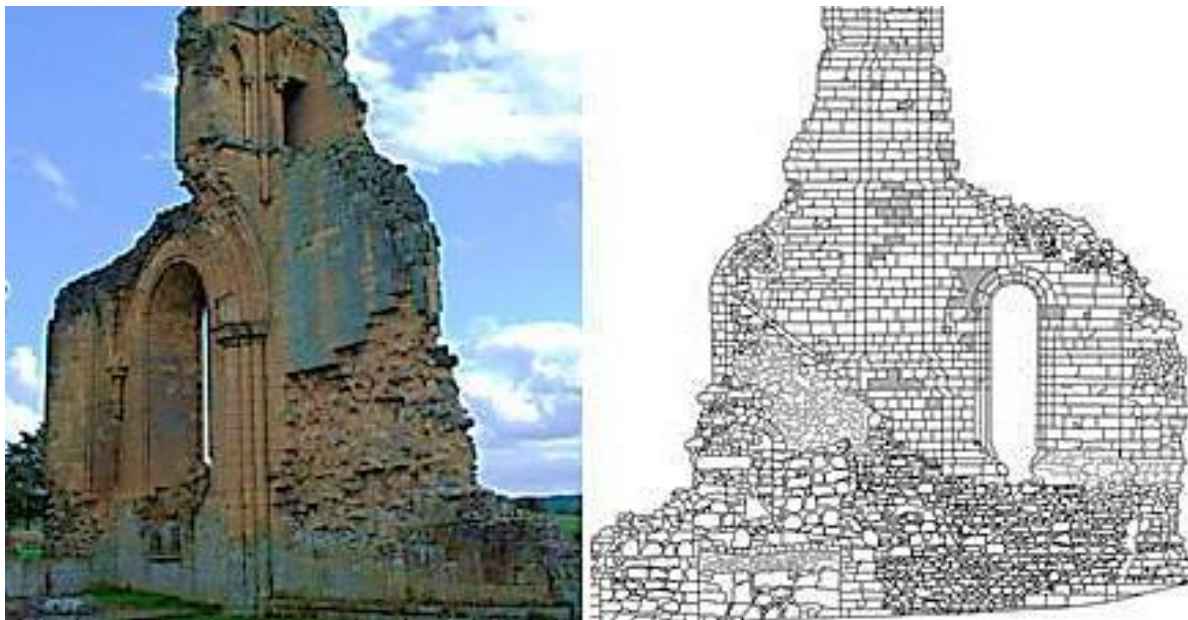


Figure 1.16: 3D scanned survey of Byland Abbey, North Yorkshire.

High end computers with large amounts of memory were and still are required to handle the very large files that the scanners produce [47]. The use of the LS became more widespread as the price of computer components, such as the Central Processing Units (CPU) and the Random Access Memory (RAM) dropped in proportion to their increase in speed and computing power. By the millennium, the possibility of being able to capture true life scenes and convert them to form a 3D image had arrived. By contrast, stereographs, the 3D photographic imaging process which had been in existence since 1860, had been overtaken by that ruby red beam that nobody knew what to do with forty years earlier. As with the camera obscura, stereoscopic views, or stereographs, consisting of two nearly identical photographs, using the camera, which had been used for recording buildings, people, and landscapes etc., for well over one hundred and fifty years, in most scientific and engineering fields, were obsolete.

### 1.18 Cost of 3D Scanners

Most professional 3D Scanners are expensive. In a comparison sheet created by *LinDarUSA®* [48] in 2012 , a competitor of *Trimble®*, the *ScanLook®* was selling from €65,400/\$80K compared with the *Trimble MX2®* (Figure 1.17) from \$90K, then add to this the cost of software, and any extra equipment required. However, at the other end of the scale, fully boxed and ready to go, the *DAVID Structured Light Scanner SLA-2® 3D-Scanner* (Figure 1.18) 3D scanner is priced at just over

€3000/\$3650 [49] and at the end of 2016, *Apple*<sup>®</sup> filed patents for a 3D scanner [50].



Figure 1.17: *Trimble MX2*<sup>®</sup> Dual Head digital 3D scanner.

Comparison of LS, their efficiency and the value for money each represents is not within the scope of this thesis and therefore is for others to determine before such a purchase is made.

Many papers exist where either machines are compared against each other [48], or in the case of Brecko *et al.* [51], cost analysis is attempted between four types of data capture, in this case using four different machines; the DSLR camera, X-ray based CT, structured light scanning and laser scanning. As well as a comparison of final specimen images obtained from each piece of equipment, this paper also contains a comparison and cost analysis including cost of equipment, portability of equipment and processing time, as well as other interesting data.

There is a range of other equipment, as well as laser scanners on the market, at even lower price points than €1000/\$1225 (see Table 1.1). *Kinect* [52] by Microsoft was claimed to be the *"fastest selling consumer electronics device"*, in the Guinness Book of World Records when it was released in 2010, and had sold over 24 million units by 2013, although not a laser scanner in the same way as the *Trimble MX2*<sup>®</sup> or the *David SLA-2*<sup>®</sup> 3D-Scanner (Figure 1.18). It was originally designed to be an accessory to the *Xbox*<sup>®</sup> computer gaming technology but has been adapted by third parties for other uses. Although there are some

drawbacks as shown by Das *et al.* in their work on replicating large paleontological specimens, the Kinect v2 sensor has become a useful tool for those with a lower budget [53].



Figure 1.18: DAVID Structured Light Scanner FDM-2 3D-Scanner®.

Within this €1000 price point, there are many other machines, perhaps two of the most well-known being the 3D Systems Sense® at approximately €450 to €500, and MakerBot's *Digitizer*®, costing about €800, both true 3D scanners, ideal for the serious hobbyist or small business/design studio. But the lowest priced laser scanner the author found was on E-bay in the spring of 2017, for €31.62; “*DIY 3D scanner main camera kit*” (Figure 1.19) including free shipping and software! No advice and very little “Product Details” were provided.

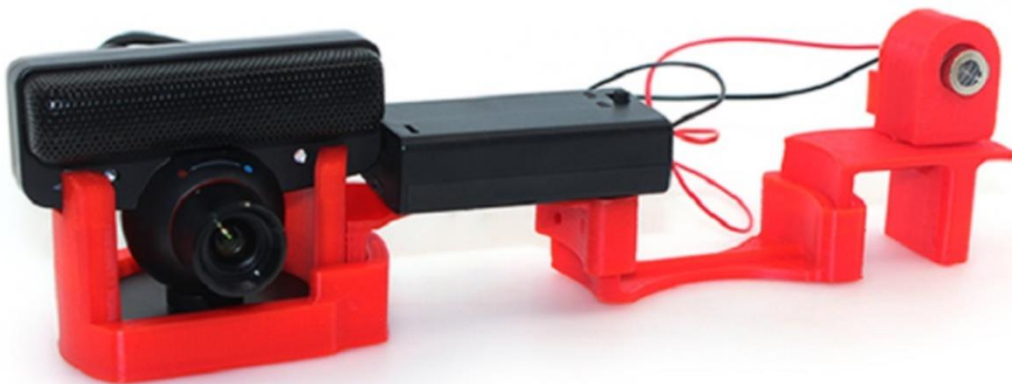


Figure 1.19: DIY 3D scanner camera Kit.

Table 1.1 is a compilation of low cost scanners, the cut-off point being \$5,250, all of which are readily available at prices as shown table, under the type of technology each employs. The lowest price found (as of Spring 2018) was the

basic Microsoft *Kinect*® priced at \$97, whilst the highest price found was the Shining 3D *EinScanPro+*® at \$ 5,199.

Table 1.1 Details of Popular 3D Scanning Technologies priced up to \$5,250.

Product	Technology (see below)	Resolution	Market Price* (US\$)	System
<b>Stationary 3D Scanners</b>				
Shining3D EinScan SE / SP	SL	1.3 M Pixels	\$1,199 - \$2,299	Windows
iiIDScan PrimeSense 3D Scanner	SL	640x480	\$1441	Windows
NextEngine 3D Scanner HD	LT	0.1 mm	\$2,995	Windows
MakerBot Digitizer	LT	500µm	\$788	Windows, OSX, Linux
David SLS-2	SL	60µm	\$3,275	Windows
Matter and Form MFS1V1	LT	250µm	\$499	Windows, OSX
<b>Handheld 3D Scanner</b>				
Shining3D EinScan Pro / Pro+	WLS	0.1 mm (HD) - 0.3 mm	\$3,999 - \$5,199	Windows
XYZprinting Handheld	SL	1500µm	\$170	Windows, OSX
Occipital Structure Sensor	SL	500µm	\$379	iOS, Android, OSX, Windows, Linux,
Cubify Sense	ToF	900 – 1000µm	\$400	Windows
Fuel 3D Scanify	PhG	350µm	\$1,386	Windows
3D Systems iSense	PhG	500 – 1000µm	\$73 - \$409	iOS
Microsoft Kinect	ToF	1280 x 960 px	\$97	Windows
<b>DIY 3D Scanner Kit</b>				
FabScan Pi	LT	0.25mm	\$100 - \$200	Raspberry Pi
Turntable for Mobile Phones	PhG	n/a		Android, iOS
Murobo Atlas	LT	0.25mm	\$209 - \$244	Raspberry Pi
BQ Ciclop	LT	0.3 to 0.5 mm	\$240	Windows, OSX, Linux
<b>3D Printer Scanner</b>				
XYZprinting Da Vinci 1.0 All in One	LT	250µm	\$500	Windows, OSX
XYZprinting Da Vinci 1.0 Pro 3-in-1	LT	250µm	\$700	Windows, OSX
AIO Robotics Zeus	LT	150µm	\$2,499	Windows, OSX, Linux

\*AMAZON PRICES 2018

Abbreviations	
PhG	Photogrammetry
LT	Laser Triangulation
WLS	White Light Scanning
SL	Structured Light
C	Contact
ToF	Time of Flight

### 1.19 Virtual 3D Representational image

CAD computer software such as Adobe's *Photoshop LE*<sup>®</sup> and *Photoshop Elements*<sup>®</sup> [54] have been able to stitch 2D digital photo images together for a number of years, creating panoramic views of city, sea or landscapes. More recently there were several software programs capable of stitching 150 or more, high resolution digital images together to form a 3D image [55].



Figure 1.20: Examples of 3D virtual textured point cloud data images.

1999 saw a breakthrough in the algorithm that launched photogrammetry software no longer requiring matched photographic scenes, but able to capture and create large point clouds from very large photo sets (Figure 1.20). The efficiency of the software which can convert digital images taken with a DSLR camera is so high, that it can turn billions of point cloud data points into 3D images within hours. This must now be a threat that the LIDAR world, with such disadvantages as the high cost of scanning and associated equipment, collecting data, slower speed of processing and the steep learning curve needed on the

research and understanding involved in utilising the entire point cloud, must now consider [56].

## 1.20 3D Reliefs

### 1.20.1 *Bas-relief, Sunken and Raised Relief*

To the uninitiated or casual observer all of the above methods are the same, or similar; reliefs being an artistic method of expression hovering between a 3D sculpture and a 2D painting or drawing, often described as 2.5D art. *Bas-relief*, from the French meaning “lower”, and sunken reliefs are those where the drawing or pictorial image has been cut into a brick, stone, wood or metal surface.

In the main, raised relief is where the surrounding material has been cut away to lower the original surface and leave the subject matter to stand proud. All the aforementioned techniques are several thousand years old, with examples of *bas-relief* being found from around the world (Figures. 1.21 & 1.22), in all of the early civilisations such as Chinese, Egyptian, Persian, Greek and Indian, as well as from the Mayan period in South America.



Figure 1.21: Roman pot shard – *Bas-relief*.

Today these forms of relief can be found on coins, both ancient and modern, jewellery such as brooches and rings, and on the walls of buildings as *bas* or *high-reliefs*, where the art work can be protruding almost 100% from the surface.

Several modern techniques exist to copy or improve on the originals, where the different types of relief have been created using different starting criteria; examples cited here include restoration of brick and stone relief, an art form as practised by the Han Dynasty, (c206 BCE-220 AD). They recorded their

individual personal achievement, local events or national military campaigns and victories [48].

In 2011, Wang *et al.* [57] proposed a method using 3D models as input data to generate sunken reliefs, in which the incised lines form the contours below the surface, whilst the heightened forms are on the surface level. By overlaying the feature lines, further refinement was achieved, enhancing the final visual impact on the viewer. The final digital 3D generated mesh was then used, via appropriate software, for machining real geospatial parts either using AM or computer numerical control (CNC) technologies.

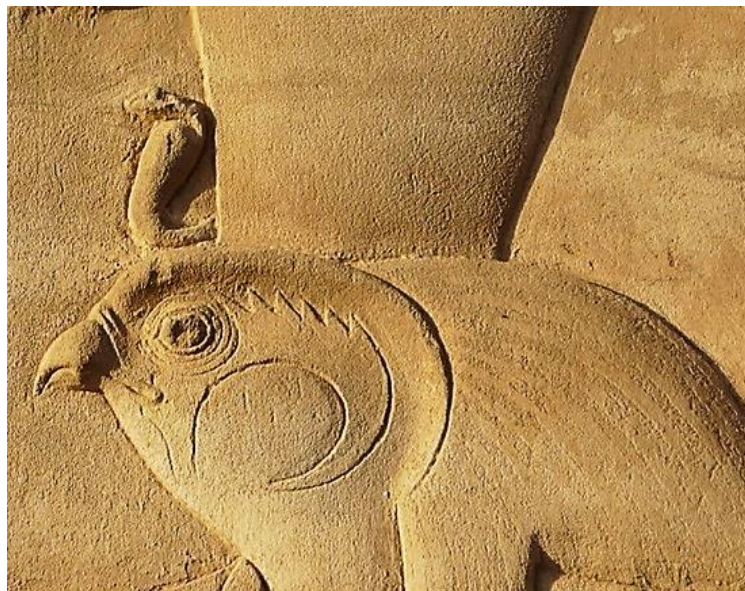


Figure 1.22: Egyptian Horus raised-relief.

In a similar vein, in 2013, Yu-Wei Zhang *et al.* [58] looked at replication by computer generated 3D mesh of line-based sunken relief, as found largely in the Ancient Egyptian artwork. Their aim was to find a way of combining the contour incised lines, which form the first outline sculpture, with the remaining sunken, variable depth features, leading to changing shadow and thickness under strong lighting conditions, in which replication had been problematic.

A further interesting computer based method of reconstruction of *bas-relief* carving, is a system for semi-automatic creation of bas-relief sculpture as described by Weyrich *et al.*, in 2007.

*"the unique challenge of squeezing (3D) shapes into a nearly-flat surface while maintaining as much as possible the perception of the full 3D*

scene. Our solution to this problem adapts methods from the tone-mapping literature, which addresses the similar problem of squeezing a high dynamic range image into the (low) dynamic range available on typical display devices..... Given a 3D model, camera, and a few parameters describing the relative attenuation of different frequencies in the shape, our system creates a relief that gives the illusion of the 3D shape from a given vantage point while conforming to a greatly compressed height” [59].

Their problem was to maintain the centuries old artistic principles of *bas-relief* starting with a geospatial model, a camera view of the model and a selection of controls such as output height (relief height) and overall breadth and width, taking into account the amount of detail to use or reject and the final material to be used in presenting a semi-automatic computerised solution.

Working with more conventional oil paint based art works, where the paint on canvas forms a raised relief, Peng *et al.* [60], in 2015 were experimenting with UV Ink-Jet technology, whilst gaining some success they felt that many problems were still to be overcome before high value art work would be replicated by the use of 3D fabrication technology.

### 1.20.2 Image-Based Displacement



Figure 1.23: Full rendered computer relief.

Finally, the focus of this thesis is on image based displacement (IBD), which is seen as a relatively new original digital method, combining both bas and raised relief, whereby a 2D painting, drawing or relief (see Figure 1.22) is photographed by a digital camera and the data is transformed into an AM replicated object, the image being imprinted to appear both below and above the surface.

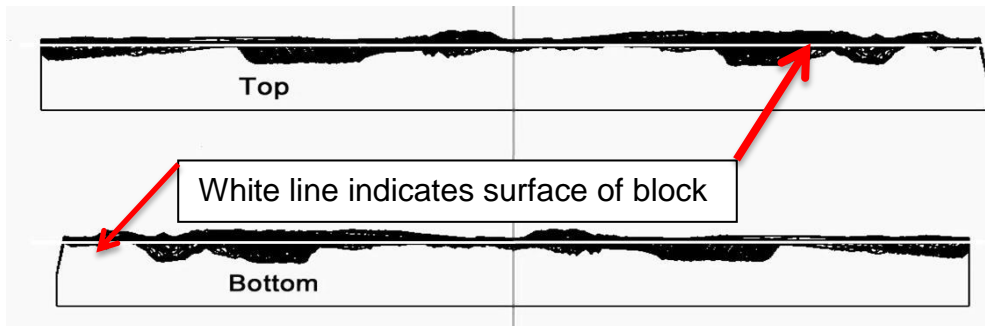


Figure 1.24: Top and bottom of block showing surface displacement according to grey scale colour intensity.

By converting the coloured image into a “grey scale” image (Figure 1.23), the points of the mesh created, move relatively to the grey colour intensity of the digital image, which displaces the surface geometrically (Figure 1.24). A coloured textured mapping system can be applied to the whole surface so that a digital computer file is produced which can be 3D AM fabricated as a raised or bas surface with the original colour picture printed on top of the relief (Figure 1.24).

## 1.21 Historical Summary

This section intended to outline and shows how, over the millennia, scientific knowledge has increased since the prehistoric cave paintings of early man and, together with the development of his tools, has contributed to the development, expansion and experience of the human mind. The desire to create, understand and problem solve, through reason and intuition, has led us to resolve many questions that have been asked over the centuries. And yet the solutions to many past problems have in fact created new ones for us to ponder over. One might argue that replication/recreation of artifacts or *objets d'art* by modern technology such as AM is no further advanced than when hammer and chisel were employed to produce the very objects we aim to replicate. But it is perhaps the by-products of such technologies that can recreate bone or teeth for implants, or make the availability of relief pictures for the visually impaired more accessible to a wider

population. Long slow processes were involved in reaching the digital age of photography and the technology used in this research is part of this process, aiming to show that with simplification and affordability, the early philosophers, mathematicians and engineers will have been well rewarded.

## Chapter 2: Literature Review and Research Objectives

### 2.1 Introduction to Photogrammetry

3D imaging has been in existence since the invention of Lenticular's Stereoscope in 1860. Thus, the idea of a 2D image being converted to a 3D image is not new. In 1934 when Photogrammetry was being defined, roll film was the media that was being used in cameras; this continued up till the late 1950's when cassette or cartridge format film, superseded roll films, in the small format popular *snapshot* cameras of the time; but the professional photographers continued to use roll film in expensive *Rolleiflex* and *Hasselblad* cameras. By the 1960's Single Lens Reflex (SLR) cameras (a development of the camera obscura), although expensive, were being bought by the serious amateur photographers, and these still used roll film. The big change in the recording method was to come in the later 1970s with the event of the laser and digital imaging systems. So the definition of photogrammetry still holds true as it was the "*processes of recording, measuring and interpreting photographic images*" [28]. It is the process, the capture of data and its use, which was of prime importance, not the system of recording the images (by DSLR camera, 3D scanning, magnetic resonance imaging (MRI), computed tomography (CT)) by which it was achieved. Hence, there are many systems which now come under the overall umbrella of photogrammetry.

Whilst not directly linked with the main theme of this research, the Medical section (Chapter 2.3) of the literature review grew from the interest developed in the research and work with the Egyptian artifacts in conjunction with The Kendal Museum, Cumbria. UK., and the research that followed in finding a suitable crown for Horus, the mythical God of Ancient Egypt. The reading of Steele *et al.*'s [61] unveiling of an Egyptian mummy and the recreation of its' skull, led by progression to the research work being undertaken by non-invasive methods on a variety of objects from antiquity, Egyptian mummies included, by others in the field. From as early as 1997, when the fragile Degas figurine was scanned and recreated [62], the beginning of the potential of the combination of these technologies was first seen. The use of MRI and CT scanners was not intended to be involved in any photogrammetry research for this dissertation, but these uses were being developed at the same time in the medical field for Orthopaedic

reconstruction; all this background information proved useful knowledge in what was being slowly achieved in the scientific world, including how the use of these technologies together with AM or RP (originally called Rapid Prototyping), was advancing and the software that was being developed alongside these advances, so that digital photographic data could be processed as well as scanned data, to produce virtual 3D images.

## **2.2 Overview**

There are many methods of employing photography and 3D scanning to capture data under the general heading of photogrammetry, as there are uses. The differing technologies of data capture can be split into several categories: data capture, by 3D scanners only, a combination of 3D scanners and DSLR cameras and modern 3D stereoscopic digital cameras such as seen in Figure 1.10. Under the heading of laser scanning there are machines which now included MRI, CT, data capture by Close Range Photogrammetry (CRP), UAV and by single or multiple DSLR cameras. Laser Triangulation, White Light Scanning, Structured Light, Contact, and Time of Flight are also covered under the generic term of 3D scanning.

Since the late 1990's, 3D scanning has moved to the predominant non-invasive method used to replicate both large and small 3D objects, such as large historic buildings and small statues. The practice of using scanners in the fields of Archaeology, Medicine, Terrestrial and Aerial Field surveying is well established, but sometime later saw the beginning of combining photo digital capture with laser scanners, which has more relevance to this research.

## **2.3 Medical**

Significant results in the use of scanners were obtained in 2003, when the Rapid Design and Manufacture Centre in Strathclyde University, Glasgow, (in collaboration with the Royal Museum of Edinburgh and the University of Edinburgh) undertook to reproduce a 3500-year-old Egyptian mummy. With the use of an MRI scanner they were able to produce 3D virtual images of the artifact without removing the age-old bandages which were preserving it [61]. As part of the Glasgow centred research, with a software package called *Shapesnatch*®, a photo projector (substituted for the LS) and digital camera were used to capture a

series of fine line photographic images projected onto a Greek Comedy mask. 6.2 megapixel resolutions were used to ensure the data capture produced good results. In both instances an AM duplicated model of both the head and the mask were produced.

With the “*The development of a collaborative medical modelling service*” together with CT and MRI scanning, with what was then called rapid prototyping (RP), full scale models of human parts such as skulls were fabricated. These parts could be drilled, cut and reconstruction plans could be designed to aid complex surgery units (these units consisting of CAD engineers, AM technicians as well as medical staff) assisting the front line clinicians, Sugar *et al.* [63].

By 2008, Stockmans *et al.* [64] shows that orthopaedic surgeons were combining the techniques of LS and AM, building patient-specific surgical guides for patients with deformed bone structures. When presented with a case of a deformed radius, the radius being the shorter of the two arm bones, in a boy’s arm, a replica of the arm’s deformed bone was made, allowing the surgeons to examine and pre-plan their operation well before the patient was anywhere near the operating table. The pre-surgery combination of CT/MRI scanning and CAD/CAM plus AM technology, has been used by surgeons to prepare the surgical drilling guide used in the operation. In the X-ray image shown in Figure 2.1, the deformed bone can be seen, with the complete set of plates and drilling guides to aid and secure the reconstruction of the repaired deformed arm shown in Figure 2.2 [64].



Figure 2.1: X-ray showing deformed arm bone.

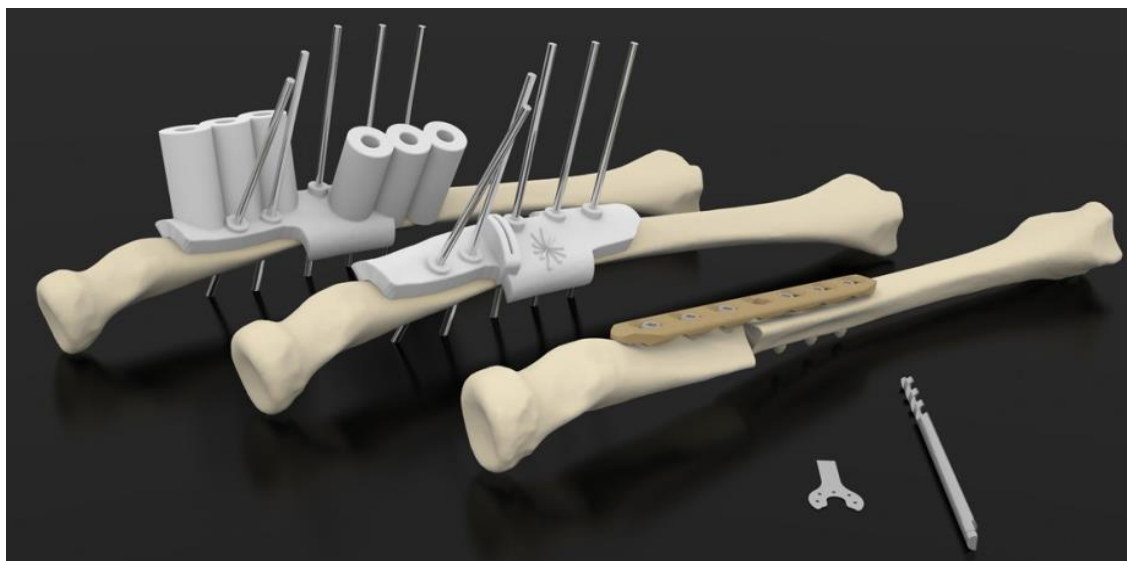


Figure 2.2: Drilling guide for fixing plate attached to model of bone<sup>1</sup>.

Only a couple of years later, surgical clinicians had become so competent in the techniques of CT scanning and computer assisted surgical planning as to lead discussion papers on the pros and cons of computer-assisted versus non-computer-assisted preoperative planning, as in the work of Leong *et al.* [65].

By 2014, more than 60 studies had been undertaken in orthopaedic surgery, of which 14 had focused on the manufacturing of AM osteotomy guides using stereo-lithography (SL) or selective laser sintering (SLS) processes. The materials used in the processing could be sterilised to the required hygienic level, both cutting guides and replicated bones being patient-specific. Popescu *et al.* [66], felt the need to create a platform (POIGO) which would bridge the communication gap between orthopaedic surgeons and additive manufacturing engineers. Both groups had their own very specific complex professional language. The design and manufacturing of all components with patient-specific guides (PSG) required collaboration between surgeons and engineers. This often resulted in the misunderstanding of requirements either from the medical or the engineering viewpoints. This acronym is from the original Romanian:

*“Platforma online inteligenta colaborativa pentru proiectarea si fabricarea ghidajelor personalizate in chirurgia ortopedica”.*

This translated to “intelligent online platform which can support guides designed for manufacturing process” [67].

---

<sup>1</sup> Patient-specific drills@ Materialise 2015. Courtesy of Filip Stockman Torstein Husby. All rights reserved

POIGO (Figure 2.3), a system with protocols and knowledge support for both surgeons and engineers, now ensures that the correct questions are asked at the correct time, that a surgeon follows the correct procedure when requesting a PSG and that the engineer and designer of the surgical guides understands the implication of, for instance, where a screw or drill hole might or might not go into a bone. This workflow procedure ensured the maximum efficiency, from all members of a very complex team, working at the cutting edge of their field for the ultimate benefit of the patient.

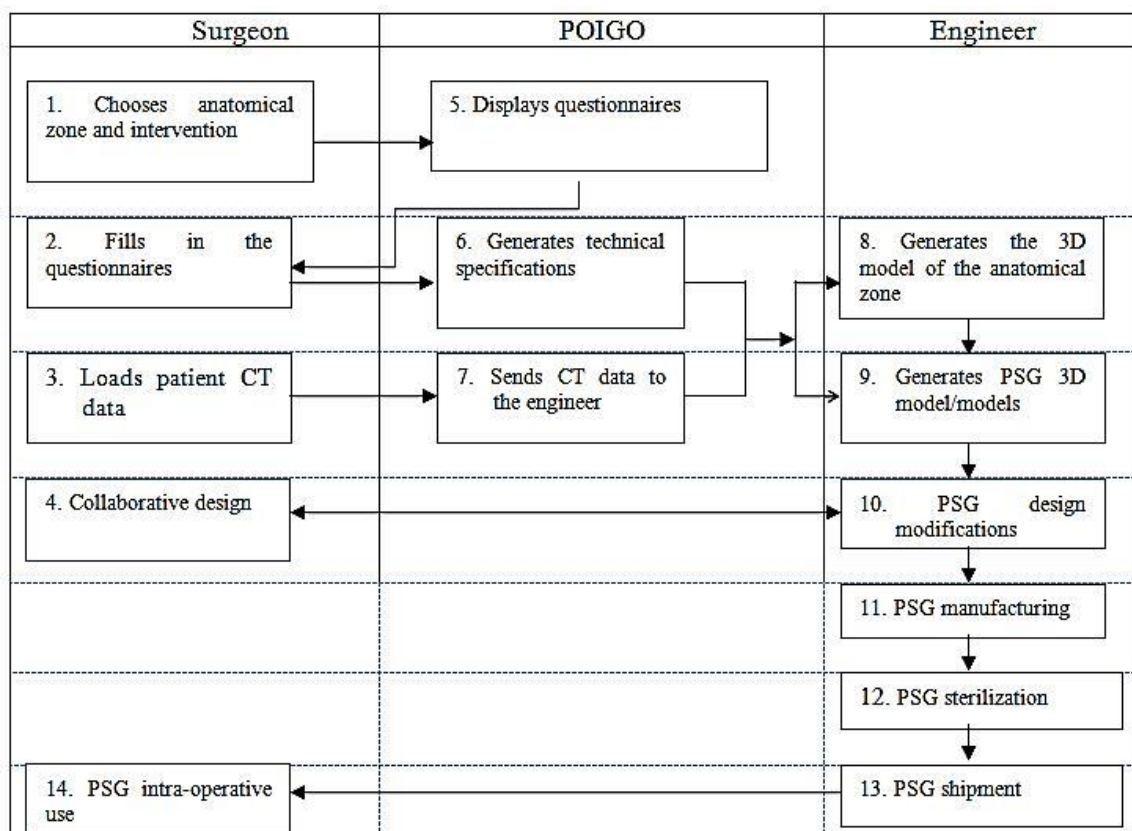


Figure 2.3: Bridging the gap between Surgeon and Engineer [66].

## 2.4 Archaeology

Using a similar combination of LS and DLSR, at the medieval church of Pozzoveggiani near Padova, Italy, and with the use of several software programs, a self-access web information portal was created in 2010 [68]. On analysis of the final access and viewing results, it was found that of those interviewed, only those with a “*greater computer knowledge and understanding of computer software*”, were able to gain full benefit and access to the portal. But it

was a step towards a full interactive multi-media system with the potential of bringing complex virtual exploration of artifacts and archaeological sites to the interactive computer screen.

As the processing power of computers increased and became widely available, at affordable prices, and from the early *Photoshop Elements*®, which could digitally combine several 2D photographs into one, software programs have improved so it is now possible to digitally combine multi view photographs, taken from 360°, into 3D virtual representational images. This has now led to the possibility of 3D images being created without LS intervention.

One such photogrammetry-based survey technology, aDoFting *ZScan Survey System*® (Menci Software, Arezzo), a development of the stereoscope, was used in 3D digital capture of medieval capitals on a church in Aosta, Italy. This was used for the purpose of building models to assist in future conservation of artifacts, and the building of a spatial Information System for tourist information. The moveable camera, mounted on a horizontal bar, took three digital images of each position from a different angle. The overall field of vision of each position was overlapped by about 30%. As a result of the complex detail of the capitals, from each prime camera position in the horizontal, digital capture in a higher and lower position in the vertical was also taken, but with the maximum rotation angle of 15° so as to minimise any photographic distortion. In all, 72 high resolution pictures, each 10.2 megapixel, were taken of each capital. Secondary software was used to process and clean the virtual point cloud images, which then allowed different types of model visualization rendering to be created, to assist in further research [69].

More recently, in 2011, Verhoeven [70] using stereoscopic photography and processing the digital images with *PhotoScan Pro*®, produced a series of virtual 3D images. By virtue of the many output formats this software can produce, including PDFs, file/image sharing is made easy. It was noted that although *PhotoScan Pro*® claim to be able to process, in theory, a very large number of photographs, in practical terms there is a maximum of approximately 1024 images. Verhoeven records that the relationship between the processing time, speed, quantity and high resolution data, are all interlinked. The more detailed the photogrammetric data, the greater the speed of processor needed with a computation time penalty.

Waite *et al.* [71] commenting on a research paper presented at the 2014 Computation and Journalism Symposium, elaborated in an article written for the American Journalism Review [72] on their use of *PhotoScan Pro*®. His colleague and co-writer, Kreimer, pre-programmed a flightpath for a drone and flew two missions over the archaeological site of Antiochia ad Cragum in Southern Turkey. Using a Canon *Powershot SX260*® on the drone, 2,800 aerial images were taken after flying over the whole site, the whole operation taking about an hour. However, he reported that the processing of two sets of images, one with 249 and the other with 949 images, took eight hours and 30 hours respectively. But he admits to only having 8GB of RAM, whereas AgiSoft in their manual suggest for that quantity of photographs 15 to 45GB of RAM [55] is required, plus an i7 central processing unit (CPU).

As with any new technologies that emerge, standardisation or benchmarking is required, and to this end an investigation into the use of photographic digital image capture, and benchmarking of datasets was recently attempted [73]. Nguyen *et al.* evaluated and compared four current software processing programs, testing some 40 objects to evaluate the systems and finally choosing one object which was then subjected to four separate datasets. Each dataset had a constant resolution of 1600 x 1200 pixels and a varying number of input images, from 30 to 7. In another test a constant number of 30 images were used, but the resolution was progressively downgraded from 1600x1200 to 200x150 pixels.

Basantia *et al.* [74] investigated the different techniques and characteristics of both photogrammetry and LS, but the advantage of photogrammetry is that expensive LS equipment is not used and experienced technicians are no longer required to operate this equipment, since by using a relatively modest DSLR camera, 3D virtual images are obtainable.

## 2.5 Museums

There has been a trend of hands on exhibits in museums over the last few years, in order that all members of the public might more readily engage with the collections normally housed behind glass cabinets. To fulfill this need, institutions such as Kendal Museum, Cumbria [75], are interested in exploring potential

opportunities from emerging technologies so as to replicate artifacts within their collection, in line with their mission statement:

*“To safeguard and enhance all of the collections for the benefit of all Museum users, improve the visitor experience, to increase learning opportunities and ensure that the Museum has a sustainable future”.*

The Kendal Museum collection was established in 1796, as a ‘Cabinet of Curiosities’. While the museum’s value is in its collection of original objects, replicas of specific objects have their place. Due to the delicate nature of most objects, they are unable to be handled by the public. Replicas are very useful for handling sessions, especially for school sessions and loan boxes.

Being able to replicate actual museum collection objects would be of great benefit to teaching in local schools about the Egyptians and the material held in the collection. In product design, Caulton [76] found that replicas or prototypes give the handler a chance to experience the size, texture and weight of objects. Feedback from participants in such pre-tooling and pre-manufacturing sessions, often result in minor changes to the original design of a product, saving companies large amounts of money by modifying designs before being sent to the markets.

Zheng *et al.* [77] set out the challenge quite clearly in the title of their 2016 paper “*3D Printout Models vs. 3D rendered Images: Which is Better for Preoperative planning?*”. The teams participating in the study suggested that both methods greatly improved post-operative knowledge on planning, but on answering a pre-set “Quality of the Surgical Plan Questionnaire”, those who were given the 3D fabricated models (as opposed to 3D rendered images) showed a higher score in the quality of the surgical plan.

Conversely it is obviously not possible to be physically present at all the sites around the world to see or examine museum collections or visit ancient monuments. Many museums are presenting on their web sites, 2D graphics of the artifacts in their possession. Those museums with the resources and expertise are able to create 3D virtual images on their web pages which are accessible to all. To this end Georgiev [78] presented a set of ‘Tools’ for exhibiting or displaying 3D graphics in web pages using the HTML5 standard.

This allowed complex 3D images to be added into the web browser using an Application Programming Interface called WebGL [79]. Several applications were presented which allowed users with limited software development skills to upload complex graphics onto their websites so as to be viewed by the wider public. As Georgiev points out, this can be used by e-Commerce and e-Learning sites and once the software tools have been embedded into the author/developer's existing web site, the complex 3D graphics become available on all devices and web browsers.

## 2.6 Cultural Heritage

In 2003, Gee [80] argued that good computer and video games enhanced the learning experience in young children, that "*games allowed players to be producers and not just consumers*". He observed children playing mythological and superhero video games, then looking to supplement their own knowledge by investigating books from the library or surfing the web at home, thereby learning outside the environment of the school.

The concept of teaching cultural heritage via the use of the computer and the internet is nothing new and *Data Games* explores the possibilities in great detail [81]. Games such as *MuseumVille* [82], use the databases of European museums, libraries and galleries and create a learning game whereby the player can create a collection or build a gallery, catalogue and hunt for lost treasures. Millions of artifacts, books, drawings and paintings can be accessed through *Europeana* [83], by means of which a virtual trip though Europe's institutions can be had by all, without moving from the classroom or home computer - this vast amount of digital data can be accessed at the touch of a few keys. Long *et al.* [84] surveyed the way in which the digital age, over the last 10 years, has transformed the way Art historian scholars, librarians and teaching methods have changed, and has transformed access to collections and resources across the world, without the original objects themselves losing their prime importance.

Bontchev [85], in 2015 classified 14 types of modern entertainment video games, the most popular being the "*Action packed and Shootem up*" type, and a whole raft of others, but whilst the analysis and comment is not within this dissertation, it must be noted that many contain what might be termed an "*educational or cultural*" element. However, there is a classification which has

been termed “*Serious Games*” and contains among other things, documentary games which might depict past battles, or historic events, and although these were developed for “*fun*” they are used for educational purposes due to their accuracy and realism. As Bontchev observes:

*“Contemporary methods of preserving cultural heritage rely highly on digitization and archiving as foundations for developing various virtual heritage applications. During the last two decades, video games proved to be an interactive visual media able to incorporate virtual heritage in amazing and highly appealing ways. At the same time, each video game represents a valuable artifact reflecting technological, socioeconomic and historical issues of its creation. Therefore, video games are an essential and integrated part of modern cultural heritage and themselves need preservation efforts.”*

The gaming technology, for example, is now used for virtual museum visits or a virtual visit to an ancient Egyptian Temple, now with a 3D option. With the widening availability of 3D software that can convert artifacts from 2D images into 3D virtual objects and can then be included into a video scene, plus the use of Flash or Adobe Shockwave to ‘fly’ or ‘walk’ though a recreated (or scanned) ancient monument set, even more realism can be added to the final 3D rendered video game.

Digitisation of artifacts is now allowing us to resurrect and supplement large quantities of documentation which has been amassed by historians and archivists over centuries of knowledge gathering. As suggested by Schuhr and Lee [86], classical fine line drawings (as well as rough archaeological sketches) of historic buildings, scenic views, and relief works etc., have already been supplemented by 2D photographs and Victorian 3D anaglyphs since the late 1860’s (Lenticular 3D images - see Figures 1.6 and 1.7), as well as the more modern version of 3D images as seen through coloured lensed glasses. With the choice now of buying a TV with “*Avatar*” type 3D stereoscopic capability, there is nothing to stop all of our cultural heritage monuments and artifacts from being digitally preserved and made widely available to the public.

Add a few more technologies such as reverse engineering (RE), photogrammetry and AM, and with the modest equipment discussed, digital files can be created, uploaded and downloaded, to be fabricated using one of a number of AM (or 3D printing) technologies, enhancing the experience of cultural heritage investigation and research, either in the home or classroom [87]. These geometric models, if printed in the basic white Nylon 12 (polyamide) or white Acrylonitrile Butadiene Styrene (ABS), depending on which machine is used, can be painted by hand, for further enhanced realism.

*“Making unauthorized copies of physical objects protected by copyright is copyright infringement, whether those copies are made with a 3D printer or a whittling knife”* [88].

This of course opens up the greatest minefield of the digital age, in managing the intellectual copyright of institutions who own the artifacts. But as digital technology changes now at an ever faster pace, leaving old technology obsolete, within twenty years software and its compatible hardware will no longer be able to be accessed by the majority of the population. There cannot be many households still owning a workable *Sinclair ZX Spectrum*<sup>®</sup> [89] or *Vic20*<sup>®</sup> [90] and the tapes that held the data. Yet many would argue that the games played on them form part of our early childhood computer heritage and should be preserved. However, as Mailer [91] points out, the problems encountered by those who try and preserve such digitised data not only include the technical problems of reconstruction of these programs by building emulators. But in doing so the copyright of those who hold the licences is infringed by the very nature of having to *hack* into the original course code to save the data. Trying to obtain permissions from licences whose companies have long since disappeared or have been swallowed up several times in corporate buyouts is, as Mailer points out, virtually impossible. Those who strive to save this type of digital heritage referred to as ‘orphaned’<sup>2</sup> or abandonware<sup>3</sup>, need to be protected from complex legal challenges from those who no longer market, distribute or sell these old

---

<sup>2</sup> Orphan works are works still protected by copyright whose owner is unidentifiable or untraceable.

<sup>3</sup> Abandonware means software (such as old video games), which is no longer commercially distributed/sold and for which product support is no longer available. It is thus “abandoned” by its manufacturer. Many games that are abandonware are also orphan works.

video and computer games, and within the EU copyright reforms provision must be made for such activities.

As seen from the last two sections of this chapter (2.5 and 2.6), the biggest challenge for museums, which traditionally viewed their role as guardians of our heritage and of the copyright of the artifacts and Intellectual Property (IP) that they held, is that they were prohibited from the reproduction of items of third party interest, to the detriment of being able to replicate artifacts which could be used for scientific research or educational purposes. Pantalony's [87] guide of 2013 goes some way to help those in charge of museums with this very confusing problem and legislation, in normal peacetime circumstances. These issues not only affect local museums around the world, but even more so in the larger internationally renowned museums and art galleries at a time when there is much destruction and looting from war zone areas of artifacts thousands of years old representing irreplaceable cultural heritage [92], which had been stored and preserved in museums, and which have now been destroyed. IP and copyright might be a fine ideology to uphold, but digital replication and archiving perhaps would have been the saviour of such doomed relics, as the digital files themselves could have been moved from one place to another, and although it might not have been possible to save the original artifact, at least copies could have been replicated, using the technology of photogrammetry, 3D scanning and AM fabrication techniques.

By utilising and combining some of the aforementioned techniques, it should be possible to reconstruct some of the lost monuments with the help of Crowd Sourcing. Access to most World Heritage sites, and many lesser sites, is now made possible by the huge growth of international tourism, but a visit to a monument site may be impossible whilst the destruction is occurring, which may be by the hand of nature or of man, and when it is gone it cannot be replaced. Stathopoulou *et al.* [93] when trying to reconstruct a 150 year old historic stone bridge, which had collapsed and partially been swept away by a very heavy rain storm, turned to the public via the web for help. Designing a crowdsourcing platform, they were able to collect 2D data images of the bridge. These images not only formed the basis for a virtual 3D image reconstruction, but helped its architects and builders ensure that the small details of the bridge construction were not lost.

## 2.7 Aerial Surveillance

The use of UAV's increases due to the lower price points, ease of acquisition from retail outlets, reduces weight of digital cameras as well as the improved resolution of the digital images. Photogrammetry is the ideal technology to utilise for UAV surveillance of large areas of land [94], whether to study crop growth [95], tree top crowns [96], alien plant species [97] or archaeological sites [98], to name but a few. The techniques for this type of digital image collection are developing and the camera formats and UAVs are still under review [99]. The small *GoPro®* cameras as fitted, typically, to cycle helmets and retailing under £100 seem to be the camera of choice for these drones. Although written in 2005, for those starting with UAV surveillance Neumann's short paper is a good introduction to those who wish to.....

*“..... purchase a new camera system or to contract aerial image acquisition, it is important to recall some of the main camera parameters and to understand the differences between the old traditional analogue cameras and the new state of the art digital cameras” [100].*

In January 2015, the *BBC News*<sup>4</sup> carried a feature titled “Game of drones: As prices plummet drones are taking off”, quoting that a *DJI Phantom Drone* had been purchased with an *iPhone* compatible *GoPro®* camera fitted to the drone, for £750. The rig was being used and flown by a local estate agent, to fly over local properties he hoped to sell. Six months later, two reports appeared in the media, one in early June about the confiscation of a drone and the possible prosecution of the drones' owner because he flew it over the Wimbledon Tennis Courts<sup>5</sup>. The second report was in *the Times*; the story was of a drone having flown within 50 feet, of an *Airbus A320* at 1,700ft, as the plane was descending in preparation to land at Heathrow Airport. This was the second such incident reported within the year<sup>6</sup>.

---

<sup>4</sup> 16<sup>th</sup> January 2015. BBC Business News

<sup>5</sup> 29<sup>th</sup> June 2015. London Evening Standard

<sup>6</sup> 30<sup>th</sup> June 2015. The Times Newspapers Ltd.,

The police have given out warnings that the flying of drones in most instances is illegal and both confiscation and prosecution can be expected by the controller/owner, if caught. So although the use of drones in conjunction with photogrammetry has proved very useful in the capture of digital images of many scientific, cultural and archaeological projects, it seems highly probable that without police and/or Civil Aviation authority and an appropriate pilot's licence, the use of drones, as a tool for aerial photogrammetry, has a limited lifespan, for all but the professional flyers.

But for those who are determined to fly and can practise this new art of aviation, far from the madding crowds, Ashmore, in his paper, "Drones in Archaeology:..." [101], works through the four main techniques, which must apply to all aerial surveying work, not just archaeology. He briefly looked at: camera or video use; 3D Mapping; Thermal Imaging; and LINDAR, the use of laser-based remote sensing. Finally, he looked in more detail at the best ways for its use above archaeological sites. With the use of a *DJI Phantom 2* quad copter [102] and a software program called *Ground Station*, the operator was able to control the drone using an iPad or iPhone. Having control of the drone, there was further software, *Vision* [103], which controlled the camera functions and included a safety function which would return the Drone to its original take-off site if WiFi contact was lost with the ground controller. His conclusion was that if one operated and flew with care, drones are a great asset for non-invasive site recording, especially of inaccessible sites, and with the right camera rig, for data collection for 3D visualisation modelling.

## **2.8 Archiving and storage of Data**

In this research, it is shown that with the use of photogrammetry, virtual 3D models can be created, without a high level of computer expertise and without the use of relatively expensive or complicated 3D LS equipment. High resolution point cloud image data files are created, and are then converted by additional software programs to the files needed for AM machines to replicate the photographed item and produce geometric representational models. The use of this technique could contribute to the reproduction, restoration or repair of damaged or broken antiquities by non-invasive methods at modest cost and by

lay persons, who are computer literate but not necessarily expert in the use of specialised software or complex laser based scanning technologies.

The amount of data that needs to be stored when undertaking projects as described, can be considerable. There are the images of the original artifacts, the sets of photographic data that has been acquired to the many different stages of possessed file format that accumulate. All needed to be organised and stored for future research or archiving. In a 2015 presentation in Los Angeles [104], Bennett, a Digital Production Librarian and Archivist, sets out a clear and logical method in how to handle such data, at the same time giving a useful overview of the many types of file format and the computer software that read these different formats. Having asked the question "*How do you organise all of this data*", the final part of his presentation goes some way to answer the questions posed.

## **2.9      Heritage Lost and Gained**

### **2.9.1      The Crosby Garrett Helmet**

The Crosby Garrett Helmet is an example where Photogrammetry and AM technology could have combined and would have played an important part in preserving part of the historic local heritage, in this example in Cumbria. It could very well apply to any community anywhere in the World, it was in the replication, even if not full size, of objects that have been found in the local area by residents of the local community. Due to the unique, historical and in many cases monetary value of the objects, the local museum or gallery may not necessarily be able to afford to compete with the World price paid at such an institution as Christie's when the objects are placed under the auction hammer. Alternatively the object may be deemed too important a find to be housed in the local museum and is moved to a major City museum such as the Victoria & Albert or the British Museum in London. In the worst case scenario, the item, having been sold on the World Market, moves out of the country altogether, depriving not only the local people of their historical cultural heritage but also the Nation.

Such was the case with the Roman Helmet and face mask found in the North West of England, so rare that only two other such helmets have been discovered in the UK. It was found in a field by a treasure hunter with a metal

detector and became known as '*The Crosby Garrett Helmet*' (Figures 2.4 and Figure 2.5) [105].



Figure 2.4: Bronze Copper helmet and mask [106].

Named after the village near where it was found, it was discovered in May 2010 in pastureland in the small hamlet near Kirkby Stephen, Cumbria, UK. Before it went to auction, a full study and conservation was conducted so at least some form of provenance was established as to its historical and cultural importance [107].

Although well over £1 million was raised through private, public and National Heritage donations, it was sold at a London auction and fetched £2.2 million from an anonymous private phone bidder. After much protest from the public, the anonymous buyer allowed the helmet/mask to be displayed at the Royal Academy exhibition '*Bronze*'<sup>7</sup> – a prestigious international exhibition, before moving for a few months to Carlisle's Tullie House Museum, Cumbria.

---

<sup>7</sup> In the Main Galleries, Burlington House - 15 September - 9 December 2012



Figure 2.5: Children look eyeball to eyeball with their cultural history [106].

Finally moving to the British Museum for a further period of display, and it may well have now been taken in to a private collection or out of the country by its owner, forever.



Figure 2.6: Pre cleaned Helmet.

However, the technology was available, and still is, for an attempt to be made for a good geometric replica of the original Roman Helmet, part of our

cultural heritage, to be fabricated, although not as good as having the original but better than simply a 2D digital image.

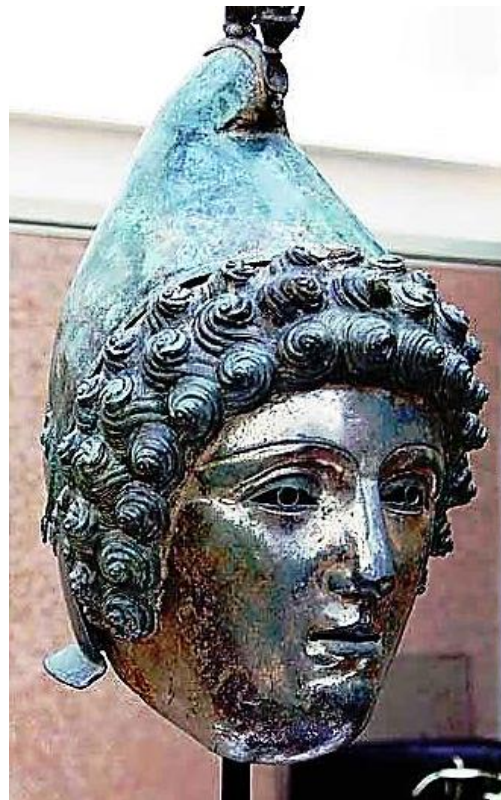


Figure 2.7: Helmet after cleaning – as displayed at Christie’s 2010.

The helmet, when found and being made of copper alloy [108], would have had a covering of a dull platina or oxidation from having been in the ground for many centuries (Figure 2.6).

This would have been the ideal time to use the photogrammetric techniques as described in this thesis. The helmet, which now, if it were photographed or 3D scanned, having been cleaned, would present problems from the light reflection or scatter off the cleaned metal surface, as per the cleaned reflective face when it was displayed at Christie’s for the auction (Figure 2.7). As discussed in Chapter 6, if there were any glare, flair or reflective light, then this would cause distortion to the processed photographed digital image. This glare can cause “spikes” to appear on the artifact, as in Geoffrey Mann’s Victorian Candelabra “Shine” [109]. The camera or laser beam cannot distinguish what is surface and what is reflection. These and similar problems are common and have been discussed by the author previously [110].

## 2.9.2 Tlingit Community of southeast Alaska, USA

On a larger scale, replication of tribal artifacts for educational purposes using a Konica *Vivid 9i* laser scanner and a CT scanner, has taken place in America. The Smithsonian Institute has collaborated with the National Museum of Natural History in New York, USA, to replicate sacred objects, with examples shown in Figures 2.8 and 2.9<sup>8</sup>, from the Tlingit Community of southeast Alaska, USA [111]. After one hundred years of petitioning by the Tlingit people, these sacred and ceremonial artifacts were repatriated to their rightful home with the elders of the community.

Through the use of 3D digital technology, and close co-operation between The Tlingit people and Smithsonian Institution, the near perfect physical replicas were made, so that the reproduced artifacts can still be studied and seen by the wider population for both pleasure and education. These artifacts were and still are religious and sacred items still in use by the Tlingit people. By creating the reproductions with minor imperfections, the reproduction artifacts are no longer considered holy by the community and can be used or stored in a museum.



Figure 2.8: The Kéet S'aaxw hat.

This example, which used a much more complex and expensive method than photogrammetry, could have been attempted using the photogrammetry

---

<sup>8</sup> From the Smithsonian's collection

techniques as described above, (the scanner sells for about \$12K). These examples show the feasibility of preservation, whilst providing security against loss of artifacts and allowing study and educational access to items not normally available to the general public.



Figure 2.9: *Kaagwaantaan* clan Sea Monster Hat.

The two replicated objects discussed above, representing local and national heritage, are good examples of an artifact that could have been reproduced, (the Roman Helmet), and one that has been reversed engineered by photogrammetry and reproduced using AM technology, (the Hats of the Tlingit people).

## 2.10 Research Objectives

### 2.10 Development of Simpler Data Capture and Processing

In 2013 the European Commission funded a project entitled “3D icons” [112] with the aim of digitising between 3000 and 4000 artifacts as high resolution 3D images that could be viewed on personal computers and on the internet. This project brought together 16 institutions from 11 European countries with a time imposed deadline to finish at the beginning of 2015. Several methods of data capture were employed using a selection of different capture and processing software [113-115]. As a result of this project, papers from some of the participating institutions have appeared, but all seem to have stopped short of

producing physical models or replications of the artifacts that were digitised as this was not in the original project brief.

A combination of DSLR cameras and 3D scanners were used by the institutions whom were funded by the EU, unlike many UK institutions like Kendal Museum, where funding for such projects is limited or non-existent. However, a simplified method, as shown in this thesis, could be employed by computer literate museum staff to produce good quality replicated models of the museum artifacts at minimum cost.

## **2.11 Technology for Computer-literate Operatives**

As reported in May 2016, there were 80 software programs claiming to be able to convert 2D digital photographs into 3D images or data models [116]. Several commercial computer software programs are available with a proven and reliable record to “stitch” multi-view photographs together to produce a 3D image. From the mid 1970’s, techniques have evolved to *stitch* images to produce 2D photo-mosaics [117] and by the late 1990’s commercial computer programs such as Adobe’s *Photoshop Elements*<sup>®</sup>, as documented in Redwood’s “*Photoshop Elements History*” [54], were widely available, being able to *stitch* full colour 2D digital captured photographs together, creating panoramic views of city, sea or landscapes [118].

So important was the goal of being able to align and stitch photographic images together that in 2006, Szeliski, compiling a tutorial on *Image Alignment and Stitching*, was able to reference over 200 relevant papers, some dating back to the mid 1970’s [119]. However, within the last few years, software has become available capable of stitching 100 or more high resolution digital images together to form a virtual 3D representation.

It is shown that with the use of photogrammetry, virtual 3D models can be created, without a high level of computer expertise and without the use of relatively expensive or complicated 3D LS equipment. With the use of Autodesk’s *123D Catch*<sup>®</sup> [6] and AgiSoft’s *PhotoScan Pro*<sup>®</sup> [7] as primary processing software, high resolution point cloud image data files are created, and are then converted by additional software programs such as Netfabb’s *StudioPro*<sup>®</sup> [9] to the files needed for additive manufacturing (AM) machines to replicate the photographed item and produce geometric representational models. The use of

this technique could contribute to the reproduction, restoration or repair of damaged or broken antiquities by non-invasive methods at modest cost and by lay persons, who are computer literate but not necessarily expert in the use of specialised software or complex laser-based scanning technologies.

## **2.12 A Cost Effective, Cheaper and Safer System**

Much has been written about the pros and cons of the use of 3D Scanning, and such phrases from James *et al.* as:

*“Acquiring appropriate data commonly requires expensive instrumentation and/or significant expertise”* [120]

are not uncommon in the published papers and journal articles; the quoted author continues :

*“..... camera-based approaches retain advantages over laser scanning for applications requiring detailed data from remote, rapidly changing or spatially limited areas, through their low cost nature and low bulk. Furthermore, unlike laser scanners, cameras can be easily mounted on lightweight unmanned aerial platforms such as kites and model helicopters to obtain near-vertical coverage.”*

Although aerial data collection by UAV has not been a requirement of this research nor explored, one can imagine that the data collector would need some training in flight planning and in how to handle an airborne light craft, but the data processing is virtually the same, as seen from the many papers using this method of aerial data acquisition. Remondino *et al.* covers all of the main requirements as well as a list of typical uses, such as forestry and agriculture, archaeology and cultural heritage and more. As well as examples of field work, a warning is included that regulations in many countries are being reconsidered with regard to the use of UAVs, the technical specifications and areas where they can and cannot be used [121].

The *Guardian* newspaper reported about a “drone” that was flown over Huddersfield by a member of staff at Maplin, who sell such vehicles. It included a reference to the Civil Aviation Authority (CAA) who won a court case against a UAV hobbyist in Barrow-in-Furness [122]. Perhaps the use of UAVs in remote

locations is a very good method of data collection but clearly in many parts of the UK, and other parts of the world, for all intents and purposes it is not an option to pursue without official CAA clearance.

A discussion regarding the costs of LS equipment has been included in Chapter 1.18. It is difficult to predict how prices of the better quality equipment will change or how the entry level LS will improve to close the differential between the top and bottom of the market. But in the main, the data supplied has been backed up by Straub *et al* in their article on small inexpensive scanners, which require manual intervention around stationary subjects, large freestanding (nearly) instantaneous units or very high cost scanners that capture the data within seconds [123].

Finally, there are hazards associated with the use of lasers. This has been thought to be acute enough at Lancaster University to have been brought to the attention of users by Lancaster University's managing technical staff, who have published and widely circulated a warning document: "*Lancaster University laser policy extract – Hazard Classification for Lasers*" [124]. This also comes with a "*Laser Registration Form*" to be completed together with a Risk Assessment to be undertaken and submitted to the University Safety Office.

In this warning is seen another reason for using a camera: a child, young person or person of any age, for that matter, would be far less likely to come to harm with a DSLR camera than with a Laser Scanner.

## **2.13 Systems Utilisation**

### **2.13.1 Local Community projects**

Chapter 2.6 has shown how the internet can be used as a database for building cultural heritage projects; another extension of this idea is that of Photo Tourism, as proposed in a system in which the internet is trawled for all the photographs of one particular location. The example quoted returned over 15,000 photos on a Google search for Notre Dame Cathedral [125]. Snavely *et al.* were able to convert hundreds of these images into 3D point cloud geometric representation and by way of using a state-of-the-art image based modelling system, created *Scene Visualisations*. They were able to "fly" around popular world sites in 3D by morphing between photos, also adding information and details about the

locations visited. Whilst some of the methods used by Snavely may seem very advanced, it is not beyond many local community computer groups or U3A (University of the 3<sup>rd</sup> Age), where a wealth of knowledge already exists, to undertake similar projects but with the use of simpler and cheaper hardware.

### 2.13.2 Educational Institutions

Amongst the many case studies which are documented here, one involved the reproduction of a modern clay vase, whilst two other examples dealt with 3500 year old Egyptian clay artifacts from the Kendal Museum, Cumbria (UK). All three objects were successfully recreated using AM technology, one on a fused deposition modelling (FDM) machine and the other two on a selective laser sintering (SLS) machine. These models were also printed using two AM colour fabricators, the 3D Systems *Projet 660*<sup>®</sup> [126] and the Mcor *IRIS*<sup>®</sup> machines. Although ownership of such colour fabricating machines is not within the budgets of most educational institutions, except perhaps universities, replication models could be made using such technology, by commissioning from third party bureaux, many operating over the internet.



Figure 2.10: Entry Level Desktop AM machine - *UP!3DPP*<sup>®</sup> [127].

Some of the models have been printed on an entry level FDM machine, a *UP!3DPP*<sup>®</sup> printer (Figure 2.10), or a *RepRap*<sup>®</sup> printer (Figure 2.11), showing that such machines, which are within the budgets of many schools, are more than just

the latest novelty. A recent search on e-Bay produced many second generation clones of the *MakerBot*® (Figure 2.12), at under £1000. At the London *3DPrintShow2014*, several exhibition stands were selling these clones at takeaway and self-assemble prices, as low as £500 (€600).



Figure 2.11: Entry Level Desktop AM machine - *RepRap*® [128].

In this thesis, the whole process is shown, from digital capture of artifacts to their AM replication. This includes entry level printers as shown in the illustrations, (Figures 2.10 to 2.12). By using moderately priced equipment and software, as suggested and used by the author, the methods described could be and are being integrated into school curriculums to teach modern technology at many, if not all, year levels. The advantage of this process is that 3D scanners are not required to capture the data necessary to produce 3D CAD images, and experienced technicians are no longer required to operate this equipment. By using a relatively modest DSLR camera, and understanding the simple principles which are laid out in this thesis, good results are obtainable. A comparison between photogrammetry and 3D scanning, their techniques and characteristics has been shown [74].



Figure 2.12: Entry Level Desktop AM machine - *MakerBot*® [129].

### 2.13.3 Museum and Gallery Staff

Whilst a museum's value is in its collection of original objects, replicas of specific objects have their place. Due to the delicate nature of many objects, they are unable to be handled by the general public. Replicas are very useful for handling sessions, especially for school visits and loan boxes. Loan boxes are often used by rural schools where it is difficult to arrange actual visits to the museum. The school then can hire a box of material for a term and undertake practical activities at their own site using museum resources. Loan boxes and handling collections often consist of un-accessioned objects (not in the main museum collection), or if the museum has large amounts of the same type of original material some can be used. Loan boxes may have original Victorian and Roman material, but in the case of Egyptian collections it is rare to have an original handling collection.

At present, the schools' Egyptian loan box at Kendal Museum, Cumbria, UK, where part of this research was conducted, is made up of general replicas (not items in the collection), and photocopies of documents and photos. Another area which is now in the UK school curriculum is the medieval period, but most items held by the museum are too delicate or fragile to handle, especially by school children.



Figures 2.13: Children handling the Museum replicas.



Figure 2.14: Children handling replicated models of 3,500 year old Egyptian artifacts.

Replicas, even if not exact in all detail, give the handler a chance to experience the size, texture and weight of objects, if the original object cannot be handled. The experience becomes far more tactile than just looking at a 2D black and white or colour photograph. In Figures 2.13 and 2.14 the children are seen handling replicated artifacts from the Egyptian Collection at a Kendal Museum's open day. The original items having been digitised previously by the author, as described in Chapter 3.7. Part of this process was published in 2014 in the specialist publication *Ancient Egypt* (see Appendix C) [130].

#### **2.13.4 Non-invasive Replication of Unique Objects**

Photogrammetry can be used as a non-invasive method of image data capture for AM geometric representation of *objets d'art* and historic cultural artifacts, limited only by the build envelope of the AM machines, but in some cases, if the original model is too big for an AM machine, the CAD models can be sectioned and joined after physical fabrication. An example where this combined technology could have played an important part in preserving the historic local heritage is in the replication, even if not full size, of objects that have been found in the local area by residents of the local community. Due to the unique, historical and in many cases monetary value of the objects, the local museum or gallery may not necessarily be able to afford to compete with high auction prices.

Such was the case with the Roman Helmet and face mask found in the North West of England, so rare that only two other such helmets had been discovered in the UK. It was found in a field by a treasure hunter with a metal detector and became known as '*The Crosby Garrett Helmet*' (Chapter 2.9.1, Figure 2.6).

However, the technology was available, and still is, for an attempt to have been made, for a good geometric replica of the original Roman Helmet, part of our cultural heritage, to be fabricated, not as good as having the original but better than simply a 2D digital image.

Replication of tribal artifacts for educational purposes using a Konica *Vivid 9®* laser scanning and a CT scanner, has taken place in America. The Smithsonian Institute has collaborated with the National Museum of Natural History in New York, USA, to replicate sacred objects (Chapter 2.9.2, Figures 2.8 and 2.9), from the Tlingit Community of southeast Alaska, USA [111].

### **2.14 Product Promotion for Business**

Previous research by the author considered the diverse use of AM technology in industry in a variety of countries by small businesses (SME's) and how these technologies impacted on small companies [110]. The discussion is still very relevant to the many small traditional Craft Design businesses (who are not necessarily using AM technology at present), but also the companies who have encompassed the AM technology within their Design or Research and Development departments.



Figure 2.15: Contemporary  
Designed Bottle [131].



Figure 2.16: Goveshy [132].



Figure 2.17: Morling [133].

With the use of CAD or Photogrammetry, these companies could replicate their designs, on a smaller scale, to include a company logo discreetly embedded onto the surface so as to protect their design and property rights. These small artifacts could then be sent to potential clients as examples of their work for sale. Typically, Figures 2.15 to 2.17, taken from the Craft Councils Collection, are some of the artifacts that have been shown at Craft Councils Fairs over the years and are not dissimilar to some of the items and figurines that the author has replicated in this work (see Figures 2.18 and 2.19).

Many of these companies, both large and small, can be seen flourishing at such events as the *Craft Councils* annual International Art Fair for Contemporary Objects “COLLECT” which ran in 2015 at the Saatchi Gallery, London. This type of Fair, along with the many Trade Shows around the world, are where the exhibited items on display are hand crafted, limited editions or even “one off” creations. The designers are there to “showcase” their wares in the hope that the designs are seen by buyers of large companies, who might want to distribute or mass produce for the commercial markets around the world.



Figure 2.18: Clay Head.



Figure 2.19: Glazed Clay Bottle.

By the use of photogrammetry, as described in this thesis, a simple and relatively inexpensive approach is used to digitise and produce not only virtual images, but near perfect replicated models of the original hand crafted *objets d'art*. These virtual models can be used to create multiple samples of these designs in a much quicker and more economical way than trying to replicate by hand each time a sample is required by a potential client.

## 2.15 Spatial and Tactile Experience by Blind and Visually Impaired

One of the most well-known and respected organisations for the blind and partially sighted, is the Royal National Institute for the Blind (RNIB), who amongst

many other things, for many years have organised Braille reading and text books as well as audio recordings for the many people who are disabled in various degrees due to their loss of sight. In conjunction with and independently of the RNIB, many theatres and art galleries now have events where blind and visually impaired people can hear descriptive accounts of plays being performed or guided tours of sculpture in galleries. The National Gallery in London, for example, has a running program called “Art through Words” [134]. Each session begins with a detailed description of a painting or sculpture, ending with a visit to the gallery.



Figure 2.20: Mona Lisa by Leonardo De Vinci.



Figure 2.21: AM *Bas-relief* of Mona Lisa – shot from above.

Many of the sculptures could be copied in the ways described in this thesis and reproduced using AM techniques. In the case of large pieces, scaled models would not only reduce the cost of production but make access more available. A marble or stone bust weighing several kilos might be reduced in size and replicated as a hollow model, easily transported in a carry case or box.



Figure 2.22: AM *Bas-relief* of Mona Lisa – shot just above horizontal plane.

Although not a detailed part of this research, looking back at the IBD process as described in Chapter 1.20.2, this process can be and has already been used to replicate paintings and drawings so as to replicate 2D images in a 3D format. Figure 2.20, a relief of the Mona Lisa by Leonardo De Vinci, is just one such picture where this technique has been tried and tested. The enigmatic smile has been distorted a little in transforming the image, under harsh side lighting the highs and lows of the picture can be clearly seen in Figure 2.21, and blind and partially sighted people have been able to identify the *bas-relief* picture-gram. Deep shadows are cast by a lamp shining on Figures 2.21 and Figure 2.22 caused by the furrows in the 3D print replicas.

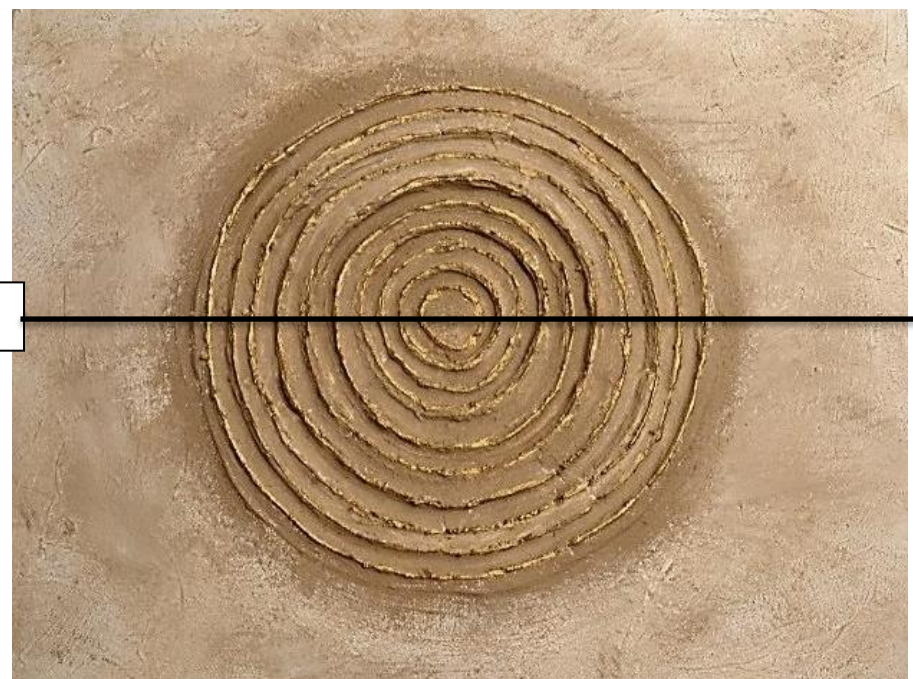


Figure 2.23: Original relief painting showing position of cross section A/A.

In the author's own work, a raised relief painting was successfully replicated as seen in Figure 2.23, and in the cross section of the digitised STL file (Figure 2.24), the raised and indented pattern is clearly visible. It must be noted that the method used to produce the relief painting (see Figure 2.21) was not the same as in the example given for the Mona Lisa [135]. Figure 2.23 was produced using Autodesk 123D Catch®, as will be discussed in Chapter 4.

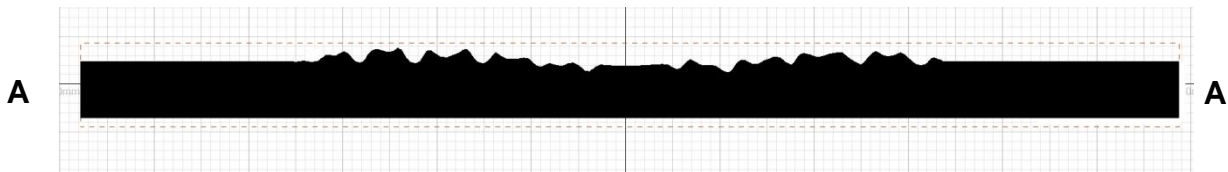


Figure 2.24: Horizontal cross section of STL virtual image.

These techniques were by no means new, (the ancient Egyptians were experts over 4000 years ago using their own technology), but a new application of an existing idea. By the late 1990's, software was available from Delcam's *ArtCAM Insignia®* and *ArtCAM Pro®* [136] (the software was acquired by AutoDesk in 2014 [137]). This software was able to transform 2D images into 2.5/3D relief, using CNC technology, later to be upgraded to support 3D printing.

Stangl *et al.* [138] discussed, in October 2015, the importance of 3D printable accessible tactile pictures (3DP-ATP) when supporting visually impaired children with literacy development, and although many teachers and organisations have shown a great interest in developing these materials the task is far more complex than obtaining a 3D printer and learning fabrication skills. The study suggested a way in which the community of 3DP-ATP designers can benefit from a set of online support tools to meet the challenges of creating for these children. For those needing a more immediate answer to the problem a collection of tactile story books can be downloaded ready for 3D fabrication from the internet [139].

## 2.16 Conclusions

### 2.16.1 Literature Summary and Gaps in Knowledge

In reviewing the literature during this research, an attempt has been made to include information relevant to the research itself. Most of the research being

conducted deals with the different methods of 3D scanning, with or without the use of a digital camera. Others have dealt with the problems associated with computer software or the merits of one piece of software or scanner over another, and analysed the results. Although the use of large multi-camera installations has become increasingly popular in the commercial world of AM replication, very little has been investigated as a combination of photogrammetry, small artifacts, single digital camera/compact and AM fabrication. In a variety of situations, the benefits for the user to have or hold a replicated artifact, rather than 2D photographic images of the object, have also been shown. This research also looked at an example of a potential missed opportunity to preserve local heritage, as well as the potential use of single camera photogrammetry for promotion of business for SME's.

In all scenarios, using non-invasive RE methods, very little attempt, if any, was made by others to follow through the whole process; nor to simplify the methodology and to compare the final AM results with the existing replicated artifacts. The impact of the use of camera lens filters, or whether to shoot in RAW or camera ready Jpeg images, and how third party photographic software could enhance the original photographic data, had not been explored. Nor had the cost implications of processing high and ultra-high quality point cloud digital images on a tight budget. Nor had investigation taken place into why high quality PC images should be processed in the first place when the AM printers that were available to the end user could only output medium to low grade resolution objects (say 100µm or less) unless used only for 3D virtual displays.

In this research, the issues discussed above have been explored and answers provided to these questions, thereby contributing to a gap in the knowledge within the field of photogrammetry and AM fabrication.

## Chapter 3: Tools of the trade - Hardware and Software

### 3.1 Photographic Hardware

This Chapter is broken down into three main sections, describing the equipment used in this research. Most of it was purchased from high street stores or, in the case of the studio lights, second hand via the internet. Two pieces were constructed or “fabricated” from components bought from well-known DIY shops. The first part, a corner joint (see section 3.7.1) formed part of the light tent and proved to be very useful but rather fragile. It was decided to reconstruct the joint in *SolidWorks*<sup>®</sup> and then fabricate it using an AM machine. The other, a multi camera test support frame, was built using *SolidWorks*<sup>®</sup> and fabricated using an AM printing machine. Although successful in concept, in its present form, this proved to be very susceptible to vibration and needed to be more robust in construction. Due to time restraints this was not pursued.

### 3.2 The Camera

One of the main objectives of the research was concentrating on the ease of reproducing artifacts without complex hardware or software. A mid-range Nikon *D3100*<sup>®</sup> DSLR camera was used (Figure 3.1), the digital data obtained being in camera ready (CR) \*.jpg format.



Figure 3.1: Nikon *D3100*<sup>®</sup>  
DSLR Camera.



Figure 3.2: *AF-S DX Zoom-Nikkor 18-55mm f/3.5-5.6* – Zoom Lens.

This camera came “bundled” with the choice between two lenses, either a 50mm fixed focus lens, or *Nikon 18/55mm DX*<sup>®</sup> auto focus lens (Figure 3.2). At the time of purchase, in 2012, this cost £350.00

### 3.3. The Lens

A standard fixed focus prime 50mm lens, which has a wide f1.4 or f1.8 aperture and minimum lens distortion and very good depth of field (DoF) was considered, but the *Nikkor 18/55mm DX®* auto focus lens was chosen, being directly compatible with the camera and able to automatically refocus around the subject from the many positions and angles encountered. Minimum lens distortion was achieved by keeping to the higher focal length end of 35/55mm on the lens. These factors were considered more advantages than the advantage of the fixed lens which was that a fixed lens has a greater DoF, and slower shutter speeds which were required if the aperture was not as wide. A resolution of 3456 x 2304 pixels equates to just under 8 megapixels. An Ultraviolet (UV) filter was attached to the lens, as is common practice, as much to protect the lens as to shield from UV light.

#### 3.3.1 Close-up-Lens

A set of Close-Up (CU) Lenses were purchased in case any of the as yet unknown artifacts to be photographed proved too small for the 18/55mm lens to cope with. These CU lenses act like other filter lenses and screw directly onto the front of the primary lens, allowing the camera to remain at a distance without having to move closer to the subject, providing additional magnification of the subject.



Figure 3.3: Typical set of Close up lenses.

The problem of sharp focusing with three-dimensional subjects can be a critical component in close up or *macrophotography* and the all-important depth-of-field is significantly reduced. Closing the aperture to a smaller f/stop will compensate for this, but an increase in lighting levels or a slower shutter speed is then required. The CU lenses, as seen in the Figure 3.3, are generally labelled on

their sides with their relative “strength” or magnification using a measure of optical strength called “dioptre”.



Figure 3.4: The Warrior – effect of - f/18 @ 35mm +0.



Figure 3.5: The Warrior – effect of - f/18 @ 35mm +4 dioptres lens.



Figure 3.6: The Warrior – effect of - f/18 @ 40mm +10 dioptres lens.

A lens labelled “No. 1” would be a relatively mild close-up attachment; those labelled “No. 2” or “No. 4” would be relatively stronger. Close-up lenses are

commonly available in magnifications from +0 dioptrre to +10 dioptrres, notice difference in curvature of lens. In the examples above (Figures 3.4 to 3.6), the position and distance of camera from the subject, is the same for all three shots, in this instance at 140mm. Only the CU lenses where changed. The first image (Figure 3.4), has been exposed without any additional lens. In the second image, a +4 dioptrre lens has been screwed onto the primary camera lens and for the third image (Figure 3.6), a +10 dioptrre lens has been added. The effect of the close up, or enlargement of the images is quite clearly seen.



Figure 3.7: Models shot at 140mm distance.

Figure 3.8: Models shot at 140mm distance but with +10 dioptrre lens.

The two photographs (Figures 3.7 and 3.8) show the advantage of using the close-up lens on a small object, the camera came within 140mm of the artifact. The Peruvian chieftain, left, is only 40mm high and detail could have been lost if the data set had been taken without the +10 dioptrre lens. The two photographs were shot using a green backdrop, producing good contrast for the larger figure but not quite so good for the smaller one.

### 3.3.2 Neutral Density Lens

As with the CU lens, neutral density (ND) lenses were purchased as a precaution for situations that might occur where the prevailing lighting conditions might be too bright for the required focusing. An ND filter is usually plain grey, or semi/half

grey (Figure 3.9), but it is a neutral grey, so whatever light it lets through does not affect the colour, just the brightness.



Figure 3.9: Selection of Neutral Density square and round Filters.

The ND filters also screw onto the front of the primary lens or, in some cases, fit into a screw-on frame. The camera's automatic exposure system works out the filter factor. If for example, an 8x filter is used, the camera will reduce the shutter speed from, say, 1/125sec to 1/15sec to compensate for the three stops extra light required. Or the aperture will be opened up from f/22 to f/8. As can be seen, the use of an ND filter allows the camera operator more flexibility in controlling the variables encountered on the camera settings.

### **3.4 Additional Camera Equipment**

Although different methods of data capture were employed throughout this research, a sturdy tripod was always used with the camera, as well as a release cable directly fitted to the camera. This additional equipment enabled the camera positioning to be more precise if the camera was to be moved as in Chapter 4, method 1, or as in method 2, maintain a constant position. Although the lens used has a “*Vibration Reduction (VR) function*”, the use of a cable release ensured there was minimum camera shake.

An *Omega® HHLM3 Light meter* (Omega Engineering Inc.) was used to read the ambient light, ensuring that there was an even spread of light around the

subject. A range could be selected and read, from 20 lux, 200 lux, 2000 lux or 20,000 lux, with the facility to hold the current reading. Although this meter was available it was in effect seldom used as the camera was able to compensate adequately for all lighting conditions.

### 3.4.1 Compact Camera Support Frame

As mentioned in the introductory paragraph of this Chapter 3.1, a multi camera test support frame was designed and built, which it was hoped would hold three compact cameras. A series of tests was planned, using much cheaper cameras, all of which retailed for under £120.00 and which were all of the “*point and shoot*” design. The test rig was constructed using a curved steel hollow pipe, so as to ensure each camera had an almost identical radial distance from the subject (seen from above Figure 3.10). Three evenly spaced camera shoe brackets were attached to the pipe (Figure 3.11).



Figure 3.10: Frame curvature as seen from above.

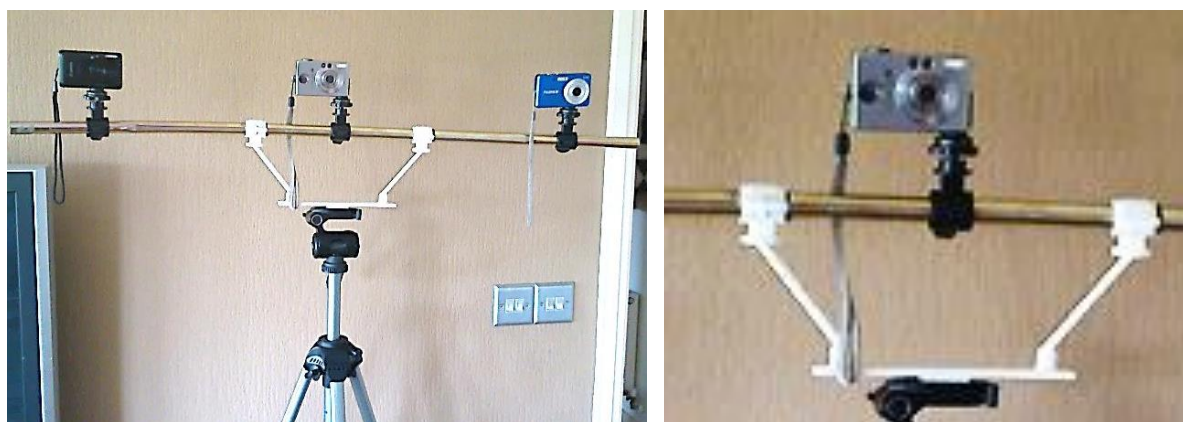


Figure 3.11: Curved pipe supporting three compact cameras.

Figure 3.12: AM support arms and frame.

This assembly was then supported by two nylon arms attached to a frame, which had been printed using an AM machine (Figure 3.12). This lower frame was clipped into the camera shoe on the tripod. Unfortunately there was not enough rigidity in the two supporting arms, whose spring or flexibility meant that although each camera could be operated under exactly the same condition of distance and light, the cameras vibrated, enough for the digital images obtained to be blurred. It was realised that this was an engineering weakness in that the materials used to construct the frame were too flexible. If time had permitted, a new sturdier/thicker frame could have been fabricated in steel to overcome this problem and the cameras linked to a cable release.

### 3.4.2     Turntable and other Props

The camera was used in two basic ways to capture the data images of the artifacts: in the first method, the camera was moved around the artifact on a tripod, in a 360° circle.

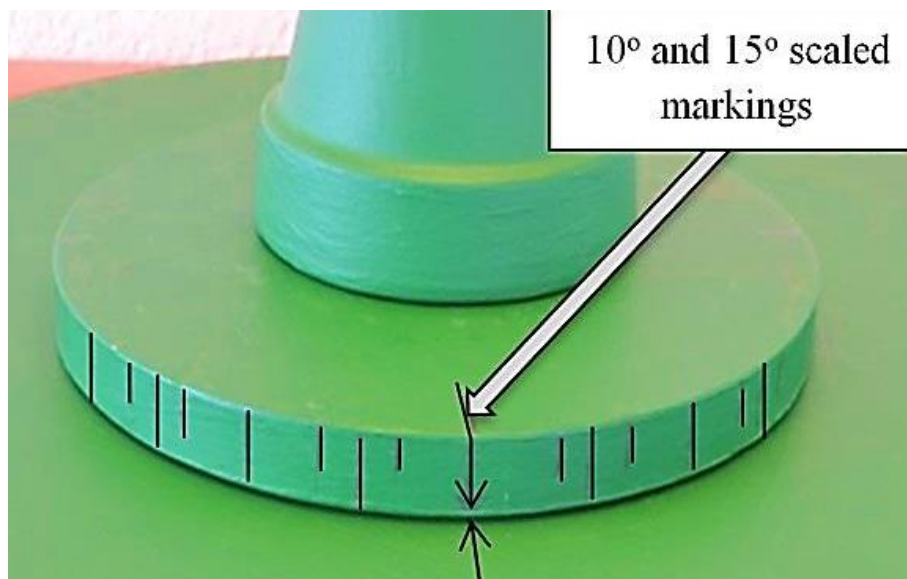


Figure 3.13: Close-up of turn table showing degree markings.

In the second method the camera was stationary on a tripod and the object to be photographed was rotated on a turntable in a 360° circle (Figures 3.13 and 3.14). According to how much detail was required to be captured from the subject, so the number of digital images required to capture and processed, increased or decreased. The object was placed on the turn table which was rotated either through 10° or 15° per photograph. The turntable and supporting

pot, on which the prime object was placed, were also painted to match the Chrome Key covering. A rotation of  $10^\circ$  produced 36 images per rotation whereas a rotation of  $15^\circ$  produced 24 images per rotation.



Figure 3.14: Turn table as in use.



Figure 3.15: Use of cord to control radial distance.

For another indoor photo-shoot, this time of a relief painting (Figure 3.15), the object painting was left hanging on the wall, directly facing indirect light

coming from a window on the left of the photograph. In this series of image capture, the camera was moved in a semi-circle around the hanging picture. Note the cord (arrowed in photograph) tied to the tripod leg and the top of the central heating radiator, thus keeping the cord tight maintained the radial distance from lens to subject.



Figure 3.16: Use of pole to control radial distance of camera position.

In another series of photographs, the camera is kept at the same distance from the subject by the use of a simple pole (arrowed in photograph) attached to the tripod leg (Figure 3.16). By keeping the camera at the same distance the size of the digital images and DoF was kept as near constant as possible.

### 3.5 Compact Camera Test - *Canon IXUS 100 IS<sup>®</sup>*

Although the *Nikon D3100<sup>®</sup>* was extensively used throughout, and because of the failure of the three compact digital camera frame (see Chapter 3.4.1), a small pocket digital compact *Canon IXUS 100 IS<sup>®</sup>* camera was used to take images of a few objects. It came with 12.1 megapixels, 3.0x Optical Zoom and an optical image stabilizer. This camera could also take high resolution images but could be set at a lower picture resolution of 1600 x 1200 pixels, equating to just under 2 megapixels. This camera was ideal to compare a low resolution point and shoot to the more complex *D3100<sup>®</sup>*. Although this camera has since been superseded

by a new model, it can still be purchased for under £120. These images and results were used as comparison data in a later chapter (see Chapter 7).

Two methods of digital data capture were employed by the use of the Nikon *D3100*<sup>®</sup> and these form the bulk of the discussion in future chapters, together with the specific operating conditions in which objects were photographed. The first part of the process was the acquisition of the digital data images using the single DSLR camera. According to the type of processing software employed, some 60 – 150 images were taken from different angles, for the digital data sets needed for processing, ensuring that there was an image overlap of about 10-20%. The images were taken using a mid-range resolution of 4608 x 3074 pixels. The final part of the process was the conversion of the 2D digital images to 3D CAD models, using the appropriate software as recorded in the examples cited, and transferring this data to the AM machines which were used in the fabrication of the artifacts to produce the geometric models.

The advantage of this single digital camera process was that 3D scanners were not required to capture the data necessary to produce 3D CAD images, and experienced technicians were no longer required to operate this equipment. By using a relatively modest DSLR camera, good results were obtained. A comparison between photogrammetry and laser scanning, their techniques and characteristics has been shown by Barsantia *et al* [74].

Details and results of the three artifacts that were used for a set of trials with different camera settings are found in Chapter 7. A processed 3D digital image for each artifact is compared with one taken with the *Nikon D3100*.

### 3.6 Lighting

The approach employed for lighting and camera positioning for the artifacts was different in each method used, the common factor being that shadowless, flat lighting was required to illuminate all the artifacts, as any shadow distorted the image captured and processed by the software. Highlights or reflections that the lighting might have created coming off the objects could also cause distortion to the digital image. In most cases, if the lighting level was low, the camera was able to compensate by the combination of shutter speed or aperture opening. Where small apertures were required, because a greater DoF was required to

obtain maximum sharpness, the lighting level if raised too much could cause reflective flare. In such an instance the shutter speed would be lowered.

For future research, it might be useful to measure both the level of brightness (lumens) emitted by the light source in relation to the reflective spectral brightness (flare) of the light, to ascertain the point at which the digital image is distorted by this spectral interference. As there are so many different reflective surfaces, the outcome for such research may show that there is very little, if any, common ground to substantiate a given set of rules, thus proving that such an idea is unworkable and each object photographed must be tested to find the optimum level at which the flare results in the degradation of the digital image.

### **3.6.1      Light and the Kelvin Scale**

The ideal lighting conditions, in which to photograph the objects, was an even, shadowless illumination, from above and around the object. During prolonged visits to Spain over the winter months, where the natural lighting is generally much brighter and stronger than in Northern England where the author lives, it was possible to take advantage of natural outdoor lighting conditions, and several separate lighting environments were used. As will be shown, no photographic sessions took place in direct sunlight.

The Kelvin scale is the standard method of describing the colour temperature in a variety of situations (Figure 3.17). Although the terms temperature and degrees are still used, degrees were deemed obsolete in 1967 by the International System of Units (SI) but still in common use in the media industries [140]. The optimum word however is colour, and the scale ranges from 10,000K representing the cold blue light of the northern sky through to 5,000K, the bright white noon daylight, and finishing at 1,000K, which represents the very warm red glow of a candle flame. Even the description “temperature” can paradoxically be counter-intuitive, because the higher the temperature, the “colder” (cooler) the colour. The “hot” colours - the reds - are at the bottom of the scale, whilst the cooler colours - the blues - are at the top end of the scale [141]. Through the use of compensating lens filters, the mood of the captured photographic image can be changed, although modern DSLR cameras can be set to automatically compensate for these colour variations.

Colour temperature is not so important for the data capture of artifacts that are to be fabricated using monochromatic AM technologies, as the \*.stl file carries no colour information across to the AM machines, and the final colour of the replicated model is the colour of the material which is utilised, although the heating, melting and cooling process can turn a white powder or filament into a slightly cream coloured model. If on the other hand colour printed replication of artifacts is required, the colour temperature of the digital images is important, as the colour bias will be carried through to the final fabricated model and could cause the colours to be too red or too blue.

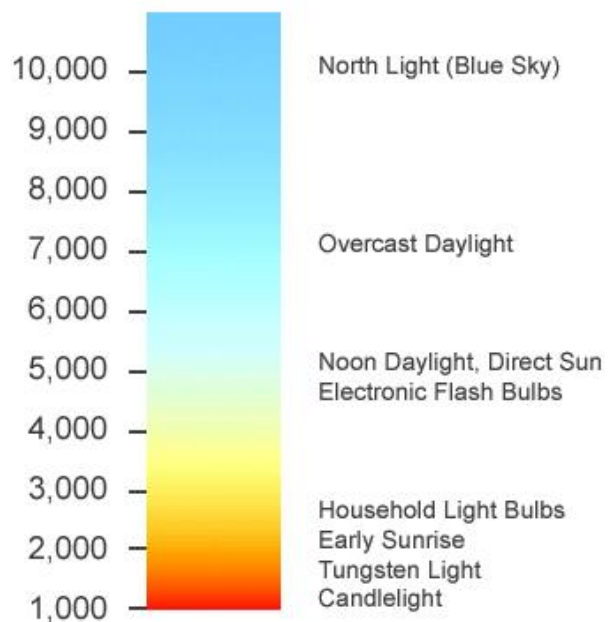


Figure 3.17: Colour Temperature – the Kelvin Scale [140].

In the UK, all photographic capture was conducted indoors with the use of mainly fluorescent artificial lighting (Kelvin scale approximately 5,000K), with one exception, which was an outdoor trial session at Morecambe Bay (Kelvin scale approximately 7,000K). This also allowed for a comparison to be made between the use of controlled artificial indoor lighting and bright outdoor sunlight (Kelvin scale approximately 3,500-4,000K). Unless actually measured with a meter at a specific moment in time, natural light by its very nature changes and therefore is usually within a scale range, hence the use of “approximately” above. Artificial light on the other hand, can be made to a particular colour temperature [141] and when a tungsten or fluorescent light is purchased, this colour temperature can be specified.

However, it was found that, as long as the correct amount of illumination (lumens) was used, ensuring even, flat, and shadowless lighting to illuminate the artifacts, no discernible difference was observed between indoor artificial lighting and natural bright daylight. This was due to the camera compensating for the difference in white light balance (see below). The indoor image data capture was either in an “*Open Room*” environment (i.e. the living room of the author’s domestic dwelling), or with the use of the Light Tent, which by virtue of its portability, could be set up in any area. A further method was using an unusual non-portable walk-in light tent, in Spain (see Chapter 3.7.2).

### 3.6.2 Basic Lighting Equipment

Two *bip*® fluorescent floodlight control units on telescopic stands were used, each with 3 separate switched 100watt bulbs (Figure 3.18) and white diffusing front covers to prevent any strong shadows being cast. Each tube was “Cool White” equating to Kelvin scale 5000K. In addition, two smaller additional lights were also used, these having 45W, 4000K fluorescent bulbs (Figure 3.19). These small differences in colour temperature, known as White Balance in camera terms, are automatically adjusted by the *D3100* camera:

“as digital cameras have a far greater capacity to compensate for the varying colours of light” [142].



Figure 3.18: *bip*® fluorescent floodlight.



Figure 3.19: Single bulb 45W floodlight.

### 3.7 White Balance and Grey Scale

As discussed in Chapter 3, the DSLR camera that was used had a built-in mechanism for compensating for the varying colours of lighting conditions used throughout this thesis and was set at Auto White Balance mode throughout. The arguments for or against manually setting the White Balance and use of Grey Cards, and the science behind colour is not within the scope of this thesis. Many might perceive the use of Grey Cards as an essential part of Photography and might question the use of automatic camera settings for White Balance. This type of technology is standard with all modern digital cameras and can be deactivated by the camera operator if required. Without this auto compensation, the varying lighting colour, as can be seen from the Kelvin scale, causes the artifacts or scene colours to change.

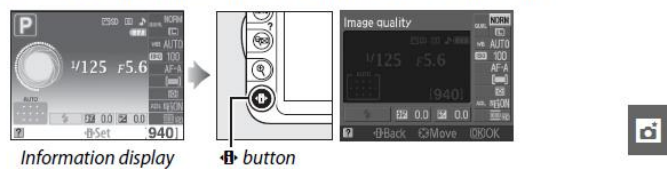
#### White Balance

White balance ensures that colors are unaffected by the color of the light source. Auto white balance is recommended for most light sources; in P, S, A, and M modes, other values can be selected if necessary according to the type of source:

Option	Description
AUTO Auto	Automatic white balance adjustment. Recommended in most situations.
Incandescent	Use under incandescent lighting.
Fluorescent	Use with the light sources listed on page 88.
Direct sunlight	Use with subjects lit by direct sunlight.
Flash	Use with the flash.
Cloudy	Use in daylight under overcast skies.
Shade	Use in daylight with subjects in the shade.
PRE Preset manual	Measure white balance or copy white balance from existing photo (90).

**1** Place the cursor in the information display.

If shooting information is not displayed in the monitor, press the  button. Press the  button again to place the cursor in the information display.



**2** Display white balance options.

Highlight the current white balance setting in the information display and press .



**3** Choose a white balance option.

Highlight an option and press . To return to shooting mode, press the shutter-release button halfway.

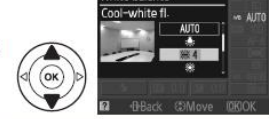


Figure 3.20: A page from the Nikon Manual [143].

Both to the human eye and the camera sensors that record the image, the colouring can become either too blue (cold) or too red (warm). This in turn would have an adverse effect on the final AM production if fabrication of the model would be enabled using a colour machine. When the camera is set to Auto, the camera sensors automatically search for the mid-grey hue within the scene and set the white balance mode accordingly, as shown in the camera manual on White Balance (Figure 3.20) there are eight White Balance options within the camera settings menu. Before any condemnation of the Auto White Balance mode on cameras the following should be considered.

### **3.7.1 Accuracy of the Colour requirement**

If absolute colour accuracy is deemed imperative, this problem can be overcome by the use of “Grey Cards” [144]. For example, for the studio photographer who is shooting commercially for a shopping catalogue, this colour accuracy is very important. The buyer, looking through a clothing catalogue, expects the colour of the fabric of a blue shirt or red dress, as seen on the printed pages of a catalogue, to be exactly the same colour as the goods they receive on purchasing the item of clothing.

The grey card is a means of setting or calibrating the camera’s exposure, manually, by providing a “colour” reference point for the prevailing lighting conditions. This referencing works because the grey card is a neutral tone and lacks any colour. All images captured under those lighting conditions will reflect those settings. Under constant studio lighting, the use of grey card will be ideal, but if a photoshoot is taken outdoors, perhaps on a sunny day with light cloud cover, or a semi overcast sky with the sun periodically coming through, the lighting might well change from image to image as the cloud cover rolls across the sky or the sun hides behind a cloud. When set to manual, the white balance will have to be reset with the grey card for every cloud shadow and lighting change. This is not ideal if at an outdoor sporting event where fast response is required by the camera operator, or if photographing a single object outdoors, from perhaps 120 different angles, as would be the case in AM replication by using a single camera for reverse engineering of the object.

The other way of compensating for such a lighting colour change would be in pre-processing of the digital images with a program such as *PhotoShop CS5*,

Adobe *Lightroom* [145] or other such digital manipulation software, which all have settings for the correction of White Balance within a set of images. Having selected and corrected a specimen image from the batch, the setting for the correction can be synced to the rest of the data set. This can be achieved provided the camera operator has access to these highly specialised and expensive programs and is skilled in the use of them.

### 3.7.2 Consistency in Colour printing

If colour accuracy in the printing of the artifacts is still paramount, as in the example above for the shopping catalogue, then the next step to consider is the graphics technology and photographic printing requirements for printing of the colour images and the media to be used, in this case paper. There are international colour matching standards that ensure the consistency of the colour of ink and the print media used. British Standards [146] indicate that there are some 25 ISO standards covering the colour and consistency of printing ink, prepress digital data exchange, colour monitor for soft proofing etc.

Pantone 213	Pantone 214	Pantone 215	Pantone 216	Pantone 217	Pantone 218	Pantone 219	Pantone 220
Pantone 221	Pantone 222	Pantone 223	Pantone 224	Pantone 225	Pantone 226	Pantone 227	Pantone 228
Pantone 229	Pantone 230	Pantone 231	Pantone 232	Pantone 233	Pantone 234	Pantone 235	Pantone 236
Pantone 237	Pantone 238	Pantone 239	Pantone 240	Pantone 241	Pantone 242	Pantone 243	Pantone 244
Pantone 245	Pantone 246	Pantone 247	Pantone 248	Pantone 249	Pantone 250	Pantone 251	Pantone 252
Pantone 253	Pantone 254	Pantone 255	Pantone 256	Pantone 257	Pantone 258	Pantone 259	Pantone 260
Pantone 261	Pantone 262	Pantone 263	Pantone 264	Pantone 265	Pantone 266	Pantone 267	Pantone 268
Pantone 269	Pantone 270	Pantone 271	Pantone 272	Pantone 273	Pantone 274	Pantone 275	Pantone 276
Pantone 277	Pantone 278	Pantone 279	Pantone 280	Pantone 281	Pantone 282	Pantone 283	Pantone 284
Pantone 285	Pantone 286	Pantone 287	Pantone 288	Pantone 289	Pantone 290	Pantone 291	Pantone 292
Pantone 293	Pantone 294	Pantone 295	Pantone 296	Pantone 297	Pantone 298	Pantone 299	Pantone 300
Pantone 301	Pantone 302	Pantone 303	Pantone 304	Pantone 305	Pantone 306	Pantone 307	Pantone 308
Pantone 309	Pantone 310	Pantone 311	Pantone 312	Pantone 313	Pantone 314	Pantone 315	Pantone 316
Pantone 317	Pantone 318	Pantone 319	Pantone 320	Pantone 321	Pantone 322	Pantone 323	Pantone 324
Pantone 325	Pantone 326	Pantone 327	Pantone 328	Pantone 329	Pantone 330	Pantone 331	Pantone 332
Pantone 333	Pantone 334	Pantone 335	Pantone 336	Pantone 337	Pantone 338	Pantone 339	Pantone 340
Pantone 341	Pantone 342	Pantone 343	Pantone 344	Pantone 345	Pantone 346	Pantone 347	Pantone 348
Pantone 349	Pantone 350	Pantone 351	Pantone 352	Pantone 353	Pantone 354	Pantone 355	Pantone 356
Pantone 357	Pantone 358	Pantone 359	Pantone 360	Pantone 361	Pantone 362	Pantone 363	Pantone 364

Figure 3.21: Small part of the Pantone colour chart [147].

Colour standardisation exists in many countries around the World with as many colour charts as there are colours and systems of colour classification (for

example, see Figures 3.21 and 3.22). There also are colour charts, tables and wheels to convert one system to another so as to ensure consistency [148].

How any one colour may be affected by the material on which it is being printed must also be taken into account. Certain industries evaluate the material to be printed based on a standard of whiteness and type of surface coating; perhaps there is a matt, a gloss or a semi-gloss finish to the surface to be printed. The definition of absolute white must also be considered and if this surface to be printed on is perceived as white, how far it deviates from this and appears as a faint tint of yellow or blue [149]. These issues are covered by the ASTM E313 standard [150], and the ASTM standard for the use of colour in the workplace (ANSI Z535.1-6. Colour Codes) [151]. Such topics must be evaluated in colour printing so as to achieve consistency and accuracy of colour.



Figure 3.22: BSI Fan Deck 475 colours [152].

### **3.7.3      Uniformity of AM printers and inks.**

The printing press, along with the inks used, as well as paper technology, have evolved over many years, with time enough to confer, standardise and optimise consistency and accuracy so as to produce, results that meet the same international standards internationally. However, AM colour printing and the technology of the inks, machines and media used are by comparison still in the very early stages of development.

In 2014, Mcor Technologies Ltd., claimed that their IRIS machine conformed to an international (ICC) standard based colour profile [153]. This standard was also embedded into the driver software as well as computer screens resulting in a what-you-see-is-what-you-get technology [154]. However, for a paper/resin based modelling machine nothing is forthcoming from the company about the standardisation of the paper or resin colour used and if such hues in colour are masked by the ink or have a “sun glasses effect”, turning each colour into a hue of its original ICC colour.

Assuming that most of the materials used to fabricate the models on AM machines are mainly monochromatic (white), the materials used should conform to any whiteness indices such as ASTM E313, the index used to measure the whiteness of materials such as paper, paint and plastics. This information is important, if for example, it is intended to colour print an object in a consistent shade of blue, conforming to a BSI colour chart number. Having quoted such a BSI number, this could then be converted to other colour tables such as RAL, RGB or CMYK charts, ensuring consistent colour printing on any machine anywhere in the World. The material used must, if white, also conform to a specific shade of white, so as to ensure consistency from batch to batch.

Two major AM colour printing machine manufacturers were asked the following questions about their products, as well as modified versions of the questions being put to both BSI and ASTM:

*“Do 3D printing machines comply with any 3D printing colour accuracy standards or do the ink colours comply with BSI, CIE, ASTM or other standards?”*

*“Assuming that most of the materials used to fabricate the models on all your machines are mainly white, do the materials you use conform to any whiteness indices such as ASTM E313, the index used to measure the whiteness of materials such as paper, paint and plastics?”*

Examination of sales of AM printing machine data and materials data sheets has not confirmed any such international standard conformity, and no response was received from the companies that the author contacted to verify that such

standards exist nor that any consultation exists between AM manufacturers, printing ink or material suppliers.

### **3.7.4 Auto White Balance camera mode**

The use of the Automatic camera setting for most situations has been recommended by camera manufacturers. If the end result of a camera photoshoot is to produce a landscape, portrait, or any other type of printed media image where colour must be true to life, consistent, or totally repeatable, or where special effects are required both in videos and other multi-media, the camera operator must maintain control over the final appearance of images produced by the control of the white balance via the use of grey cards. The reproduction of such media is at a very advanced stage, and as seen in the preceding sections, international standards have been established in every aspect of image production and reproduction. The importance of these international colour standards were shown in a court case in 2012 where the chocolate company Cadbury won the right to stop its rival Nestlé from using Cadbury signature colour Pantone 2685C purple, on the Nestlé wrappers [155].

Although ASTM and BSI have evolved a number of international standards that cover many of the aspects of processing AM products, nothing appears to cover colour or the colour fabrication of AM products [156] [157]. If the model is to be made of single, solid materials, white, black etc., and the digital files are converted to \*.stl files ready for most AM printing machines, the subtleties of the colour hues will be totally lost within the \*.stl file and will not be required by the AM machine. Whilst most AM manufacturers will point to the consistency of their material, ink and machines, as yet there is no standardisation between these manufacturers. In 2012, in an article about the emerging markets in 3D colour printers, Joe Titlow stated:

*“Several 3D printers are available that give you the option of seeing your part in one or more colours. Each printer, though, handles colour differently.....”* [158].

As yet, there is still no standardisation agreed by all or any of the parties involved in this technology.



Figure 3.23:  
Original Photograph.



Figure 3.24:  
Screen shot point cloud image.



Figure 3.25:  
Mc or *IRIS*<sup>®</sup> model.



Figure 3.26:  
Stratasys *PolyJet J750*<sup>®</sup> model v1.

Figures 3.23 to 3.26 of the Eureka Man, which is 65mm high, illustrates the above quote by Titlow. Although the colouration of the point cloud image (Figure 3.24) is not an ideal colour match in comparison with the original (Figure 3.23) the *IRIS* colour model (Figure 3.25) however closer to the point cloud colouring than the *PolyJet J750*<sup>®</sup> model v1 (Figure 3.26). Both machines used the same colour “wrl” file which was processed using AutoDesSys software *formZ 8 SE*<sup>®</sup>.

Figures 3.27 to 3.29 highlighted a similar issue as above. With Figures 3.27 and 3.28, the colouring was a near matched but with the PolyJet model (Figure 3.28) the replicated model had a very distinctive red bias rendering the black and grey colours a dark or light mauve respectively. The flesh skin tones had taken on a reddish hue.



Figure 3.27: Original Sobekhotep model.

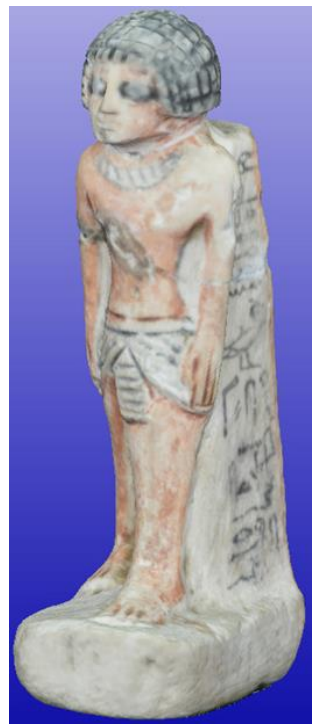


Figure 3.28: \*.wrl file created in *formZ 8 SE*.



Figure 3.29: Model from *PolyJet J750*®.

On examination of the PolyJet machine it was found that the colour mismatch was due to a printing cartridge having been changed from clear to yellow, prior to the printing of these models, and the yellow ink was not fully flowing through to the printing head.

Although claiming to be able to produce more than 36,000K colour options together with automatic colour mapping [159], the machine did not seem to have a facility to colour check against the original software image file (\*.vrml file) and colour compensate accordingly. This it seemed was left to the machine technician/operator – by which time the artifact had been fabricated, wasting time and money.

As a result of this colour printing problem, another model of the Eureka Man was fabricated on the *PolyJet J750*® machine (Figure 3.30) which confirmed that the original \*.vrml file was correct. This new model was also a very good match to the original Mcor *IRIS*® paper fabricated model.



Figure 3.30: Re-printed colour model from the *PolyJet J750®* machine v2.

This thesis concerns the simplicity of operation with limited prior “expert” knowledge for an alternative method to LS, for replication of artifacts. The use of manual setting on the camera, in the most part will not contribute to better or more accurate fabrication of monochromatic AM models, and until there is international standardisation within the industry, there is no justification for the use of the Manual setting on the camera for AM colour printing and replication. A *true to life* colour model will not be any more effectively produced using a Manual rather than with using an Auto setting, but with Manual, there are all the added complications that the manual mode entails.

### 3.8 Light Tents

#### 3.8.1 Light Tents Construction

The first was a specially constructed DIY light tent made from 20mm plastic tubing and suitably fabricated to make a 1 metre square enclosure, covered in white poplin fabric with a front opening. It was constructed so as to make it as portable and as versatile as possible, and the finished version could be used with or without a Chroma Key backdrop, as seen in the Kendal Museum workshop (Figure 3.31) without the backdrop, and if appropriate without the outer poplin covering as in Figure 3.32.



Figure 3.31: Light tent set up in museum workshop – with poplin cover.

In order to obtain strong contrast between the subject matter that was being photographed and its background, interchangeable Chroma Key [160] backdrops were used, either white or green, depending on the colour of the subject. As seen in Figure 3.31, the lights, (with their own muslin covers) were placed outside the tent, allowing the fabric to soften the lighting effect and disperse any shadows.



Figure 3.32: Light tent set up without poplin cover but showing Chroma backdrop.

In Figure 3.32 the frame was used to support the Chroma Key backdrop, here shown without the cotton poplin outer covering. This technique was presented at the ESDA 2014 Biennial Conference in Denmark and later published by ASME (see Appendix A) [161].

### 3.8.2 “Studio” Lighting Conditions - Spain

No supplementary lighting equipment was needed in one of the Spanish settings, as the objects were photographed outdoors on the veranda under an off-white canvas awning, measuring 3 metres x 4 metres, and, by pulling the side blinds and roof canopy closed, a large walk-in light tent was formed. The very bright sunlight was diffused through the canvas, so as to create a shadowless, evenly lit work space, with a colour temperature of around 3750/4500K – a little warmer in temperature than the indoor working area in the UK, (less cold blue light, more warm yellow).

To show that data capture can be undertaken in the simplest of circumstances, the alternative method discussed in this thesis used natural outdoor light. In this example, the very bright sunlight had to be shaded by an awning to ensure that there were no excessive shadows or highlights (Figure 3.32) which would distort the digital image.



Figure 3.33: Spanish walk-in-light tent.

This lighting set-up was under very bright sunny Spanish skies, but, ironically the ideal natural lighting is under grey dull cloudy skies, as shown in Figure 3.34, taken outdoors in Morecambe Bay, in the north of England. As can be seen, although the sculpture is covered with small mosaic semi glazed tiles, there are no highlights and minimal shadows, ideal lighting conditions! This type of shadow would not distort the digital images when the time came to process the photographs into 3D point cloud images.



Figure 3.34: Under grey, dull, northern English, cloudy skies.

If at all, the shallow shadows might show as differential colour tones, and even if this did present a problem, a second camera session needed, it would then require the use of reflector panels placed on the ground, to eliminate any shadow. However, these reflector panels would then need to be masked out in a pro-processing session.

### 3.9 Open Room Studio

As previously discussed, the method of lighting and camera positioning for the artifacts was different in each case study, as was the surrounding environment, but the common factor was that shadowless, flat lighting was required to illuminate all the artifacts. All reflective surfaces were covered (television and glass coffee table), to stop any light flare or reflection. The same was true for any highlights or reflections coming off the artifacts that were being photographed, as these caused distortion or “noise” to the processed digital image. In Figure 3.35 the windows were covered with translucent blinds so as to diffuse the natural

daylight and help create a shadowless room. The main indoor lighting consisted of two *bip*® fluorescent floodlight control units on telescopic stands, with white diffusing front covers.



Figure 3.35: Typical artifact – indicated - being photographed in an open room setup using florescent lighting.

Although available for use as “fill in” lighting, the two small lamps with 45W 5500K bulbs were not required in this setting. One can see that the indirect daylight was utilised if available and counterbalanced on the opposite side of the room from the windows by the two large floodlights.



Figure 3.36: Light Tent under the florescent lighting, including ceiling downlights.

Apart from the room having small bright inset LED lights in the ceiling, the room had four larger inset ceiling lights, each fitting taking 2 x 18w fluorescent bulbs. Under normal conditions these would have been standard “warm white” at 2000/2700K but for the duration of this research, the front two were changed to match the floodlight at 4500K. By placing the subject artifact under these ceiling lights, any shadows created by the natural light coming in through the windows or from the floodlight was eliminated. In Figure 3.36 the Light Tent can be seen resting on a low table, also under the central fluorescent ceiling lights, whilst the large fluorescent lamps are used as the primary source of lighting, supplemented by the two smaller lamps.

### **3.10 Alternative “Open Studios”**

In Figure 3.37, a photo-shoot had taken place with the minimum of equipment. This was outside under a Spanish *Naya*, or undercover veranda. Under very bright sunlight conditions, the enclosure provides very soft light, and only a contrast green Chroma Key backdrop was required. This covered the pedestal which a turntable was placed upon.



Figure 3.37: Photogrammetry under a Spanish *Naya*.  
Backdrop hung from wall.

The turntable was the same colour as the backdrop and used to rotate the artifact. In the author's right hand can be seen the camera cable release switch. Hanging from a picture hook on an inside wall, back in the UK, a different artifact was being photographed but with the same backdrop. The use of two large floodlights had to be used to compensate for the bright Spanish sun. This set of photographic data (Figure 3.38) was to use *PhotoScan Pro*® and the whole front and back of the photo frame was required for the final 3D image. The photo frame was therefore placed on a turn table and rotated before a static camera lens.

In another indoor photo-shoot, this time of the relief painting (Figure 3.39) the object painting was still hanging on the wall, directly facing indirect light coming from a window on the left of the photograph. In this series of image capture, the camera was moved in a semi-circle around the hanging picture. A cord was tied to the tripod leg and the top of the central heating radiator which was just below the relief painting (Figure 3.15).



Figure 3.38: Backdrop hung from wall but with lighting - Indoors in the UK.



Figure 3.39: Relief painting photographed whilst still hanging on wall.

The cord was kept tight and used a central pivot line, as the tripod and camera move in a semicircle around the painting.



Figure 3.40: *Infinite-Realities* multi camera studio [162].

By comparison, in Figure 3.40 the multi camera studio of *Infinite Realities* contained over a hundred cameras poised ready to take a single synchronised shot of a human figure to produce an AM figurine.

### 3.11 Software

As referred to in chapter 2.12 there are 80 software programs claiming to be able to convert 2D digital photographs into 3D virtual images. On investigation, it has been found that many are still in development and are not necessarily available for use, except experimentally. Several commercial computer software programs are available with a proven and reliable record to “stitch” multi-view photographs together to produce a 3D image. The primary research task investigated how well these software programs converted the original digital 2D image into 3D CAD models and ultimately physical AM enabled models. The results obtained were compared with the original photograph of the object or the object itself.

The research investigated the tactile surfaces of the replicated models and compared them, where possible, to the original objects; it considered whether those replicated models, when scaled up and down, lost surface detail and whether the AM models created could have been substituted for the original. The research wanted to discover if one could consistently reproduce objects using much cheaper equipment than the standard 3D scanners, and how user-friendly the camera generated digital image processing software was. Three main software programs were used and will be discussed within the context of this research.

With a little training and the simple equipment being used, staff employed at galleries and museums could reproduce part of their collections by non-invasive methods using reverse engineering. If good copies could be fabricated of objects, normally held behind glass cabinets in such museums, visitors including school children might become more engaged with ancient history, culture or modern sculpture. Instead of just looking at the pieces behind glass, the model reproductions could be handled by all.

#### 3.11.1 AutoDesk – 123D Catch®

At the beginning of this research, AutoDesk had not long released *123D Catch*®, as a free Beta 8 product, which had been developed originally from *Inventor*.

AutoDesk had added a 3D printing system to a CAD modelling program, claiming that anybody could produce 3D virtual images that could be made into model replications. This free app was available from the *App Store*. These three methods of data capture – PC, iPhone and iPad - use the AutoDesk's *Cloud Internet* service which transforms the digital data images into virtual 3D models.

Their publicity speaks of allowing ....

*“.... users to capture the world around them in 3D while on the go. Imagine the potential for photos of vacation memories, family or other mementos brought to life in 3D. Captures made in 123D Catch can also be used as the foundation for further 3D modelling, 3D animation, or used to create a 3D printed object.”*

Whilst the author has only used the PC version of *123D Catch*<sup>®</sup>, and as will be seen in Chapter 4.1, with quite good results, one questions the skill and dedication of the users to obtain results “*on the go*”. Autodesk's use of the words “*.... as the foundation for...*” and “*.. potential for...*” might indicate the potential problems that can be encountered by the novice or casual user.

*123D Catch*<sup>®</sup> is part of a family of products, and the user can take advantage of a worldwide user group with a focus on 3D design and personal fabrication of their own models as well as the usual blog pagers for support and help. As one of the largest software companies, it has now invested in the entry level 3D printers in line with the profile of its user group. Autodesk also introduced *cloud storage* for design projects whilst connected to any of its products, allowing free flow of data files between other users, hence allowing users to share files between products. This also encouraged the downloading of models to be “*home*” fabricated or printed by third party fabricator services, of which there are many.

### **3.11.2 Agisoft – *PhotoScan Professional*<sup>®</sup>**

Founded in 2006, this is a Russian based organisation operating out of St. Petersburg. As an innovative research company with focus on computer vision technology, Agisoft LLC has gained expertise in image processing algorithms, with digital photogrammetry techniques setting the direction for the development of applied software tools. Agisoft were very supportive of the author's proposal to

use their software *PhotoScan Pro*<sup>®</sup>, as an alternative to *123D Catch*<sup>®</sup>. Over the years that it was in use in this research, there were several updates, and the company has been gaining a very good reputation, as seen by the numerous times it is now used in a variety of photogrammetric research products and quoted in research papers from around the world. As with Autodesk, it has a very good help line and blog, which is hosted by Alexey Pasumansky, with whom the author has had several email dialogues and much help from his technology team.

With *PhotoScan Pro*<sup>®</sup>, the operator has much more control over how the images are processed, as all the computation is done on one's own computer. With the use of *123D Catch*<sup>®</sup>, there is less control over the processed digital data, as this is sent via the internet to be "cloud processed" by AutoDesk. However a much higher computer specification is required to process the data on one's own computer which must be at least an i5 or preferably i7 CPU with a minimum 16GB memory [55]. The author's PC was updated to 32GB RAM before ultra-high resolution 3D image data could be processed.

Unfortunately, unlike *123D Catch*<sup>®</sup>, the software did not have the facility to convert the captured images into a video. If required, this could be done using a proprietary video processing program.

At the conclusion of this research over fifty objects had been processed using photogrammetry as the core digital data collection method. With the use of these two programs, the majority of 3D point cloud images were produced and converted from 2D \*.jpg files to 3D \*.obj files.

### **3.11.3 Netfabb GmbH – *Studio Pro*<sup>®</sup>**

The two primary software programs used in this research, as discussed in the two preceding sections, processed the digital data and produced an \*.obj file. This final \*.obj file had to be further processed to produce a format that AM machines could read so as to fabricate the models; for which an \*.stl file had to be produced.

For this secondary process, the author used Netfabb GmbH *StudioPro*<sup>®</sup>. This German company was founded in 2009 and, as part of *FIT AG and FIT Additive Manufacturing Group*, has had access to a large machine factory of laser sintering, electron beam melting, injection moulding, vacuum casting and 3D

printing technologies in metal, plastic and other materials. The author has met several of the company directors at several trade shows in London over the last few years.

*Studio Pro*<sup>®</sup> has been in use since the start of the project and was occasionally updated over the time and was able to perform all the modifications required by the author, resize, hollow out etc., and convert the files to the required \*.stl format.

Other software programs, which had the same processing function, such as *Mesh Lab*, were trialled for a short period, but a much greater in-depth, specialist knowledge of the structure of point cloud images and 3D virtual imaging was required. As an ongoing free community/university project, which was being modified at regular intervals, on balance and without exception, *Studio Pro*<sup>®</sup> was much easier to use.

The success rate achieved was good but depended on controllable factors:-

- 60% very good fabricated models with very good surface detail.
- 30% recognisable and acceptable models, but with some loss of detail.

The failure rate of the finished models was of the order of 10 to 15% and was due to (now) known reasons. The failings of this research are fully discussed in Chapter 6.

### **3.11.4 DeskArts - 3Data Expert<sup>®</sup> 10.1**

*DeskArts* was founded in 1989 as a continuation of research projects started at the Helsinki University of Technology. Their sponsors asked the research group to develop industrial design software, emphasising Design, rather than the traditional Engineering features such as seen in *SolidWorks*<sup>®</sup>.

Whilst looking for a company to print colour AM models, the opportunity arose to use a *ZCorp* printer, (now part of the 3D Systems group), and a *Mcor Technologies*<sup>®</sup> paper rapid prototyping, colour printing machine. *DeskArts*' main program *3Data Expert*<sup>®</sup> relabelled under the company name as *AutoDesSys Inc.*, and marketed as *formZpro*<sup>®</sup>, was the supporting software for both companies. These machines read VRML files (known as \*.wri) which convey the colour information to the printing machine. *DeskArts* allowed the author a licence for both programs so as to investigate the different formats and enable some models

to be fabricated in colour. The programs also read the standard \*.stl and \*.obj files and had many of the features of *PhotoScan Pro*® and *Studio Pro*®.

### 3.11.5 Dassault Systèmes *SolidWorks*®

This software program called *SolidWorks*® has been a software engineering tool for creating 3D parametric CAD models since 1993. In this research, *SolidWorks*® was also used to recreate the 3-way corner joint as used in the light tent (see Chapter 3.8.1 Light Tent Construction).

*SolidWorks*® Screen shots



Figure 3.41: Amphora stand.

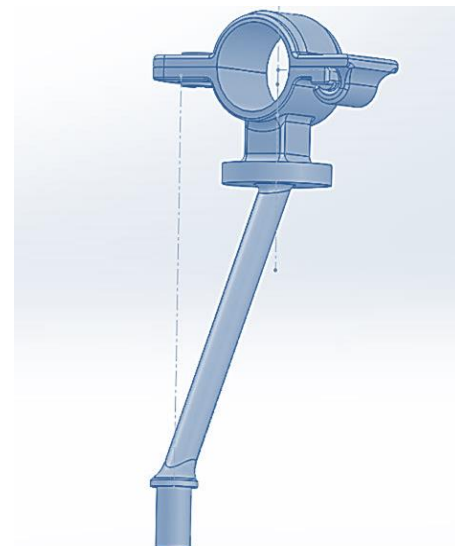


Figure 3.42: Arm of compact camera frame.

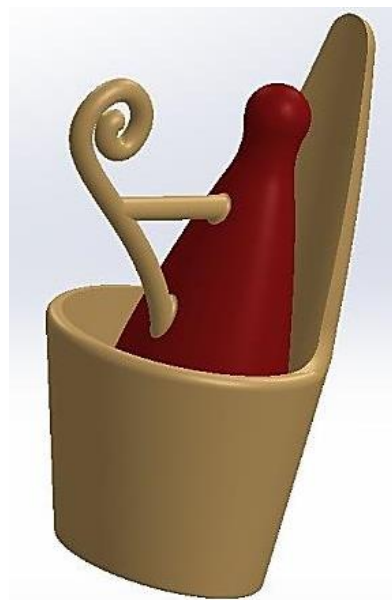


Figure 3.43: Final rendering of Horus's Crown.

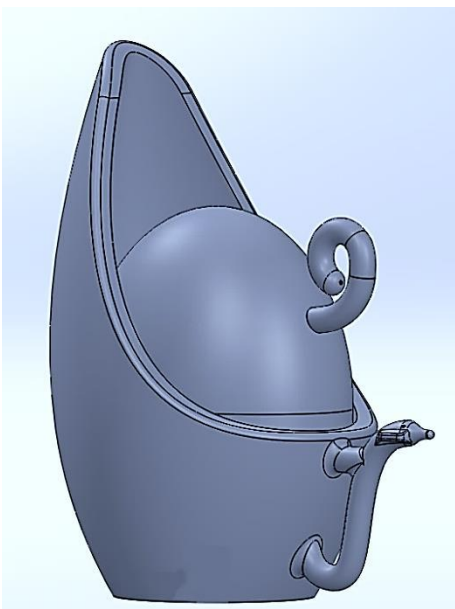


Figure 3.44: Alternative un-rendered version of Horus's Crown.

The compact camera frame (see Chapter 3.4.1), was used to support three compact cameras, and to create two crowns for the Egyptian god Horus (see Chapter 6.9), as well as a stand for an Amphora type jug (Figure 3.41). In the photographic screen shots below, part of the camera support frame is seen as a SolidWorks® screen shot (Figure 3.42) and the two Crowns made for Horus (Figures 3.43 and 3.44).

### **3.12 Software Summary**

To conclude, with the use of photogrammetry, 3D models can be created, without a high level of computer expertise and without the use of relatively expensive or complicated 3D scanning equipment. The software used in this research for the primary processing were: Autodesk's *123D Catch*® and Agisoft's *PhotoScan Pro*®. In addition, the high resolution point cloud images produced were filtered and converted to \*.stl files by *StudioPro*®, ready for AM machines to replicate and produce geometric representational models.

All three programs were relatively straightforward to use with user-friendly interfaces. The use of these techniques, as will be seen in future chapters, contributed to the reproduction, restoration or repair of damaged or broken antiquities by non-invasive methods at modest cost and could be used with only a little training by laypersons who are computer literate but not necessarily expert in the use of specialised software.

## Chapter 4            Methodology for 3D Reconstruction

### 4.1        Method 1

#### 4.1.1      Open Room Studio – Setting the Scene

As discussed and seen in Chapter 3.8, the object to be photographed was placed on a pedestal in the room so as to allow the camera, which had been attached to a tripod, and the camera operator, free movement around the object (Figure 3.23). Any reflective surfaces were covered so as to eliminate any glare which stray light might cause by reflection. The furniture in the room was also moved so that it did not impede the camera movement, but at the same time it was best placed so as not to have to reposition them again, as both the subject and surrounding furniture were required by the computer software, in order to stitch each frame of the digital images together to form the final 3D virtual image.

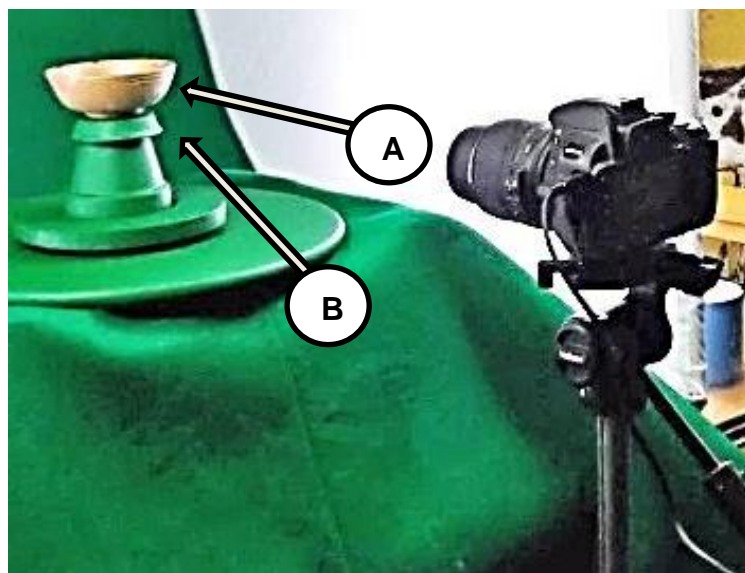


Figure 4.1: Data Capture - Advantageous camera angles.

Any movement of background objects might cause a mismatch of the image data stitching process. The Clay Head, seen in Figure 2.18, one of many of the objects to be photographed in this thesis, was the first object to be processed, and is seen resting on a flat table top. On later photoshoot sessions, it was found much more advantageous to place the artifact on a raised upturned flower pot (Figure 4.1). This allowed for the camera angle to be well below the horizontal plane (see arrow A) and thus to capture more detail from this obtuse angle (see arrow B).

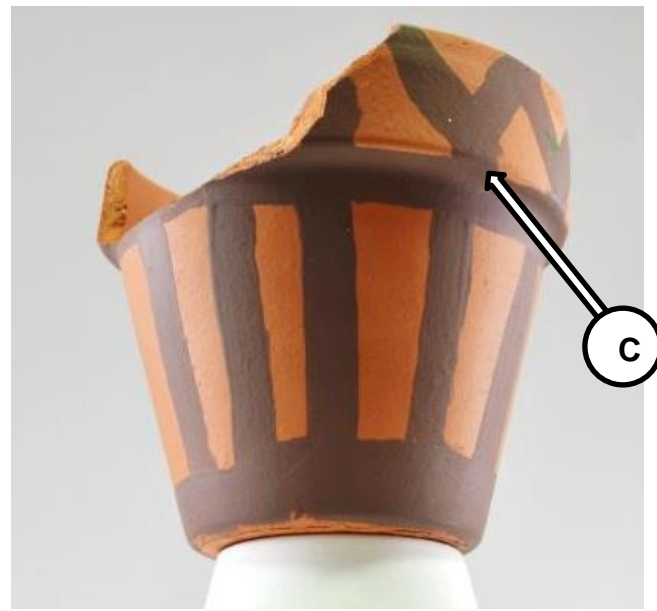


Figure 4.2: Data Capture - Supporting model above horizontal plane.

By raising the artifact above the horizontal plane, as seen in Figures 4.1 and 4.2, more detail was obtained, for example, from the underside of the protruding ridge (see arrow C, Figure 4.2), improving the quality of the digital data image and therefore the finished surface detail of the replicated model.

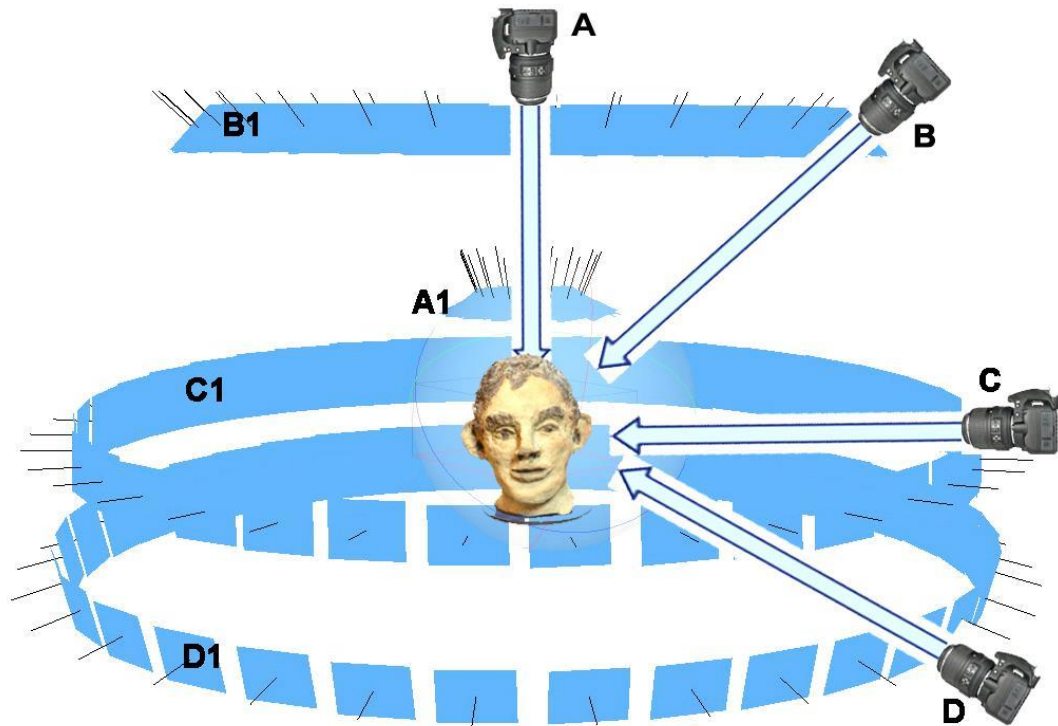


Figure 4.3: Correlation between camera position and horizontal image deviation.



Figure 4.4: Four frames from part of the Data set of 75 photographs.

Figure 4.3 shows the camera positions seen from the horizontal plane, A1–D1 representing the different angle plane of each photograph, as clarified in Table 4.1. Figure 4.4 shows four frame which form part of the data set of 75 photographs that were sent for processing via the internet cloud using *123D Catch*<sup>®</sup> software.

Table 4.1: Correlation between camera positions and horizontal image deviation.

Camera position <b>A</b>	90° above Horizontal plane photographic capture position <b>A1</b>
Camera position <b>B</b>	35/40° above Horizontal plane photographic capture position <b>B1</b>
Camera position <b>C</b>	Horizontal plane = 360° photographic capture position <b>C1</b>
Camera position <b>D</b>	35/40° below Horizontal plane photographic capture position <b>D1</b>

#### 4.1.2 Data Capture – *123D Catch*<sup>®</sup>

Using *123D Catch*<sup>®</sup> software, as discussed in Chapter 3.8, 24 objects were photographed both indoors and outdoors, and processed using this software. Those data sets that were taken indoors used the basic method, as described above (Chapter 4.1.1) the photographs taken outdoors were taken as described in Chapter 3.7.2.

Using *123D Catch*<sup>®</sup> as the primary digital software, the research established a procedure as tabulated below, but it must be emphasized that this might not be the appropriate procedure or methodology when other data processing software is used to process the digital images (Figure 4.5).

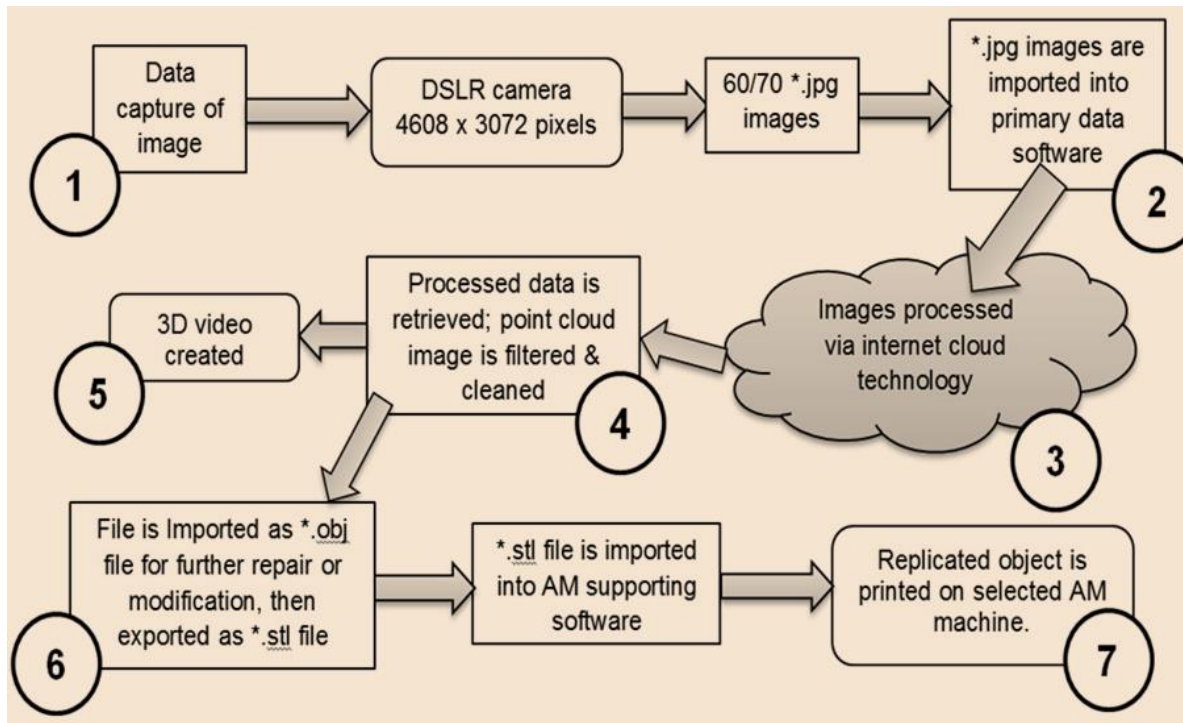


Figure 4.5: *123D Catch*<sup>®</sup> Data processing Flow chart.

To date, the research has identified a procedure in keeping with the aims and objectives of simplicity. The software program used for the processing showed, on several objects, digital photogrammetric problems, which have been identified but have yet to be addressed and overcome. It has been found that even at the lowest lighting conditions, excessive glare or flare can be present on the digital image, and this can be the cause of distortion. The surfaces of several of the original objects have been found to be too reflective, causing the digital image to be distorted.

The flow chart, seen in Figure 4.5, shows seven major stages in which digital data is captured by use of a DSLR camera (or other) to produce from sixty to seventy-five \*.jpg images which are then imported into the primary digital software. The individual images can then be checked for quality and sent via internet cloud technology to be processed. As Verhoeven [70] points out, the time taken for this process is dependent on the quantity and quality of the images, (as

well as internet speed) but a reduction in either can result, as Nguyen *et al.* show [73], in processed image data which is badly degraded.

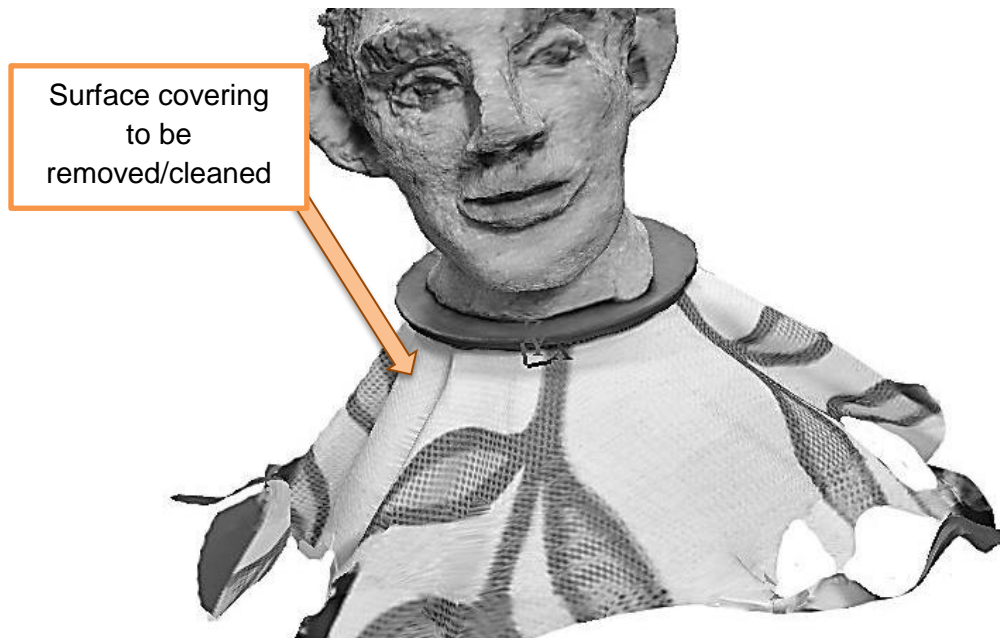


Figure 4.6: Close-up screen shot of image waiting to be cleaned.

Having retrieved the point cloud image, filtering or cleaning of background clutter/noise of the image was required (see Figure 4.6 and Figure 4.7). Many of the original artifacts were placed on a patterned cloth (or even newsprint) which covered the plinth on which the artifact was placed.

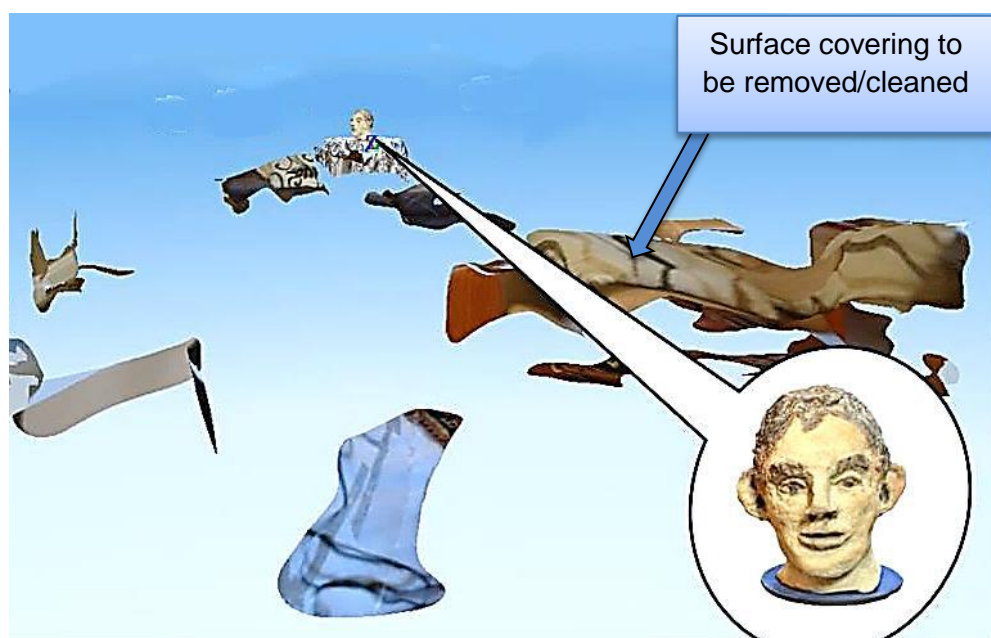


Figure 4.7: Clay head identified in blown up image amongst background “noise”.

This cloth, or covering, was then removed from the returned processed image, simply by highlighting the area and pressing the delete button within the software indicated.

As will be seen in Chapter 6, this patterned cloth helped in the repair of incomplete data.

The file was then ready to export as an \*.obj file into secondary software programs, in this instance *StudioPro®*. This created 3D textured mesh which could be further repaired or enhanced. Figure 4.7 is a complete frame of the returned data file before it was cleaned.

This technique was presented at the ESDA 2014 Biennial Conference in Denmark and later published by ASME (see Appendix A) [161].

#### **4.1.3 Computer Data Primary Processing**

The first part of the process was the acquisition of the digital data images using the DSLR camera. The images were then sent by the internet to be “cloud processed” using an AutoDesk facility but the number of images that could be sent was limited by the pre-requirements of AutoDesk. In the author’s view this was a partial limitation on the quality of the final replicated models. Between 60/75 photographic images were taken from different angles, encircling by 360° and arcing by 30° above and below the horizontal plane around the object, and if required directly from above, ensuring that there was an image overlap of about 15-20%. To start with, the images were taken using a mid-range resolution of 3456 x 2304 pixels, but after several data sets were collected and in one or two instances where greater detail was required, the higher resolution of 4608 x 3074 pixels was used. It was very important that the image was of a high quality, being lit well, with no deep shadows and with the best possible focus and so it was decided that in order to obtain the best possible data images, without any time lost for processing, a standard format of 4608 x 3074 pixels would be used throughout the whole photographic data image capture.

The images were used to generate a point cloud data set, and cloud processed to turn the \*.jpg images, which had been uploaded from the camera, into either a \*.3dp data file, or ready to export as \*.obj or \*.dwg files. After some time, a notification by email from Autodesk came with information that the processed files were ready to download back into the software program running

on the “home” computer. The returned point cloud image had now been transformed into a 3D image which could be viewed from all angles, but it still required to be *cleaned* or filtered to eliminate background noise that had been captured along with the primary object, such as other articles or furniture that were in the line of focus when the digital image was recorded by the DSLR. Having been cleaned, the data file was then ready to be imported into third party software programs, the most common file type being \*.obj or \*.dwg files.

## 4.2 Case Studies

The three examples that are cited here are taken from a series of studies using *123D Catch®* software. The first two were both eventually successful, proving that the process worked, and the third highlighted some of the problems to be resolved by further research. Where there was a problem in the quality of the data capture such as noisy or distorted data, which caused problems in the final virtual image, the detail of the remedy or repair is dealt with in Chapter 6. In some cases there was not an answer to the problem and more tests and trials will have to be conducted at some time in the future.

### 4.2.1 Clay Head



Figure 4.8: Original Clay head.



Figure 4.9: Clay Head - Screen shot of textured processed digital image.

This artifact was a handmade, matt glazed, painted clay head, approximately 105mm high by 95mm deep. Three attempts were made to photograph this head with alterations being made to the camera settings at each attempt (Table 4.2). All three images were in focus, showed good detail and were well lit under indoor fluorescent lighting (Figure 4.8). The final, textured digital image, is seen in Figure 4.9. But in two data sets, the processed image had a hole under the chin, see arrowed in Figure 4.10, and in another data set, a distortion appeared on the crown of the head (indicated in Figure 4.11). For further details, see Chapter 6.

Table 4.2 shows the results.

Table 4.2: Camera data – Clay Head.

<i>Figure</i>	<i>Resolution</i>	<i>Images</i>	<i>Focal length</i>	<i>Aperture</i>	<i>Shutter speed</i>	<i>Result</i>
4.8	3456 x 2304	Original digital images				
4.9	3456 x 2304	60	55mm	A*	1/60	Final data set - Good result
4.10	2304 x 1536	52	55mm	f/5.6	A*	Hole under chin.
4.11	3456 x 2304	40	55mm	A*	1/60	Top of head defect

A\* = Automatic setting on camera

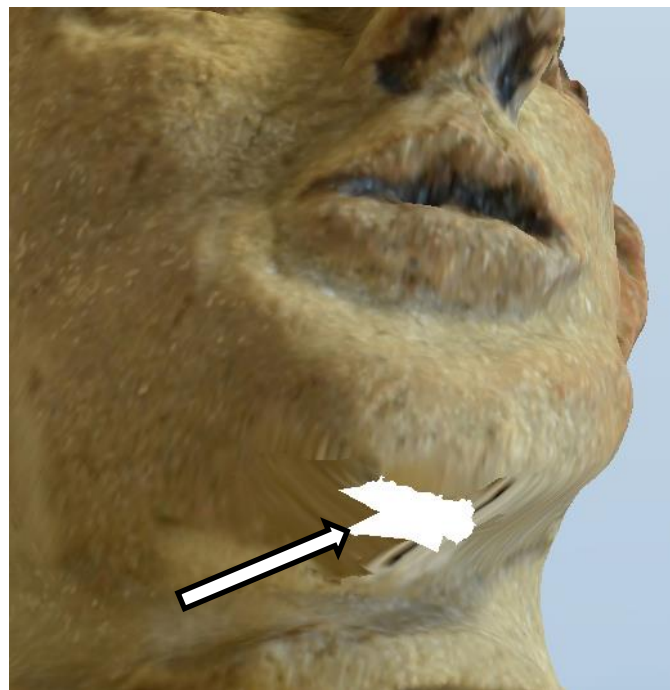


Figure 4.10: Digital model of Clay Head - hole under chin.

The processed photo-textured 3D mesh images (see Figures 4.10 and 4.11) could have been repaired using *StudioPro*<sup>®</sup> but by increasing the number of images, more angled shots and greater image overlap, complex repairs to the point cloud and textured mesh were eliminated (Figure 4.12).



Figure 4.11: Distortion on the back of head.

By selecting the appropriate control in the editing section of *123D Catch*<sup>®</sup>, a wire frame (Figure 4.12) alone, wire frame and texture, or texture only model could be obtained. This would facilitate the model repair if required.

The final data file of the head (Figure 4.13) was processed to create an \*.stl file using *StudioPro*<sup>®</sup>. Finally the file was sent to the *Stratasys*<sup>®</sup> FDM machine to create the geometric model.

The model was instantly recognisable as a copy of the original and although the FDM model is a little smaller than the original (Figure 4.13), being 80% of the original size, the tactile surface finish was much smoother than the rough, prickly feel of the original. Seven artifacts were reproduced successfully using a *Stratasys*<sup>®</sup> FDM machine and a further 5 remained at a stage waiting to be fabricated. It was found that a mid-range resolution size of 3456 x 2304 pixels produced enough definition for the production of FDM models and that increasing the number of pixels per image resulted in either the *PhotoScan Pro*<sup>®</sup> software not being able to cope or the processing time greatly increased.

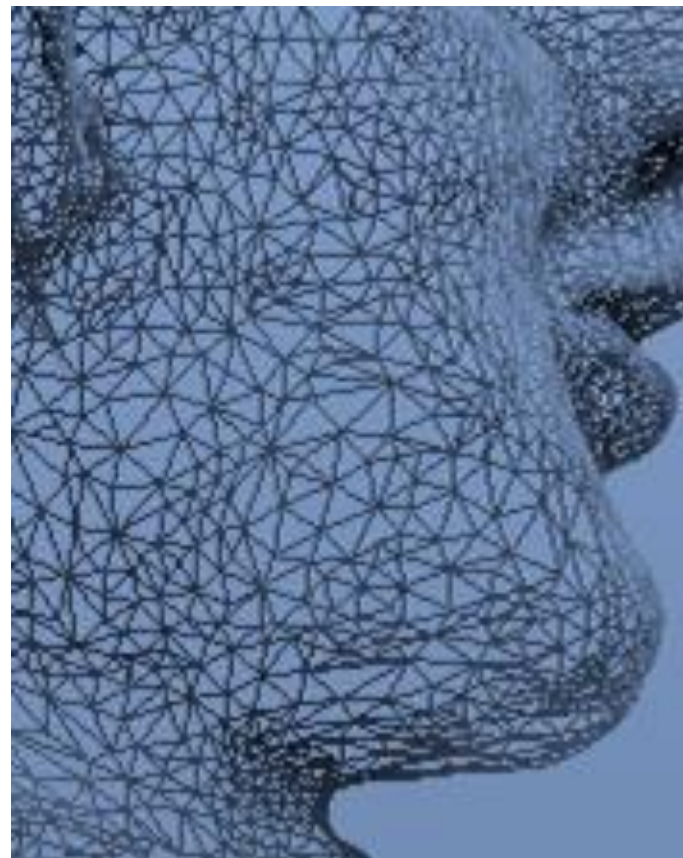


Figure 4.12 : Clay Head - Section of point cloud mesh.

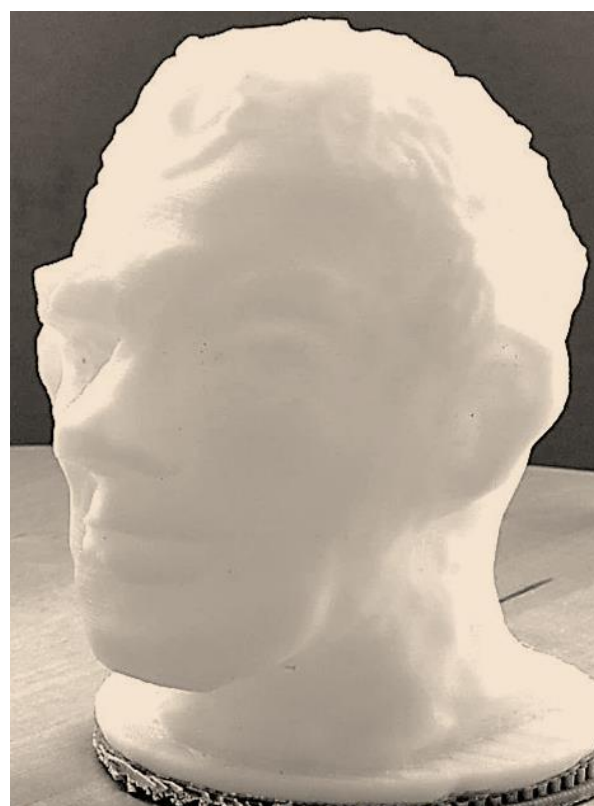


Figure 4.13: Final Geometric Representation FDM Clay Head model.

This could be attributed to similar geometric errors caused by the size of the extrusion nozzle and tool path of the *Stratasys*<sup>®</sup> machine as described by Brooks *et al.* [163], where the surface detail on FDM models was directly related to the size of the extrusion nozzle diameter and by increasing the software capability or processing time, the physical capability of the nozzle was the controlling factor.

#### 4.2.2 Unglazed Ceramic Vase

This second object was an unglazed ceramic vase that had been coated at some time in the past with a chalky type of whitewash, much of which had come off due to weathering, see Figure 4.14.



Figure 4.14: Original digital image of Ceramic Vase.

The difficulty in photographing this artifact was that it was hollow, so two surfaces, not just the outside but also an inner surface, had to be digitally captured. The vase was much bigger (200mm x 220mm) than the clay head, and the photographs were taken outdoors in the light tent (Figure 3.24).

Table 4.3: Camera data – Clay Vase.

Figure	Resolution	Images	Focal length	Aperture	Shutter speed	Result
4.14	3456 x 2304		32mm	f/11	A*	Original digital images
4.15	3456 x 2304	17	32mm	f/11	A*	Good image <b>but</b> holes inside
	3456 x 2304	57	32mm	Auto	1/60	Took extra 17 images
4.16	3456 x 2304	72	32mm	f/11	A*	Extra 15 images stitch in - Good
A* = Automatic setting on camera						

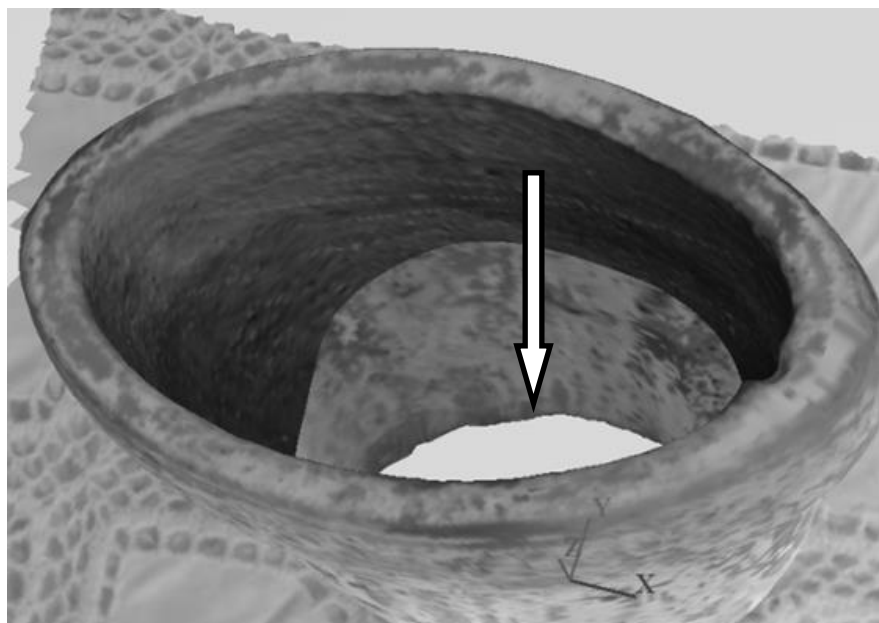


Figure 4.15: Initial processed image – Hole in bottom & side of vase.

Table 4.3 shows the camera data from three separate data capture sessions of the unglazed Vase. After processing the first 52 images the returned virtual image was seen to have a hole in its base (Figure 4.15).

Another 17 images were taken with greater emphasis on the inside of the vase. The software program allowed for manual addition of additional images, (see Chapter 6, Figure 6.7). After this manual addition, the new set of 72 images was resent, via the internet, to be cloud processed by Autodesk. This cloud process took from one to two hours depending on the speed of the internet connection and the computer CPU processor. This addition of images

cured the problem of the hole in the base as seen in the textured image Figure 4.16.

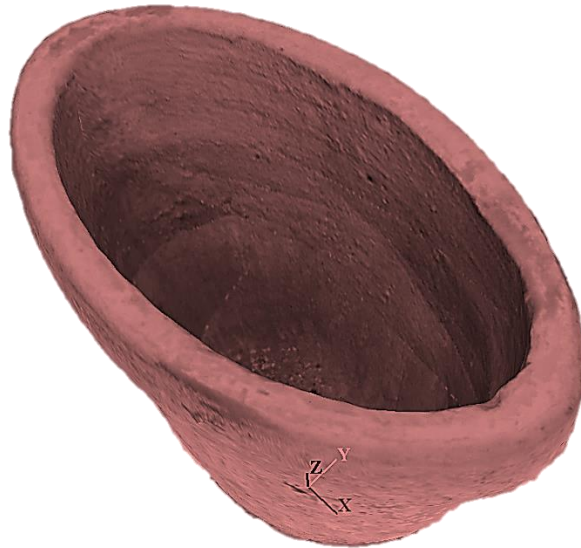


Figure 4.16: Hole removed from vase after an extra 15 images were added.

#### 4.2.3 China Figurine

Three attempts were made to photograph this 70mm high, 1920's porcelain figurine (Figure 4.17), using *123D Catch*<sup>®</sup>, but unfortunately without total success. Table 4.4 gives details of the digital image camera data of the china figurine.



Figure 4.17: Clean, crisp, sharp image of China figurine.

In the first attempt, 66 digital images were recorded and as seen, typically in Figure 4.17, all were clean crisp images, well focused. However, the internet cloud processing returned from *123D Catch®*, was unable to combine 13 of the images from the data sets.

Table 4.4: Camera data – China Figure.

Figure	Resolution	Images	Focal length	Aperture	Shutter speed	ISO	Result
4.17	3456 x 2304	Original digital image					
4.18	3456 x 2304	66	55mm	f/5.6	A*	100	Processed images – distortion
	3456 x 2304	72	55mm	A*	1/60	100	Extra 6 images
	3456 x 2304	59	48mm	f/14	1/10	400	Too Dark – <b>Not processed</b>

A\* = Automatic setting on camera

Typical faults were plumes and flare showing on the virtual images, as seen in Figures 4.18 to 4.20.



Figure 4.18: Textured 3D Mesh Image of China figurine.

On the second attempt a similar result was found on the return of the processed images from *123D Catch*<sup>®</sup>, and so, of the 72 digital images originally sent, 17 had to be “hand” stitched, and sent back for reprocessing (see Chapter 6.5.6, the Ceramic Vase). By examining the image closely of Figure 4.17, it can be observed that although the main subject, the figurine, is in sharp focus, the background is not. This technique is often used in photography to emphasise the main subject, by decreasing the DoF, so that the background becomes blurred, with the effect of forcing the subject forward into the viewer’s conscious vision.

But identification of matching points, as required by the processing software on the background, has been made difficult, if not impossible. The third attempt resulted in all 59 images being rejected as too dark to process.

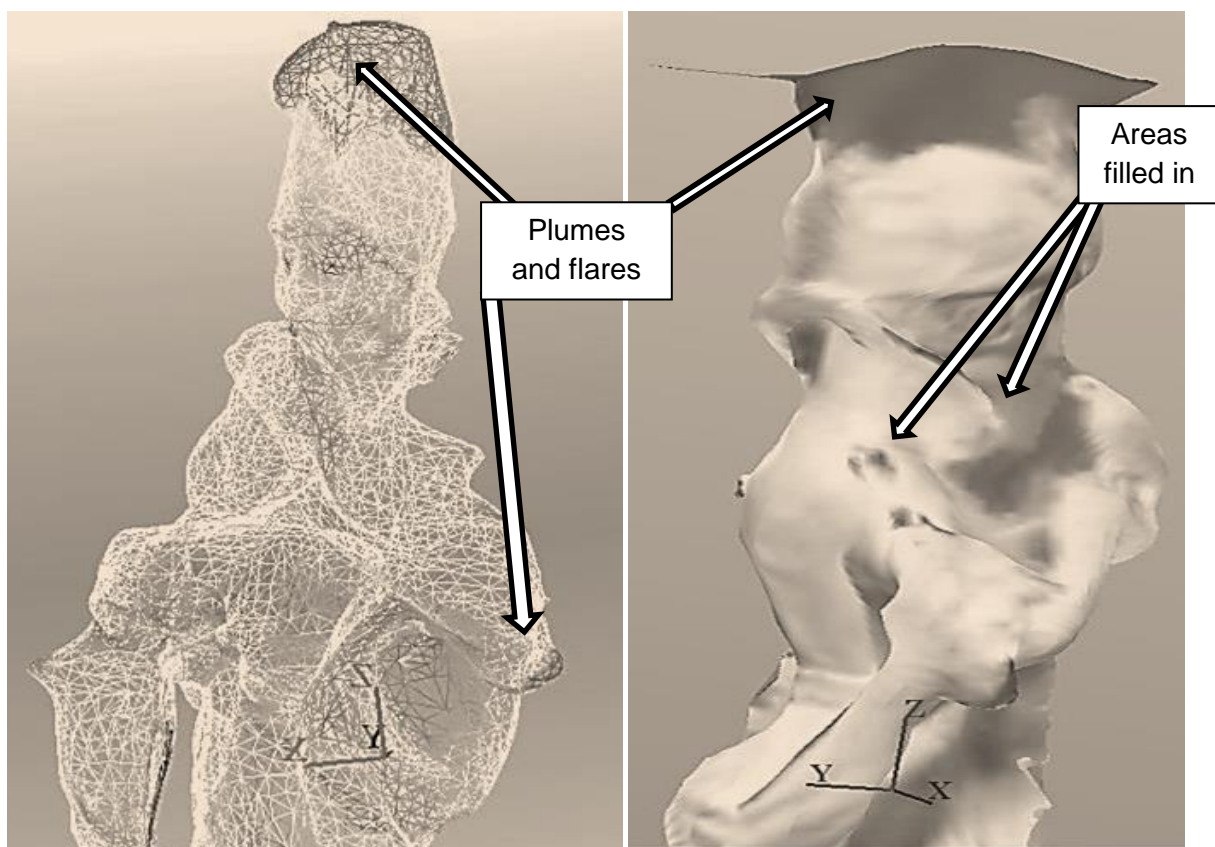


Figure 4.19: China figurine - Point cloud 3D mesh.

Figure 4.20: China figurine - Dark shadows and plumes.

It can be seen from Table 4.4, that the aperture was stopped down too much for the available light, in the hope of countering the reflective glare of the figurine, and constant slower shutter speeds were needed. This attempt rendered the

images too dark and therefore the data set was rejected by the software and not processed.

#### 4.3 Data Chart and Image Library – processed with 123D Catch®

For brevity, only the average or final data has been tabulated in Table G.1: Appendix G, ‘*Data Chart – Images processed using 123D Catch®*’ as some objects such as Figure G.08, ‘Mollusc’, were tried 5 times without success, with several attempts at photo stitching being attempted, whereas two attempts were made on Figure G.15, ‘Fat Clay’ pot, both producing good results.

Table. 4.5: 24 items processed using 123D Catch®.

*The results of the 26 items processed using 123D Catch® were as follows:-*

- 7 - FDM models were made
- 5 - models waiting to be made
- 7 - models too distorted to proceed
- 2 – models with detail too fine to be made on FDM
- 3 - models too large to be scaled down and show detail
- \* FDM model made
- \*\* FDM model waiting to be made
- # detail too small to be made
- ## Too much flare causing distortion on image

Seven models were manufactured using an FDM machine, with a further five models with \*.stl files completed see Table 4.5. For the full list of images and image numbering (numbered with prefix G), will be found in Table G.2: Appendix G, “*Photographic images, size and material*”. All these models were processed with the minimum of computation, there was no CAD reconstruction or alteration to the point cloud image or the photo-textured mesh; this eliminated the need for software experts, one of the main objectives of the research.

There are obvious exceptions in which the DSLR camera cannot compete, as in the example of the Magnetic Resonance Imaging scanning of the Egyptian mummy by Steele and Williams [61].

The three case studies that are cited in this chapter were selected because all showed similar characteristic faults which were present through most of the data collection sessions. The remedies which were applied were also typical of the simplicity in repairing any of the 25 items processed. Photo stitching, as in the 'Clay Head' and 'the Vase' (examples one and two, Figures 4.8 and 4.14), contributed to the final success by the additional of eleven more images, and there were some objects that needed even more additional images to achieve good results.

However, there were causes which could have been subjects for elimination in a future series of photographic images. In example 3 (the figurine Figure 4.17), the small dark areas on the upper side of the figurine (see Figures 4.18 to 4.20), may have been the result of highlight reflection of the shiny surface of the glazed porcelain.

The series of images used in the set of photographs for the china figurine were viewed close up. As the figurine was very detailed, picking out identifiable points was also difficult – the result possibly being that the image was therefore rejected by the software and not stitched into the main group of photographs. This resulted in a degrading of the final photo-textured 3D mesh image, producing a dark plume or shadow as seen on the tops of the head/hat and upper body, in Figures 7.18 to 7.20, as the computer software compensated for what it could not see or identify. By using ND filters and controlling, to some degree, the amount of diffused top lighting, the problem was not resolved, nor did setting the camera aperture to a mid-range f/8 or f/11 to help to give a greater DoF to the images and so facilitate the stitching of images. This problem has been noted by several other researchers who are also looking for the answer to light flare reflecting the object being photographed [120] [164, 165].

#### **4.4 Creation of 3D Video**

It was then also possible to create and record a virtual 3D video within this primary digital software. By using *123D Catch*<sup>®</sup>, a video could be created by selection or rejection of the 60/75 photographic images in the path the images had taken. The software seamlessly converted the images selected into a moving 3D virtual representation. This Bi-product could be incorporated into a longer

company promotional video or, if short clips of several artifacts were joined together, could be used as part of a multi-media presentation.

The image Figure 4.21 is a diagrammatic representation of the camera positions:-

arrowed **A** – Camera position of the image, taken at that point;

arrowed **B** – expanded frame - pointing to the actual digital image;

**C** – the original photograph from digital sequence.

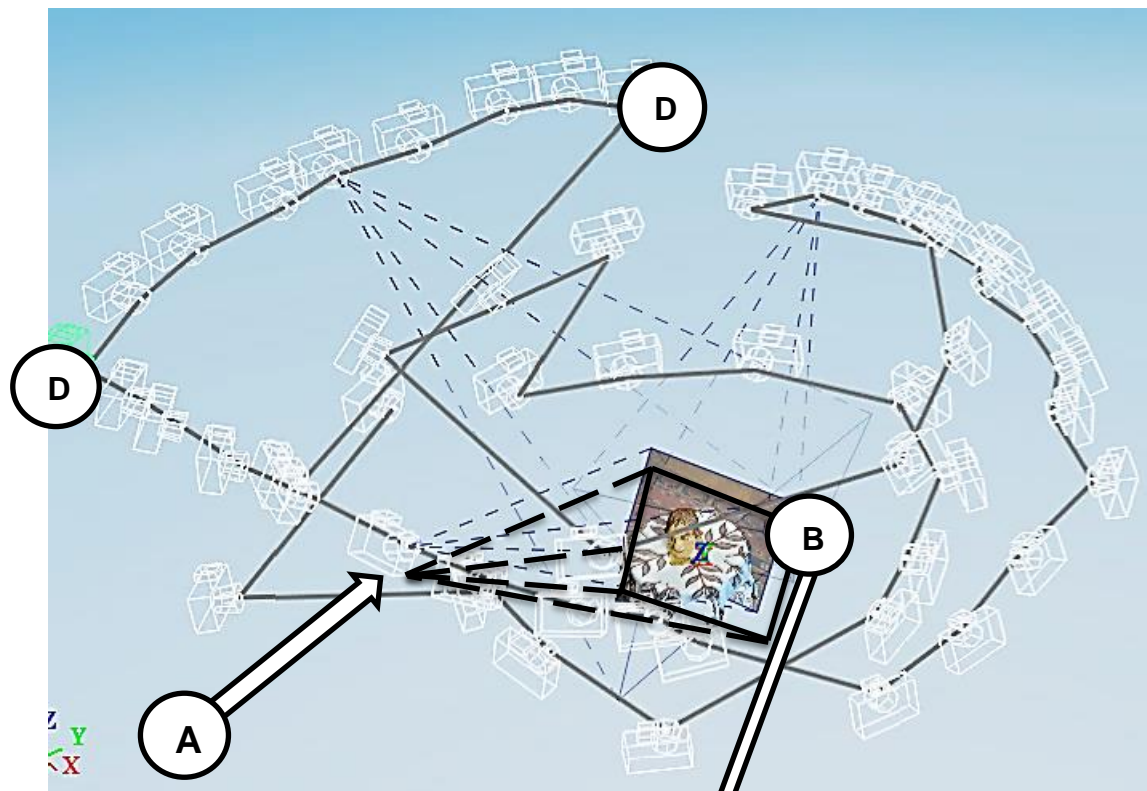


Figure 4.21: Vertical view of Video Map.

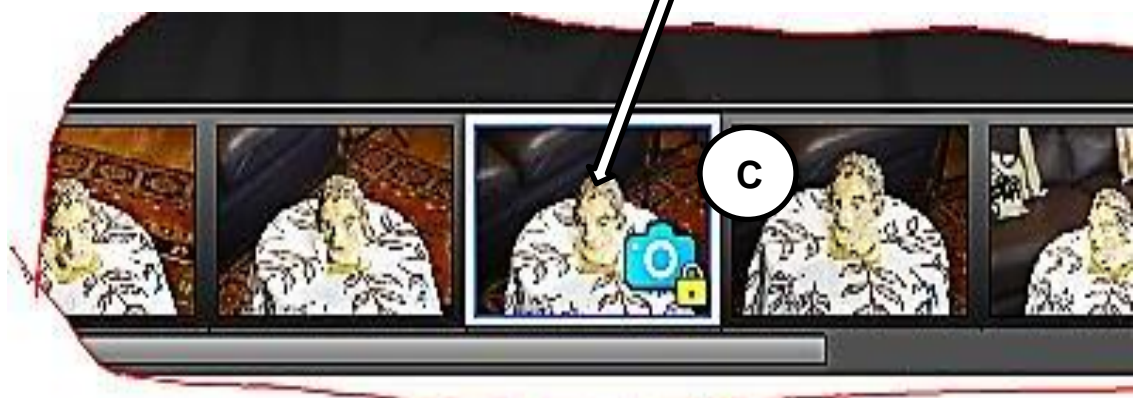


Figure 4.22: Enlargement of Figure 4.21 showing camera position and projected image of the tracking path produced by the software.

The darker grey line shows the video tracking path. Point **D**, represents the end of a series of cameras positions, and would be interpreted as a very sharp change of direction to another lower or higher level. By eliminating these corners, a smoother effect was obtainable as seen in the last diagrammatic screen shot (Figure 4.23).

The time lapse between each camera angle could be controlled and the final edited video was saved in a variety of formats ready to be imported into a documentary type movie or as a promotional video with voice commentary and music if required. The dark grey line linking each camera position (shown in small white outlines) represents the camera “tracking” path. The software allowed for the user to select and eliminate each camera position so as to smooth this tracking path as seen in Figure 4.23.

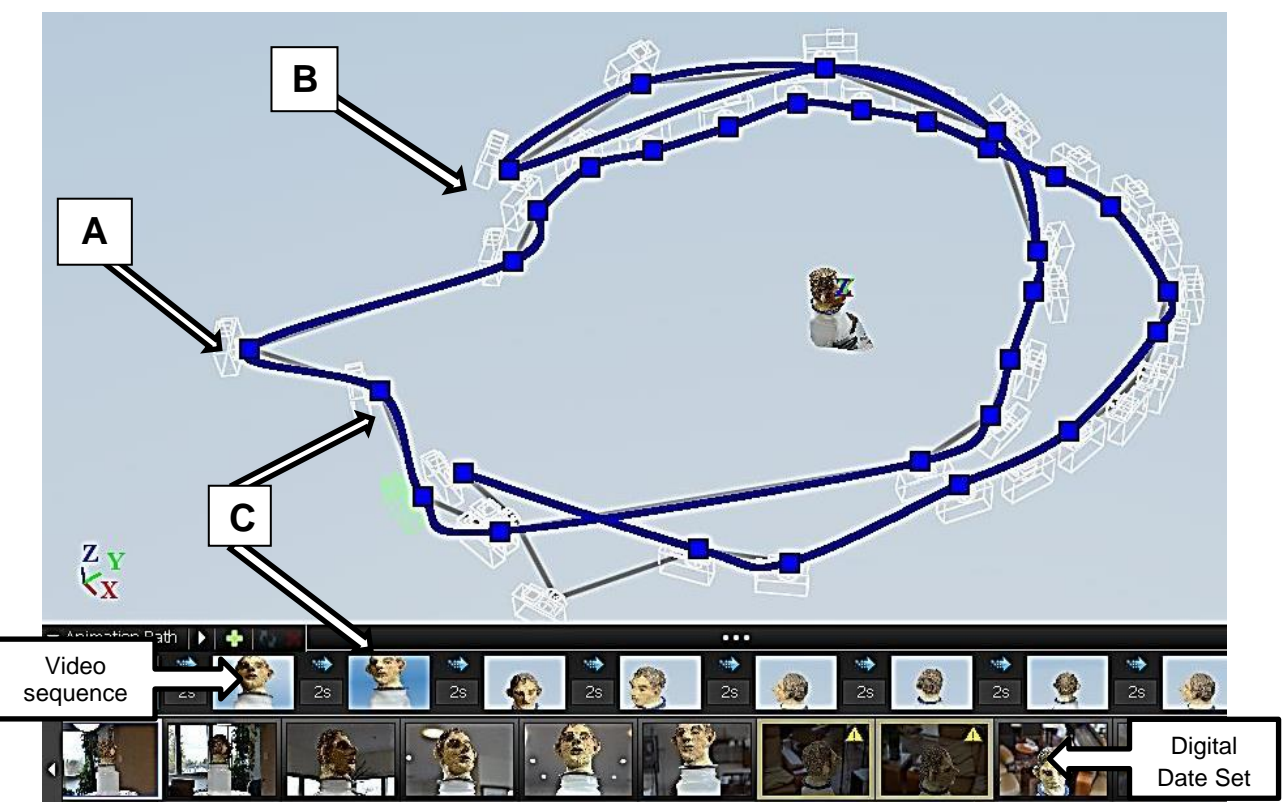


Figure 4.23: Changes that can be made to video path.

The top photographic sequence represent the images which form the video clip and the lower sequence are the original digital captured images which have been processed to form the 3D virtual model. In the above diagram Figure 4.23, points **A** and **B** represent frame positions shown in the upper line of images **C**,

some of which might very well be eliminated so as to smooth the video path even more than from the original track shown in Figure 4.21.

## 4.5 Summary

The AutoDesk software was commercially launched as freeware, aimed at the entry level AM market. Over the last few years AutoDesk has increased the portfolio of software programs that link into and work alongside *123D Catch*<sup>®</sup> such as *123D Make*<sup>®</sup>; *123D Sculpt*<sup>®</sup>; *123D Design*<sup>®</sup>, to mention just a few. As well as the free software, a fee paying licence version is now available giving additional options and tools. Hardware options also now exist to acquire 3D printers and other types of machines within the framework of this technology. Full descriptions are not within the remit of this research but can be found on AutoDesk 123D website.

*123D Catch*<sup>®</sup> has been used and reviewed in numerous research papers, as well as in this research, where it was used to process 24 objects, with mixed results, as described within this thesis. Table G.3: Appendix G, “*Capture Data Log – 123D Catch*<sup>®</sup>” contains all the day to day record and evaluation as well as photographic data of 24 artifacts. As a basic software program, it had limitations, in that it was an internet based automatic processing program with little user control. In this research, the other software programs in the Autodesk portfolio were not accessed, as they were added at later dates and therefore outside this remit, which looked only at the free, stand-a-lone software available at the start of this research, which was *123D Catch*<sup>®</sup>. Nevertheless, the video facility was found to be useful and novel, especially if used for promotional or educational applications.

## 4.6 Method 2

### 4.6.1 Light Tent technique

The second method of digital data capture used a collapsible Light Tent, as used in the Kendal museum workshop and seen in Figure 3.19 or as in Figure 3.24 in the author’s living room, its’ construction as previously discussed in Chapter 3.7.1. In Figure 4.24, the light tent was placed in an undercroft, and although the flood lights are seen in the photograph, during the daylight hours the flood lights were not used as the natural light was shadowless but quite bright. In this setting,

the natural light coming from the window behind (unshaded) helped to counteract any shadows. These examples demonstrate how versatile the light tent was, and although it took time in putting it up and taking it down, it was a very useful tool in the data capture process.

The light tent used to capture the Ammonite data was similar to Figure 3.20, in that the white linen cover was not used. In an alternative scenario, the light tent was placed in a *Naya* and as the natural light in this semi outdoor/indoor environment was very soft, only a small amount of “fill in” artificial light was needed. However a contrast green backdrop was used to enhance the contrast with the yellow/greyish coloured Ammonite.



Figure 4.24: Turn table and green Chroma Key backdrop.

In Figure 4.24 a turntable can be seen which was used to revolve the artifact around 360°. The camera was stationary, only being moved up or down in the vertical plane for every complete revolution of the subject.

As highlighted in the beginning of this chapter, only a selection of the total 24 artifacts that were processed, are discussed: those that shared a common method, both in photographic technique, or in problems that arose. The light tent was used in the process of digitally capturing images of artifacts from antiquity to the modern day: a 3,500 year old Egyptian figurine; an Ammonite fossil; stones

found in the garden; and vessels, ancient and modern. All the artifacts in this section were processed using AgiSoft's *PhotoScan Pro*® as the primary processing software. These files were then imported into *StudioPro*® (Chapter 5) to produce the \*.stl file which the AM machine required in order to print the replications. Most of the models that were made using this technique were then processed on a 3D Systems *DTM Sinterstation*®, Selective Laser Sintering (SLS) machine, in a plain white Nylon 12 (Polyamide).

#### 4.6.2 Standard Data Capture using *PhotoScan Pro*®

As seen from Figure 3.23 in Chapter 3.8 in the “open room” system of data capture, the main subject, in this case the clay head, was in a static position and the camera was rotated at a distance of approximately 1.2 to 1.5 metres away. With the light tent system of data capture, depending on the artifact’s size, the camera was placed much nearer the subject. The artifact was then rotated on a turntable between 10° and 15°, as each frame was shot, Chapter 3.4.2, Figure 3.13. This method also allowed for small objects to be photographed with the use of close-up ring lenses which screwed onto the front of the camera’s prime or zoom lens (Chapter 3.3.1).



Figure 4.25: The Egyptian Vase on the turn table.

In Figure 4.25 an original 3,500 year old Egyptian Vase can be seen on the turntable at Kendal Museum, ready to be photographed using the standard Nikon 18/55mm DX® lens. Depending how complex in design the artifacts were, up to 144 images were captured, rotating the turntable either 10° or 15° for each frame.

#### 4.7 Depth of Field

Being much nearer the subject increased the criticality of the focusing and the DoF became far more important; the closer the lens to the subject, the shallower the DoF became. Shooting at f/5.6 to f/9 in an open room became f/18 to f/22+ in a light tent. These smaller apertures required increased illumination on the subject or required longer timed exposures.

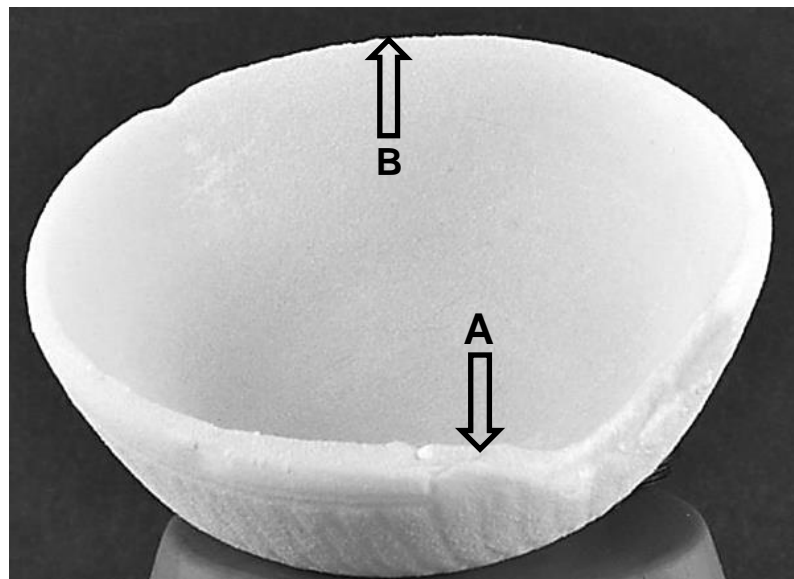


Figure 4.26: Results of out of focus images on an SLS fabricated Bowl.

On examining the bowl in Figure 4.26, a small shift in the circumference of the rim has caused the SLS model to skew. One side was thicker than the other side; the thicker side arrowed **A**, the thinner side arrowed **B**. The correct thickness is seen in the front of the bowl in Figure 4.27, tapering down from the rim to a thicker section of the body, half way down.



Figure 4.27: SLS fabricated Bowl using *PhotoScan Pro*<sup>®</sup>.

It appears that the *123D Catch*<sup>®</sup> processing software was able to match and process the model even though there was a mismatch due to a slight blurring to one side of the bowl, but the resulting model was lopsided. This was caused by the DoF being too shallow in this set of data images.

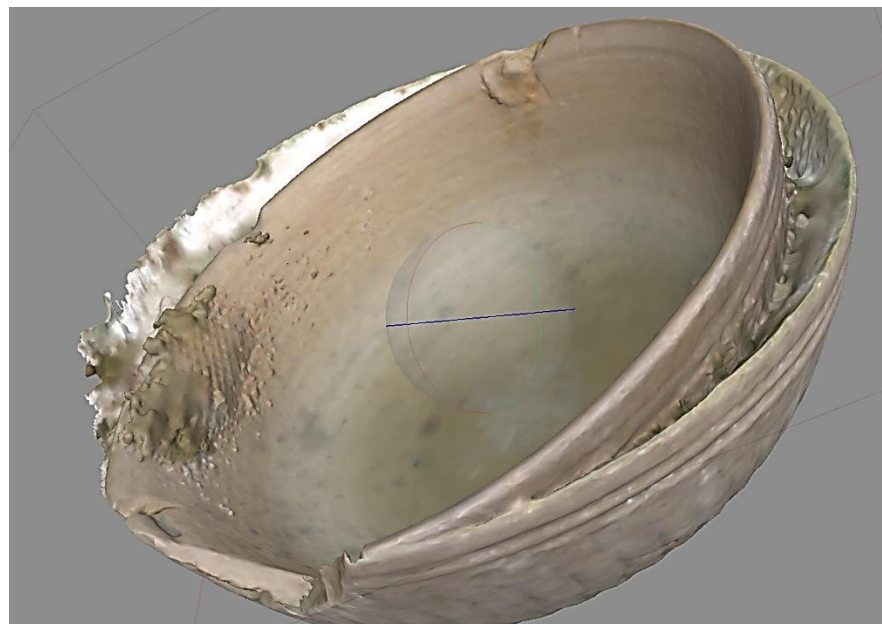


Figure 4.28: Bowl - Double point cloud image, caused by initial out of focus data.

However, the Agisoft *PhotoScan Pro*<sup>®</sup> software would not tolerate this slight blurring in the data set, and it responded by producing a double image (see Figure 4.28). The software tried to compensate for the error and filled in the gap (see Figure 4.29). Although lopsided, it was still possible to produce a \*.stl file and a physical SLS model, the lopsided result is seen in Figure 4.26.



Figure 4.29: Bowl - A texture point cloud “Fur” infill created by computer.

It was only after the author had several failures photographing this bowl, and decided to send the data set of 130 images to Agisoft for their examination that they spotted this slight blurring (out of focus) in the original photographic set and suggested a much smaller aperture, producing a deeper DoF, which produced sharper images.



Figure 4.30: Egyptian Bowl - Stitching of images c/o Agisoft.

With their expertise, AgiSoft's technicians were able to take the data set of images that had been sent to them and digitally stitch the images together, matching seven main points.



Figure 4.31: Screen shot of completed textured point cloud Egyptian bowl.

Fortunately this difficult repair technique was not required with any further images processed with *PhotoScan Pro*<sup>®</sup> (see Figure 4.30). These new, improved, in focus images, were then processed and the result was a perfectly shaped reproduction of the original Egyptian Bowl. In the photograph of the reproduced bowl, the rim is equal all around the top of the circumference (see Figure 4.31).

#### 4.8 Lens Diffraction

Figures 4.32, 4.34 and 4.35 show how important DoF is when processing the dataset to create the 3D image. If the aperture is stopped down<sup>9</sup> too far another anomaly can occur, lens diffraction, which can distort the photographic image recorded by the camera. There is a vast amount that has been written on the subject both in photographic books [166] [167], magazines and on the internet [168]. Lens diffraction is an optical effect caused by light waves spreading, dispersing or “diffracting” as the light waves pass through the aperture in the camera. This can have an adverse effect on the resolution of the digital image. The dichotomy occurs as the smaller the aperture that is used, the sharper the image becomes and depth of field increased.

---

<sup>9</sup> The expression “stopped down” is a term used to indicate a reduction in the aperture setting, or increasing the f/stop number thereby decreasing the amount of light entering the lens.



F/5.6



f/8



f/11



f/18



f/22



f/32

Figure 4.32: Contrasting sharpness between f/stop images.

However, with too small an aperture, a softening or blurring of the image can occur. At this stage the camera has become diffraction limited. There are Diffraction Limit charts and calculators [169] that assist the camera operator with these problems, but if in doubt a test can be conducted to establish if diffraction will cause a problem. Before taking the full set of images, a series of photographs can be taken, changing the f/stop each time to find the lowest one for the sharpest image (see Figure 4.32). Both the extreme images f/5.6 and f/32 in the set of six images, in Figure 4.32, are softer and not as sharp as the rest of the images. The f/5.6 aperture is too open (not enough DoF) and the f/32 aperture is too small caused by diffraction.

In the latest versions of PhotoScan Pro7 (v1.3.2/4205 – 64 bit) that was used, there is a “Quality” function in the “Photo” menu which will scan the dataset that is about to be processed and grade the quality of each image in an arbitrary scale from 0 to 1. If the score of an image falls below 0.5, it is advised by Agisoft not to use the image (see Figure 4.33).

Photos						
Label	Size	Aligned	Quality	Focal length	F-stop	ISO
DSC_0007.JPG	3456x2304		0.307131	55	F/5.6	100
DSC_0008.JPG	3456x2304		0.667857	55	F/8	100
DSC_0009.JPG	3456x2304		0.697779	55	F/11	100
DSC_0010.JPG	3456x2304		0.692618	55	F/18	100
DSC_0011.JPG	3456x2304		0.671456	55	F/22	100
DSC_0012.JPG	3456x2304		0.63805	55	F/32	100
DSC_0013.JPG	3456x2304		0.619251	55	F/36	100

Figure 4.33: The “Quality” results of the scanned images.

In the six photographs shown in Figure 4.34, all the images except the first, f/5.6, are above 0.5 on the scale as shown in Figure 4.33. The middle three images, f/11, f/18, and f/22 have the highest rating. The images seen in Figure 4.34 have been enlarged to show more clearly the softening or blurring caused by either the large aperture (f/5.6) or the aperture that is too small (f/32). As noted by a contributors on the Agisoft-on-line Forum [170], values used in the camera settings for photogrammetry, may not be valid for usual photography.



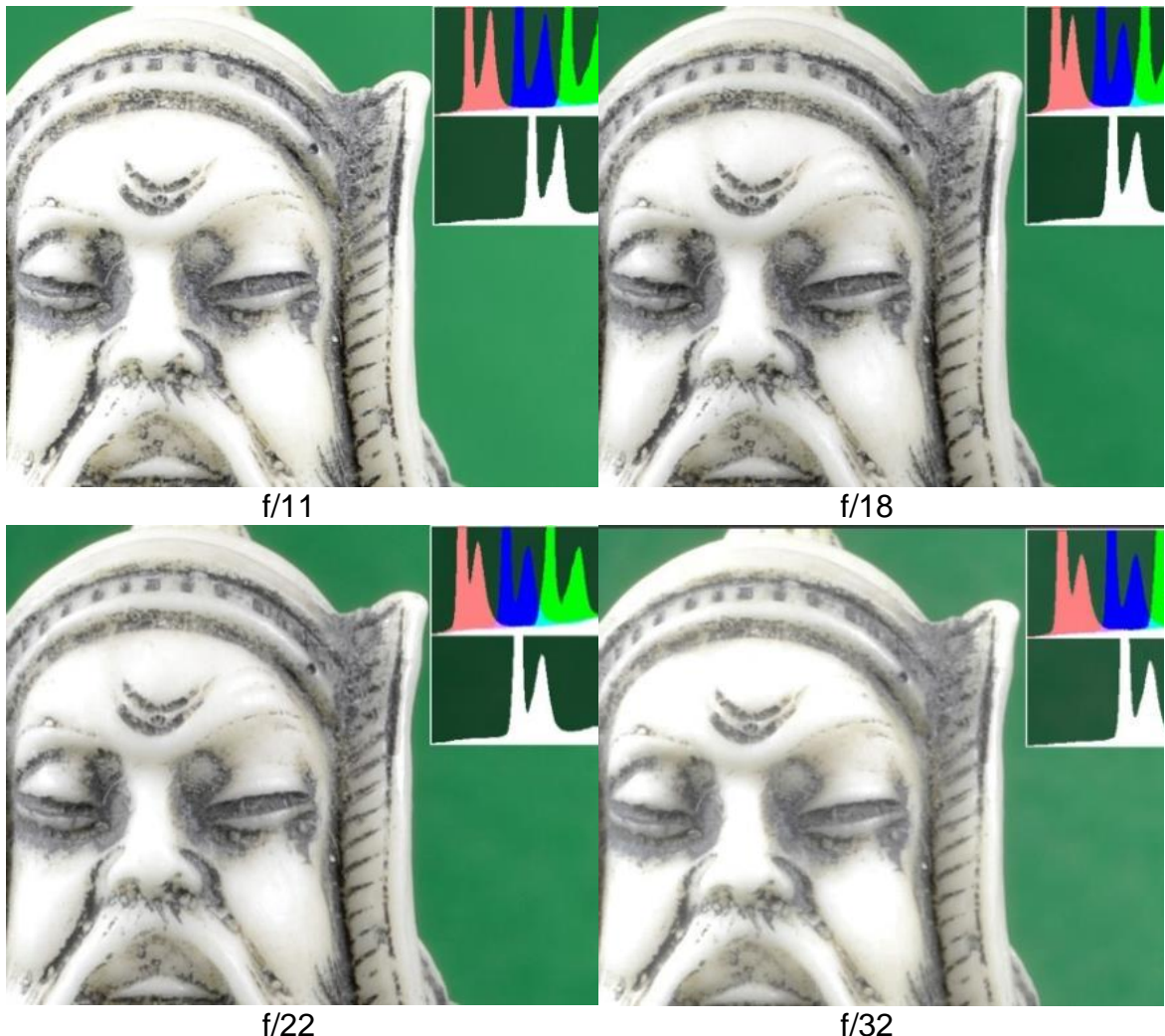


Figure 4.34: Enlarged images to show difference in sharpness.

The camera settings are a delicate balance between the a ISO value, the smallest aperture value, a long shutter speed and keeping the highest luminosity so as to produce the sharpest images for *PhotoScan Pro*®, or any other prim software, to process. There can be no hard and fast rules as each operator's equipment may differ; the best rule perhaps is to test and compare results for any given scenario.

#### 4.8.1 Histograms

Histograms and their use can be useful in showing graphically the tonal range of pixels in a photograph and can be used to edit with great precision the digital image [171]. These histograms are shown in the right hand side of each image in Figure 4.35 (screenshot from Adobe *PhotoShop CS6*®) and Figure 4.36 (screenshot from Adobe *PhotoShop Elements 11*®). Both programs show similar

information but CS6 is more spread-out. Some image editing software may show a very basic graphic image in which only Red, Green and Blue (RGB) channels are shown [172]. Most software also has the facility to show the dark and light tones - the highlights, midtones and shadows - whilst the more advanced software will have additional colour channels such as Cyan, Magenta and Yellow [145].

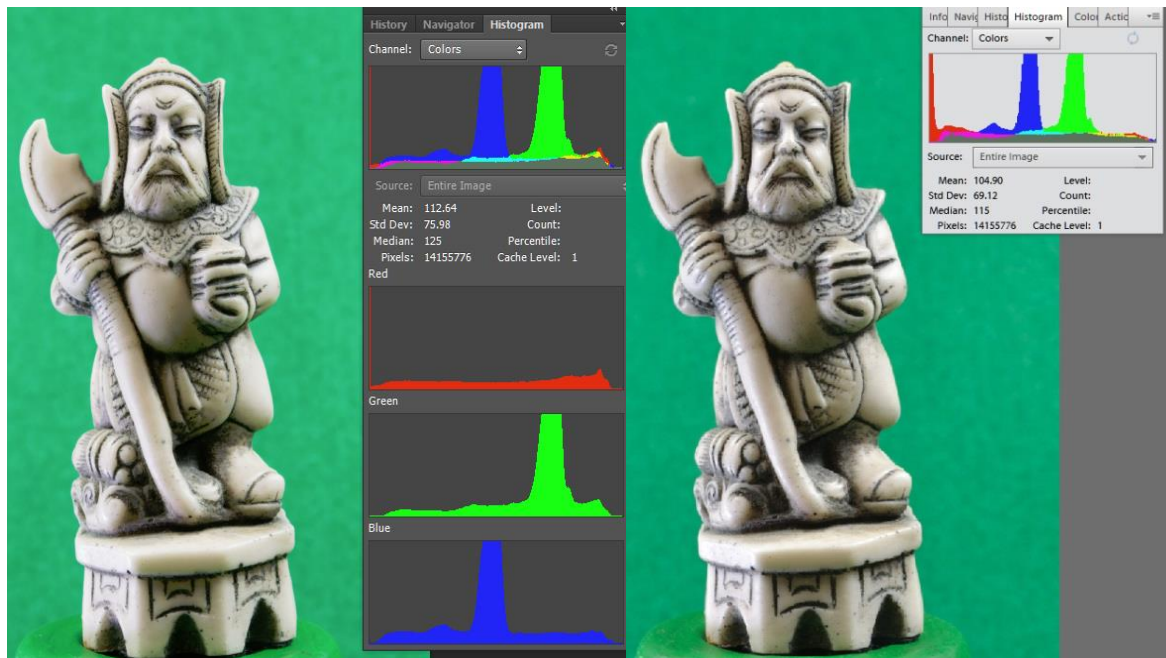


Figure 4.35:  
Histogram - PhotoShop CS6®.

Figure 4.36:  
Histogram - PhotoShop Elements 11®.

Many digital cameras also have a histogram facility in the “playback” mode and this is useful to determine and assess how an image has been exposed [142]. Depending on the camera make, this may differ from digital editing software histograms. Figure 4.37 has been taken from the Nikon User Manual and explains the symbolic images and information that appear in the screen on the back of the Nikon camera. In the histogram diagram taken from the Nikon manual (Figure 4.37) the colour distribution in the Red, Green and Blue scale as well as other information is shown. In Figure 4.34 the brightness of each image is also shown (lower histogram) and at first glance all seem similar. However, on closer examination it can be observed that each histogram is different and there are subtle differences between the colour distribution scales as well as the white scale. These scales give a visual guide to the change in tonal values when editing an image.

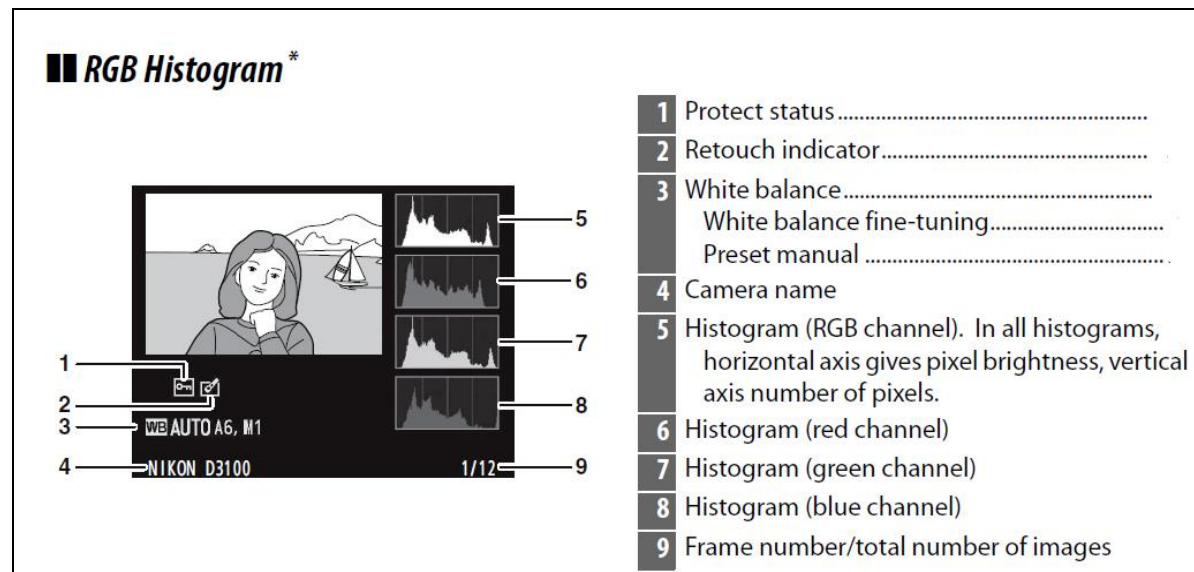


Figure 4.37: Nikon User Manual explanation of RGB Histogram [143].

It has been shown despite the potential problem of diffraction caused by stopping down the aperture too far, lens diffraction should not cause undue problems. This is on condition that a series of tests are undertaken to determine at what point image distortion occurs and how small the f/stop can be. This must be determined for each camera and lens combination, before a full dataset of digital images are taken.

As with many of the photographic processes and editing tools, it must be understood that the objective is not to produce a beautiful coloured printed image which is to appear in a glossy, expensive magazine, or hang in a national photographic gallery or museum, or a family grouping to be displayed on the domestic living room wall. Such utilisation seeks to perfect the visual image and as such may come under greater scrutiny. In such cases, if the original image is enlarged, many image defects may be visible to the viewer. However, photogrammetry in relation to reverse engineering is about achieving a set of images which satisfy the requirements of the software, software which can scan the image and reject unsuitable images, and which transforms the digital pixels into a point cloud image. This in turn produces a 3D model of the original artifact that is within the fabrication limitations of the AM machines being considered.

#### 4.9 Software control – semi automatic

In this method, the software was considered semi-automatic. It allowed far more control, by the operator, over how the data was processed. Instead of processing

the data via the internet, as with the examples in the first part of this chapter, it could be processed on the same machine, without the use of the internet, as long as the host computer had an i5 or preferably i7 CPU with a minimum 12GB memory.

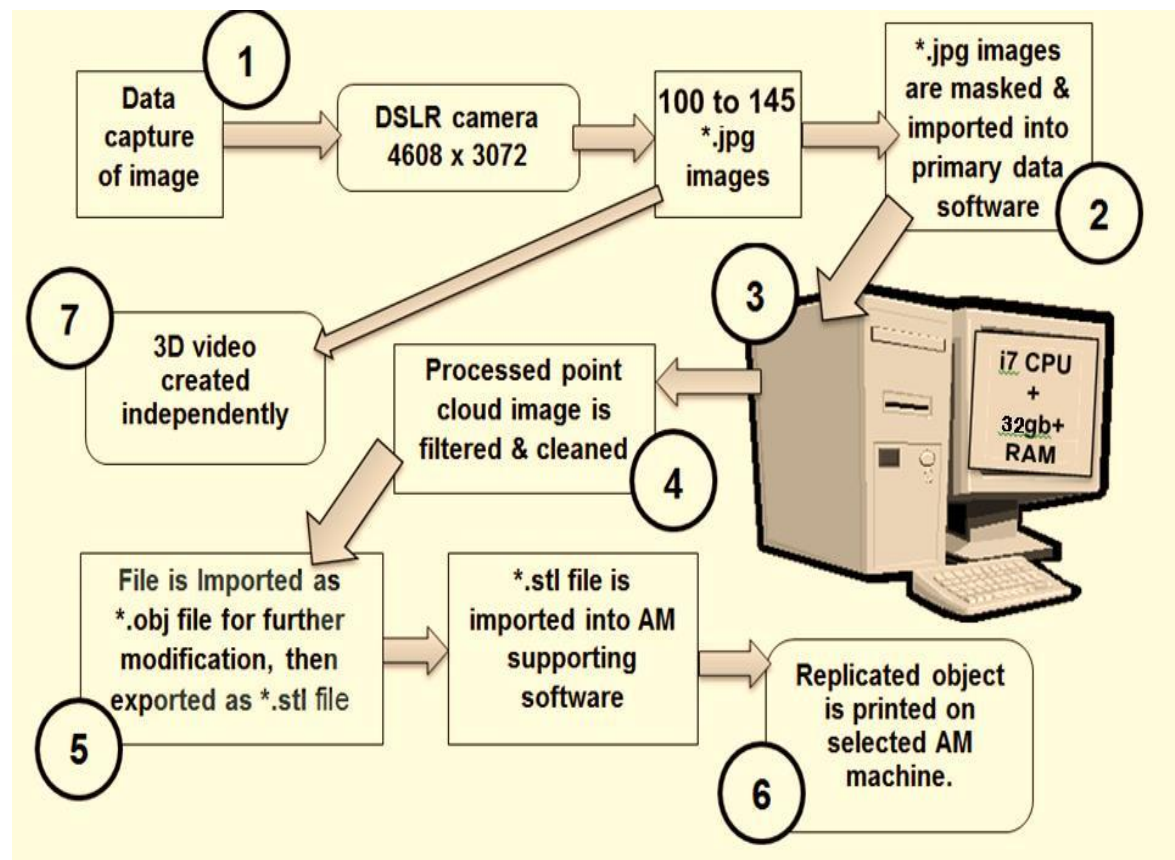


Figure 4.38: *PhotoScan Pro®* Data processing Flow Chart.

The author upgraded the computer to 32GB of memory before *Ultra High* scanned data could be processed. In Figure 4.38, the Flow chart is very similar to that in Method 1 (Figure 4.5) but unfortunately the Agisoft software did not support the creation of an independent video, although there was no requirement for internet connectivity for data processing with *PhotoScan Pro®*. The software was more demanding to use than *123D Catch®*, because it was not fully automatic, but the interface and icons employed were straightforward and easily learned. Unlike *123D Catch®* it only used the subject image and not the background to stitch the digital images together to produce a data point cloud image.

#### 4.10 Pre-Process Masking

Editing by the user began at this early stage of the process. But first, for best results, before processing the data, each image was masked from the surrounding background. This masking was possible using a built in tool in the software, as can be seen in Figures 4.39 and 4.40, the Egyptian Vase.

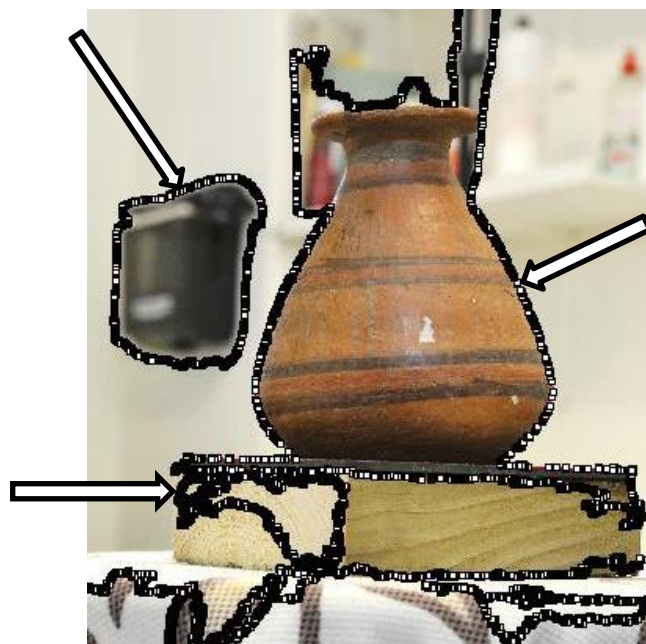


Figure 4.39: Complex masking line without Chroma Key backdrop.



Figure 4.40: Simplified masking operation when backdrop is used.

Experimentation with inter-changeable Chroma Key backdrops was undertaken; this type of backdrop provided a very good contrast between the main subject matter and its surroundings. Before the data set could be processed, each individual photo frame was masked so as to outline the subject.

It was found that the time taken to mask each digital image was considerably quicker with the use of a single plain coloured Chroma Key background. The photographic frame in Figure 4.39 is without the Chroma Key backdrop, and masking became a much more complex operation than in Figure 4.40 which used the backdrop. In both frames the masking line is arrowed.



Figure 4.41: Non-masked images of the Egyptian Vase – pre-processing.

The more RAM that was available, the faster the digital data could be processed, and the more detail that was forthcoming.

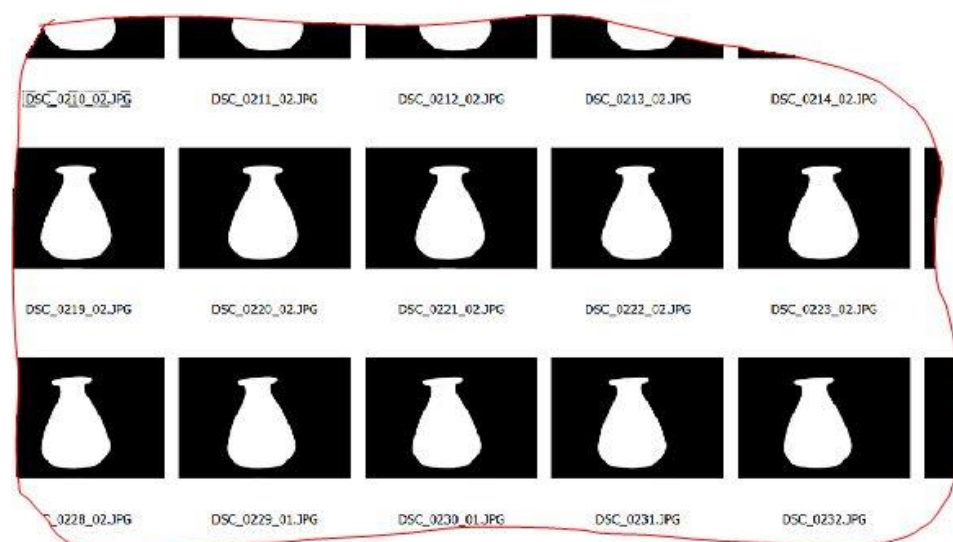


Figure 4.42: Masked images of the Egyptian Vase – pre-processing.

Figure 4.41 shows 10 non-masked images which formed part of a 130 digital data set that were shot for the Egyptian Vase, whilst Figure 4.42 shows part of the masked set, which the software uses to stitch the images together. *PhotoScan Pro*® was considered as being semi-automatic software, that is, it allowed the user some freedom to manipulate the digital image as it was being processed.

#### 4.10.1 Alternative uses for Pre-Process Masking

In the following two examples, a Concrete Mix block (Figure 4.43) and a Sea Shell (Figure 4.44), both items which had been placed on the turn table, needed additional support so as to photograph them in the best possible positions, so as to record as much data as possible. This support was provided by thin wooden sticks as seen in Figures 4.43 and 4.44. Both were photographed in an upright position with a supporting wooden stick pushed, as in Figure 4.44, into the shell, or as in Figure 4.43, supporting the back of the concrete block. Both images, Figure 4.43 and Figure 4.45, are from the data sets of images which were then masked, as described above, before being processed by the software. Masking frames are used by the software to build the final 3D images.



Figure 4.43: Original image – part of image data set of Concrete Mix.



Figure 4.44: Original image of Sea Shell.



Figure 4.45: Positive masked over sea shell support.

By examining the virtual point cloud image at each stage of processing, of which there were four, the possibility of elimination of part of the newly created point cloud virtual image was possible. Having removed the pixels, the software proceeded to the completion stage.



Figure: 4.46: Negative mask of sea shell.

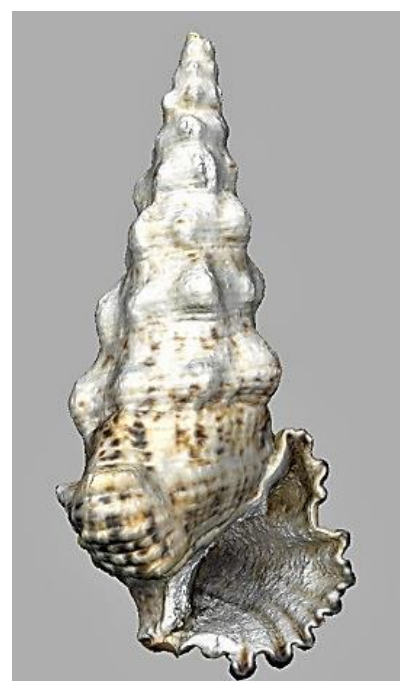


Figure: 4.47: Final textured shell.

Figures 4.45 and 4.46 show the original images having been masked, the positive and negative of the same image are shown. In the first of these images, the support can just be seen (indicated), in the negative/reverse image the wooden stick has been completely eliminated and only the cutout on the base of the shell are seen, the entry points to the shell are arrowed. The last image is of the final textured Sea Shell without the supporting wooden stick (Figure 4.47). The Concrete Mix block has been treated in much the same way except the masking of the wooden sticks cuts out data from the digital image (Figure 4.48).

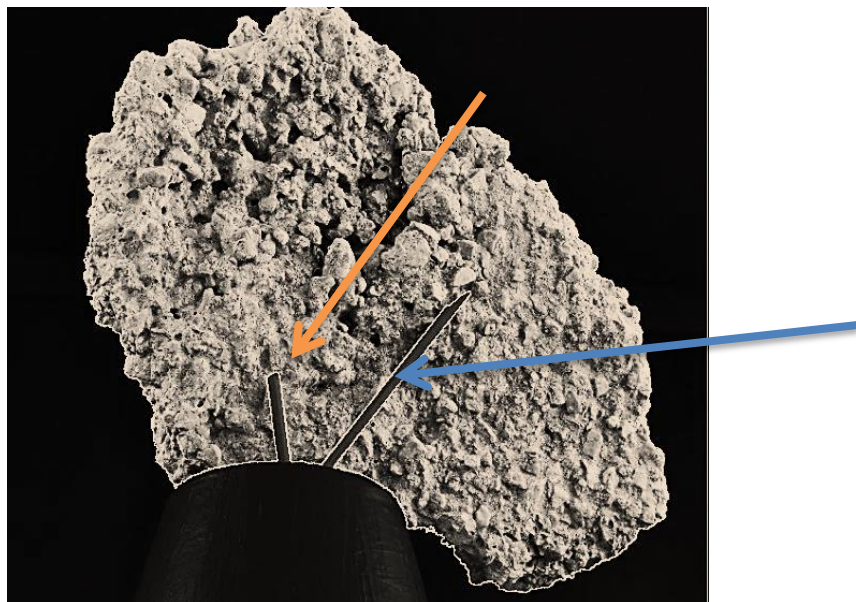


Figure 4.48: Positive mask image of Concrete Mix.

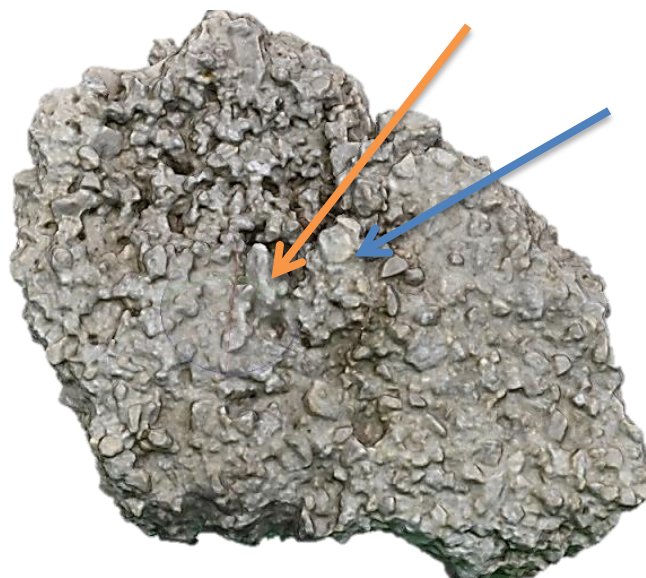


Figure 4.49: Final textured dense cloud image of Concrete Mix.

However, as can be seen from Figure 4.49, the software has compensated for this lack of data and the stones merge in to fill the void left by the masked out wooden sticks. Although the orientations of both of these images are not identical, in the center of Figure 4.48, it is possible to identify and match some of the larger stones onto the image on Figure 4.49.

The oldest and most valuable artifacts to be photographed and replicated using the light tent method were from The Kendal museum collection which was established in 1796, as a '*Cabinet of Curiosities*'.



Figure 4.50: Sobekhotep seen in center of light tent on turn table.

Three objects from the collection were initially chosen: a small bowl, approximately 120mm diameter and 45mm high (Figure 4.31), a vase 120mm high and 100mm diameter (Figure 4.42) and a statuette of Sobekhotep, son of Nehesy<sup>10</sup>, approximately 200mm high. In Figure 4.50, is the limestone figure of Sobekhotep (from the second Intermediate Period, Abydos, Tomb 537A'08, which dates to around 1500BC, and was a very important and rare figurine within the Kendal museum collection) on the turntable ready to be photographed. "This is a very important and rare figurine which represents Sobekhotep, son of Nehesy, an official who lived at Abydos during the Second Intermediate Period. The figure is somewhat crude, showing Sobekhotep wearing a round wig and a kilt, standing with the left foot forward, and has been carefully painted. The back

<sup>10</sup> Inscribed figurine excavated by Garstang from Tomb 537 at Abydos, donated in 1923 by Ruskin to Kendal Museum

pillar preserves a hieroglyphic inscription, which shows that Sobekhotep's sister Kemet gave the statuette of her brother as an offering to the god Ptah-Sokar-Osiris:

*"A boon which the king gives (on behalf of) Ptah-Sokar-Osiris, that he may give offerings to the Ka of ... Sobekhotep the justified, begotten of Nehesy, by his sister who causes his name to live ... Kemet" (Snape 1994: 310).*

Sobekhotep may have been a soldier, and so his sister may have dedicated the statue of her brother after he died in active service and was buried at Abydos (Snape 1994: 312) [75].

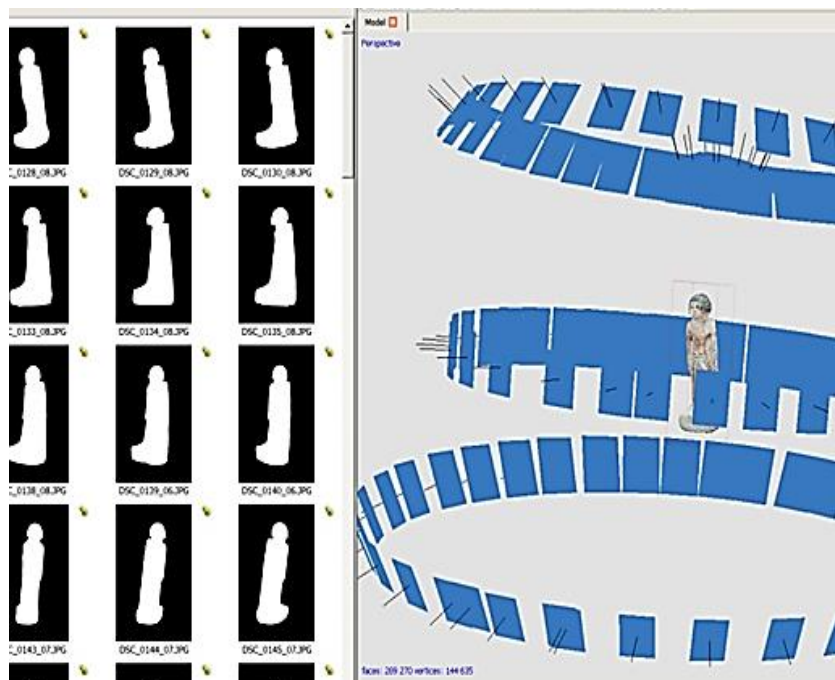


Figure 4.51: Screen shots of masked images and view of camera positions.

The method of geometric data capture was the same for all these items. In the case of Sobekhotep, the maximum amount of detail was required not just in the silhouette but also of the hieroglyphics that had been written down the sides. The camera was positioned in one of four elevations, for each data set, being higher, lower or on the same plane as the subject being photographed at elevations of 20° to 30° to the horizontal. This ensured that every part of the object was recorded and that a good overlap of images was obtained, the artifact being in the centre always at the same elevation.

In Figure 4.50, the camera can be seen close up to the subject, depending on the artifact's size, allowing for small objects to be photographed. If necessary a close up lens could be fitted. For each object on the turn table, a rotation of 10° would produce 144 images, but if more detail was thought to be required an extra 10 images would not increase the processing time significantly. On the other hand a simpler artifact needing less digital information might have been rotated only 15°, producing up to 96 images, also allowing for a few extra shots if thought necessary.



Figure 4.52: Photograph of Sobekhotep, son of Nehesy.



Figure 4.53: Sobekhotep – High resolution point cloud image.

Being nearer the subject, the focusing and the DoF became far more important, increasing criticality of the focusing. As the lens moved closer to the subject, the shallower the DoF became but by increasing the f/stop to f/18 or f/22+ this problem was overcome, however one must be aware that at such small apertures there is the possibility of a loss of image sharpness due to diffraction. At this small aperture increased illumination on the artifact or a longer time exposure is required. Although the images seen in Figure 4.51 are the masked

negatives, the subject matter, Sobekhotep, filled each frame. The images in the frames were not cropped or altered in any way as to do so would confuse the software in the processing stage and distort the stitching process. The detail that is shown in Figure 4.52, an original photograph, can be seen quite clearly in the final processed screenshot of the high resolution digital images (Figures 4.53 and 4.54). The file of this image, a \*.obj file, was now ready to import into *StudioPro*<sup>®</sup> to produce the \*.stl file required for the non-colour AM machine. If colour printing had been available the file would have been imported into DeskArts' *3Data Expert*<sup>®</sup> to produce the \*.wri file.

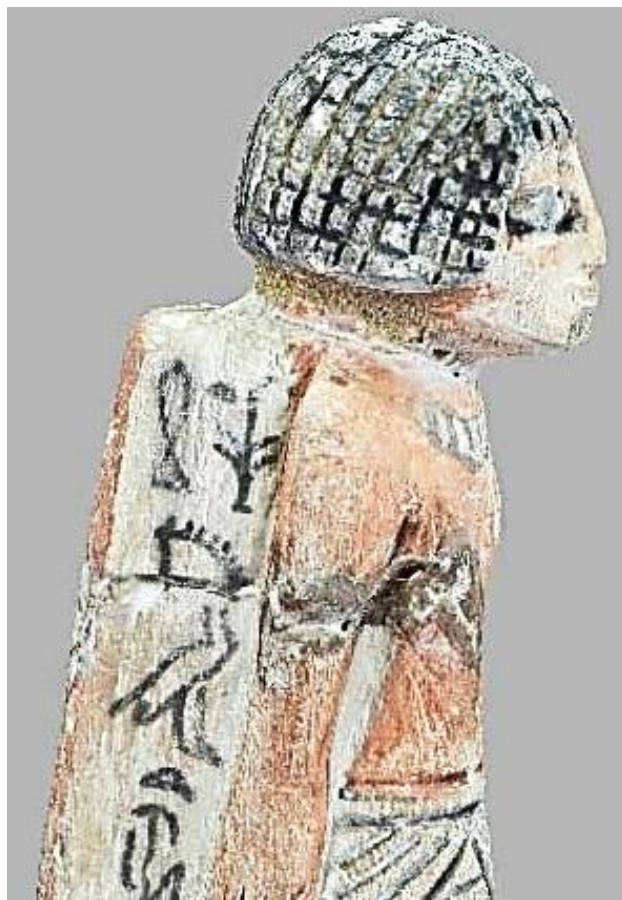


Figure 4.54: Sobekhotep - Enlarged detail of high resolution image.

#### 4.10.2 Digital Photographs, Point Cloud and Polygon Images

The mesh which forms the outer skin of the 3D model, as shown in the high resolution image in Figure 4.54, was created from the cloud point data in the *PhotoScan Pro*<sup>®</sup> process. This is a three part process based on a multiview reconstruction of the digital photographic data taken by the camera in the original

shoot, as shown in Figure 4.51. In the first part (“Align Photos”) the software identifies and estimates the camera positions and alignment, identifying common matching positions on the image captured, forming a “sparse” point cloud data image. This sparse point cloud, which is the first stage of the process, can be exported into other third party software and used as a 3D reference model (see Figure 4.55).

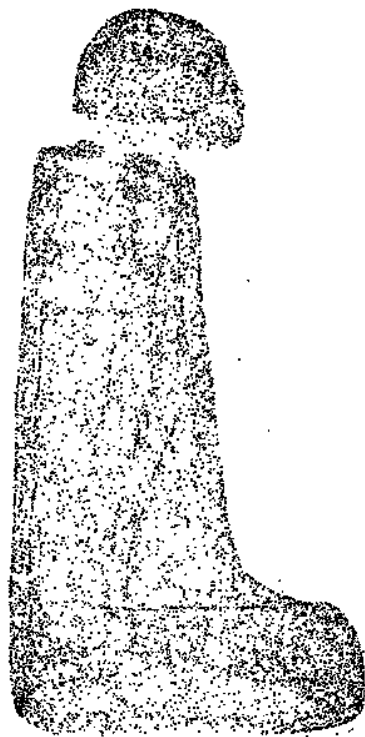


Figure 4.55: Sparse point cloud – 13,639 points.

In the second stage, as seen in Figure 4.56, (Build Dense Cloud) the software builds on the sparse cloud data using the estimated camera position data and the photographic image data, building a “dense” cloud image. Whereas the sparse cloud point data may be thousands of points, the dense cloud data is in the millions. As discussed in section 4.10, *PhotoScan Pro*<sup>®</sup> allows the user to specify five densities of cloud points: Ultra High, High, Medium, Low or Ultra Low. The decision on which density to use impacts on the equipment available, the processing time taken, and the resolution of the mesh created. This in turn results in the detail created and replicated in the final 3D model.

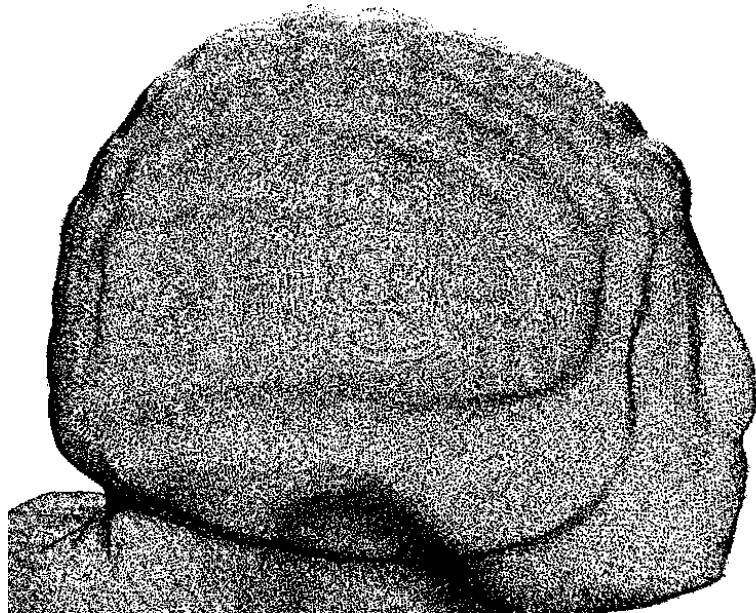


Figure 4.56: Medium Build Dense Cloud -1,044,192 points.

It is only during the “Build Dense Cloud” process that the software uses the GPU, as can be seen from the section taken from the “Workflow Log” (Figure 4.57), where not only is the CPU used, but unless the GPU card has built in RAM, the action will fail to proceed or become so slow that the machine will stop working. This was experienced by the author before upgrading both CPU RAM and the GPU card. The alternative working of the CPU and GPU has been highlighted for clarity in Figure 4.57.

The log records the number of points in the cloud that have been processed/created for each device (Device 1 is the CPU and Device 2 the GPU). In this instance the image that was being processed at “High Density”. The time taken for this section is also recorded. The Device 1 and Device 2 performance information shows that for the calculation for the depth map stage of processing, the Device 2 (which was the new GPU card) was processing at about 4 times the speed of the CPU card. Due to some changes in the processing algorithms, Agisoft have since removed this information on the newer versions of the program [173]. This section initializing at 10.00.25 and finishing in just over two hours at 12:08:07

```

2017-02-04 10:00:25 Initializing...
2017-02-04 10:00:25 initializing...
2017-02-04 10:00:26 selected 138 cameras from 138 in 1.638 sec
2017-02-04 10:00:26 Loading photos...
2017-02-04 10:00:33 loaded photos in 7.083 seconds
2017-02-04 10:00:33 Reconstructing depth...
2017-02-04 10:00:34 [GPU] estimating 895x2074x160 disparity using 895x1037x8u tiles, offset -84
2017-02-04 10:00:34 [CPU] estimating 822x2113x192 disparity using 822x1057x8u tiles, offset -85
2017-02-04 10:00:35 timings: rectify: 0.234 disparity: 0.811 borders: 0.25 filter: 0.156 fill: 0
2017-02-04 10:00:35 [GPU] estimating 936x2055x128 disparity using 936x1028x8u tiles, offset -19
2017-02-04 10:00:36 timings: rectify: 0.234 disparity: 0.608 borders: 0.281 filter: 0.265 fill: 0
2017-02-04 10:00:37 [GPU] estimating 909x2054x128 disparity using 909x1027x8u tiles, offset -20
2017-02-04 10:00:38 timings: rectify: 0.265 disparity: 4.009 borders: 0.188 filter: 0.093 fill: 0
2017-02-04 10:00:38 timings: rectify: 0.234 disparity: 0.64 borders: 0.281 filter: 0.14 fill: 0
2017-02-04 10:00:38 [CPU] estimating 863x2079x192 disparity using 863x1040x8u tiles, offset -109
2017-02-04 10:00:39 [GPU] estimating 839x2076x192 disparity using 839x1038x8u tiles, offset -74
2017-02-04 10:00:40 timings: rectify: 0.281 disparity: 0.889 borders: 0.281 filter: 0.156 fill: 0
2017-02-04 10:00:41 [GPU] estimating 760x2088x256 disparity using 760x1044x8u tiles, offset -56
2017-02-04 10:00:42 timings: rectify: 0.265 disparity: 1.092 borders: 0.249 filter: 0.156 fill: 0
2017-02-04 10:00:43 [GPU] estimating 739x2137x288 disparity using 739x1069x8u tiles, offset -33
2017-02-04 10:00:43 timings: rectify: 0.265 disparity: 4.306 borders: 0.14 filter: 0.172 fill: 0
2017-02-04 12:05:51 [GPU] estimating 664x1338x192 disparity using 664x1338x8u tiles, offset -79
2017-02-04 12:05:51 timings: rectify: 0.188 disparity: 3.244 borders: 0.155 filter: 0.095 fill: 0
2017-02-04 12:05:51 [CPU] estimating 1619x937x192 disparity using 810x937x8u tiles, offset -62
2017-02-04 12:05:52 timings: rectify: 0.187 disparity: 0.312 borders: 0.187 filter: 0.109 fill: 0
2017-02-04 12:05:52 [GPU] estimating 709x1421x192 disparity using 709x1421x8u tiles, offset -51
2017-02-04 12:05:53 timings: rectify: 0.141 disparity: 0.374 borders: 0.156 filter: 0.078 fill: 0
2017-02-04 12:05:55 timings: rectify: 0.141 disparity: 3.619 borders: 0.172 filter: 0.171 fill: 0
2017-02-04 12:05:56 [CPU] estimating 1629x1211x192 disparity using 815x1211x8u tiles, offset -35
2017-02-04 12:06:01 timings: rectify: 0.25 disparity: 4.867 borders: 0.124 filter: 0.094 fill: 0
2017-02-04 12:06:01 [CPU] estimating 1367x1322x224 disparity using 1367x1322x8u tiles, offset -161
2017-02-04 12:07:57 [CPU] estimating 515x1358x256 disparity using 515x1358x8u tiles, offset -57
2017-02-04 12:07:59 timings: rectify: 0.031 disparity: 1.56 borders: 0.11 filter: 0.031 fill: 0
2017-02-04 12:07:59 [CPU] estimating 580x1168x288 disparity using 580x1168x8u tiles, offset -105
2017-02-04 12:08:01 timings: rectify: 0.031 disparity: 1.857 borders: 0.124 filter: 0.016 fill: 0
2017-02-04 12:08:01 [CPU] estimating 709x1421x192 disparity using 709x1421x8u tiles, offset -65
2017-02-04 12:08:03 timings: rectify: 0.047 disparity: 1.747 borders: 0.11 filter: 0.078 fill: 0
2017-02-04 12:08:07 finished depth reconstruction in 7653.61 seconds
2017-02-04 12:08:07 Device 1 performance: 93.9739 million samples/sec (CPU)
2017-02-04 12:08:07 Device 2 performance: 419.511 million samples/sec (Pitcairn)
2017-02-04 12:08:07 Total performance: 513.485 million samples/sec

```

Figure 4.57: A section of “Working Log”.

In 2015 an American computer hardware specialist [174] recommended i7 CPUs and 128Gb RAM with GPU cards with a minimum of 4Gb on each card. In extreme cases, where very high numbers (i.e. in the hundreds) of images are to be processed, and very high 3D resolution images are required, as in some aerial surveillance scenarios, computers are required using a quad GPU setup each

with 12Gb on board, plus pairing of CPU's with 512Gb RAM to cope with the additional GPUs.

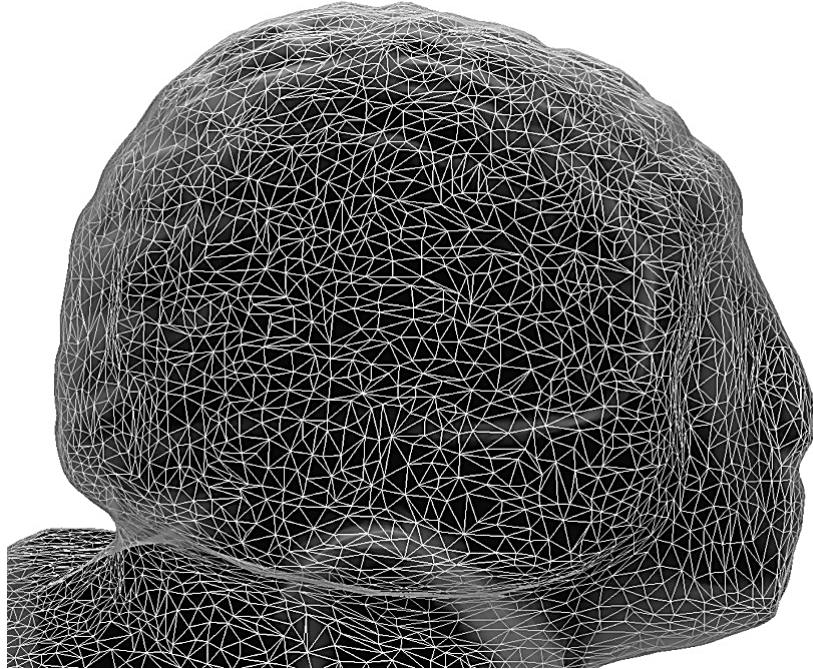


Figure 4.58:

Medium Build Polygon Mesh –  
69,862 polygons.

In the third stage of the process, “Build Mesh”, the 3D polygonal mesh is created, and depending on the density of the point count, a number of polygons or triangles are created, forming the surface detail of the 3D model (see Figure 4.58). This represents the original photographed object’s outer surface or skin, and is dependent on the original “Dense Cloud” or “Density Build” setting which can be changed by the operator.

Figure 4.58 has been created from the Medium Dense Cloud computation and the total polygons representing the whole Warrior total some 69,862, whereas the High resolution Dense Cloud image produced a point cloud count of 4,273,135 and a polygon count of 841,356. Enlarging the image to the same size as Figure 4.58, the polygons are too densely packed to be able to be individually distinguishable.

At this point, within the software program *PhotoScan Pro*<sup>®</sup>, there exists a simple editing section, whereby holes can be closed in the mesh, surface smoothed, detached or floating parts/debris removed and mesh decimation carried out. For further complex editing and manipulation, the file can be saved in a variety of formats and exported into programs such as was used in the thesis.

Having created the mesh, the final action is to build the textured image covering the surface of the model, creating a replica of the original artifact. The software does this by using the original photographs and, selecting the sharpest images to map the surface of the model, as shown in Figure 4.54.

#### 4.11 High and Low Resolution Images

As explained in the above chapter, the operator has a certain amount of control when using *PhotoScan Pro*®, in processing the final 3D point cloud image; but even this control was limited to the processing capacity of the computer. Guidi, *et al.* [113] discuss the control that the operator has over this software, a semi-automatic commercial program.

However, in processing a range of artifacts in this research, on average, the following factors played a key role in determining the time taken and quality achieved: the difference in the “Build Dense Cloud” function within the Agisoft’s software was determined by both the computer’s CPU and the Graphic card’s GPU - from Ultra High to Ultra Low (Figure 4.59).

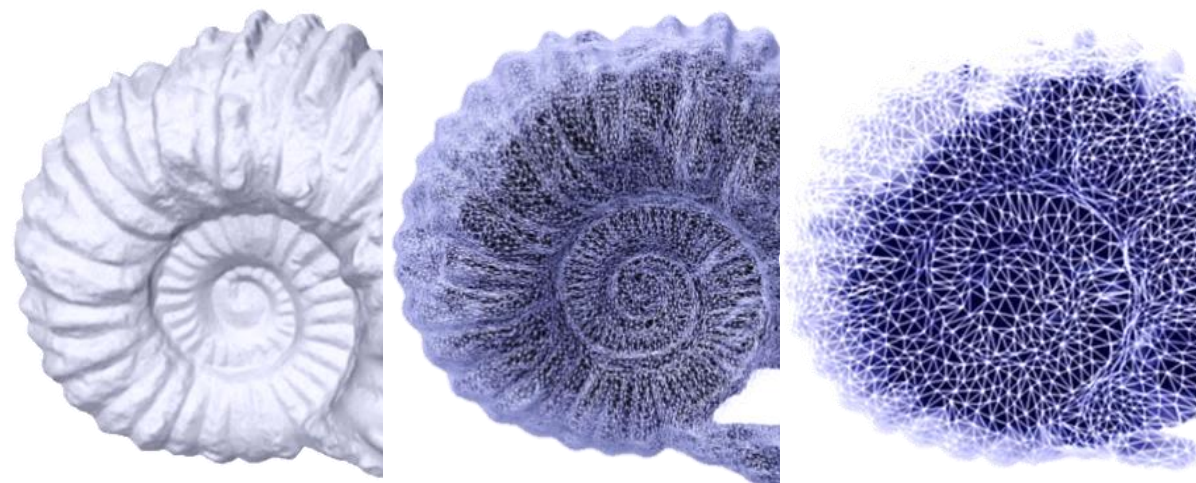


Figure 4.59: Three types of mesh – depending on the number of polygons created.

Ultra-High mesh

Medium mesh

Ultra-Low mesh

Table 4.6: Ammonite Fossil - wire mesh data.

Mesh type	Ultra-High	Medium	Ultra-Low
Polygons	4,846,416	527,150	460,304
STL file size	236,642 kb	25,740 kb	22,476 kb

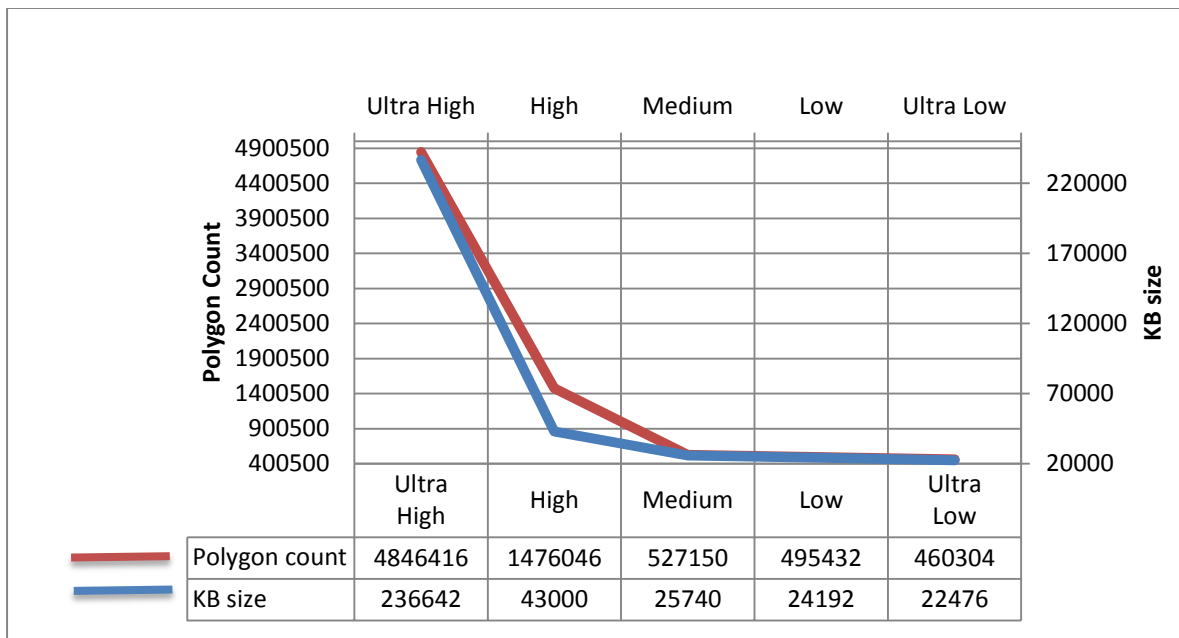
Mesh types vs Number of polygons vs Size of STL file.

Table 4.6 gives an indication as to the extra detail that is built into the mesh and the corresponding increase in file size, from Ultra-High to Ultra-Low resolution. The time factor and whether the CPU stopped functioning was due to the fact that an i7 CPU specification was being used; and whether the computer had 16MB, 32MB or more RAM, or if the GPU had additional RAM built in to the processor. Only the smallest of objects with a relatively simple profile, could be processed with 16MB RAM using *Ultra-High* setting.

Sections of this research were presented at the CIRP 25th Design Conference, and subsequently published in Procedia CIRP (see Appendix B) [121].

The processing times in the Ammonite fossil seen in Figure 4.59, increased from around 30-45 minutes for the Ultra-Low build (using 16MB RAM) to up to 6 or 8 hours for Ultra-High (using 32MB RAM), as well as increasing the size of the final STL file: which then was reflected in the quality of the AM build.

Table 4.7: Polygon Mesh count in relation to Kb file size.



Even with an i7 CPU, with only 16MB of RAM, in trying to build an Ultra High definition image, the computer ground to a halt within a very short time of a few minutes. The detail of the complex mesh which is formed is shown in Figure 4.60, being of Medium resolution. This ultra-high detail of the build was in itself controlled by the capabilities of the AM machine used, whether the machine could print in layers of say (typically) 100µm or (with recent advances) 16µm, or

even if the fine detail of an ultra-high resolution could even be printed on any of the current AM technologies.

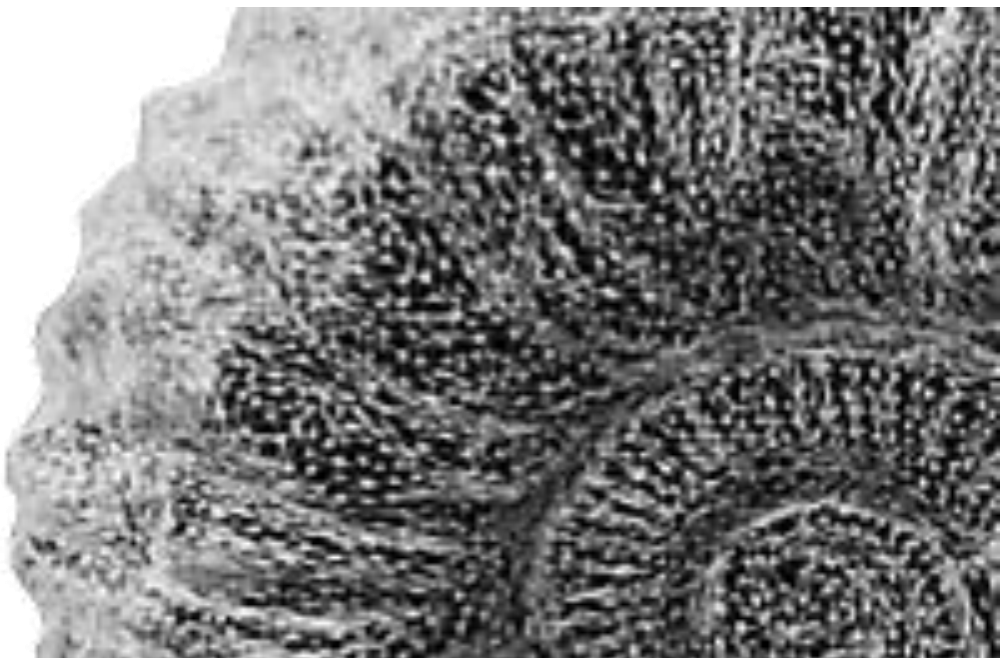


Figure 4.60: Section of polygon mesh enlarged from Medium resolution image.

Table 4.7 shows the huge increase in size of the \*.stl file, which was converted by *StudioPro*<sup>®</sup>, as the polygon count increased.

Table H.1: – Ammonite Data Sheet - “*Triangles (Polygons) size in relation to Kilobytes size of File*” see Appendix H, for expanded details.

Table H.2: - Ammonite Data Resolution Statistics “Processing 40 images with *PhotoScan Pro*<sup>®</sup> - *Mesh Statistics*”. See Appendix H, for comparative images.

#### 4.11.2 Print Problems Associated with High Resolution Data

The size, in Kb's, of the resulting \*.stl file, at the top end of the charts (Tables 4.9 and 4.10), was too large for most current AM machines to handle and therefore the polygon count had to be degraded or reduced. Using the current software that was at the disposal of the author at the time of the research, the data image was degraded. This would have been done by the software on a non-selective basis, i.e. the polygons, both on the outside and inside, would be reduced on an equal basis. This was far from ideal, as surface detail was inevitably lost from the original artifact to replicated model (Figures 4.61 and 4.62).

The replica was printed on an SLS machine in nylon and because of the large size (112mm x 65mm x 82mm high) it was more economical to have the hollow model cut in half, and printed in two sections rather than one whole object see Table 4.8.



Figure 4.61: Original Ammonite fossil.



Figure 4.62: Hand painted SLS replica.

There now exists a current generation of software, which unfortunately the author did not have access to, which will degrade the polygon count on a selective basis. Therefore the inside of the model could be reduced to meet the required Kb size, whilst the outside skin or shell would remain the same. This

preserves the detail which is so obviously important to maintain the integrity of the replicated model.

Table 4.8: Third Party Hollowed out Model Costs – August 2014

		H/L mm	W mm	D mm	Kb size	Poly count	Volume cm <sup>3</sup>	Density %	Shapeways	i-materialise	3DPrintUK.co.uk
G.12	<b>Large White Pot</b> Ceramics White Nylon 12	800		280					€ 15,415.97		
J.28	<b>Egyptian Bowl</b> Ceramics White Nylon 12 SandStone	44	112	112	9,926	203,282	66.31	12.65	€ 26.16 € 59.75 € 47.22	€ 41.25 € 80.00	
J.42	<b>Sobekotep</b> Ceramics White Nylon 12 SandStone	162	49	80	15,666	320,824	62.15	10.70	- € 52.84 € 44.42	€ 66.67 € 88.00	£72.71
J.43	<b>Roman Jug</b> Ceramics White Nylon 12 SandStone	134	86	90	25,001	512,000	155.89	15.88	€ 54.23 € 111.60 € 107.38	€ 71.86 € 115.20	
J.47	<b>Spanish Botijo</b> Ceramics White Nylon 12 SandStone	204	108	107	40,741 29,288	834,372 599,808	305.01	13.10	€ 100.98 € 205.09 € 207.55	€ 209.60	
J.50	<b>Concrete Mix</b> Ceramics White Nylon 12 SandStone	158	116	44	43,184	884,390	91.46	11.73	- € 71.70 € 64.08	€ 94.00 € 104.00	
J.51	<b>Whole Ammonite</b> Ceramics White Nylon 12 SandStone	112	90	41	72,073 25,740	1,476,046 527,150	67.81		File too Large	€ 70.89 € 92.80	
Half	<b>Half Ammonite</b> Ceramics White Nylon 12 SandStone	112	90	41	45,018	880,620	42.61			€ 44.89 € 68.02	
60mm sq	<b>Sq Ammonite</b> Ceramics White Nylon 12 SandStone <b>Utra polyamide</b>		60	60	23,157 45,439	474,234 930,582	24.40	16.87	€ 29.16 € 20.16 € 30.18	€ 27.86 € 12.01 € 15.82	
25mm sq	<b>Ammonite Frame</b> Ceramics White Nylon 12 SandStone <b>Utra polyamide</b>										
H.53	<b>Horus</b> Ceramics Green White Nylon 12 SandStone	181	54	72	36,598 17,054	749,524 349,262	76.60	10.90	€ 29.38 € 61.87 € 54.11	€ 80.06 € 97.60	£86.84
H.59	<b>Sq Frame</b> Ceramics White Nylon 12	275	205	15							

High or Medium definition

\*see Appendix G (Table G.1 and G.2) and Appendix J (Table J.1 and Table J.2)

This problem also exists if replication models are requested from third party fabrication companies, as there is usually an upper limit either on the polygon count or on size of file that can be uploaded to their servers. To overcome the downloading and fabrication problem, some companies now have software that will degrade the file before it is finally submitted to be fabricated. But, it does not overcome the problem of down grading the detail of the model, the information about which is being held within the high polygon count.

#### **4.12 Bench Marking the Models and Adapting to the Limitations of AM Technology**

There would be very little advantage in processing the data and obtaining a high resolution digital image if the AM machine that was being used to fabricate the model could not:

- a) accept and process the high kb. \*.stl file produced; or
- b) build the fine detail required in the model.

In such an instance, the only possible justification for the time taken and the cost of the higher specification hardware needed to process the data would be to use the digital 3D images for display purposes on a monitor, which in an educational environment would be a very good combined learning tool. Such decisions are obviously for the operator/educator to make before the second processing stage is undertaken in converting an \*.obj file to an \*.stl file. For example, the very specialised, Swiss made, Cytosurge *FluidFM*<sup>®</sup> 3µm micro-technology machine (FluidFM stands for fluidic force microscopy) introduced in the summer of 2017. This machine can print metal objects with a smaller diameter than a human hair. Also included is a list of web sites that publish yearly lists of “Top 10” reviewed printers.

Figures 4.63 to 4.66 show the four models (all enlarged to provide more clarity) from the data sets that were fabricated on a high resolution 14µm Stratasys *PolyJet J750*<sup>®</sup> printer with a layer resolution as fine as 14µm and accuracy as high as 0.1 mm. Figure 4.67 is the original photograph model (also enlarged) for comparison. These are from a section of the Warrior figurine that was used throughout this research. The first four images are from a photoshoot session where the data set was shot in RAW format. The last image is from the original

Camera Ready Jpeg data set that was first taken at the beginning of this research.



Figure 4.63:  
Ultra-High resolution **Jpeg** model.



Figure 4.64:  
Ultra-High resolution **Tiff** model.



Figure 4.65:  
High resolution - **Jpeg** model.

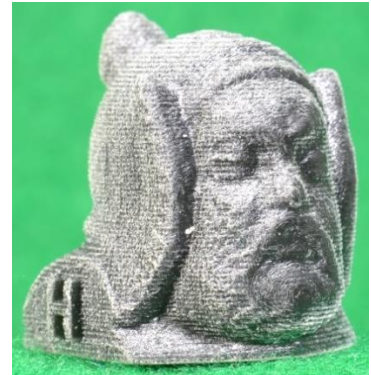


Figure 4.66:  
High resolution - **Tiff** model.



Figure 4.67:  
Original photograph of Warrior.



Figure 4.69:  
Original model size 25mm high.



Figure 4.68:  
**CR Jpeg** model.

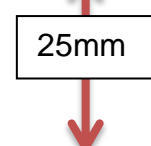


Figure 4.70:  
Fabricated model size 25mm high.



Figure .71: Bench mark model heads.

Model Number	File Type
1 -	<b>High -Tiff</b>
2 -	<b>High - Jpeg</b>
3 -	<b>Camera Ready - Jpeg</b>
4 -	<b>Ultra-High - Jpeg</b>
5 -	<b>Ultra-High - Tiff</b>

The RAW data set (which is discussed later in Chapter 9) was then processed into Tiff and Jpeg format and processed into five separate \*.stl files, Ultra-High to Ultra-Low, plus the original CR Jpeg file. Figure 4.69 indicates the actual size of the original model and Figure 4.70, fabricated model; both are shown in order to indicate the relative scale of the enlarged images Figures 4.63 to 4.66. In all, eleven heads were fabricated on the Stratasys *PolyJet J750*<sup>®</sup> and as a comparison one head (the CR model) was also printed on several other machines - full details can be seen in Table M.1 in Appendix M.

It can be observed from studying the four images Figures 4.63 to 4.66 that at such a small size, the perceived difference between the models is minimal, if any, and as the figures are so irregular in shape it would be very difficult to measure the slight irregularities between the Warriors' heads. The minimal differences are shown in the group of heads in Figure 4.71. If a more accurate comparison were needed, then one way might be to 3D scan each fabricated model and superimpose the results on top of a scanned image of the original Warrior figurine.



Figure 4.72: Medium resolution - Jpeg and Tiff models.

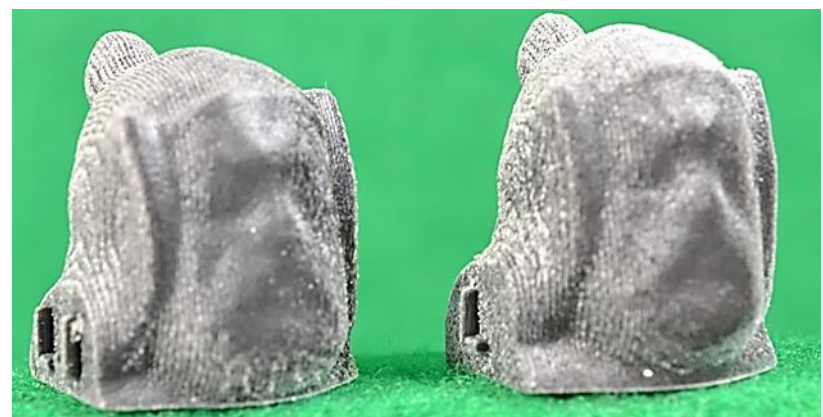


Figure 4.73: Low resolution - Jpeg and Tiff models.

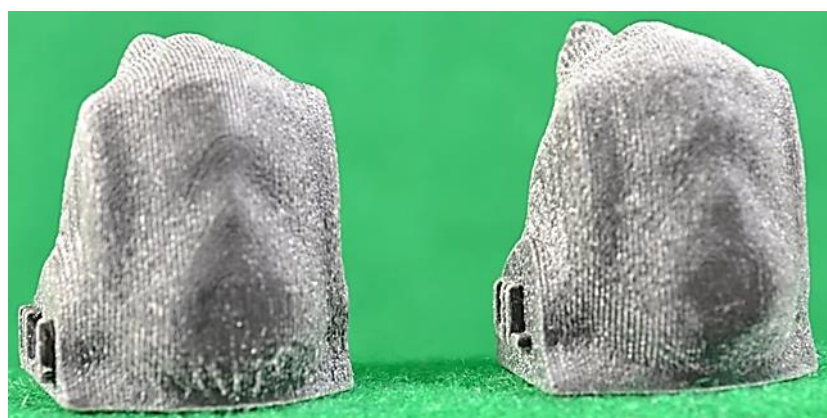


Figure 4.74: Ultra Low resolution - Jpeg and Tiff models.

But then other considerations would have to be factored in, such as monitor resolution, or if hard copy were required, 2D printer resolution, paper quality, ink quality etc.

Figures 4.72 to 4.74 show how the final 3D replicated models degrade as the processing resolution is downgraded in the Agisoft software. Both the medium resolution models in Figure 4.72 are just about acceptable for detail if

rapid prototype models are required, but as shown, the penalty is the loss of detail, though still giving the overall dimensions and look of the original.

The Low and Ultra Low renderings (Figures 4.73 and 4.74) in both Jpeg and Tiff models have lost all facial and hood detail, and in the Ultra-Low model the side hood “wings” have been partially integrated within the head. But if speed is paramount then just over 16 minutes for the Low resolution and 10 minutes for the Ultra-Low resolution was all that was required for the time taken for processing of the \*.stl file, ready to fabricate on an AM machine.

The greatest distinction between the models is the layer direction, which can be seen clearly comparing the UH Jpeg (Figure 4.63). UH Tiff (Figure 4.64) and the CR Jpeg (Figure 4.68). With small models such as the Warrior, it is purely a personal choice whether it is better to be built vertically or horizontally, but if a series of models are to be fabricated and kept together for comparison, as seen in Figure 4.76, then it would be aesthetically better if the grain is the same on all models.

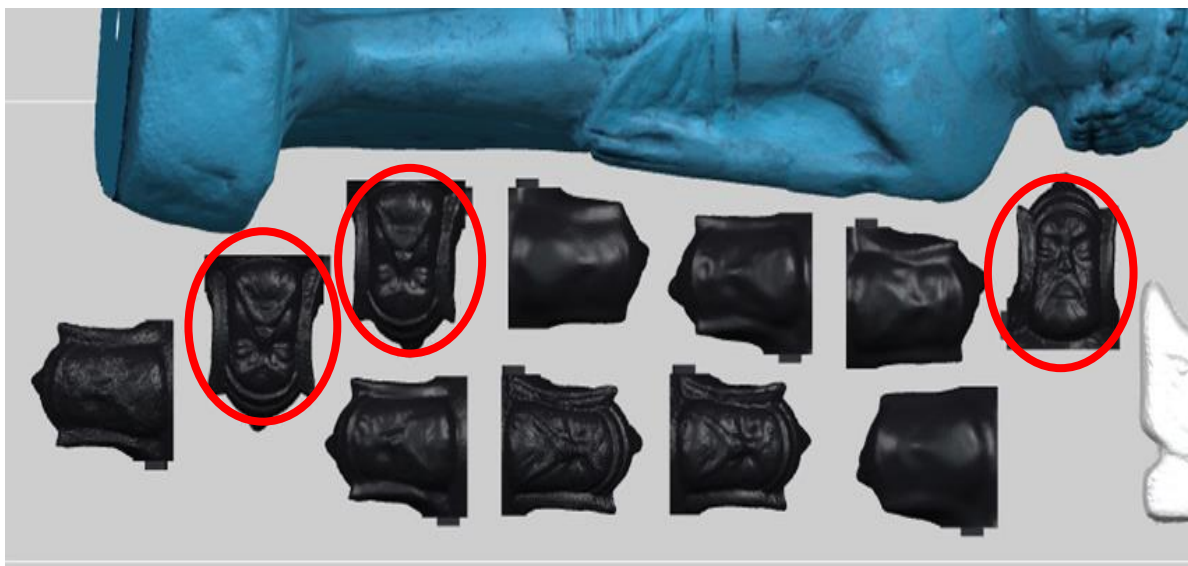


Figure 4.75: Layout of models for printing on the *PolyJet J750*®.

Depending of which type of AM technology was employed, a larger model may be have been prone to stress, strength or stiffness limitations if it was printed in an incorrect orientation [175], especially for FDM models, fortunately this was not so for poly-jet fabricated models.

Although all the models were printed in the same z axis orientation, on examination of the screen shot from the GrabCAD® Print software (see Chapter

4.13) the orientation of three heads, in the x and y plan are different from the rest; hence the different layer direction indicated by the red arrows (see Figure 4.76).

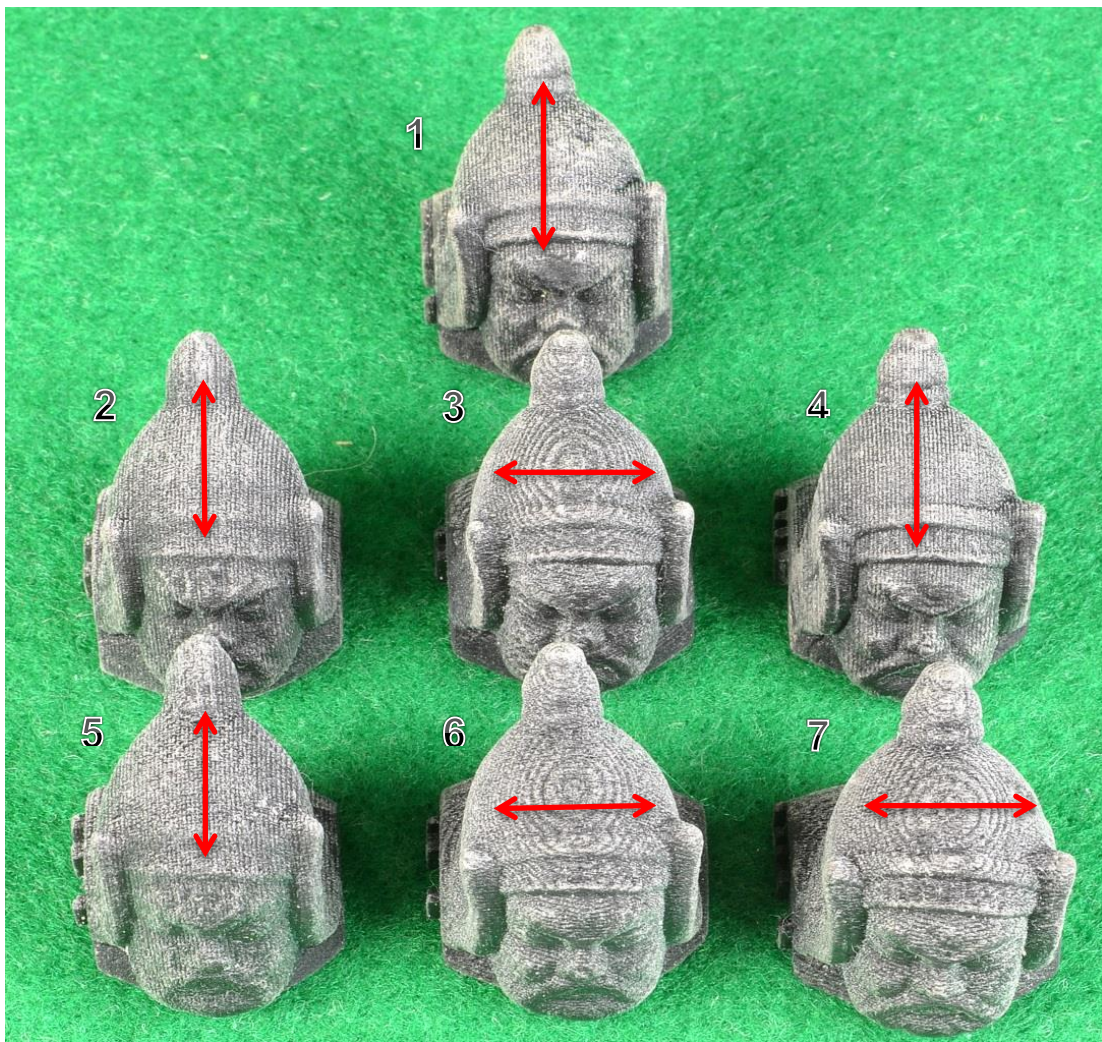


Figure 4.76: Top view of heads showing layer direction.

#### Detail of Figure 4.76

Image Number	Resolution Type
1 -	Camera Ready - Jpeg
2 -	Medium - Tiff
3 -	High - Tiff
4 -	Ultra-High - Tiff
5 -	Medium - Jpeg
6 -	High - Jpeg
7 -	Ultra-High - Jpeg

The number by each photograph indicates the type of file that each model derives from and its position in the photograph (see Table 4.14). The *GrabCAD*<sup>®</sup>

software comes with the Stratasys *PolyJet J750*<sup>®</sup> printer and is used to facilitate the fabrication process within the AM machine.

Table 4.9: Numerical data comparison Hollow Heads - Stl files.  
Netfabb processed Jpeg, Tiff, and CR Jpeg.

W: 21.2mm D: 24mm H: 25.mm

	Figure 4.63	Figure 4.64	Figure 4.65	Figure 4.66	Figure 4.67
	Jpeg image	Tiff Image	Jpeg image	Tiff image	Jpeg image
Resolution	Ultra-High	Ultra-High	High	High	CR (high)
Volume m <sup>3</sup>	3.33	3.46	3.35	3.38	3.31
Area m <sup>2</sup>	31.15	31.94	31.14	31.13	30.97
Triangles	694,612	833,298	174,676	185,918	131,130
Stl file size kb	33,917	40,689	8,530	9,079	6,403
Time to process*	960 mins	2030 mins	150 mins	150 mins	75 mins

\* The processing time taken by *PhotoScanPro*<sup>®</sup>, in minutes, was based on the original full size model not the head only.

Table 4.9 shows the numerical data of the four Warrior heads in Figures 4.63 to 4.66. This table shows a clear difference between the file size and processing time of the Ultra High models and the original CR model. The difference in detail can be observed between the model head photographs in Figures 4.63 to 4.66, having all been printed on a 14µm machine, as have the models shown in Figures 4.71 to 4.73. Appendix M (Table M.1) contains details of the Warrior Head data pertaining to volume, surface area, number of triangles, size of files etc., of each type of Jpeg or Tiff file.

In Chapter 9, a more in-depth look at the RAW v CR images is undertaken but for the smaller model, without obvious problems as discussed in Chapter 8, the question must arise as to the justification of processing RAW images versus CR Jpeg images. The extra time and resources required to process RAW images as shown in this operation, as opposed to the Camera Ready Jpeg images which produced equally good results, cannot be justified.

#### 4.12.1 AM 3D Printing Machine Envelope Build and Resolution Detail

Table 4.9 has been compiled to assist those who may be apprehensive as to which AM machine to use. This list was compiled in July 2017, and is by no means complete. New AM machines were being introduced on a very regular

basis, both at an entry level and at high end specification, with fine layer resolution, as well as new materials for these machines.

Table 4.10: AM 3D Printing Machine Envelope Build and Resolution Detail\*.

Machine Name	Build Envelope	Layer Thickness /Height		Extruder Nozzle Diameter	Filament Size	Data file format						
		mm	inch									
<b>Fused Deposition Modeling (FDM) or - FFF (Fused Filament Fabrication)</b>												
<b>3D Systems</b> <a href="http://www.3dsystems.com/3d-printers">http://www.3dsystems.com/3d-printers</a>												
CubePro	285 x 230 x 270 mm 242 x 230 x 270 mm 200 x 230 x 270 mm	0.0027" 0.0079" 0.0118"	70 μm 200 or 300 μm	0.35 mm 0.50mm	1.75mm	g3d, stl						
CubeX	274 x 265 x 241 mm	0.0027" - 0.0196"	70 - 500 μm									
<b>AIO Robotics</b> <a href="http://www.zeus.aiorobotics.com/">http://www.zeus.aiorobotics.com/</a>												
Zeus	203 x 152 x 145 mm	0.08"	80 μm	0.35mm		aio, .obj, .ply, .stl						
<b>AirWolf</b> <a href="https://airwolf3d.com">https://airwolf3d.com</a>												
HD2x	289 x 203 x 305 mm	0.0024" - 0.0158"	60 - 400μm	0.50mm	2.00mm							
Axiom Dual Drive	305 x 203 x 241 mm	0.0016" - 0.004"	20 - 100μm	0.35mm 0.50mm 0.80mm	2.88mm	g3d, stl						
Axiom AW3D	318 x 203 x 254 mm	0.0016" - 0.0158"	20 - 400μm									
Axiom AW20	318 x 305 x 508 mm	0.0024" - 0.008"	60 - 200μm									
<b>CEL</b> <a href="http://www.cel-robox.com">www.cel-robox.com</a>												
Robox - RBX01	210 x 150 x 100 mm	0.008" - 0.012"	200μm - 300μm	0.3mm 0.8mm	1.75mm							
<b>Dremel</b> <a href="http://www.cooksongold.com/Jewellery-Tools">http://www.cooksongold.com/Jewellery-Tools</a>												
Idea Builder	140 x 230 x 150 mm	0.004"	100μm		1.75mm	stl, g3d						
<b>Delt Maker</b> <a href="https://www.deltamaker.com/">https://www.deltamaker.com/</a>												
dm2 - 3dp	240 x 240 x 260 mm	0.004"	100μm		1.75mm	stl						
dm2T - 3dp	240 x 240 x 457.5 mm											
dm2XT - 3dp	240 x 240 x 558.8 mm											
<b>Da Vinci</b> <a href="http://eu.xyzprinting.com/eu_en/Product/">http://eu.xyzprinting.com/eu_en/Product/</a>												
1.1 plus	200 x 200 x 200 mm	0.004" - 0.016"	100 - 400μm	0.4mm	1.75mm	stl, 3w, xyz						
Junior	150 x 150 x 150 mm	0.004" - 0.016"	100 - 400μm	0.4mm 0.3mm								
Junior 1.0w		0.004" - 0.016"	100 - 400μm	0.3 mm								
2.0A Duo Twin Nozzle	200 x 200 x 150 mm	0.004" - 0.016"	100 - 400μm	0.3 mm								
<b>Lulzbot</b> <a href="https://www.lulzbot.com/">https://www.lulzbot.com/</a>												
Mini	152mm x 152mm x 158mm	0.002" - 0.012"	50 - 500μm	0.35mm	3mm							
TAZ 4-6	280mm x 280mm x 250mm	0.05"	300μm to 1200μm	1.2 mm 0.35mm 0.5 mm	3mm	multi software						
<b>Maker- Bot</b> <a href="https://www.makerbot.com/">https://www.makerbot.com/</a>												
Replicator +	295 x 195 x 165 mm											
Replicator mini +	101 x 126 x 126 mm	0.004"	100μm	0.4mm	1.75mm	stl, obj						
Replicator Z18	300 x 305 x 457 mm											

Machine Name	Build Envelope	Layer Thickness /Height		Extruder Nozzle Diameter	Filament Size	Data file format						
		mm	inch									
<b>New Matter</b> <a href="https://newmatter.com/">https://newmatter.com/</a>												
<b>RoBo</b> <a href="https://robo3d.com/">https://robo3d.com/</a>												
MOD - t	125 x 150 x 100 mm	0.004" - 0.016"	100μm - 400μm	0.4mm	1.75mm	stl, obj						
<b>Stratasys</b> <a href="http://www.stratasys.com/3d-printers">http://www.stratasys.com/3d-printers</a>												
Mojo	127 x 127 x 127 mm	0.007"	178 μm	1.75mm or 3.00mm	stl	Cartridge						
uPrint SE	203 x 152 x 152 mm	0.0010"	254 μm									
uPrint SE plus	203 x 203 x 150mm	0.0010" or 0.013"	254 μm or 330μm									
Dimension 1200es	254 x 254 x 305 mm	0.0010" or 0.013"	254 μm or 330μm									
Dimension Elite	203 x 203 x 305mm	0.010" or 0.007"	254μm or 178 μm									
Fortus 250mc	254 x 254 x 305 mm	0.013" or 0.010" or 0.007"	330μm or 254μm or 178μm	Cartridge	stl							
Fortus 350mc	380 x 355 x 305 mm	0.013" or 0.010" or 0.007" or 0.005"	330μm or 254μm or 178μm or 127μm									
Fortus 450mc	406 x 355 x 406 mm	0.020" or 0.013" or 0.010" or 0.007"	508μm or 330μm or 254μm or 178μm									
Fortus 900mc	905 x 610 x 914 mm	0.020" or 0.013" or 0.010" or 0.007"	508μm or 330μm or 254μm or 178μm									
<b>Type A Machines</b> <a href="https://www.typeamachines.com">https://www.typeamachines.com</a>												
Series 1 Pro	305 x 305 x 305mm	0.002" - 0.0118"	50μm - 300μm	0.4mm	1.75mm	stl, obj, 3mf						
<b>UP!</b> <a href="http://up3dprinters.co.uk/">http://up3dprinters.co.uk/</a>												
Box 3d	205 x 255 x 205 mm	0.004" - 0.016"	100μm - 400μm	0.4 mm	1.75mm	stl						
Plus 2	135 x 140 x 140 mm	0.006" - 0.016"	150μm - 400μm									
Mini 2	120 x 120 x 120mm	0.006"	150μm - 350μm									
<b>Ultimaker</b> <a href="https://ultimaker.com/">https://ultimaker.com/</a>												
Original +	210 x 210 x 205 mm	0.008"	upto 20μm	0.4 mm	1.75mm 2.85 mm	stl, obj, X3d,3mf, bmp, gif, jpg, png						
Ultimaker 2+	223 x 223 x 205 mm	0.002"	600μm - 20μm	0.25mm - 0.8mm								
Ultimaker 2 Go	120 x 120 x 115 mm	0.008"	200μm	0.4 mm								
Ultimaker 3	215 x 215 x 200 mm	0.008"	20μm - 200μm	0.4mm 0.8 mm								
<b>Velleman N.V.</b> <a href="http://www.velleman.co.uk">http://www.velleman.co.uk</a>												
K8200	200 x 200 x 200 mm	0.008"	200μm	0.5 mm 0.35mm	3 mm 1.75 mm	stl						
K8204 upgrade												

\* A selection of AM printers as of October 2017 - not all manufacturers information was available

Machine Name	Build Envelope	Layer Thickness /Height		Resolution dpi	Min. Size Resolution	Data file format								
		mm	inch											
<b>Binder Jetting (BJ)</b>														
<b>ExOne</b> <a href="http://www.exone.com/Systems/Production-Printers">http://www.exone.com/Systems/Production-Printers</a>														
Exerial	2200 x 1200 x 600mm	0.011" to 0.020"	200μm - 500μm	100μm		Xprep								
S-MAX + Phenolic	1800 x 1000 x 600 mm													
S-MAX	1800 x 1000 x 700 mm													
S-Print	800 x 500 x 400 mm													
M-Print	800 x 500 x 400 mm	0.006"	150μm	63.5μm - 150μm		stl, cli, slc								
M- Flex	400 x 250 x 250 mm	0.004"	100μm	66μm - 150μm										
Innovent	160 x 65 x 65 mm	0.002"	50μm	66μm - 150μm										
<b>Direct Light Projection (DLP)</b>														
<b>Norge/ Prodways</b> <a href="http://www.prodways.com/en/">http://www.prodways.com/en/</a>														
L5000	400 x 330 x 400 mm	0.0098" – 0.0059"	25μm – 150μm	605 x 605 x 1016dpi		stl, 3mf								
L6000	800 x 330 x 400 mm													
L7000 - 2head	800 x 330 x 400 mm													
L5000D	400 x 330 x 200 mm													
L600D	800 x 330 x 200 mm			784 x 784 x 1016 dpi										
D35 - 2 head	720 x 230 x 150 mm													
V6000	120 x 500 x 150 mm													
	120 x 350 x 150 mm													
	120 x 150 x 150 mm													
P1000	300 x 300 x 300 mm	0.002" – 0.004"	60μm – 120μm	1080 x 1920 dpi		stl, 3mf								
P2000HD & HT	250 x 250 x 320 mm	0.002" – 0.011"	60μm - 300μm											
P4500SD, HS, HT	400 x 400 x 450 mm x 400 x 600 mm	0.002" – 0.004"	60μm – 120μm											
<b>Rapid Shape</b> <a href="http://www.rapidshape.de">http://www.rapidshape.de</a>														
S30	50 x 31 x 80 mm	0.002" – 0.004"	25μm - 100μm	1080 x 1920 dpi		stl								
S30L	83 x 46 x 80 mm													
D30	110 x 62 x 85 mm													
D40	110 x 124 x 85 mm x 2													
S50 mini	76 x 42 x 80 mm	0.0007" – 0.0026"	19μm - 65μm	1080 x 1920 dpi										
S50 midi	95 x 53 x 80 mm													
S50 maxi	124 x 70 x 80 mm													
S60 mini	76 x 42 x 110 mm													
S60 midi	95 x 543 x 110 mm	0.002" – 0.004"	25μm - 100μm	1080 x 1920 dpi										
S60 maxi	124 x 70 x 110 mm													
S90	153 x 86 x 200 mm													
S90L	192 x 108 x 200 mm													
<b>Perfactory</b> <a href="https://envisiontec.com/3d-printers/perfactory-family/">https://envisiontec.com/3d-printers/perfactory-family/</a>														
P4 Mini XL	115 x 72 x 220 mm	0.0006" – 0.006"	15μm - 150μm	1920 x 1200 pix	stl									
P4 Mini	64 x 40 x 220 mm	0.0039"	100μm											
P3 Mini Multi Lens	44 x 33 x 230 mm													
P3 DDP	84 x 63 x 230 mm													
P4 DDP M	160 x 100 x 180/ 230mm	0.0039"	100μm	1920 x 1200 pix										
P4 DDP	115 x 72 x 180/230mm													
P3 DSP	190 x 120 x 180/ 230mm													
P4 DDP XL	192 x 120 x 180/ 230mm	0.0039"	100μm											
P4 DSP XL	192 x 120 x 180/ 230mm													
P4 DSP	160 x 100 x 180/ 230mm													
P4 Standard XL	192 x 120 x 180/ 230mm		1920 x 1200 pix											
P4 Standard	160 x 100 x 180/ 230mm													

Machine Name	Build Envelope	Layer Thickness /Height		Resolution dpi	Min. Size Resolution	Data file format						
		mm	inch									
<b>Direct Metal Laser Sintering (DMLS)</b>												
<b>EOS</b> <a href="https://www.eos.info/systems_solutions/metal/systems_equipment">https://www.eos.info/systems_solutions/metal/systems_equipment</a>												
M100	100 x 100 x100 mm	0.0016"	40µm									
M290	250 x 250 x 325 mm	0.004"	100µm									
M400	400 x 400 x 400 mm	0.0035"	90µm									
M280	250 x 250 x 325 mm	0.004" - 0.0012"	100µm - 500µm									
M080	80 x 80 x 95 mm	0.0012"	30µm									
<b>Fibre Laser Direct Metal Printing (DMP)</b>												
<b>3D SYSTEMS</b> <a href="http://www.3dsystems.com/3d-printers">http://www.3dsystems.com/3d-printers</a>												
ProX DMP 100	100 x 100 x 100 mm	0.0012"	30 µm	x,y - 100 µm z - 20µm								
ProX DMP 200	140 x 140 x 125 mm	0.0016"	40 µm									
ProX DMP 300	250 x 250 x 330 mm	0.0020"	50 µm									
ProX DMP 400	275 x 275 x 420 mm	0.0012" or 0.0024"	30µm or 60µm	100 µm								
<b>Electron Beam Melting (EBM)</b>												
<b>Arcam</b> <a href="http://www.arcam.com/technology/products/">http://www.arcam.com/technology/products/</a>												
Q10plus	200 x 200 x 180 mm	0.0055"	140µm									
Q20plus	350 x 380 x 380 mm											
A2X	200 x 200 x 380 mm	0.0098"	250µm									
<b>Laser Melting System (LMS)</b>												
<b>Renishaw</b> <a href="http://www.renishaw.com/en/metal-3d-printing">www.renishaw.com/en/metal-3d-printing</a>												
RenAM 500M	250 x 250 x 350 mm											
AM400	250 x 250 x 300 mm	0.0027"	70 µm									
AM250	250 x 250 x 300 mm	0.0002" - 0.0024"	25 - 60 µm									
<b>Slide and Separate Technology (SAS) - UV LED</b>												
<b>Asiga</b> <a href="https://www.asiga.com/products/printers/">https://www.asiga.com/products/printers/</a>												
Freeform PRO2 50	96 x 54 x 200 mm	0.0020"	50 µm									
Freeform PRO2 75	144 x 81 x 200 mm	0.0029"	75 µm									
PICO2 - HD	71 x 40 x 75 mm	0.00145"	37 µm									
PICO2 - 39	51 x 32 x 75	0.00153"	39 µm									
PICO2 - 50	64 x 40 x 75 mm	0.0020"	50 µm									
<b>Stereolithography (SLA) or (SL)</b>												
<b>3D Systems</b> <a href="http://www.3dsystems.com/3d-printers">http://www.3dsystems.com/3d-printers</a>												
Projet CJP 260C	236 x 185 x 127 mm	0.004"	100µm	300 x 450dpi								
Projet CJP 360C	203 x 254 x 203 mm											
Projet CJP 460plus				600 x 540dpi								
Projet CJP 660Pro	254 x 381 x 203 mm											
Projet CJP869Pro	508 x 381 x 229 mm											
iPro 8000 RDM650M	650 x 350 x 300 mm	0.002" - 0.006"	5 µm - 150 µm									
iPro 9000XL RDM1500XL	1500 x 750 x 550 mm											
RDM 750SH	650 x 750 x 50 mm											
RDM 750H	650 x 750 x 275 mm											
RDM 750F	650 x 350 x 550 mm											
ProX 800	650 x 750 x 550 mm	0.0049"	125 µm	4000dpi								
ProX 950	1500 x 750 x 550 mm											
ProX SLS 500	381 x 330 x 460 mm											
ProJet 660Pro	254 x 381 x 203 mm	0.004"	100µm	600 x 540dpi								
ProJet 4500												
ProJet MJP 2500	295 x 211 x 142 mm											
ProJet MJP 2500 plus		0.0013"	32µm	800 x 900 x 790 dpi								
ProJet 3510 SD	298 x 185 x 203 mm	0.0013" - 0.0011"	32 µm - 32µm & 29µm									
ProJet 3510 HD	127 x 178 x 152 mm											
ProJet 3510 UHD	203 x 178 x 152mm											
ProJet 3510 XHD			32µm	375 x 375 x 790dpi								

Machine Name	Build Envelope	Layer Thickness /Height		Resolution dpi	Min. Size Resolution	Data file format	
		mm	inch				
ProJet 3500 MAX HD	298 x 185 x 203 mm	0.0013"	32 μm	375 x 375 x 790dpi			
ProJet 3500 MAX HS		0.0013"	32 μm				
ProJet 3500 MAX UHD		0.0011"	28 μm		750 x 750 x 890dpi		
ProJet 3500 MAX XHD		0.0006"	16 μm		750 x 750 x 1600dpi		
sPro 140	550 x 550 x 460 mm	0.003" -	80μm - 150μm				
sPro 230	550 x 550 x 750 mm	0.006"		600 x 540dpi			
sPro 60HD	381 x 330 x 460 mm						

### Stratasys

<http://www.stratasys.com/3d-printers>

Object 24	234 x 192 x 149 mm	0.0011"	28 μm	x & y - 600dpi z - 900dpi			
Object 30							
Object 30 Pro	294 x 192 x 149 mm						
Object 30 Prime							
Object 260	255 x 252 x 200 mm	0.0006"	16μm	x & y - 600dpi z - 1600dpi			
Object 350							
Object 500	490 x 390 x 200 mm						
Object 1000 plus	1000 x 800 x 500 mm						
J750	490 x 390 x 200 mm	0.0005"	14μm	x&y - 300dpi z - 1600dpi			
				x&y - 600dpi z - 1800dpi			

### Concept Laser

<http://www.concept-laser.de/en/machines.html>

Mlab cusing & cusing R	50 x 50 x 80 mm 70 x 70 x 80 mm 90 x 90 x 80 mm	0.0006" – 0.0019"	15μm - 50μm	0.002"	50μm		
Mlab cusing 200R	100 x 100 100 mm 70 x 70 x 80 mm 50 x 50 x 80 mm	0.0006" – 0.0012"	15μm - 30μm				
M1 cusing	250 x 250 x 250 mm	0.0008"	20μm - 80μm				
M2 cusing	250 x 250 x 280 mm	0.0031"	50 μm – 500 μm				
M2 cusing multilaser							
X Line 2000R	800 x 400 x 500 mm						
M Line Factory	400 x 400 x 425 mm	0.0008" – 0.004"	20μm - 100μm				

\* A selection of AM printers as of October 2017 - not all manufacturers information was available

INDEX		Measurements			AM Printer Review Websites		
		inch	mm	micron			
AFM -	Atomic Force Microscopy						
BJ -	Bubble Jet	0.04	1	1000 μm			
CLI P -	Continuous Liquid Interface Production	0.02	0.5	500 μm			
CDLM -	Continuous Digital Light Manufacturing	0.016	0.4	400 μm			
CDR -	Control Drug Release	0.012	0.3	300 μm			
DDP -	Digital Dental Printer	0.008	0.2	200 μm			
DDSP	Desktop Digital Shell Printer	0.007	0.175	175 μm			
DLM	Digital Light Manufacturing	0.006	0.15	150 μm			
DLP	Direct Light Projection	0.005	0.125	125 μm			
DMLS -	Direct Metal Laser Sintering	0.004	0.1	100 μm			
DMP -	Direct Metal Printing	0.00295	0.075	75 μm			
DLP -	Direct Light Projection	0.00197	0.05	50 μm			
DLP -	Direct Light Projection	0.00098	0.025	25 μm			
EMB -	Electron Beam Melting	0.00078	0.02	20 μm			
ERM -	Enhanced Resolution Module	0.00059	0.015	15 μm			
FDM -	Fused Deposition Modelling	0.00039	0.01	10 μm			
MJP	Multi material Jet Printers	0.00019	0.005	5 μm			
PLS	Plastic Laser Sintering	0.00012	0.003	3 μm			
PRS -	Powder Recovery System	0.00004	0.001	1 μm			
RDM -	Resin Delivery Modules						
SAS	Slide and Separate Technology						
SDL	Selective Deposition Lamination						
SLA -	Stereolithography						
SLCOM	Selective Lamination Composite Object Manufacturing						
SLM -	Selective Laser Melting						
SLS -	Selective Laser Sintering						
STA -	Standard Triangle Language or Standard Tessellation Language						
STL -	Stereolithography						
HD	High Definition						
UHD	Ultra-High Definition						
UHDS	Ultra-High Definition - Single						
XHD	Xtreme High Definition						
XHDS	Xtreme High Definition - Single						

#### 4.13 AM Technology Software

Many AM technologies come with proprietary software, or in some cases generic software that will support a range of machines that have been produced by a specific manufacturer. The software used for illustration in this chapter supports the Stratasys range of machines: *GrabCAD*® [159] and for use with the Ultimaker FDM machines: *Cura*® [176]. Before any artifact can be fabricated, whether created by photogrammetry or LS techniques, and before it can be further processed to produce a finished model, the model's data file has to undergo one more process: it must be turned into a file that the AM machine can process. The original file could be many different formats but most popular might be either an \*.stl, \*.vrml (wrl) or \*.obj file, all containing the information to re-create the original object.

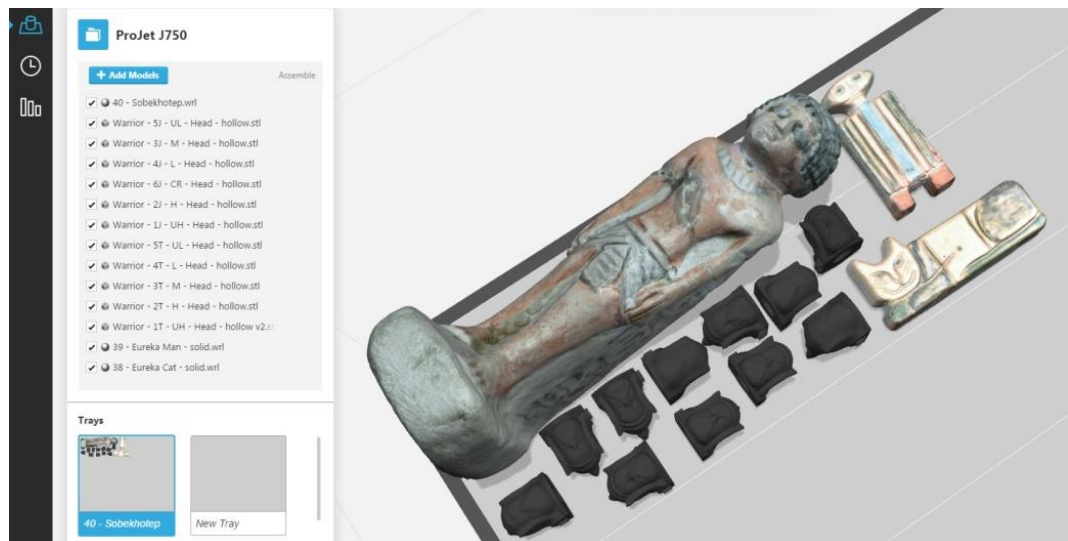


Figure 4.77:

Screen shot of a manual build platform layout from *GrabCAD*®.

The difference between file types, such as \*.vrml, is that they contain the information that can reproduce the item in full colour, whereas, for instance, the \*.stl file can only produce a monochromatic model. The software allows the operator to arrange models to be printed, either manually (Figure 4.77) or in some cases automatically (Figure 4.78) on the print tray or platform. The software, *GrabCAD*®, also checks the integrity and suitability of each model to ascertain if there are any defects within the CAD model. A defect would have stopped or hindered the fabrication process and in this software there was a function to correct or reject the model.

If a set of models is to be printed together, the automatic function may not orientate the models in the way that is required by the operator. It may be that each item has been placed in the most economical orientation for printing, but not to match the grain or layer direction which is required (see Chapter 4.12). Depending on the AM machine being used, other criteria or preferences may be set or changed in the software, such as speed, temperature of platform or nozzle, calibration of heads or lasers, etc., as well as details of the materials which can be used on any given machine.

It should be noted that with the particular layout shown in Figure 4.78 and 4.79 which is for a Stratasys Inc., *PolyJet J750*® [159] machine, a mixture of monochromatic and colour models were being printed at the same time.

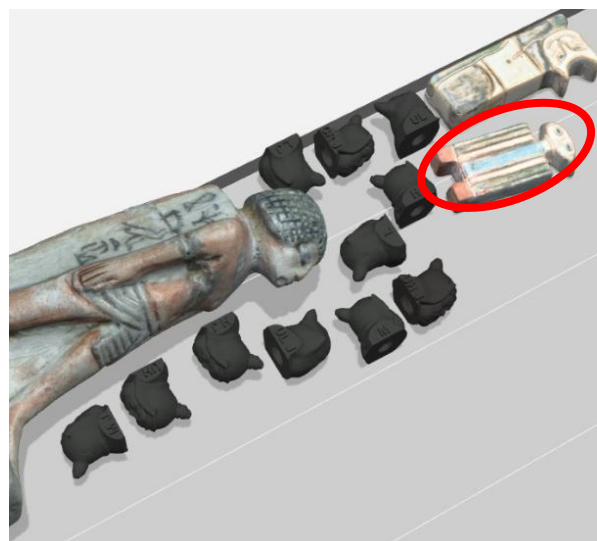


Figure 4.78:

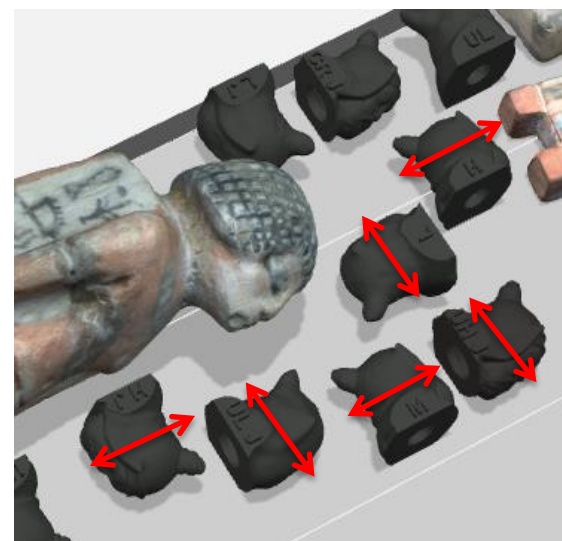


Figure 4.79:

Screen shot of the Automatic layout from *GrabCAD*®.

In Figure 4.78 it can be seen that the automatic ‘*Tray Arrangement*’ has not laid out the models in the best orientation, e.g. the model of Eureka Man (circled in red, Figure 4.78) is not square with the parallel white lines of the tray and all the model heads have been placed on their side, some with the grain and some across the grain (layer direction), as indicated by red arrows shown in Figure 4.79. The *PolyJet J750*® machine, in comparison to the Ultimaker range, is far more complex and expensive to buy. Within the *J750* machine, there exists the option to print models in full colour and multi-material, as well as the option to print some of the part in monochrome and some of the part in colour as shown

Figure 4.78. Also the layer resolution is much finer being  $14\mu\text{m}$ , as opposed to a filament FDM mono-chromatic model with the finest layer being  $250\mu\text{m}$ .

Some software, for example *Cura*<sup>®</sup>, also generates data about the model, such as the cost of material used, in financial terms as well as the quantity of material used, or the length of time required to build the model. Millimeters have been used in Table 4.15 as this is the measurement used in *Cura*<sup>®</sup> and not Microns.

Table 4.11: Slice data for Warrior model from the *Cura v2.6*<sup>®</sup> software.

Nozzle size	Print Profile used	Layer Height	Wall Thickness	Number of Layers	Time to Build	Weight of model	Time to Build with support	Weight of model with support
0.25mm	Extra Fine	0.06mm	0.88mm	1520	18hr 15min.	21g.	25hr 36min	28g
0.4mm	Extra Fine	0.06mm	1.05mm	1520	9hrs 40min	23g.	14hr 13min	31g
0.4mm	Fine	0.10mm	1.05mm	912	5hrs 59min	23g.	8hr 44min	32g
0.4mm	Normal	0.15mm	0.7mm	608	2hrs 38min.	18g.	4hr 03min	25g
0.6mm	Fine	0.15mm	1.59mm	608	3hrs 16min.	26g.	4hr 50min	35g
0.8mm	Normal	0.2mm	2.1mm	451	1hrs 39min.	25g.	2hrs 51min	37g.

Selected material – PLA Infill 18/22%

For example, by inputting the cost of the filament into the options setting in the software, an automatic costing can be calculated. Table 4.15 shows some of the data that can be obtained from the Ultimaker B.V. *Cura*<sup>®</sup> software about the Warrior model.



Figure 4.80:  
Ultimaker  $250\mu\text{m}$   
model.



Figure 4.81:  
Without supports.

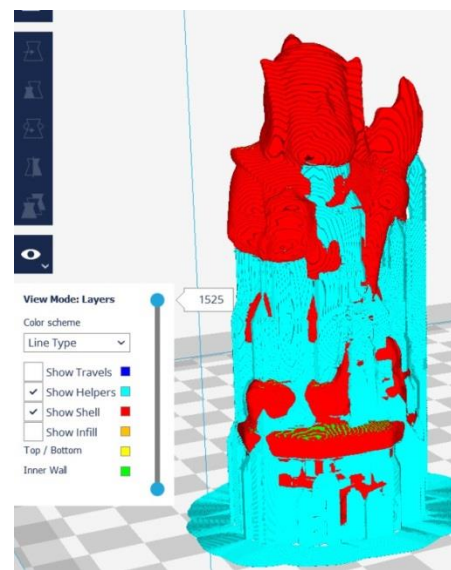


Figure 4.82:  
Model showing external supports.

In this example, the time for each model and the weight of filament used can be calculated; four nozzles were used, each with a different size orifice and using one of three preset print profiles as well as using or not using outer support structure. The quality of the model built is based on filament thickness and layer height. The higher values produced faster prints in lower resolution, lower values produced slower prints in higher resolution.

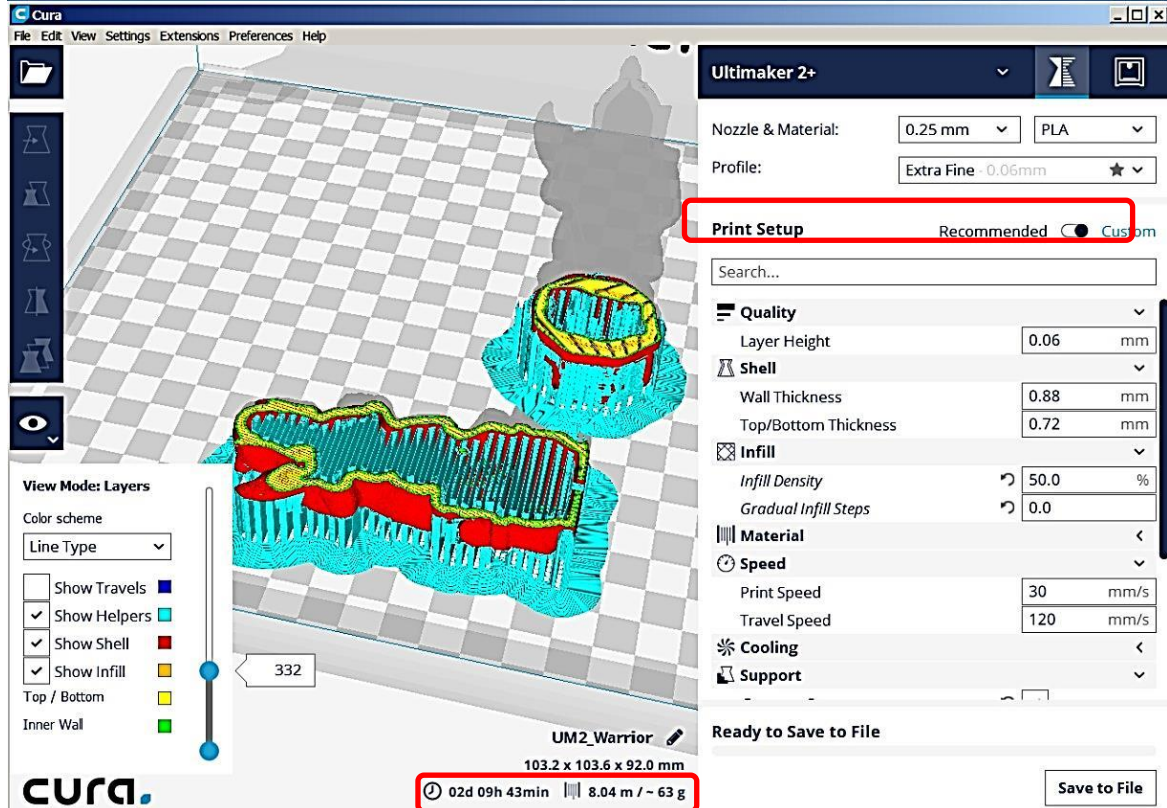
On examination of the *Cura*® software several interesting insights into the model build are explored. There are several accessible functions that the user can modify, and the result can be inspected visually by viewing on a monitor:

- The build support structure can be identified;
- The comparative thickness of layers can be assessed;
- The infill between inner shell and outer shell can be inspected;
- The G-code can be inspected.

For this exploration, the Warrior figurine has been used as shown in Figure 4.80. Both Figure 4.81 and Figure 4.82 are screen shots from the *Cura*® build software. The images show how the model would build without and with external supports, and will indicate to the machine operator the amount of post-processing work that will have to be undertaken before the model is finished. Figure 4.83 shows the comparison between the supports if the build was laid horizontally or vertically and the internal support structure that would support the model. Both the horizontal and vertical model images are shown at slice level 332, which was approximately half way down on the horizontal model, giving visual information as to the density of the inside of the artifact. On the right-hand side of the screen (highlighted in red) the operator has the ability to select how the model is constructed (Print Setup) by choosing the manually mode (Custom), either selecting from a variety of criteria or else by selecting the basic setup and allowing the program to process the model in a semi-automatic mode (Recommended).

Information is displayed in the right-hand section of the screen shot in Figure 4.83, detailing the model's construction. The section on "shell" and "infill" and could be of importance to the machine operator, showing how a model is to be handled or displayed. For example, if a model is to be kept in a display cabinet and rarely handled, a thinner outer shell and only a 20% infill might be adequate, whilst on the other hand if the model is part of a school's "hand-on" or loan box

(see Chapter 2.5), it would be prudent to increase the outer shell thickness and infill density so as to make the model more robust. This would increase the time taken to fabricate the model and increase the amount of material used and hence the cost.



The inner and outer wall – red: Between wall infill – yellow and green: Support structure - blue

Figure 4.83: Slice level 332 - showing information about the print structure of the model in “Custom” Mode.

As seen in Figure 4.83, this information is also available, automatically calculated at the bottom part of the screen (highlighted red). The operator must also take into consideration the strength and hardness of the material that is to be used, as even if the model was destined to be displayed in a cabinet it still must be robust enough to be handled in the initial fabrication, post fabrication and finishing stages of manufacturing.

By changing the nozzle size, the profile and diameter of the extruded filament, the difference in build time can be seen in Table 4.15; this difference can also be explained by observing the number of rows of material that are extruded and form the model.

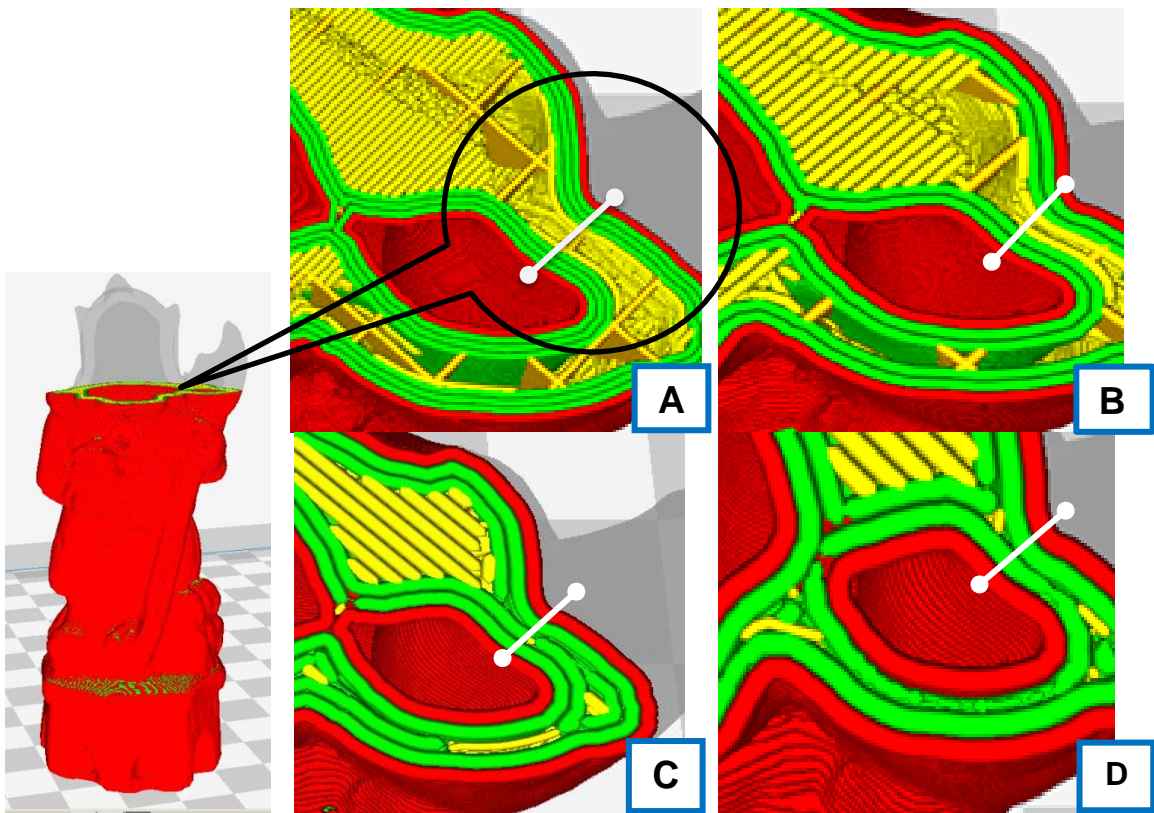


Figure 4.84:  
Slice level 1187.

Figure 4.85  
Enlargement of filament layers.

This is shown in Figure 4.84 at slice level 1187, being the point at which head and shoulders met.

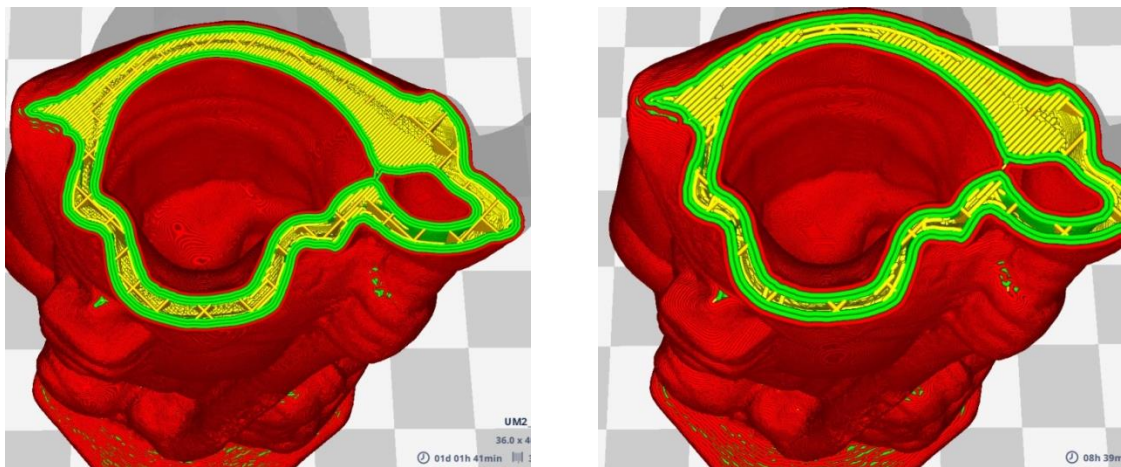


Figure 4.86:  
Extra Fine Profile - 0.25mm nozzle.

Figure 4.87:  
Fine Profile - 0.4mm nozzle.

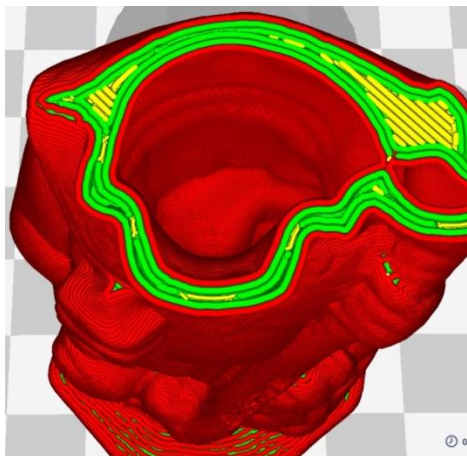


Figure 4.88:  
Fine Profile - 0.6mm nozzle

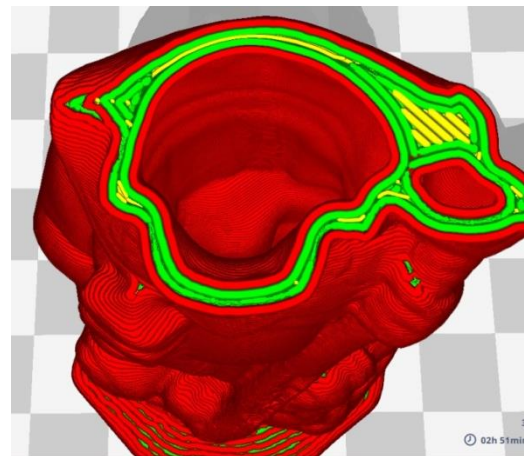


Figure 4.89:  
Normal Profile - 0.8mm nozzle

Table 4.12 shows the size and extra numbers of layers as seen in close up views in Figure 4.85 - A,B,C,D - across the white line at slice level 1187.

Table 4.12: Layers and infill per Profile/Nozzle change

	Profile used	Nozzle size	
A	Extra Fine	0.25mm	8 layers - plus infill
B	Fine	0.4mm	6 layers - plus infill
C	Fine	0.6mm	4 layers - no infill
D	Normal	0.8mm	4 layers - no infill

The larger images of Figures 4.86 to 4.89 show the internal structure which is put into place as the filament size is increased; the more internal layers, the longer the build time.

#### 4.13.1 AM Printer Drivers

One of the most well-known machine-controlling simulation software programs is CGTech's *Vericut*® [177], a software program for CNC machines which simulates the tool paths of each of its tools, enabling the operator to detect any potential errors or collisions, and to check for the optimum efficiency of the machine. The original code/program to drive CNC machines was known as G code (geometric code), NC coding (numerical control) as well as other names, and was originally developed in the 1950s to drive CNC machines from 3-axis to 6-axis machining centres. It has been incorporated in many software programs that now run the AM printers. Many of the instructions are the same for both AM and CNC machines but additional commands have been added with the development of AM printers. The code contains every instruction that the printer/CNC undertakes

in moving the nozzle/head/tool in order to lay down the filament or guide a laser beam which is usually driven using galvanometers mirrors or polygonal scanners.

Slicer programs such as *Cura*<sup>®</sup> and *Simplify3D*<sup>®</sup> generate G-code automatically from CAD models, so most users never see or program a single line of code. It is not really necessary for an AM machine operator to know, understand or be able to read what the G code means, except for interest. However, if a deeper understanding of 3D printing is required by the operator, it is essential to know about this programming language. As it is generated automatically by the AM machine software, it may not actually be accessible to the operator in all programs.

The *Cura*<sup>®</sup> software generates this G code as a text or document file and can be accessed and read by the operator, in a word processor such as Word or Notepad. This is written as a series of numerical command instructions, as can be seen in Figure 4.90, which shows a section of the code, taken at random, at slice layer 1187, and which is also the slice level of the images above in Figures 4.84 to Figure 4.89. Although outside the scope of this thesis, if required, information such as “*The NIST RS274NGC Interpreter - Version 3*” [178] or tutorials on the web such as “*G-Code Tutorial: 3D Printer Commands Simply Explained*” [179] will give the information to interpret and write or amend files created by the software.

:LAYER:1187 G0 X100.297 Y151.154 Z71.39 ;TYPE:SUPPORT G11 G1 F1200 X99.852 Y151.599 E187.3159 G1 X99.688 Y152.008 E187.32172 G1 X99.688 Y152.868 E187.33307 G1 X99.834 Y152.781 E187.33531 G1 X100.109 Y152.018 E187.34602 G1 X100.259 Y151.552 E187.35248 G1 X100.399 Y151.166 E187.3579 G1 X100.297 Y151.154 E187.35926 G10 G0 F7200 X100.133 Y151.144 G0 X99.688 Y152.008	:TYPE:FILL G11 G1 F1800 X110.36 Y163.431 E188.49825 G1 X110.322 Y163.469 G0 F7200 X110.308 Y163.2 G1 F1800 X111.197 Y164.089 E188.51485 G1 X111.235 Y164.127 G0 F7200 X111.246 Y165.656 G1 F1800 X110.438 Y166.464 E188.52993 G1 X110.4 Y166.502 G0 F7200 X110.44 Y166.443 G1 F1800 X111.027 Y167.03 E188.54089 G1 X111.065 Y167.068 G0 F7200 X109.704 Y168.818	G0 X100.173 Y151.341 G0 X100.297 Y151.154 ;TIME_ELAPSED:81827.871633  G0 F7200 X100.977 Y157.018 G0 X101.072 Y157.666 ;TIME_ELAPSED:82404.272239
--	--	--

Figure 4.90: G code from the instructions as downloaded into a word processor.

These two programs which have been investigated, *GrabCAD*<sup>®</sup> and *Cura*<sup>®</sup>, are not dissimilar to many types of AM machine software, as most of the commercial machines are driven by software in a very similar way. But the more sophisticated the machine, the more complex the process, the more feed or laser

heads, colour printing heads, base tray heating or movement, the more complex the code will be.

#### 4.14 Digital Photographic information held with the image

With all the data sets taken and processed using *PhotoScan Pro*®, the camera was set to prioritise the aperture, which had the effect of controlling the DoF but allowed for the shutter speed to be automatic. The shutter speed was not recorded in the above chart for this reason, i.e. all shutter speeds were automatic. If any of this information was important for any further research, by reference to each camera frame, the information was embedded within the digital image as recorded by the camera.

Modern digital cameras embed this information within the data and can be read by using software such as *ViewNX 2™* (Figure 4.63); this came on the supporting software disk when the camera was purchased. Table 4.13, shows a screen shot of this software information for each digital image contained within the jpg or tiff file, alongside a copy of the information for clarification.

Table 4.13: Focusing criterion for 'Live View' [143].

##### Choose an AF-area mode.

AF-area mode can be selected in all shooting modes except  and . Highlight the current AF-area mode in the monitor. Press  to display the following options. Highlight an option and press .



##### Mode

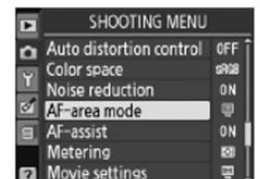
##### Description

 <b>Face-priority AF</b>	The camera automatically detects and focuses on portrait subjects facing the camera. Use for portraits.
 <b>Wide-area AF</b>	Use for hand-held shots of landscapes and other non-portrait subjects. Use the multi selector to select the focus point.
 <b>Normal-area AF</b>	Use for pin-point focus on a selected spot in the frame. A tripod is recommended.
 <b>Subject-tracking AF</b>	Track a selected subject as it moves through the frame.

Press the  button again to return to live view.

##### **Live View AF-Area Mode**

The AF-area modes for live view can also be chosen using the **AF-area mode > Live view/ movie** option in the shooting menu.



#### 4.14.1 Focusing onto the Target

There is much information as can be seen in the Table 4.17 which is embedded in the digital image as recorded by the camera's IPU. The *Nikkor AF-S DX<sup>®</sup> 18-55mm* lens is dedicated to the Nikon D3100 and for all this digital information to be recorded by the camera onto the image, the lens not only must fit the camera but be electronically controllable by the camera operational system.

Although the camera can be set to fully automatic mode, there are still decisions that the camera operator has to make, such as whether to have manual focus or auto-focus, aperture priority (AP), shutter (speed) priority (SP) or perhaps full manual control is required.

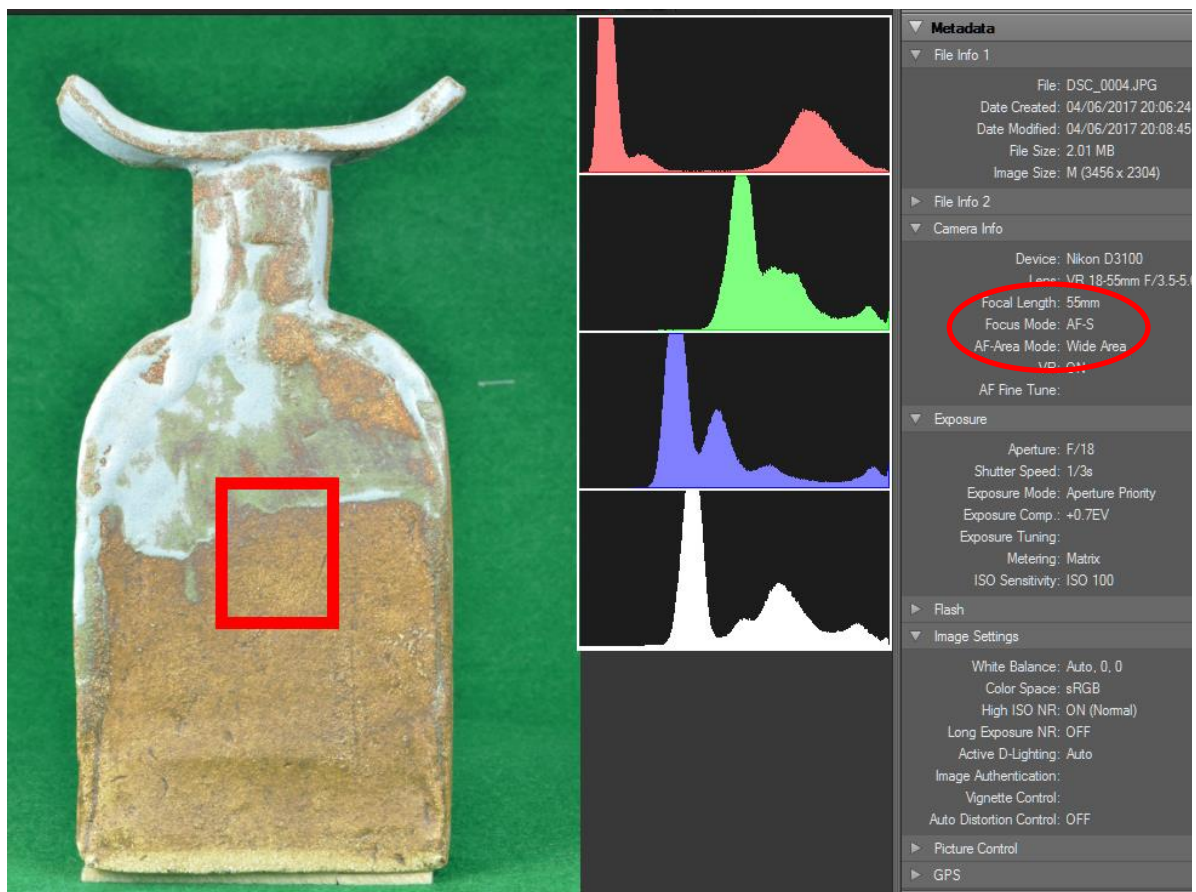


Figure 4.91: Digital information relating to the photographic image. Colour channel histograms shown separately.

The camera allows the operator to choose between several options when it comes to auto focusing. The options also allow the operator to choose between viewing the subject through the eye viewer (Viewfinder), or using the viewing screen on the rear of the camera (Live View (LV)). Either option has different

settings for the focusing point and is set through the camera “shooting” menu. Though out this research, LV was used and Table 4.17 shows the options [180], of which there are four AF-area modes: Face-priority; Wide-area; Normal-area; and Subject-tracking.

It was found that using LV was easier to see and focus on the larger screen than looking through the eye viewer. For the purpose of this thesis only ‘Wide-area’ and ‘Normal-area’ mode are used. The red square in the centre of the image shown in Figure 4.91 indicates where the lens automatically focused on the artifact. In this instance, it has been incorrectly set on the “Wide Area” setting (shown circled in red) so as to show the large focus area which should be reserved for landscapes and non-portrait subjects.

Both Wide and Normal modes work in the same way; both can be moved around the focusing frame and in both modes the camera automatically focuses on the selected target subject, the basic difference being that Normal mode allows a smaller specific area to focus upon.

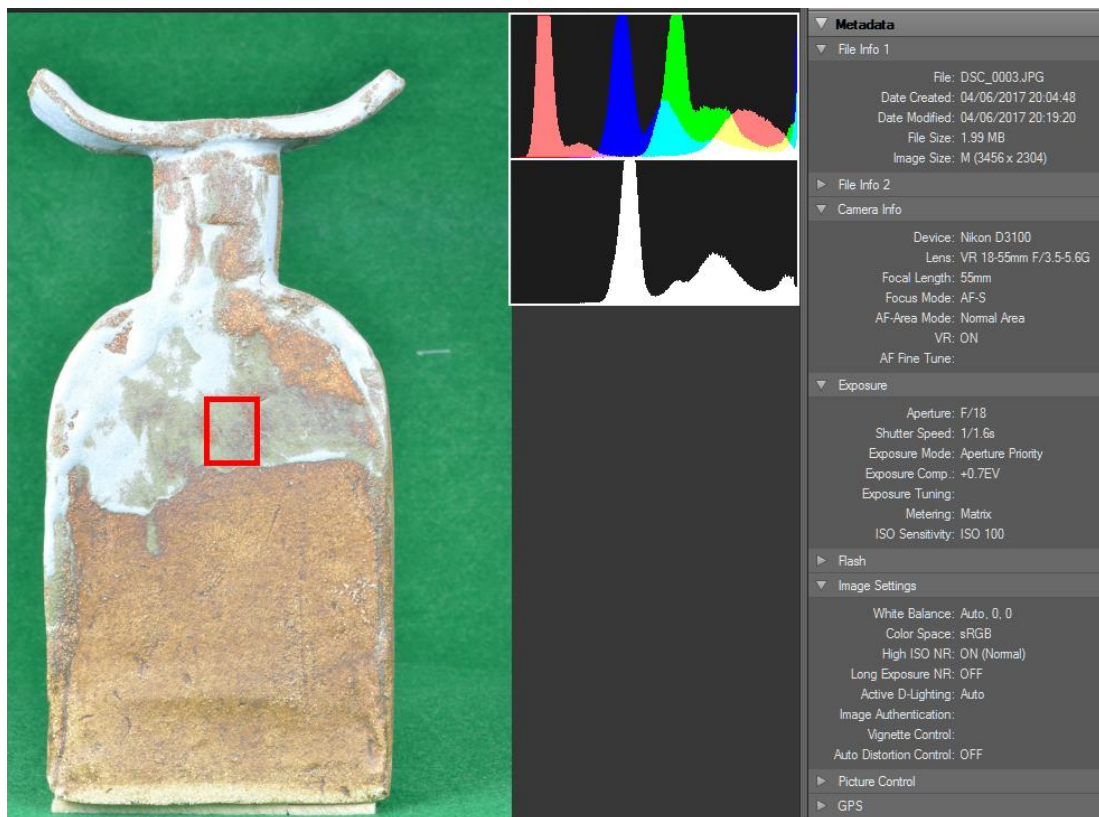


Figure 4.92: Digital information relating to the photographic image.  
Colour channel histograms seen combined.

Although very similar in their function, by using the wrong setting in photographing small objects, this Wide-area mode could automatically change the focal point if a series of images were taken consecutively, and therefore could potentially change the focus of the images.

In Chapter 4.8.1 histograms were discussed and this information plus the additional image editing facility can be found within the bundled software, *ViewNX 2™* that accompanies the camera. In the second column the colour and brightness histograms are seen, showing each channel, Red Green and Blue (RGB setting) with the option to alter many features within the software program, such as white balance, sharpness, brightness etc. In Figure 4.92 the same information is provided but in this image the red square is much smaller as the AF Area Mode has been set to 'Normal'. Also, the histogram has been displayed in a different format (an optional setting).

Table 4.14: *ViewNX 2™* table.

File Info 1		File Info 1
File: DSC_0004.JPG		File Number: DSC_0004.JPG
Date Created: 04/06/2017 20:06:24		Date created: 04/06/2017 20:06:24
Date Modified: 04/06/2017 20:08:45		Date Modified: 04/06/2017 20:06:24
File Size: 2.01 MB		File Size: 2.01 MB
Image Size: M (3456 x 2304)		Image Size: M (3456 x 2304)
File Info 2		File Info 2
Camera Info		Camera Info
Device: Nikon D3100		Device: Nikon D3100
Lens: VR 18-55mm F/3.5-5.6G		Lens: VR 18-55mm F/3.5-5.6G
Focal Length: 55mm		Focal Length: 55mm
Focus Mode: AF-S		Focus Mode: AF-S
AF-Area Mode: Wide Area		AF-Area Mode: Wide Area
VR: ON		VR: ON
AF Fine Tune:		AF Fine Tune:
Exposure		Exposure
Aperture: F/18		Aperture: F/18
Shutter Speed: 1/3s		Shutter Speed: 1/3s
Exposure Mode: Aperture Priority		Exposure Mode: Aperture Priority
Exposure Comp.: +0.7EV		Exposure Comp: +0.7EV
Exposure Tuning:		Exp. Tuning Metering: Matrix
Metering: Matrix		ISO Sensitivity: 100
ISO Sensitivity: ISO 100		ISO Sensitivity: 100

The data that was shown in Figures 4.91 and 4.92 is only a small part of the digital information which was relevant to this particular operation, and can be accessed using software provided with the camera. The program is an all-in-one

enabling the operator to transfer, view, edit and read the data from the camera [180]. For clarity, part the right-hand table in Figure 4.92 is shown as Table 4.14 where the AF-Area Mode is highlighted.

#### 4.15 Data Chart and Image library – processed with *PhotoScan Pro*®

The details of the Image library are in Table J.1: - “*Data Chart -Image processed using PhotoScan Pro*®” - Appendix J, and images referred to in this section are pre-fixed J, and can also be found in Appendix J. The original 30 artifacts were processed using *PhotoScan Pro*®, three constructed in *SolidWorks*® (Figures J.56 to J.58) and two reconstructed in *Studio Pro*® (Figures J.45 and J.46).

The following information should be noted with reference to Table J.2: - “*Photographic images, size and material*” - Appendix J, the *minutiae* for each item has been reduced for simplicity.

With most of the artifacts there was more than one attempt to obtain good data sets. With others, experimentation took place with camera settings, computer processing or photoshoot backdrops, with no other purpose than “*just to see*” what the results would be. Also some of the data sets taken in Method 1 were tried out using *PhotoScan Pro*® software. All these diversities have been logged in the appropriate Appendix G or J. Many of the objects were photographed against white and green Chroma Key backdrops or several attempts were made before a processable data set was achieved. With the Egyptian Bowl (Figure J.28), for example, there were six attempts at achieving a good data set. In fact seven attempts were made before a good clean non blurred set of the Aged Pot was achieved (Figure J.35). The data settings on the camera would have been altered with each photoshoot, as with the Egyptian Bowl, achieving the optimum DoF so as to ensure the whole bowl was in sharp focus, although difficult to achieve. Or with the ‘Fish’ Pot v2, (Figure J.44), for example, there were four photoshoot sessions, all resulting in processable data, but each session was different, e.g. background cloth, number of images – (10° or 15°) rotation, using masks or not using masks, etc. Many of the later artifacts were only photographed once and good results achieved, but this was perhaps to be expected due to experience gained on earlier objects.

From the original Roman jug (Figure J.43), two modified Roman pots were created (Figure J.45 and J.46), and were part of an experiment in the potential use of the software in an educational environment or how the software could be used to modify or morph the original artifacts into a sister object, that could be used in a history lesson in school (see Chapter 6.10.2).

Having created the long Roman jug, or to give it its proper name, a wine or grain Dressel Amphora, a stand was needed to support it (Figure J.56), as the Amphora had a point not a flat bottom. Created in *SolidWorks*®, this was seen as another potential classroom benefit.

The author, having come across the 'Horus' statuette at an antique fair (Figure J.53), and looking at one of the themes in Chapter 6 of using the technology to repair objects, felt that reinstating Horus's dignity by creating a couple of Crowns seemed a natural progression of the benefits that combining and using different software gave. Two versions were created from research photographic documentation and the 3D models were created using *SolidWorks*® (Figure J.57 and J.58).

Table J.3:- "*Capture Data Log – PhotoScan Pro*" - Appendix J, contains all the day to day record and evaluation as well as photographic data of 33 artifacts. Sections of this research were presented at the CIRP 25<sup>th</sup> Design Conference and subsequently published in *Procedia CIRP* (see Appendix B) [181].

#### **4.16      Method 3.      Adapting to Different Working Environments**

##### **4.16.1    Using a Backcloth on its Own**

The most critical part of the whole process was the data capture, the setting up of the environment in which well-focused, shadowless images could be collected by the camera. It was not always necessary to use the light tent, nor was it essential to use a backcloth for Agisoft processing; for large life size building projects this would not be possible and, as seen from Figure 4.37, it just took longer to separate background from subject without the Chroma Key background.

Working under the Naya in Spain, or in an undercroft, as long as the lighting was bright and without shadow, the resulting images captured would be good enough to process.

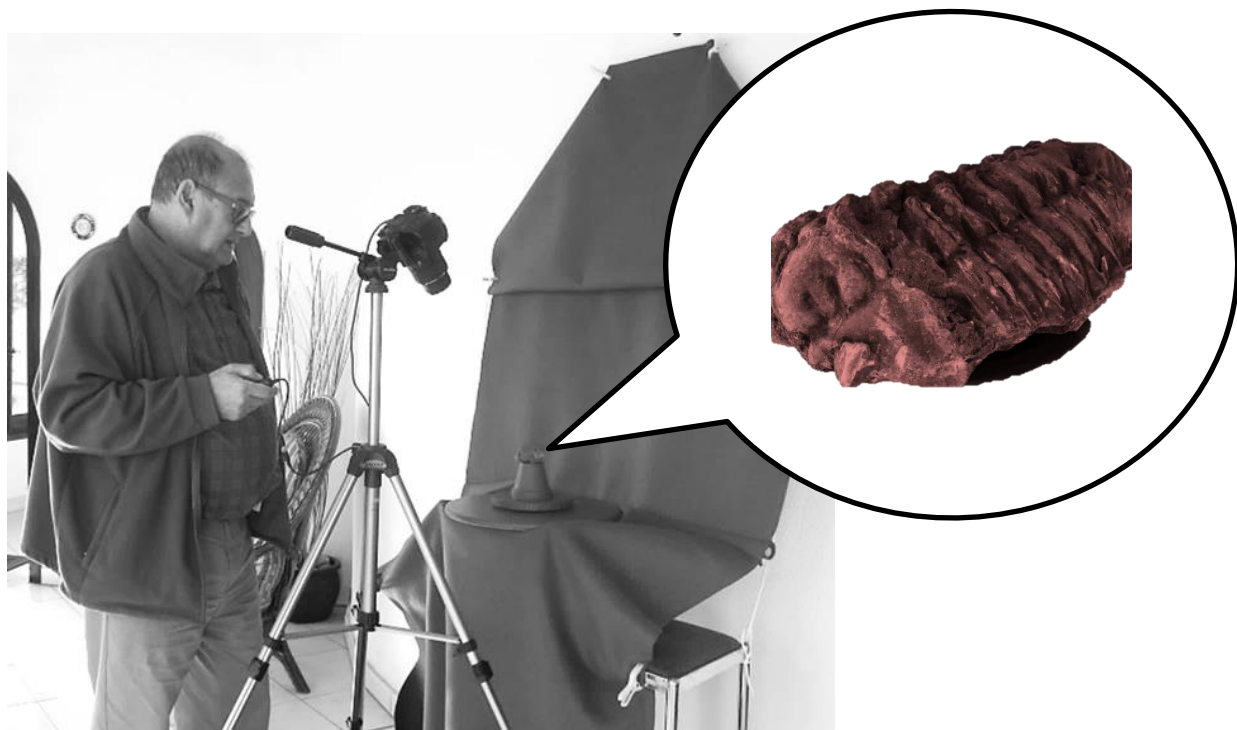


Figure 4.93: Photographing the Trilobite under a Naya with only natural light.

Hanging the backcloth on a hook, on the wall, with a few rods to hold the cloth in place and a box placed on top of a couple of stools, all covered with the backdrop, supported the turntable. This could equally have been under a tree, in the field, collecting stones or fossils. Simplicity in execution was the key in all areas of the research

In Figure 4.93, the author can be seen photographing a rusty red Trilobite (good contrasting colour) against a green backcloth, which produced a good set of images. The high resolution, point cloud image, is shown in the adjoining photograph. This Trilobite was just one of several “natural” objects that became the subject matter for research being photographed under natural light. Amongst the other objects were a piece of concrete and stone mix, an Ammonite, the Trilobite, two sea shells and two pieces of rock found in a Spanish garden. This diversification came about because of an article on the British Geological Survey [182] web site.

*“The GB3D type fossils online project, funded by Joint Information Systems Committee (JISC) [183], aims to develop a single database of the type specimens held in British collections, of macrofossil species*

*and subspecies found in the UK, including links to photographs (including 'anaglyph' stereo pairs) and a selection of 3D digital models."*

In the JISC project, many of the fossils were LS and it was decided by the author to investigate and see how such objects could be digitally captured by a single DSLR camera. Five of the objects are discussed in later chapters; all were successful in the RE and fabrication, and AM models created.

The exception was the batwing shell, which had a very shiny surface on the inside, and the reflection caused a slight orange peel effect, which would have been very detrimental to the smooth mother-of-pearl type surface this shell had in its inner surface - see Chapter 6.2.8 for full details. The remaining two objects are included in Figures 4.94 to 4.96. The first of the rocks shown was the larger of the two and had a series of natural holes going through the rock.



Figure 4.94: Original rock.



Figure 4.95: Screen shot of textured dense cloud rock image.

It weighed 3074 grams and measured approximately 190mm x 600mm x 600mm (Figure 4.94). A total of 138 digital images were taken and processed using masked images as described in the earlier section of this Chapter 4.10.1. The holes through the stone are seen in the dense cloud image of Figure 4.95. Although not fabricated an \*.stl file was created and a small stand was added, ready for display (Figure 4.96).



Figure 4.96: \*.stl image of a rock mounted on a stand and with holes through body.

The smaller rock was much smaller, being 70mm x 110mm x 40mm and weighing 219 grams (Figure 4.97). A small wooden prop (as indicated) was required as a support whilst on the turntable, but eliminated during image processing (Figure 4.98). More props could have been used for stability, but this would have entailed longer time during the masking stage prior to processing the data set (see Chapter 4.10) and also more digital image compensation by the software.

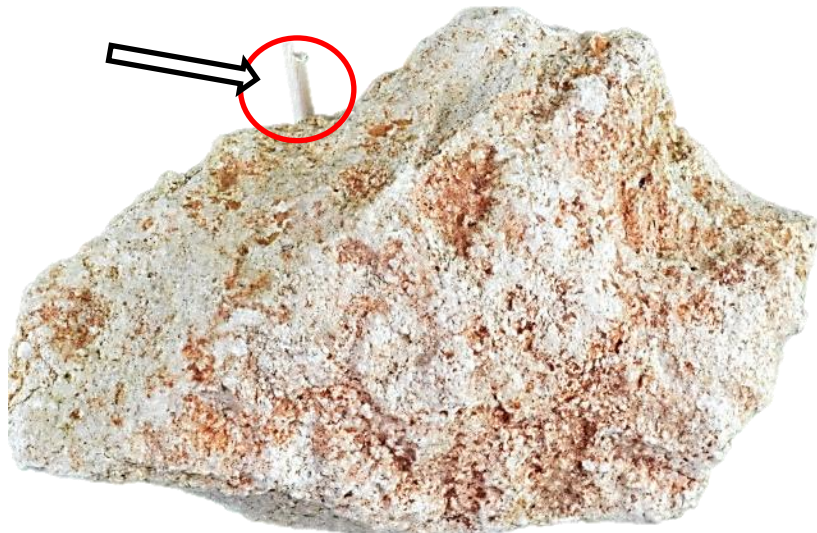


Figure 4.97: Original small rock.

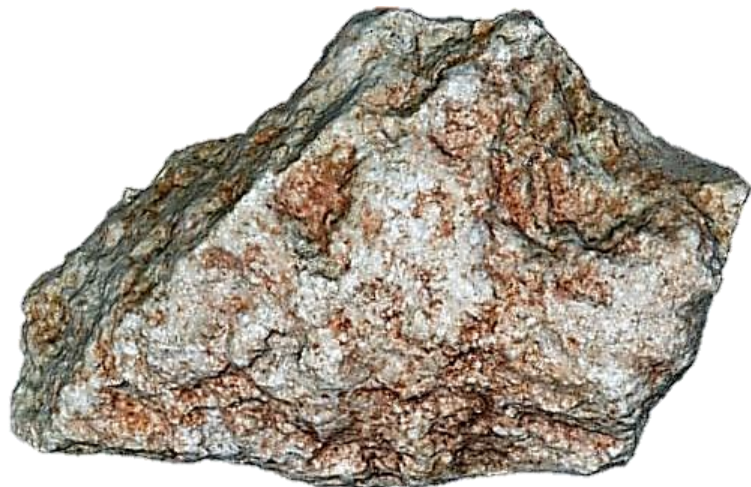


Figure 4.98: Textured dense cloud image of small rock with wood prop removed.

116 images were taken with this stone and the short prop was removed in the primary processing using the same method as with the concrete and stone mix, see Chapter 4.10

Overall this mini project with fossils, stones and shells showed that there were no major problems in replication of such artifacts except the normal type of restrictions that apply to any artifacts, and that a single DSLR camera with adequate natural lighting produced very good digital images leading to successful replicated models.

#### 4.16.2 Hanging on the Wall



Figure 4.99: Relief canvas - Camera positions seen from above looking down.



Figure 4.100: Relief canvas - Camera positions as seen from horizontal plane.

In this photoshoot session (Figure 4.99), the subject was a multimedia “Relief” canvas which was hanging on a wall. The natural light was coming from a window directly opposite the canvas giving a bright shadowless illumination to the subject. Setting up the camera, as seen in Chapter 3.4.2, the series of 63 images were captured in one session.

The camera was moved through the vertical plane 180°, then back again but moving the camera up in the horizontal plane by approximately 40°. These two planes can be seen in the Figures 4.99 and Figure 4.100.



Figure 4.101: Selection from the Photographic sequence of 68 images.

As in Figure 3.15, the camera distance in relation to the subject would have been maintained, in this instance by a pole, not a cord, tied to the tripod keeping it an equal distance from the wall. In the nine images from the photoshoot of 63 the changing angle can be seen in Figure 4.101. This series of images were processed using *123D Catch®* and no additional photographs were added, only the normal cleaning when the processed file was returned by Autodesk. Here was an example that had broken all the aforementioned “rules”, but in reality emphasises two golden rules, good lighting and good overlap of images produces good 3D models.

#### **4.17 Coded and Non-Coded targets**

Chapter 4.14.1 refers to the importance of correct focusing of the camera lens on the object that was being photographed so as to ensure sharp images were captured. The camera could be set, either automatically or manually, to focus on an area of different sizes known as the ‘*target area*’. The size of this area was dependent on the object’s size. This procedure should not be confused with Coded or Non-Coded targets.

Due to the irregular geometric form of most of the artifacts that have featured in this thesis, the use of coded or non-coded targets has not been required. The other reason for not using these has been the non-invasive method of data capture, as shown in the use of surface coverings to help reduce flare which might be caused by the lighting conditions and the reflective nature of the artifacts’ surface (see Chapter 6.2).

None of the artifacts were subjected to any surface markers which might help in the alignment of images during the point cloud image processing. Chapters 5.2, 5.3 and 5.4 demonstrate the straightforward processes for re-orientation, resizing, measuring and where required the re-scaling of the models without the use of any markers or coded or non-coded targets which could have been used in the original photographs to calibrate, orientate and measure the replicated artifacts. Coded and non-coded targets are prepared markers that can help reconstruct a 3D model of a scene. There are two types of markers, the difference being that the non-coded target looks like an ordinary full circle or a figure (circular /rectangular) with 4 four segments (Figure 4.102).

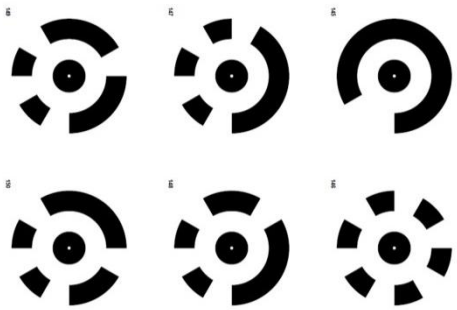


Figure 4.102:  
Agisoft non coded targets [7].

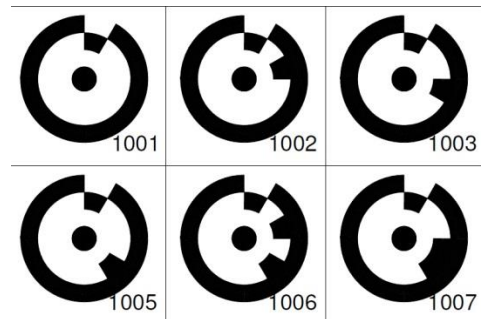


Figure 4.103:  
Coded targets [184].

Whilst the coded target has a ring sectioned into black and white segments around the central full circle (Figure 4.103). They can be used for creating points on curved or flat surfaces that do not have distinct feature points, and for highly accurate measuring between any given points.



Figure 4.104: Quadra 1 - underwater target frame.

The size and shape of the targets can vary, as can their use. Digitisation of the human face by Galantucci *et al.* [185] used small coded targets of the type seen in Figure 4.102, whilst for an underwater project monitoring red coral in the Mediterranean Sea, Drap *et al.* [186] used two types of rectangular frames measuring 23x27x1.5 cm, with a series of smaller targets printed on the top frame surface as shown in Figure 4.104. If aerial photogrammetry is undertaken using a UAV, as might be used in mining or archaeology [187], and depending on the height reached by the UAV, much larger targets are required so as to be identified in the digital images captured by the camera. There are many examples

of coded and non-coded targets and many of the software programs used have their own specifically designed targets (see Figure 4.105) [188].

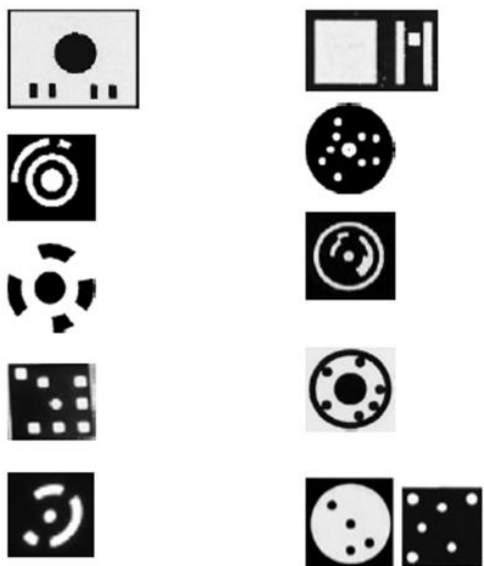


Figure 4.105: Selection of target shapes.

Agisoft, in their manual [7] give the following advice/warning about the use of non-coded targets:

*“Non-coded targets are more appropriate for aerial surveying projects due to the simplicity of the pattern to be printed on a large scale. But, looking alike, they do not allow for automatic identification, so manual assignment of an identifier is required if some referencing coordinates are to be imported from a file correctly.”*

It was felt that using both coded and non-coded targets added another layer of complexity to the process for RE of artifacts and as shown in Chapters 5.2 to 5.8, the software used could accommodate resizing, measuring etc. If the objects to be photographed are complex in form and shape, with lots of matching and identifiable points, taking an extra quantity of images is worth the extra time, rather than struggling with the additional complexities of targets.

#### 4.18 Summary - Methodology 2 & 3

Many of the current research papers have used *PhotoScan Pro*<sup>®</sup> to process the digital information that has been obtained from a variety of sources and to turn that captured data into 3D virtual images. The resulting point cloud files still have

to be processed by another software program to make them readable by AM machines. This research found that unlike Autodesk, AgiSoft's program was best run and produced best results on high end CPU's with more than average RAM, ideally computers running a minimum i5 but preferably an i7 processor and a minimum of 32GB RAM; 132RAM was ideal (or more) with GPU cards with a minimum of 4GbRAM on each card. This enabled the program to handle far more photographs, at realistic speeds (time taken to process), and therefore created more detailed meshes. Unfortunately in most cases processing artifacts at High or Ultra High resolution produced data files too large for the current AM technology to handle, but the virtual screen images were excellent. Unlike *123D Catch*<sup>®</sup> a video option was not available with the version of *PhotoScan Pro*<sup>®</sup> used. The operator, however, had far more control in how the input data was processed, did not need an internet connection for processing the data, and was confronted with a relatively simple interface, a good internet blog site to consult, as well as a very fast e-mail help desk. Overall the program produced some very good point cloud images which went on to produce excellent reproduction replications of the artifacts in question.

## Chapter 5: Secondary Processing

### 5.1. Using *StudioPro*<sup>®</sup>

Netfabb's *Studio Professional*<sup>®</sup> was used for all of the research, and was upgraded in to the latest versions as the research progressed.

The photographic images from the data capture were processed as described in Chapter 4, using either AutoDesk's *123D Catch*<sup>®</sup> or AgiSoft's *PhotoScan Pro*<sup>®</sup>. As seen in Figures 4.5 and 4.32, both these methods used the primary processing software to convert the images into dense cloud virtual 3D images. In the case of *PhotoScan Pro*<sup>®</sup>, they could exist in this state as Ultra Low resolution through five stages to Ultra High resolution. This could be seen in the example of the Ammonite Fossil (Chapter 4.11, Tables 4.9 and 4.10), with a range of over 4.8 million polygons, or triangles, to the lower end of 0.45 million polygons. This digital information could have been saved in a selection of formats, but in this research, all files were saved at this stage, using the above software, as \*.obj files, ready to be imported into *StudioPro*<sup>®</sup>.

It must be remembered and as stated by Netfabb, *StudioPro*<sup>®</sup> is essentially software for AM file preparation, not for constructing or reconstruction of the original data file. Holes and other minor errors therefore are repaired in the most simplistic way. If there was a defect with the original \*.obj, file it had to be repaired, (as will be discussed in Chapter 6), before it could be imported into *StudioPro*<sup>®</sup> for final processing and conversion into an \*.stl file for the AM machines to fabricate 3D models.

The second stage of processing started when the data had been imported into *StudioPro*<sup>®</sup> in the form of a 3D textured mesh. Until exported as an \*.stl file, *StudioPro*<sup>®</sup> stored the file as a netfabb project file with an extension \*.fabbproject or *StudioPro*<sup>®</sup> Data, the software forming its own unique format. In all versions of this software, the \*.psd file lost all colour references and this information could not be restored and used on a colour AM machine. Where colour was important, a different software package was used, e.g. *DeskArts 3Data Expert*<sup>®</sup>.

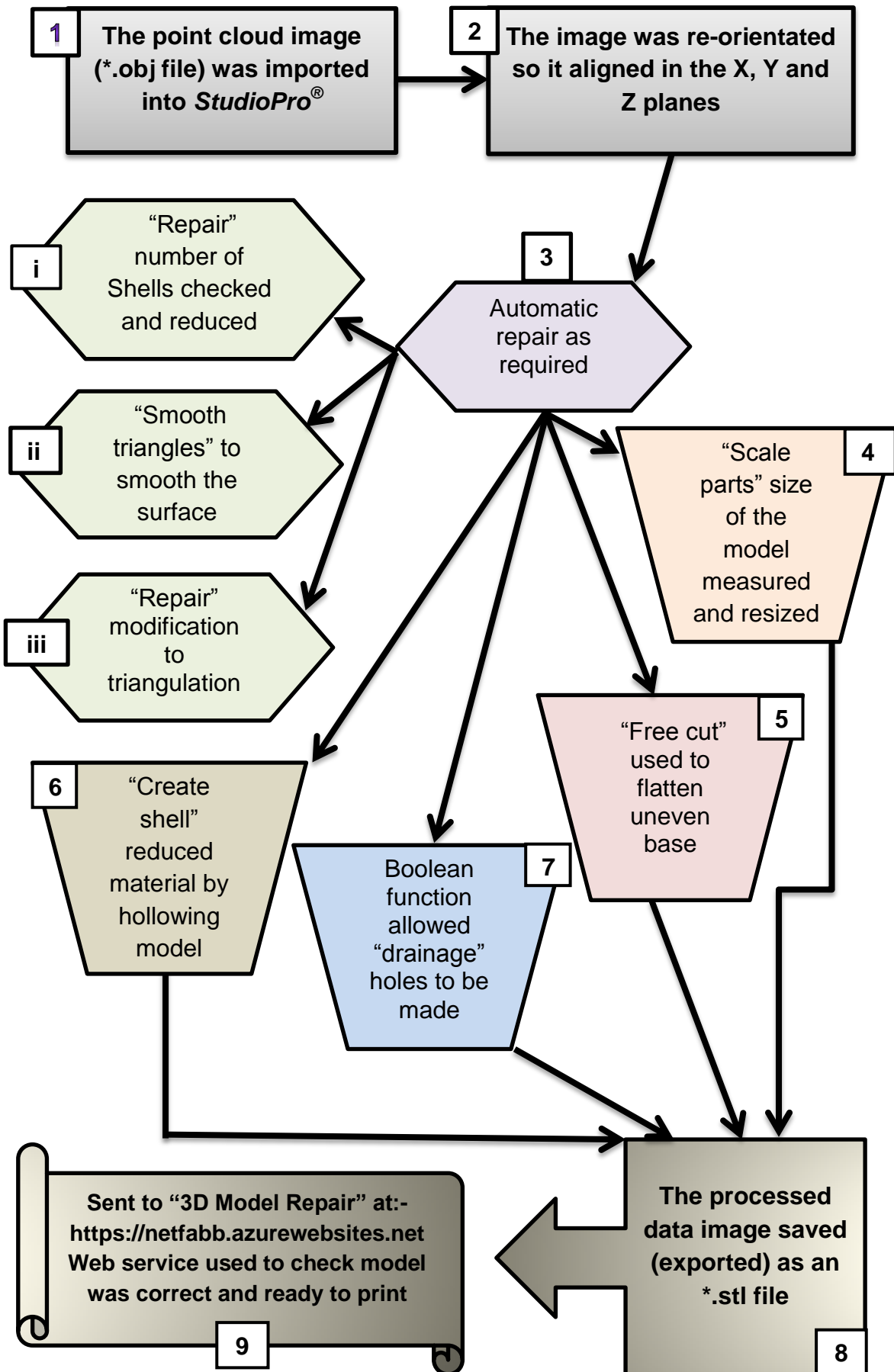


Figure 5.1: Main data processing functions of *StudioPro®*.

Figure 5.1 shows the main data processing sequence using *StudioPro*<sup>®</sup> and is explained as follows (though not necessarily in this order, nor were all operations required on every model):

1. The point cloud image (\*.obj file) was imported into *StudioPro*<sup>®</sup>.
2. The image was re-orientated and repositioned so it aligned in the X, Y and Z planes, represented by a square or oblong outlined box.
3. Automatic repair and “Apply repair” were used as required for minor repair work.
  - i Using the “Repair” function, the number of “Shells” was checked and reduced as required.
  - ii If required, the “Smooth triangles” command was used to smooth the surface.
  - iii Using the “Repair” function, modification to the triangulation of the model could be carried out (see Chapter 6.2).
4. The size of the imported model was measured and resized using the “Scale parts” function so as to match the original dimensions of the artifact.
5. The base of the object was not always flat, due to the method of data collection. The “Free cut” function was used to rectify this problem by cutting off any irregularities. The model was then rechecked for height measurement.
6. The amount of material used in fabrication was reduced by hollowing the model and using the “Create shell” function. 2.5mm – 3mm was usually sufficient thickness for the shell wall.
7. If required, drainage holes were made in convenient positions using the Boolean function. This allowed any unused powder or liquid to be removed when using the SLS or SL processes.
8. The processed data could then be saved (exported) as an \*.stl file.
9. Finally, if required, the model could be uploaded, via the internet, to “3D Model Repair” [189]. This web service was used to check that the model was correct and ready to print; this facility, provided free by Netfabb, ensured that the model was 100% error free.

Of the many features of *StudioPro*<sup>®</sup>, the preceding list of functions proved to be the most useful in the completion of the models, examples of which are shown below in Chapters 5.2 to 5.8.

## 5.2 Re-orientation

Although re-orientation of the model is not essential, it helped the operator visually when working on the video monitor to have all models orientated in the same axis. It was also important that when measuring the virtual image against the original artifact, all data was in the same orientation so as not to distort the model.

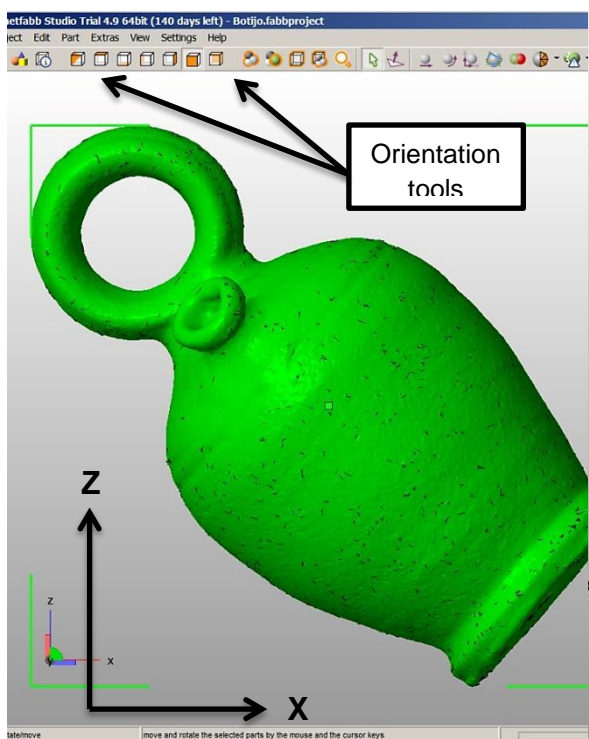


Figure 5.2: Original imported image.

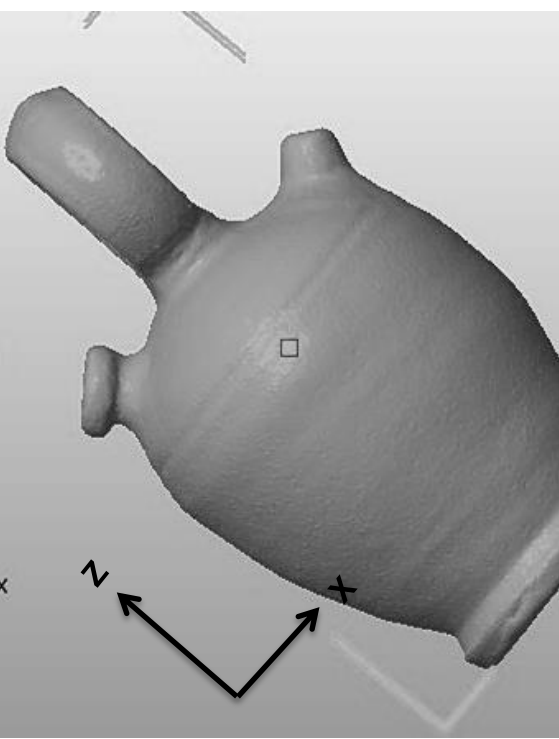


Figure 5.3: Re-oriented image of Botijo.

When the data was imported from *123D Catch*<sup>®</sup>, the image usually, but not always, appeared on the monitor in the correct orientation but in its own arbitrary scale. When importing an image file from *PhotoScan Pro*<sup>®</sup>, the orientation was never in the desired orientation of Z (Up), X (to the Left), and Y (Forward).

By selecting one of several controls from the tool bar (i.e. front, back, top, right side, etc.), the model was realigned to the correct orientation. The image in Figure 5.2 shows the orientation of the Botijo.obj file just as it was imported into the Netfabb software program. Once the image had been re-oriented as in

Figure 5.3, it could be noticed that the Z and X planes had moved and the jar was now in the correct axis. In Figure 5.4 the jar is in the correct upright position, the Z axis pointing upwards and the X axis parallel with the bottom of the jar.

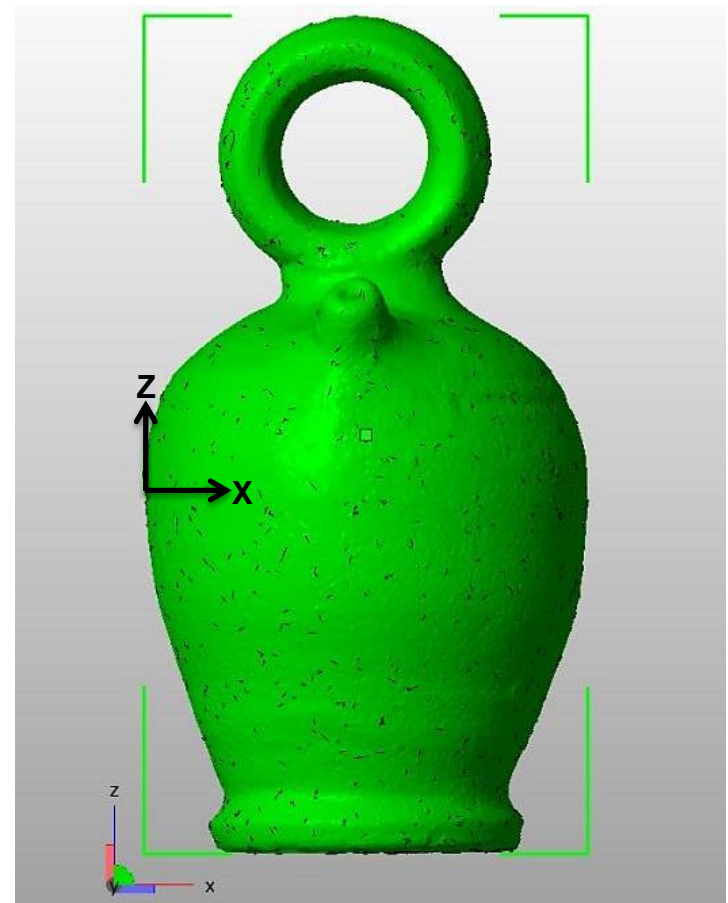


Figure 5.4: Botijo - Front facing - correct orientation.

The orientation of the XYZ plane is explained in the Agisoft manual as follows:-

*“The local camera coordinate system has origin at the camera projection centre. The Z axis points towards the viewing direction, X axis points to the right, and Y axis points up.”*

This is different from *StudioPro®*, where Z axis points upwards as seen in Figure 5.5. X axis points to the left and Y axis points forwards.

*123D Catch®* has the option to change the upwards position of orientation and define the world co-ordinate system, but as the default orientation was the same as AgiSoft's *PhotoScan Pro®* this was not altered (see Figure 5.5). However, it was a simple operation to change the orientation of the object within this program if required. If the orientation of the component was changed in

*PhotoScan Pro*® before the image was exported and saved as an \*.obj, it would be imported into *StudioPro*® retaining the new orientation.

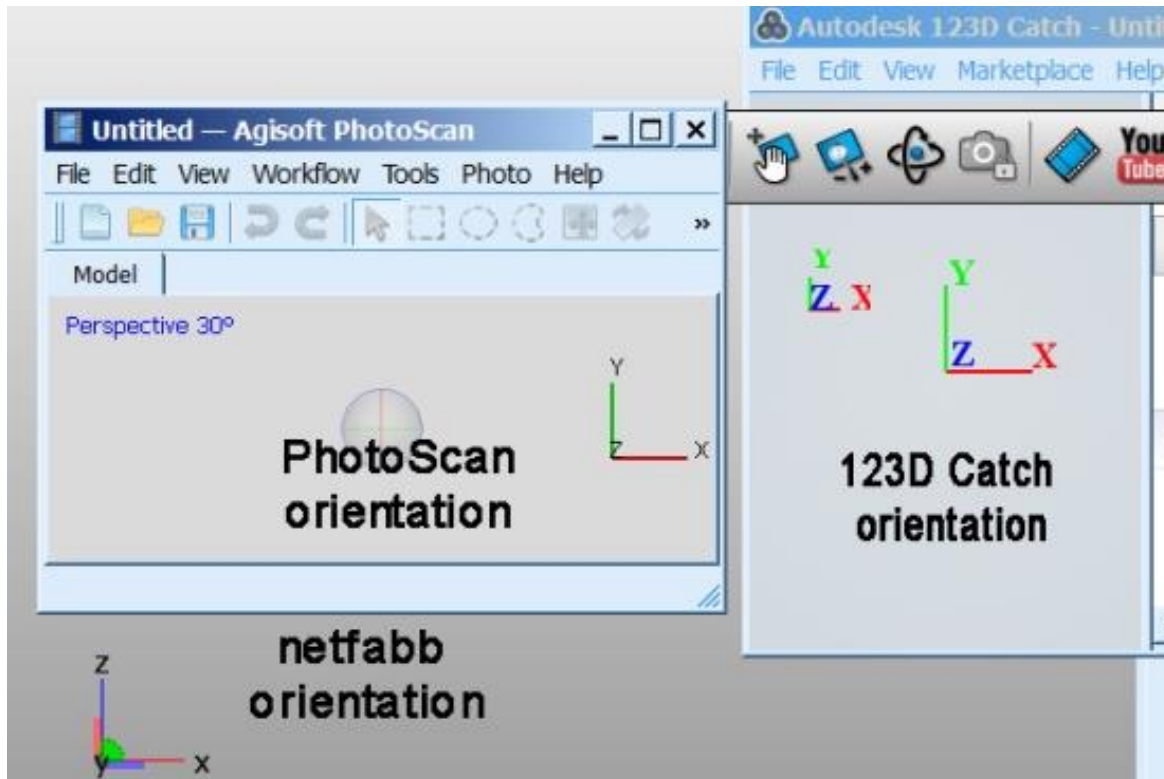


Figure 5.5: X,Y,Z Axes orientation of the three programs.

As seen in Figure 5.6, the orientation axis is the same for both images, the screen shot image on the left is from *StudioPro*® whilst the right hand image is from *PhotoScan Pro*®.

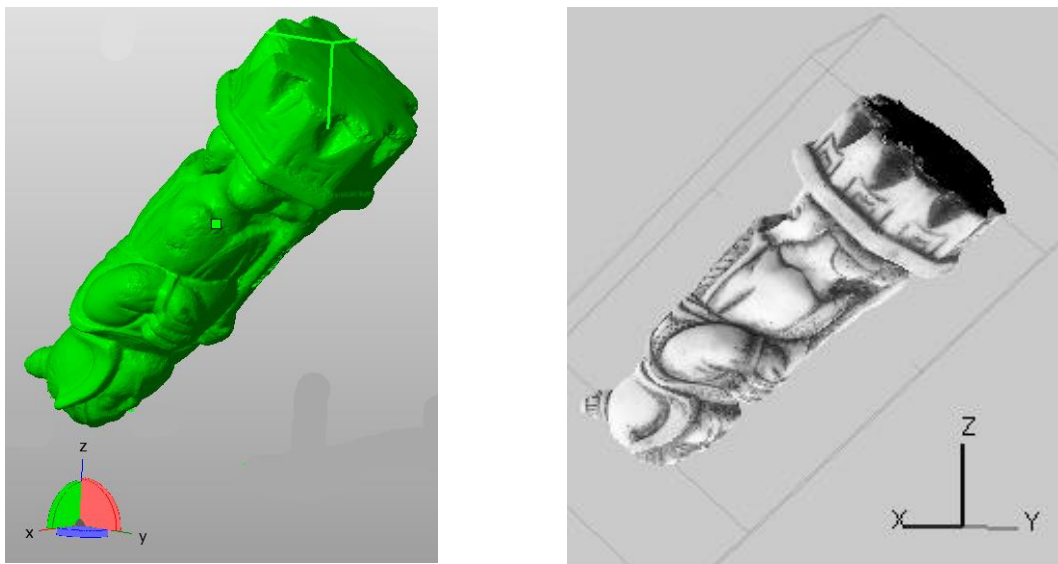


Figure 5.6

Imported orientation of the Warrior into *StudioPro*® from *PhotoScanPro*®.

Fortunately, within *StudioPro*<sup>®</sup>, it was a simple task to change the orientation of the imported image of the component, should the imported orientation be different from what was required. The “Rotate Parts” function could be used by the operator who could control the rotation in all directional planes to ensure that the model was reoriented to the desired plane (see Figure 5.7), by filling in the required figures into the rotation chart.

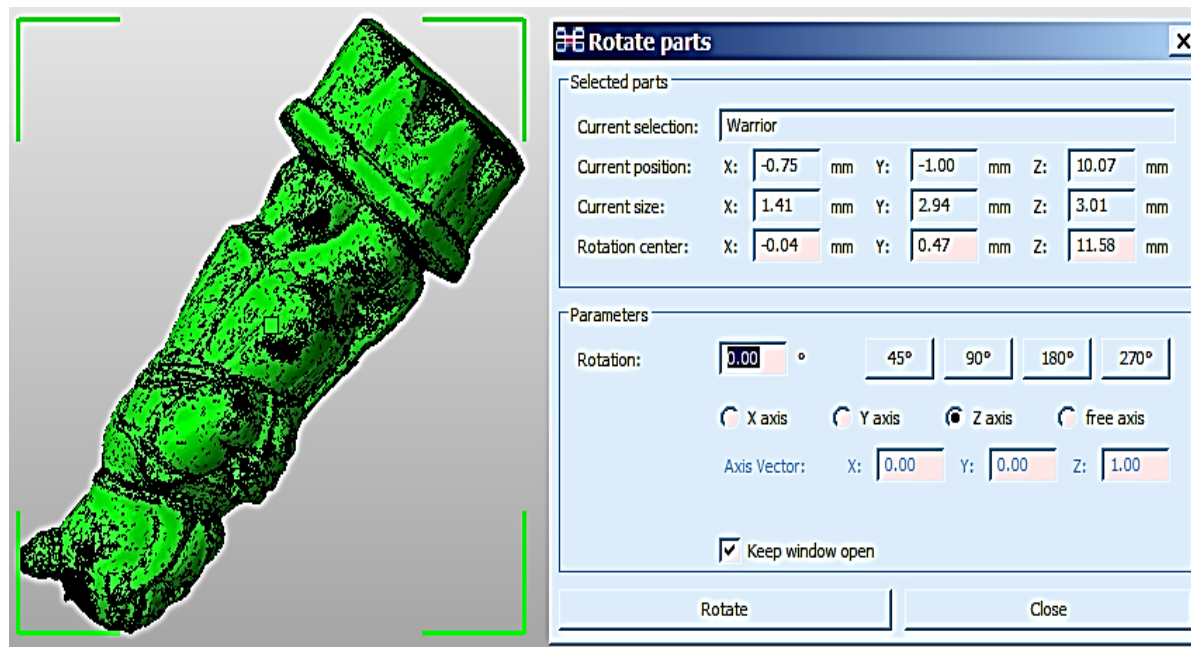


Figure 5.7: Orientation of imported part and rotation table for realignment.

### 5.3 Measuring the Digital Image

The measuring tool was upgraded in the later versions of the software and was able to perform a variety of functions such as: depth of shell; point to point; angles; radius; and highlighting points on an image, all of which were able to be screen captured for later publication in documents if required. It was found that the resulting dimensions of the 3D image obtained from the primary software when imported into *StudioPro*<sup>®</sup> did not match the original dimensions of the object photographed. This raised the question of whether the images had been reduced by a set percentage, or whether they had been created in an arbitrary scale.

A selection of models was chosen and the dimensional data of each item tabulated as shown in Table 5.1. The models were measured having been re-oriented as in Figure 5.4, where the Z axis points upwards, X axis points to the

left and the Y axis points forwards. The scale-up factor and percentage increase needed to augment the model to full size was calculated for each model.

Table 5.1: Dimensions of imported models into *StudioPro®* from *PhotoScanPro®*.

	Imported size	Actual size	Scale-up factor	% A	% B
<b>Eureka Cat</b>					
Height	0.44	35.00	79.55	1.26	7954.55
Width	1.01	80.00			
Depth	0.20	16.00			
<b>Warrior</b>					
Height	3.43	90.00	26.24	3.81	2623.91
Width	1.31	35.00			
Depth	1.48	35.00			
<b>Horus</b>					
Height	1.43	178.00	124.48	0.80	12447.55
Width	0.48	72.00			
Depth	0.58	54.00			
<b>Sobekhotep</b>					
Height	3.06	200.00	65.36	1.53	6535.94
Width	0.90	20.00			
Depth	1.51	40.00			
<b>Clay Dog</b>					
Height	0.95	90.00	94.74	1.06	9473.68
Width	1.30	140.00			
Depth	1.92	180.00			
<b>Clay Bottle</b>					
Height	0.90	200.00	222.22	0.45	2222.22
Width	0.46	100.00			
Depth	0.22	40.00			
<b>Botijo</b>					
Height	3.48	100.00	28.73	3.48	2873.56
Width					
Depth	1.86	110.00			

- Import Size = model size as imported into *StudioPro®* from *PhotoScan Pro®*.
- Actual size = Actual size of original artifact.
- Scale-up factor = Actual size divided by imported size.
- % A = percentage size of imported model against original model.

- % B = percentage size of imported model against scale-up factor.

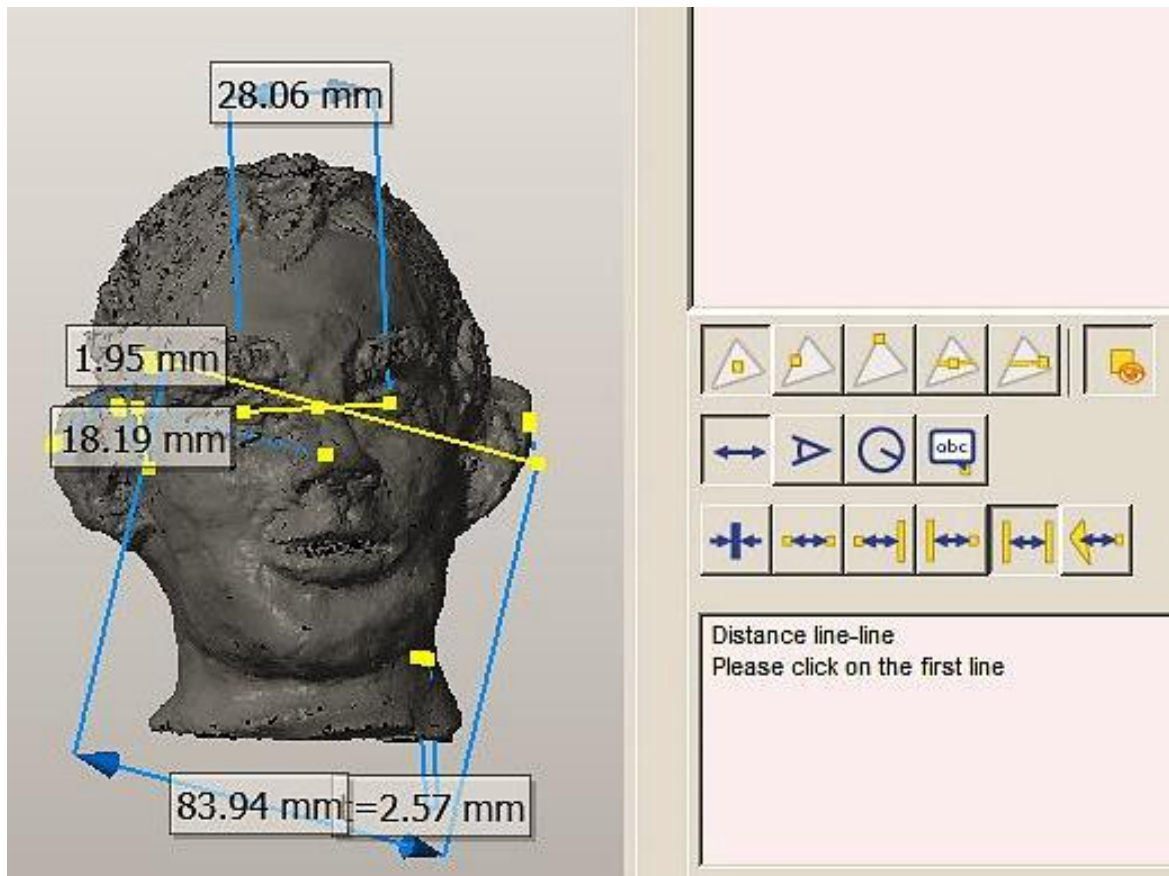


Figure 5.8: Measuring tools and essential dimensions displayed on model of head.

On examination of the data presented in Table 5.1 it must be concluded that the scale reduction of each model is an arbitrary one and not governed by any percentage increase or decrease within the software. The dimensions selected, together with a selection of measuring tools, can be displayed as seen in Figure 5.8.

In the example of the Warrior (Figure 5.9), when photographed, the model was standing on a plinth, the camera was unable to capture any data for this lower area and in processing, the software filled the area between the edges forming a bulge. To ensure the maximum dimensional accuracy, the slicing off of any such bulge or distortion was performed after the model was resized up to its original artifact dimensions. If for example, the slicing took place before re-sizing the Warrior, one might be deceived into thinking that the bulge was insignificant as the excess to remove might be measured in the hundredth of a millimetre.



Figure 5.9: Removal of bulge at bottom of model.

As indicated in the Table 5.1, the Warrior model, before resizing, was only 3.43mm high. The bulge indicated in Figure 5.9 was the result of the processing and had to be levelled by slicing it off along the red line, otherwise the model when fabricated would have toppled over. When calculating the ratio to rescale the model, see Chapter 5.4.

As discussed in Chapter 5.2, to ensure accuracy, rescaling this was best done in the same orientation as model and artifact. The camera was unable to capture any data for this area and in processing the software filled the area between the edges.

#### 5.4 Scaling and Resizing

Obtaining accurate measurements for large objects such as buildings or monuments could have been a problem, but it was not within the scope of this thesis, which only concerned itself with smaller sized artifacts and those which could be easily measured. Huang *et al.* [190] attributes this measurement problem to the use of long focal length lenses which produce limited field of vision when measuring such large buildings. Their solution was to use a digital camera

capturing images in both horizontal and vertical directions from each station position. Using this method with either a 300mm or a 600mm lens to....

“achieve millimetre scale accuracy at distances ranging from 40m to 250m”.

The two separate features of measuring and scaling, which existed in the *StudioPro®* software, were of great importance, as the final dimensional accuracy of the finished AM replicated artifact could be fine-tuned. This was needed to scale up the model to full size, thus ensuring that an exact dimensional copy was obtained.

#### **5.4.1 Scaling Using *PhotoScan Pro®***

As previously discussed in Chapter 4.17, sizing and scaling could be performed in *PhotoScan Pro®* using “Coded targets”, which were printed markers that can be positioned in the scene, around the target object, before photos were taken. These would be used by the software as reference points for coordinate system and scale definition or as valid matches between images which would help the camera alignment procedure via “Align Selected Cameras” option [191].

#### **5.4.2 Scaling Using *123D Catch®***

Within the basic *123D Catch®* software, there was a facility to resize the 3D model, and there were two methods of achieving this. In the first method, by using the “Creation Tools” and specifically marking reference points and reference distances on the photographs, a scale was created, which would then transfer to the exported \*.obj file. It was not very accurate as the process relied on identifying two points where the distance was known between them. This meant the operator being able to identify exactly the same points, on several photographs, with exactly the same precision. But unless there were very specific points on the model such as a corner or identifiable point, this operation was prone to error.

In the second method, control points known as coded or non-coded targets (see Chapter 4.17) were established at the initial scene which was to be photographed; using this method, a more reliable scaling would be obtained as the distance between control-points could be measured accurately. This was a surface measurement from point to point in a straight or curved line. Fryer *et al.*

[192] in re-assessing a project that had been established in 2004, and using the same data consisting of the original 16 images which had been uploaded to be processed with *123D Catch*<sup>®</sup>, came to the conclusion that:

*“Although not at the level of accuracies routinely achieved in normal terrestrial photogrammetry using control, the accuracy achieved was certainly useful for many applications.”*

They stated that in their view by the addition of more data (images) to the original data set of 16 images, the accuracy would have been greatly improved [192].

#### 5.4.3 Scaling Using *StudioPro*<sup>®</sup>

It was decided that the scaling tools available in *StudioPro*<sup>®</sup> were easier to use and gave a more accurate result than the scaling facilities within the primary software, as direct action was applied to the model ensuring that it was in the correct orientation first. For the purpose of this discussion, the Spanish Botijo was used for illustration (Figure 5.10).

In Chapter 5.2, the discussion centred on how to re-orientate the imported image but in this section the importance of having the correct orientation became very apparent. In the software there was an information table on the right hand side of the screen. In Figure 5.10, the \*.obj file has been imported into *StudioPro5*<sup>®</sup> and appears as though it was in the front orientation, which of course it was not.

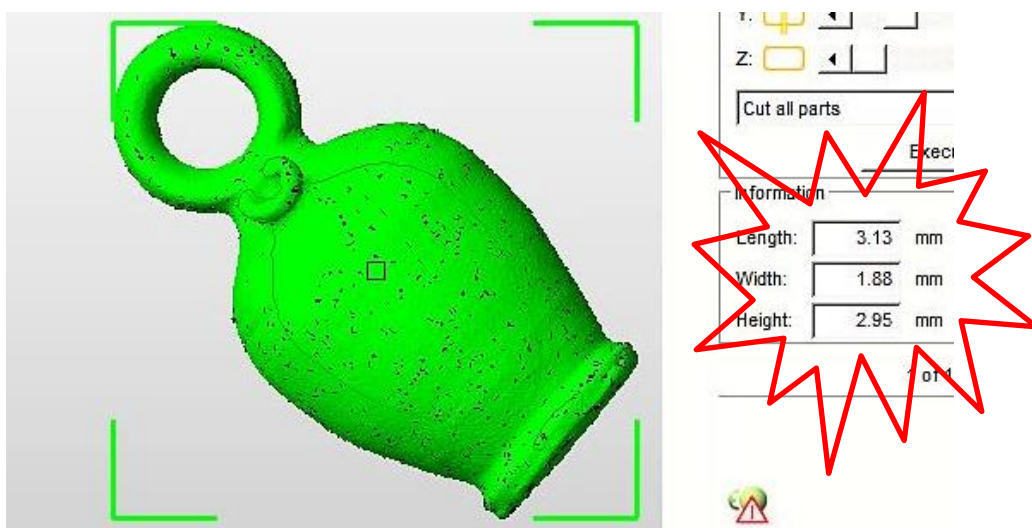


Figure 5.10: Botijo - Direct Imported dimensions and orientation.

The re-orientated image with a new set of dimensions is seen in Figure 5.10. But it will be seen that the two sets of dimensional information contradict each other. The first set of numbers are the dimensions of the model, in the orientation as imported into *StudioPro®* as seen in the screen shot, which entered the software at approximately 45°. To find the correct ratio increase needed to resize the model, the height was measured on the original artifact and divided by the model height. The software measurements were calculated in the three axes, according to the surrounding box in which the model resided.

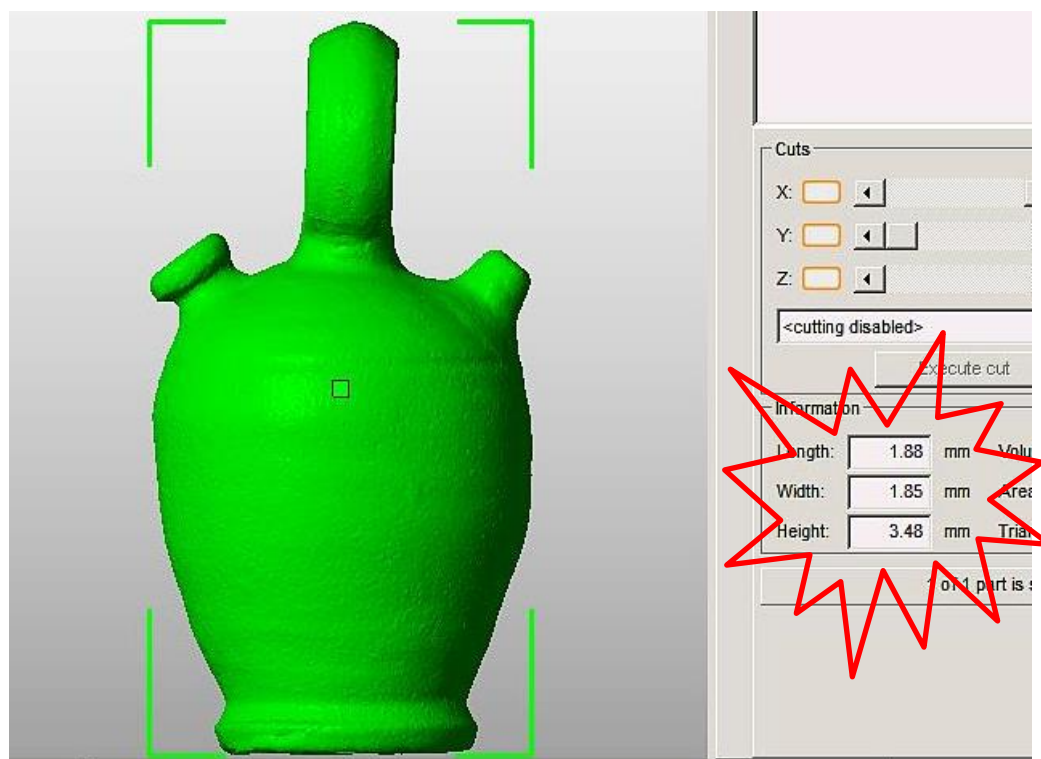


Figure 5.11: Botijo – Reoriented to correct frontal view.

By dividing the model's dimensions, into the full size dimensions (named 'dims'), the ratio or scale factor increase was calculated. Only the front of this box is seen and the corners are highlighted in green. If the first set of measurements had been used, Table 5.2 shows the error that would have occurred.

Table 5.2: 'Scaled parts' errors – Spanish Botijo

	MHZ	HS $\beta$	CH	OAH	OAW
Figure 5.10 dims Imported	2.95	67.80			
Figure 5.11 dims Re-orientated	3.48	57.47	236.21	200.00	105.00
All dimensions corrected to 2 decimal places					
MHZ = Model Height on Z Axis (mm) OAH = Original Artifact Height (mm) OAW = Original Artifact Width (mm) CH = Computed Height (mm)					
$HS\beta = \frac{OAH}{MHZ}$	= scale factor or ratio (this figure is NOT a percentage)				

Using the height dimension (the Z axis), divided into the height of the original artifact, gave the ratio by which to increase the size of the model in all the axes. When the image was rotated into the correct orientation and the ratio was used from the original Figure 5.12 (67.80) in the "Scale parts" box, the calculations were incorrect, as seen in Figure 5.11.

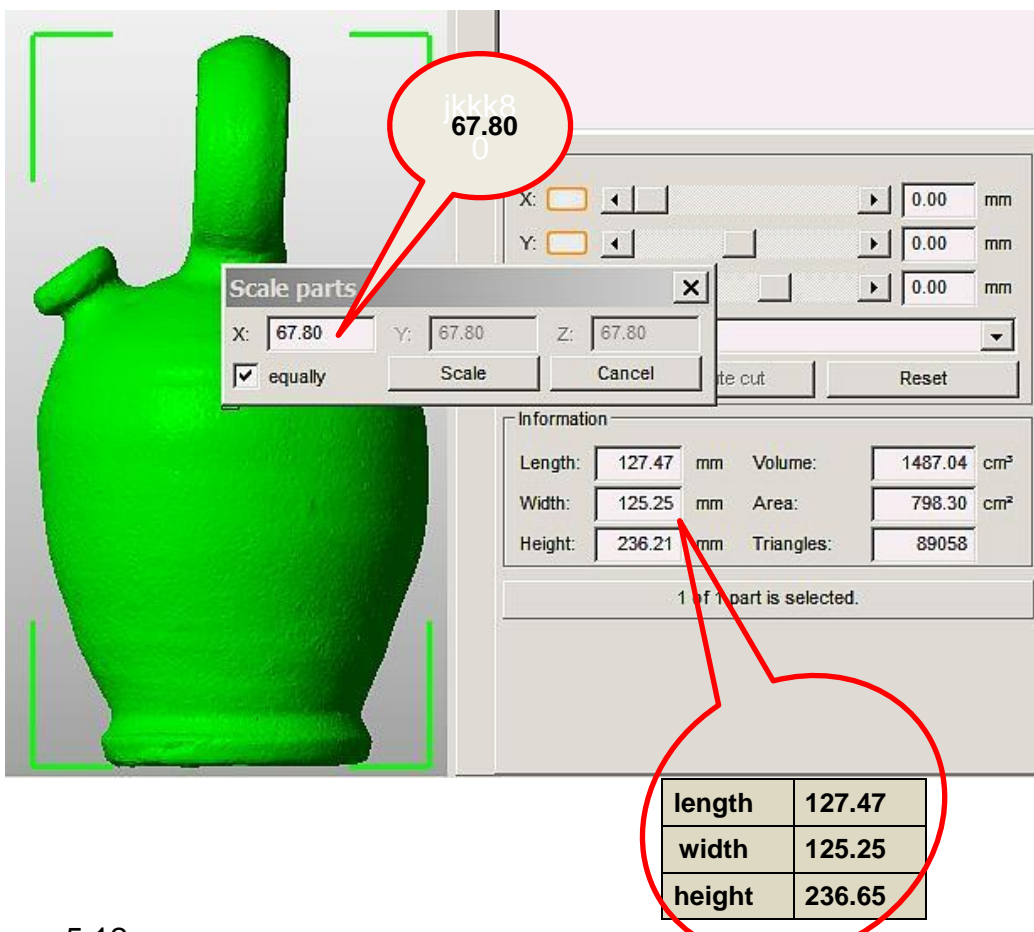


Figure 5.12:

Botijo - Incorrect ratio used – therefore dimensions are incorrect.

The actual number 67.80 is a ratio and is the amount that the model has to be scaled up or down and is neither a percentage nor has it a dimensional value.

Figure 5.13, in which the Botijo was re-orientated before any measurements were taken, shows the correct scaling ratio used and the correct dimensions produced by the software. Fortunately the interface of the “Scale parts” in the new version of *StudioPro®* has been redesigned and all the relevant dimensions have been incorporated within one table. By visually comparing the size of the 3D CAD model with the original, and by adjusting the scale factor needed to scale up the model within the software, an exact dimensional copy was obtained in all X, Y, Z axes.

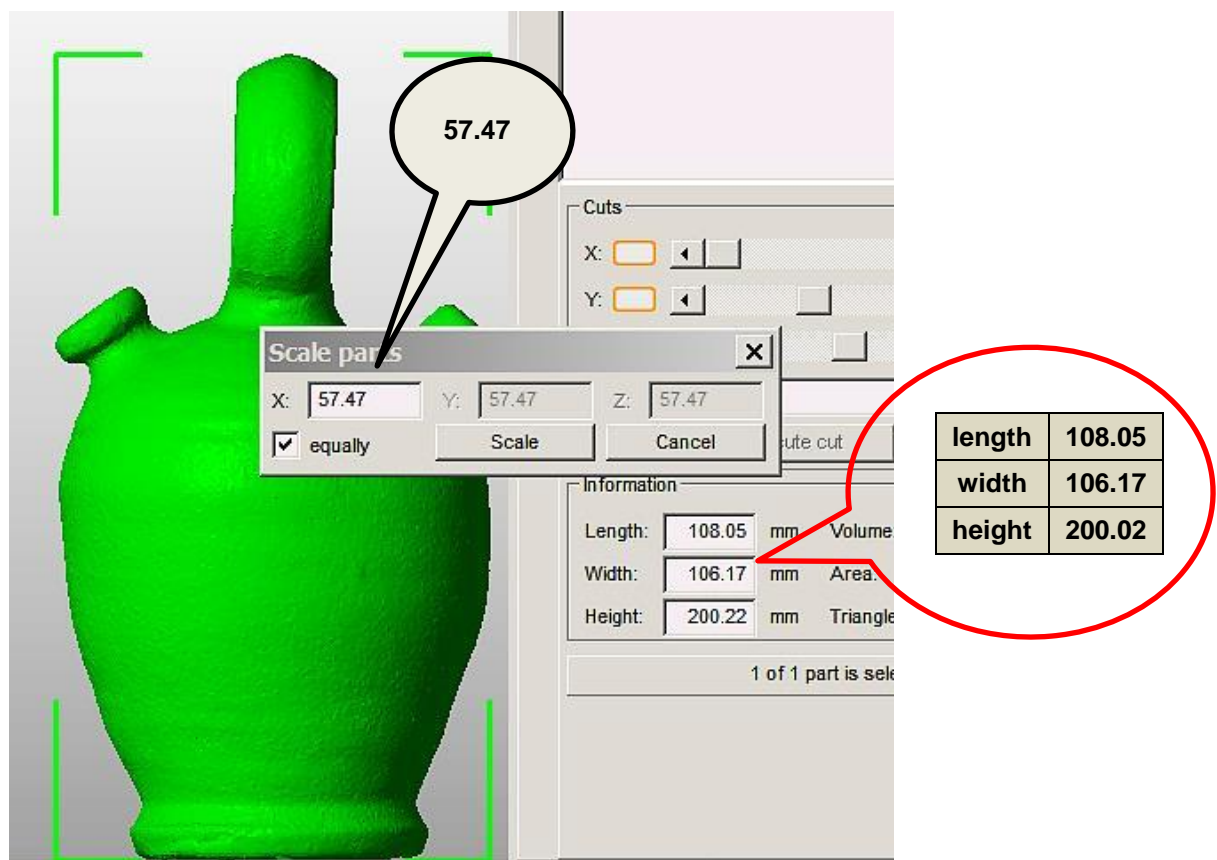


Figure 5.13: Botijo - Correct ratio obtained from correct alignment of artifact.

To make it even easier, the desired dimensions in the three axes X, Y, Z can be entered in the “Target size” box, as seen in Figure 5.14, and will be automatically re-calculated and re-sized to the measurements required. In the “Scale parts” chart in Figure 5.14 the actual size in the Z axis would have been increased by 1.5mm (depending on how large the bulge was), allowing for the

model base to be trimmed flat, and the bulge removed (Figure 5.9). By removing the tick in the “Fix scaling ratio” box, the destination size could be entered into the “Target size” boxes of all X, Y and Z axes, which meant that an uneven scaling ratio could be entered.

Importing the *123D Catch®* \*.obj files was more straightforward, although the images were in their own arbitrary scale, which was larger than *PhotoScan Pro®*. All the images were in the correct alignment in the Z axis and only had to be re-aligned in the X or Y axes.

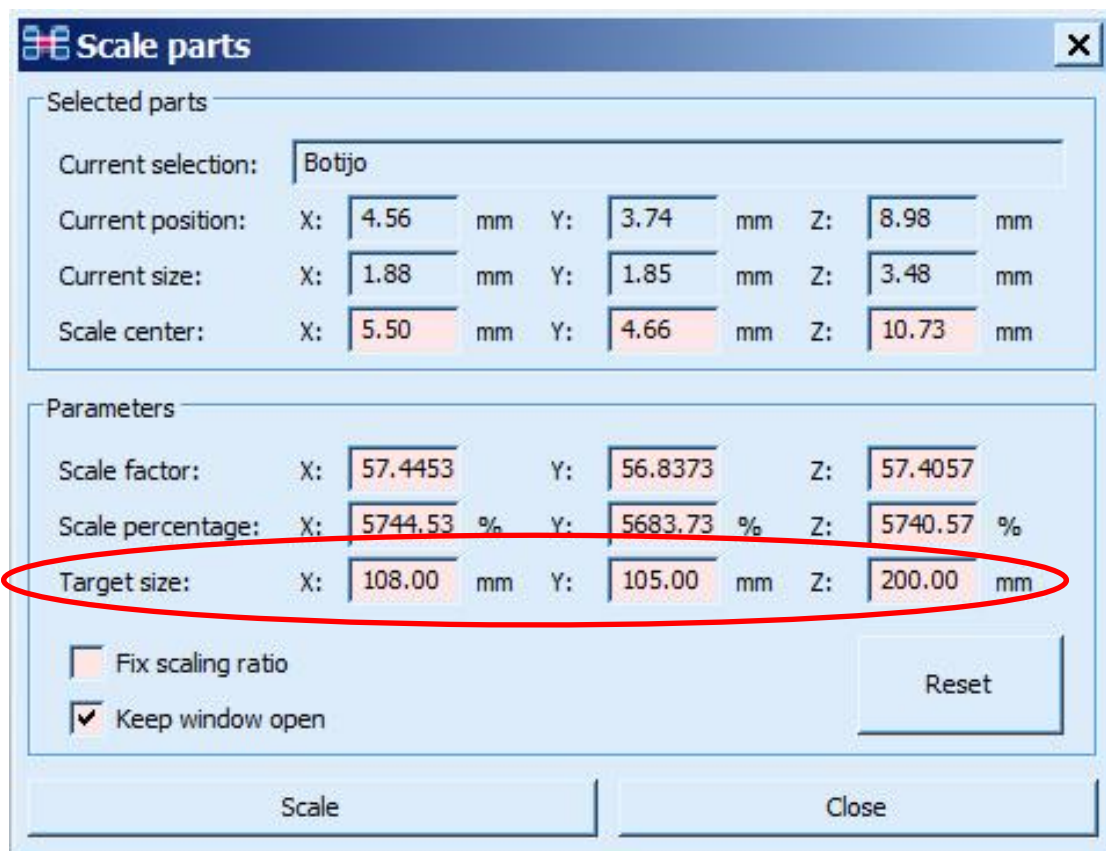


Figure 5.14: Screen shot of new version the multi-dimensional, Automatic Scaling function.

## 5.5 Slicing or Free Cutting

In most cases, if the artifact which was photographed had a flat bottomed surface, it would have rested on one of a number of small plinths. As the camera could not capture the underside of the object, a hole would be formed by the primary software in the initial processing. This hole would have been filled in on repairing the mesh, possibly forming an uneven surface.

This bulge or sloped bottom can clearly be seen in Figure 5.15 as a ridge, indicated by the arrow. The operation of levelling the bottom of the model could have been undertaken before rescaling the model, the problem being that the model was quite small and any cutting required a greater degree of precision than when the model was at full scale.

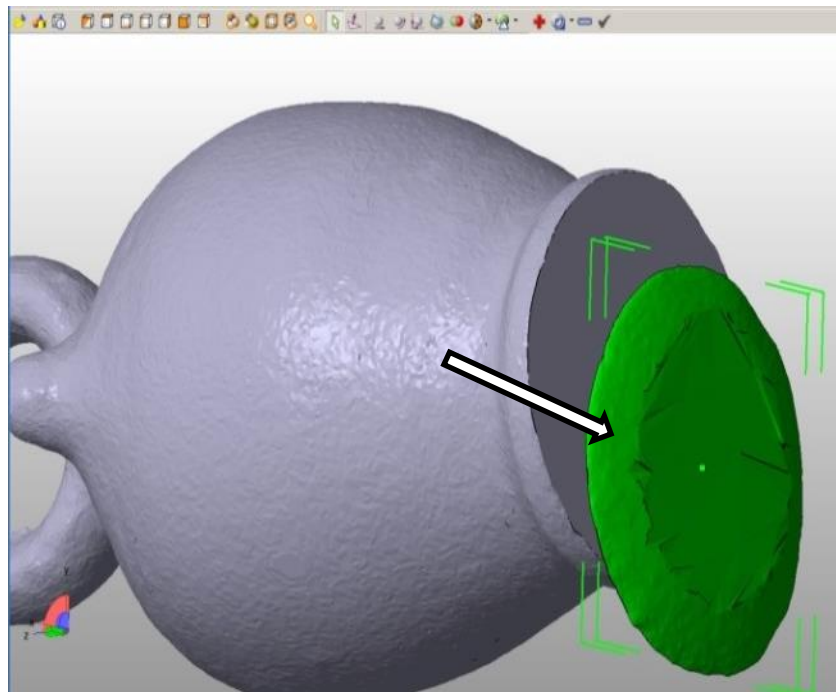


Figure 5.15: “Free cutting” tool to slice off the stepped bottom of a Botijo jug.

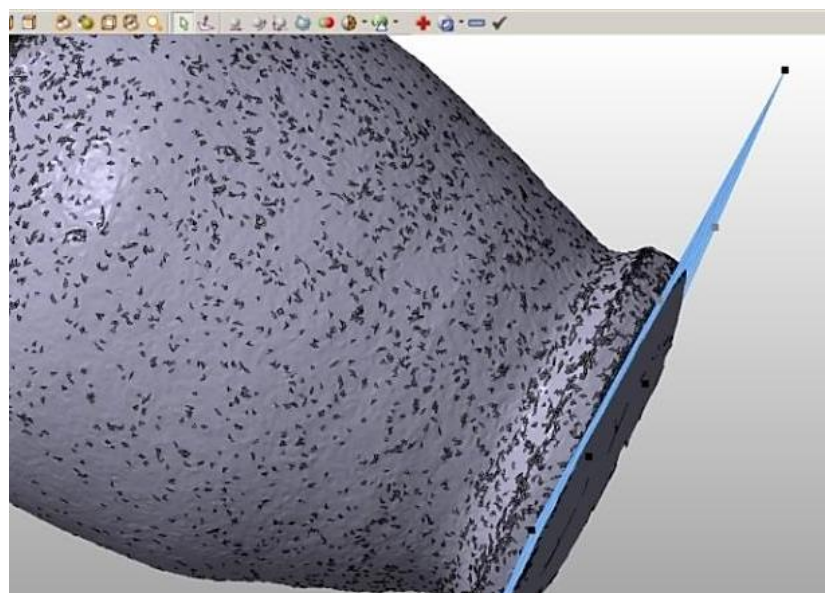


Figure 5.16: Flattening the rounded bottom of the Botijo jug.

Using the “Free cut” option, this bulge was removed, and by using the base grid to align the cutting plane, a perfectly flat plane being referenced to any other

part of the artifact was obtained by node point alignment. In some instances this free cutting option could also be performed by eye.

In Figure 5.16, the cutting plane was used as a marker for the rounded section to be sliced off and discarded. Careful observation had to be made of the perpendicular angles of the original artifact and caution had of course to be exercised when setting the base cutting plane by node point alignment; by way of an example, the integrity of the leaning Tower of Pisa would be totally lost if the base were cut at a perpendicular angle to the sides.

## 5.6 Hollowing

### 5.6.1 Shell Creation

The models that were created within the computer software were solid, but by using the “Create Shell” tool available within *StudioPro5®*, the models were hollowed or shelled. This shelling process was very important for the final outcome of the models because it reduced the amount of material that was used in the final fabrication process (see Chapter 5.6.2).



Figure 5.17: Half Ammonite Shell.

The screen shots show the hollowed out artifacts in Figures 5.17 and 5.19, both of which have been sliced in half to show how the outside contours of the

Ammonite Shell and the Botijo have been closely followed. The thickness of the models can also be checked by measuring the wall at different points scrutinising for consistency, as indicated in Figures 5.18 and 5.20.

The Ammonite was given a wall thickness of 2.5mm when the shelling tool was used in the *StudioPro®* software; however, when random selected points were measured, as shown in Figure 5.18, small discrepancies were found: on the side wall, point A, 2.51mm; at the centre of the whirl, point B, 2.55 mm; point C, the side wall, 2.55mm; and lastly point D, the flat bottom surface, 2.54mm.

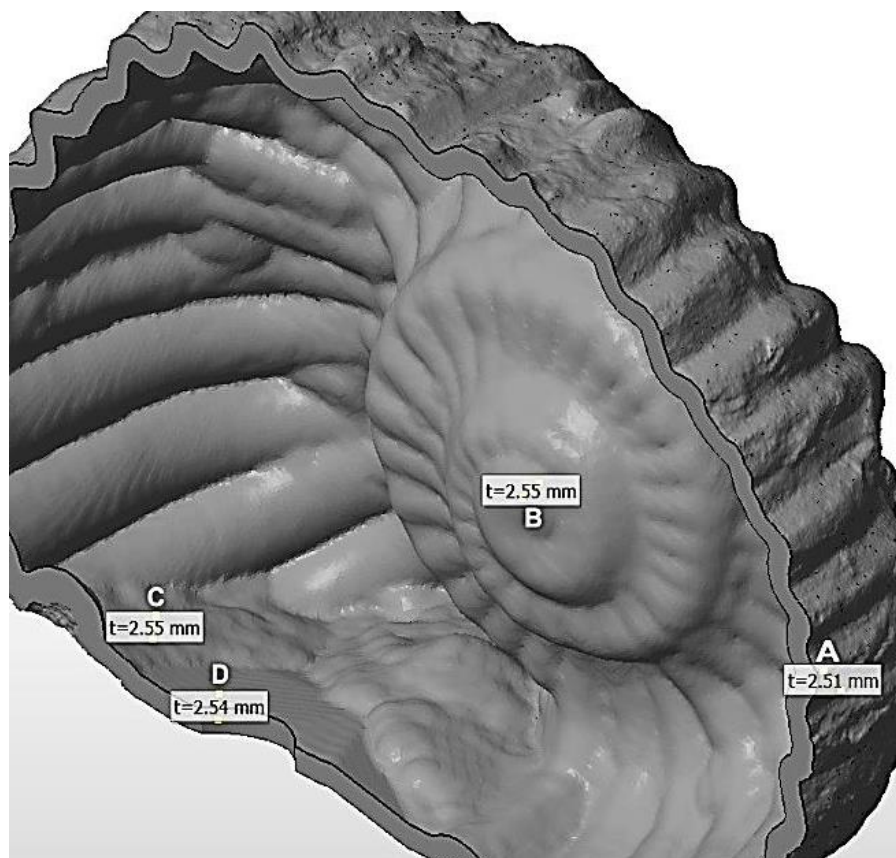


Figure 5.18: Point measurements of wall thickness of Ammonite.

However, although the differences are insignificant, 0.01mm or a maximum 0.03mm, this does seem to be a recurring inconsistency. In the other example the Botijo jar (Figure 5.19), which has smooth walls, unlike the ammonite's undulating walls, similar differences in wall thickness also occurs. There was a default tolerance setting of  $\pm 0.04\text{mm}$  (which could be altered by the user), which all measurements were within. The original wall thickness of the clay Botijo was 6mm so the model was hollowed to this same thickness. Figure 5.20 shows that random measurements on the half model reveal a similar scenario to the

Ammonite fossil model. The very smooth, inner surface followed the outside contour of the jar. Table 5.3 shows that all the measurements are within the  $\pm 0.04\text{mm}$  tolerances pre-set by the software.



Figure 5.19: Smooth hollowed Botijo.

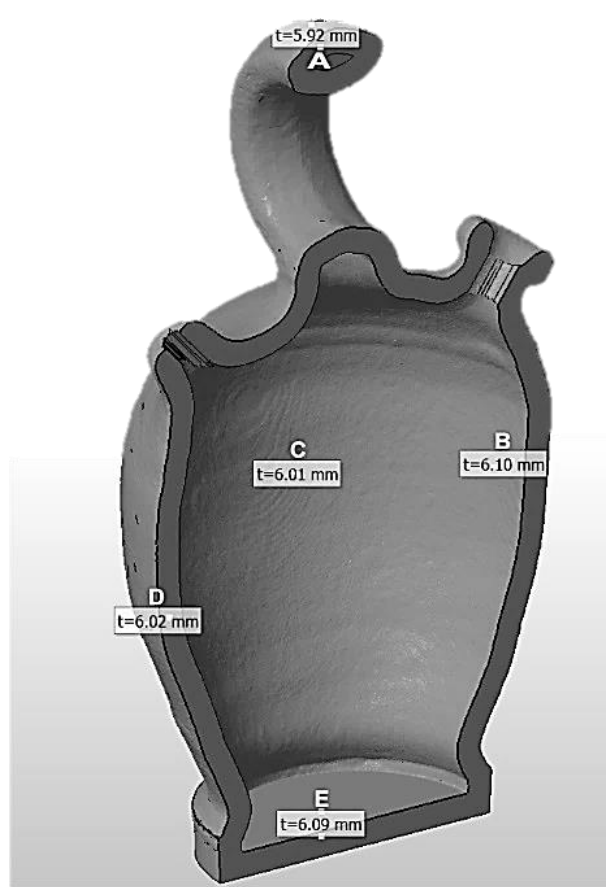


Figure 5.20: Measuring points on Botijo wall.

Table 5.3: Botijo wall thickness

Point A	Handle	5.92mm
Point B	Right side wall	6.10mm
Point C	Back wall	6.01mm
Point D	Left side wall	6.02mm
Point E	Bottom surface	6.09mm

### 5.6.2 Volume of Material used dictated by Shell thickness or Artifact attributes

The volume of material saved by the above process (Chapter 5.6.1) could be in the region of up to 80%, and could make a great difference to the final material

cost for manufacture. The hollowed out models were also faster to make and therefore the cost of machine time was reduced. As the physical weight of the model was also reduced, this could have further implications, for example, a very heavy bronze or stone artifact could be too heavy to be safely handled by a museum visitor or perhaps a child, whereas the AM replica could be engineered to be lighter in weight.

The research investigated whether the shape of the artifact had any influence on the amount of material which was saved by shelling the finished solid replicated artifact. The issue was whether a very simple shape with smooth surfaces showed a better percentage saving than a rough, heavily contoured and ridged surfaced model, taking into account that the software followed the contours of the artifact when creating the shell wall, with a wall thickness of either 2mm or 6mm, or whether the only percentage saving on materials on a pro rata basis was due to the size of the replicated item and nothing to do with shape or surface finish.

The items are illustrated and numbered in Appendix J for visual reference (see Table 5.4) and are shown to be a cross section of the artifacts that were processed using photogrammetry.

Table 5.4: Appendix J reference to illustrations

Eureka Cat	J.40	Clay Dog	J.30
Warrior	J.38	Clay Bottle	J.37
Horus	J.53	Botijo	J.47
Sobekhotep	J.42		

The artifacts were shelled in order of their original volume, i.e. the Eureka Cat being the smallest with a volume of 32.09cm<sup>3</sup> and the Botijo bottle with the largest volume at 887.61cm<sup>3</sup>.

In the illustrations given in Table 5.5 the data of the varying shell thickness between all seven artifacts was compared to see if the shape of the artifact had any influence on the percentage volume lost for the comparable shell wall thickness.

Table 5.5: Relationship between shell depth, shape and percentage volume of materials used.

Shell	Eureka Cat			Warrior			Horus			Sobekhotep			Clay Dog			Clay Bottle			Botijo		
	Size	80 x 35 x 16	90 x 35	178 x 72 x 54	200 x 20 x 40	90 x 130 x 180	200 x 100 x 40	200 x 100	200 x 100 diam.	Volume	Original % of	Volume	Original % of	Volume	Original % of	Volume	Original % of	Volume	Original % of	Volume	Original % of
Solid	32.09	100.00	46.02	100.00	218.57	100.00	405.72	100.00	580.64	100.00	622.46	100.00	887.61	100.00	100.00	100.00	887.61	100.00	100.00	100.00	
2.0 mm	13.37	41.66	17.16	37.29	59.33	27.14	81.70	20.14	115.91	19.96	112.59	18.09	108.16	12.19							
2.5 mm	16.18	50.42	20.76	45.11	72.86	33.33	100.60	24.80	142.31	24.51	139.05	22.34	133.61	15.05							
3.0 mm	18.68	58.21	24.01	52.17	85.41	39.08	119.36	29.42	166.70	28.71	164.74	26.46	158.40	17.85							
3.5 mm	21.01	65.47	27.02	58.71	97.59	44.65	137.41	33.87	190.22	32.76	189.09	30.36	182.26	20.53							
4.0 mm	23.07	71.89	29.72	64.58	108.74	49.75	154.93	38.19	211.85	36.49	211.50	33.98	205.44	23.15							
5.0 mm	26.62	82.95	34.49	74.95	129.53	59.26	188.35	46.42	252.12	43.42	254.07	40.82	249.92	28.16							
6.0 mm	29.41	91.64	38.35	83.33	148.06	67.74	219.54	54.11	288.26	49.64	293.69	47.18	291.73	32.87							

Apart from the variation in volume between the items, characteristics were chosen such as:

- smooth sides;
  - Sobekhotep, the Clay Bottle, Eureka Cat, the Botijo and Horus shared this attribute.
- rough or undulating surfaces;
  - the Clay Dog and the Warrior had both.
- protruding parts;
  - the Clay Dog had protruding ears and a tail, both the Dog and Horus had front protruding legs which were quite thin. The walls of the bottom of the legs on Horus came together to form a solid, there was also a protruding nose/beak on Horus.

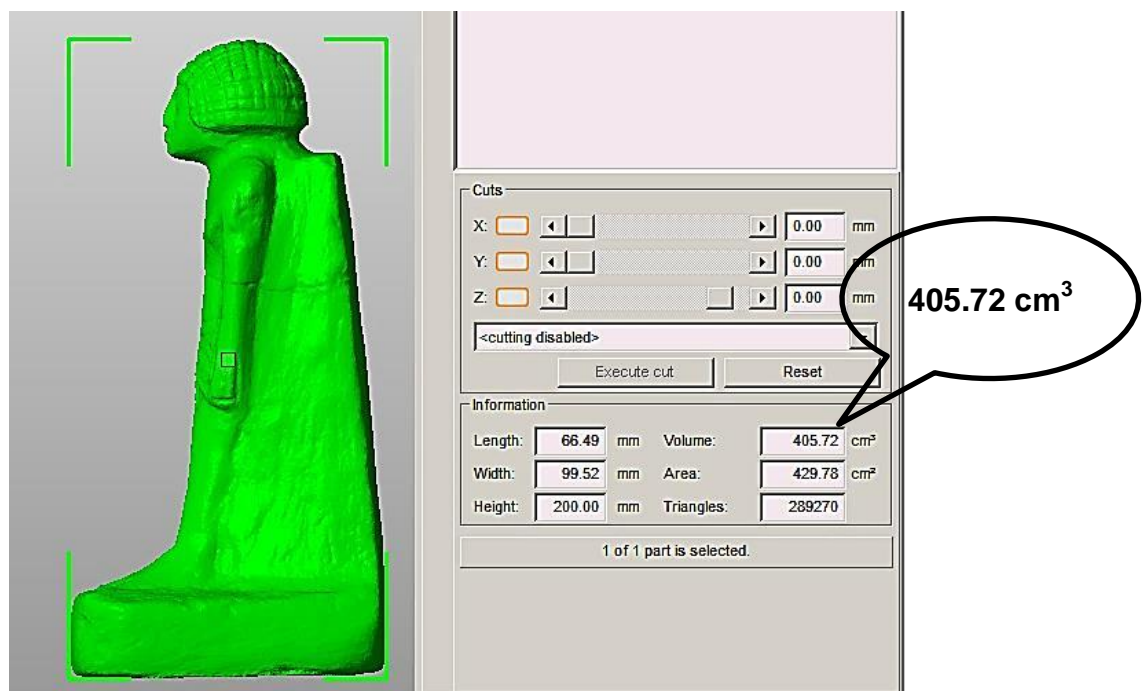


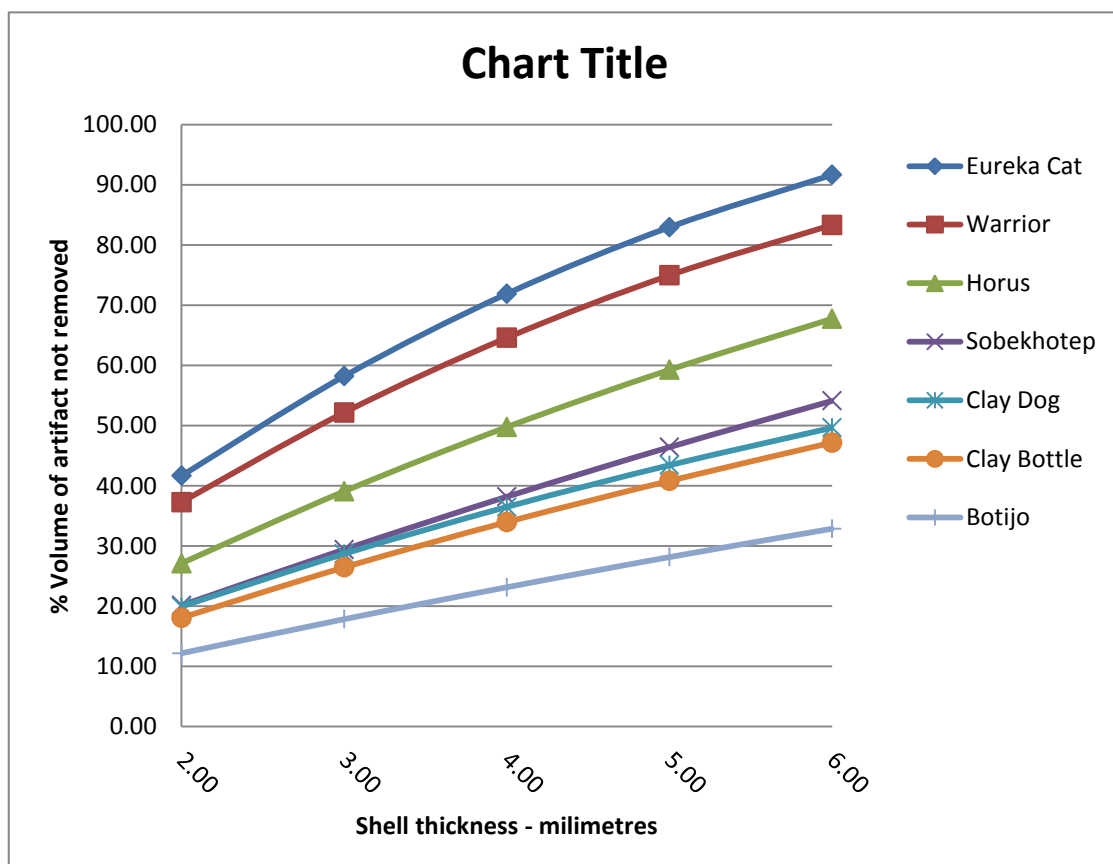
Figure 5.21: Volume of the solid figurine is displayed on chart.

Each item was shelled using a relevant 3D solid data file as a control. In Figure 5.21, the volume which displayed in the Information 'volume box' was calculated by the software of the solid figurine, before the shelling operation began. Once the shelling process was complete the volume box returned this new data. This new volume was then calculated as a remaining percentage of the original whole artifact and tabulated in the appropriate column.

Table 5.6 shows the results of these tests. Eureka Cat, the top line on the graph, was the object with the smallest volume, whilst the Botijo bottle, the bottom line, was the object with the largest volume. All the other items are in order of their volumetric size.

The only deviation was the angle of each line; this represents the wall thickness in relation to the overall volume of the object, which was most prominent as seen in the 6mm column, in which the least saving was obtained, and the greatest saving when the object was large and had thin walls. The 6mm wall thickness left only a saving of 8.36% on the Eureka Cat, whilst a 6mm wall thickness on the Botijo still saved 67.13% of the material. If the wall thickness was 2mm, the saving was 87.81% on the bottle against 58.34% on the cat.

Table 5.6: Showing differential volume according to shell wall thickness.



The only deviation was the angle of each line; this represents the wall thickness in relation to the overall volume of the object, which was most prominent as seen in the 6mm column, in which the least saving was obtained, and the greatest saving when the object was large and had thin walls. The 6mm wall thickness left only a saving of 8.36% on the Eureka Cat, whilst a 6mm wall

thickness on the Botijo still saved 67.13% of the material. If the wall thickness was 2mm, the saving was 87.81% on the bottle against 58.34% on the cat.

In conclusion, Table 5.6 clearly demonstrates that the shape, roughness or any other feature that might be selected had no bearing whatsoever on the outcome of the volume displaced within the artifact when shelled or hollowed. All the lines for each separate item on the graph were nearly identical in their trend.

### **5.6.3. Observations on Material Utilisation as used in the Replication of the Artifacts**

It must be stated from the start that no actual physical testing was carried out on any of the finished replicated artifacts. However it was observed that the larger the object, the greater volume percentage of material was removed from it, thus the larger the object, the greater amount of material would be saved, which would be the logical conclusion. Having established that it was only the wall thickness in relation to the gross volume, and not any other attributes that governed the percentage of material saving, as seen in Table 5.5 (Chapter 5.6.2), care had to be taken in selecting the shell thickness in regard to the material's mechanical properties.

Much research has been done in the past and is still ongoing by others into the mechanical properties of the materials which are now in use for additive manufacturing processes. For example, many of the AM machine suppliers, such as Stratasys Inc. and EOS GmbH, have carried out research themselves into the materials they supply and use in their machines [193] [194]. These companies also supplied tabulated test data sheets giving comparative results advising which way the replicated item should be orientated when being fabricated using a variety of different materials [195]. Meanwhile, Sherif-El-Gizawy *et al.* considered "Processed-induced Properties of FDM products", using ULTEM 9085, a thermoplastic used in aerospace, automotive and military applications [196]. As well as company sponsored reports there have been many independent pieces of research and reviews into all aspects of the materials and processes used in AM. Frazier's "Metal Additive Manufacturing: A Review" where the performance of metallic materials and AM systems are compared and the important static mechanical properties tabulated [197], is just one such report.

Ultimately, as well as the mechanical properties of the material, the “how and where” the final fabricated artifact was to be used, was also taken into consideration when deciding how thin or thick the shell was to be constructed. If the final resting place for the replicated artifact were to be behind glass in a display case, then a thinner wall might have been the choice, but the time and cost of processing will be wasted as well as the material used if the replicated artifact disintegrates in the post processing cleaning stage. If for example, the replication were to be used for educational purposes and handled by many persons, an extra 0.5mm or 1.00mm in wall thickness would go a long way towards extending its life.

## 5.7 Boolean Operation

The Boolean function within the software was a very simple way of creating drainage holes, discretely within a model. It might also be necessary to include more than one hole so as to remove as much material as possible from the inside of the model, dependent on its geometry.

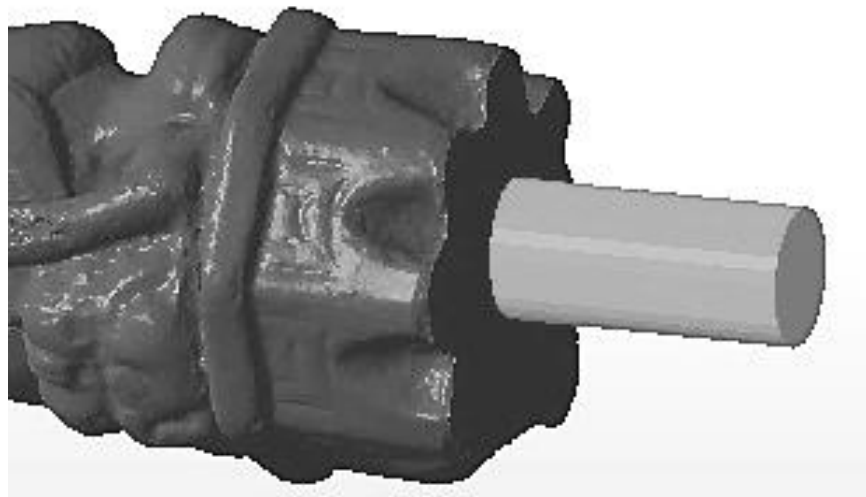


Figure 5.22: Boolean effect – light subtracted from dark.

The cylinder (which was light grey in Figure 5.22) was submerged into the body of the Warrior, seen as dark grey in Figure 5.22. The cylinder was then subtracted by using the Boolean function and the result was a hole in the base through which powder or liquid could drain (Figure 5.23).

With the powder-bed laser based AM machines, there were no internal supports to the models, so the outside walls had to be made thick enough to be

self-supporting. However, where an SL model was being manufactured, the internal structure still left areas which were hollow.

In both cases, as the laser beam melted, solidified or sintered the material that the model was being made from, unprocessed material would remain trapped inside the model, unless there was a drainage hole. As most of the powders were reusable, this would contribute to manufacturing savings, especially if powdered precious metals such as gold or silver were being used.

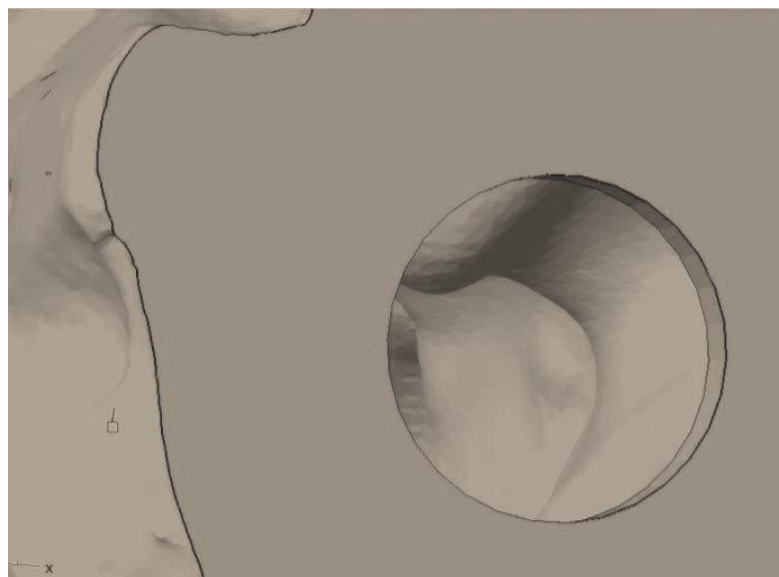


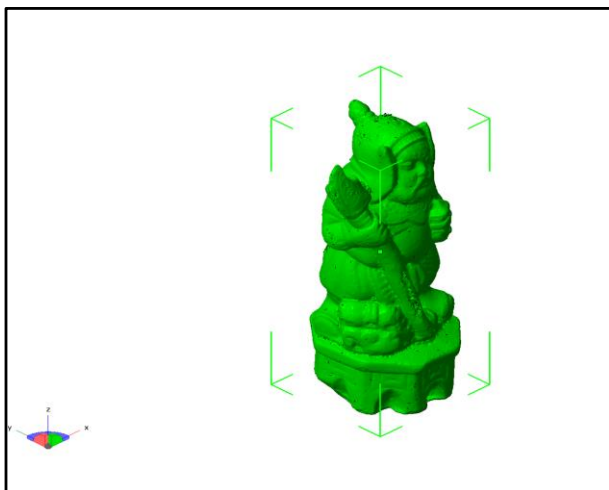
Figure 5.23: Down the drain hole and into the hollowed model.

## 5.8 Other useful features

The software also had a useful report-generating section which could be used. The report collated and provided information about the model such as its Volume, Size, Area, Number of Triangles (polygons) and even the Centre of Gravity in XYZ co-ordinates. Another report provided the size of the platform box together with the six 3D views: Top, Bottom, Left, Right, Back and Front of the model. Some of this information was very useful when models were AM fabricated by third party agencies which had limitations on physical model size (platform box) and polygon count due to the machines that they were using. Having the volume of each model, it was possible to calculate comparative costs on a £/€ per cm<sup>3</sup> for material and printing.

## Data Sheet 1

### Advanced Part Analysis.



Automatic Part Standard Analysis – created in netfabb Professional

created with



#### General analysis information for part: Boolean operation of 2 parts (Warrior hollowed, Cylinder)

Analysis date:	2015-06-17	Mesh is o.k.	1
Min:	X: -31.995 mm; Y: -35.737 mm; Z: -21.652 mm	Holes:	0
Max:	X: 3.005 mm; Y: -0.738 mm; Z: 67.611 mm	Boundary edges:	0
Size:	X: 35.000 mm; Y: 34.999 mm; Z: 89.263 mm	Boundary length:	0.000
Volume:	15604.864 mm <sup>3</sup>	Bad edges:	0
Area:	15853.527 mm <sup>2</sup>	Flipped triangles:	0
Points:	156553	Average wall thickness:	0.492 mm
Edges:	469683	Surface is closed:	1
Triangles:	313122	Surface is orientable:	1
Center of gravity:	X: 18.504 mm; Y: 17.333 mm; Z: 37.554 mm	Shadow area:	895.546 mm <sup>2</sup>

#### Wall thickness analysis:

Critical distance (threshold):	0.400 mm
Critical surface:	5.000 %
Test on critical distance:	FALSE
Total area which has an area below the threshold value:	0.001 mm <sup>2</sup>
Number of clusters:	425
Area of the largest cluster:	1.792 mm <sup>2</sup>

#### Up skin and down skin analysis:

Angle of the up skin:	45.000 °
Angle of the down skin:	45.000 °
Minimum size of the component:	0.100 mm <sup>2</sup>
Area size of the up skin area:	1248.697 mm <sup>2</sup>
Area size of the down skin area:	1364.034 mm <sup>2</sup>
Number of down skin counts:	118
Number of down up counts:	144

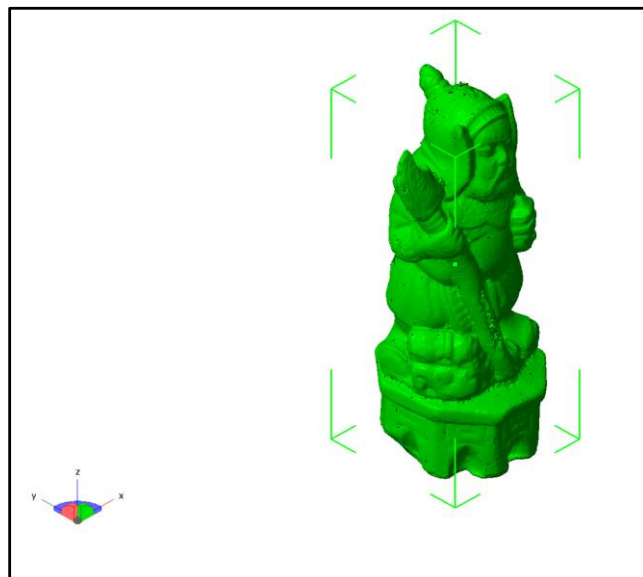
[Name of responsible person]  
[Position, Department, Company]

Signature \_\_\_\_\_

Figure 5.24a: Netfabb model information report – Part Analysis.

## Data Sheet 2

Platform views.



Automatic Part Standard Analysis –  
created in netfabb Professional

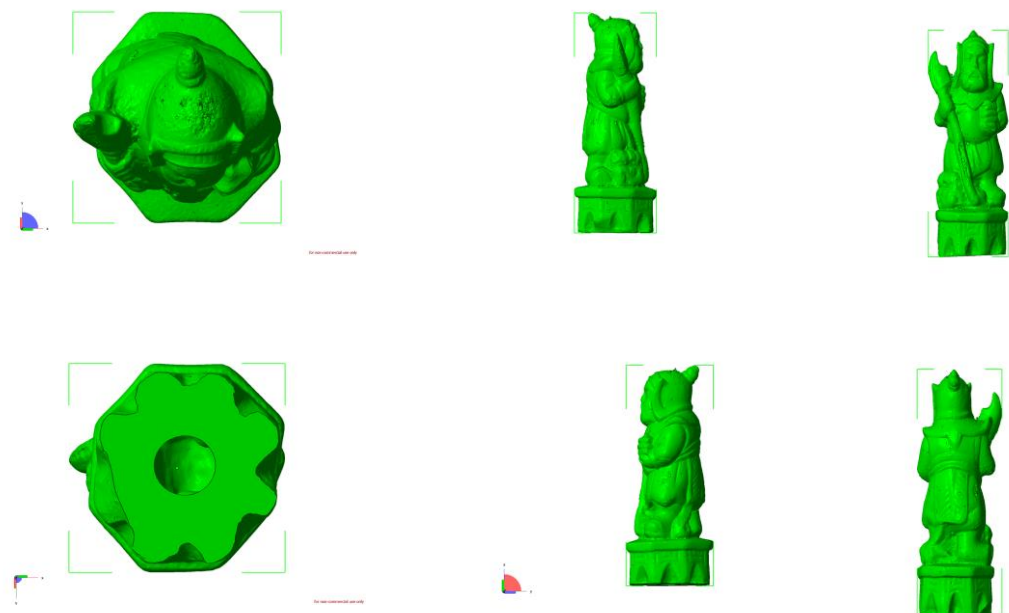
Platform Name:  
Warrior hollowed and  
hole. fabbproject

Report creation date:  
2015-06-17 18:39

Parts on Platform:  
1 parts ( 15604.864 mm<sup>3</sup> )

Outbox Size:  
35.000 mm  
34.999 mm  
89.263 mm

### 3D View



Created with netfabb Professional 5

[ Name & Signature ]

 netfabb®

\_\_\_\_\_  
\_\_\_\_\_  
Date

Figure 5.24b:

Netfabb model information report – Platform Views

These reports also included the possibility of adding the operator's details such as name, date and data file name, which were helpful in keeping documented records of work progress. With the powder-bed laser based AM machines, there were no internal supports to the models, so the outside walls had to be made thick enough to be self-supporting, and these reports also included such information about the walls. These reports, the Part Analysis report and the Platform report of the "Warrior" model, produced by the software as Data Sheet 1 and 2, see Figure 5.24a and Figure 5.24b, (Data Sheets 1 and 2).

## 5.9. Summary

As originally stated, the *StudioPro*<sup>®</sup> software was designed to prepare the files of third party software into \*.stl files for further AM fabrication. The software would check for a number of common faults which occurred in the process of converting photogrammetry images into point cloud data and reducing the number of shells that may be created in this process. Using the automatic repair function, the software would look for holes or badly aligned triangles/polygons, would correct such faults, would smooth surfaces, and would prepare \*.obj files. The software would also import and convert the data from over 30 other types of data files, leaving them ready to export into \*.stl files for AM fabrication. If the repair function was left unchecked, all holes would be filled, but any hole larger than 3mm across, on the surface, would be flattened out in the repair process, and at that point would be detrimental to the finished model, especially on a rough or undulating surface. As seen in Chapters 6.2 to 6.4, repair to the mesh might not be the answer; but retaking, adding photographic images and reprocessing the image data set would be needed.

Conversely, if the area was on the underside which was a flat bottom surface, this flattening effect might be beneficial. In Figure 5.25, the underside of a trilobite fossil was repaired using the automatic feature and the large hole was filled in by the mesh. Being the underside, this was the area on which the trilobite stood on the turntable and no data could have been captured there. As this area was flat, the large hole being filled in as a flat area by the mesh was beneficial to the overall replication of the model. Resizing from either of the primary software programs was straightforward as long as the correct orientation was first

established; this enabled the exact size of the original artifact to be replicated in all axes.

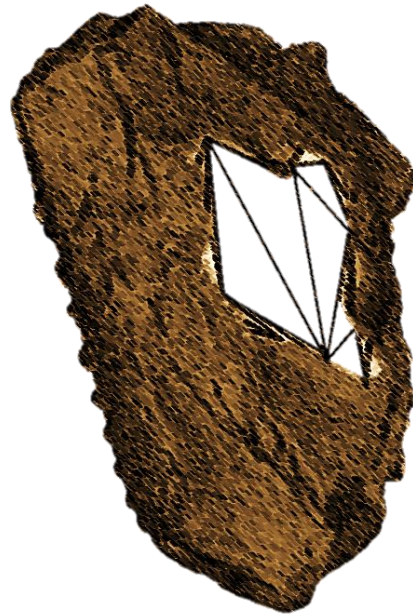


Figure 5.25: Automatic mesh lines filling in the large hole of the Trilobite.

## Chapter 6: Repair, reconstruction and construction

### 6.1 Repair of Noisy, Distorted and Incomplete Data

#### 6.1.1 Returned Noisy data

When Method 1 (Chapter 4.1) was used to process the digitally captured images, the returned processed point cloud image, as seen in Figure 6.1 (head identified) had to be filtered, or cleaned, to eliminate background noise that had been captured along with the original subject, such as other objects or furniture (arrowed) that were in the line of focus when the image was recorded by the DSLR. The software lasso tools allowed the user to highlight the area of the section of image to be cleaned and delete it. Unlike the Agisoft process, where the background was masked from the main subject, these background objects were used by the AutoDesk cloud program to stitch and build the overall central object.

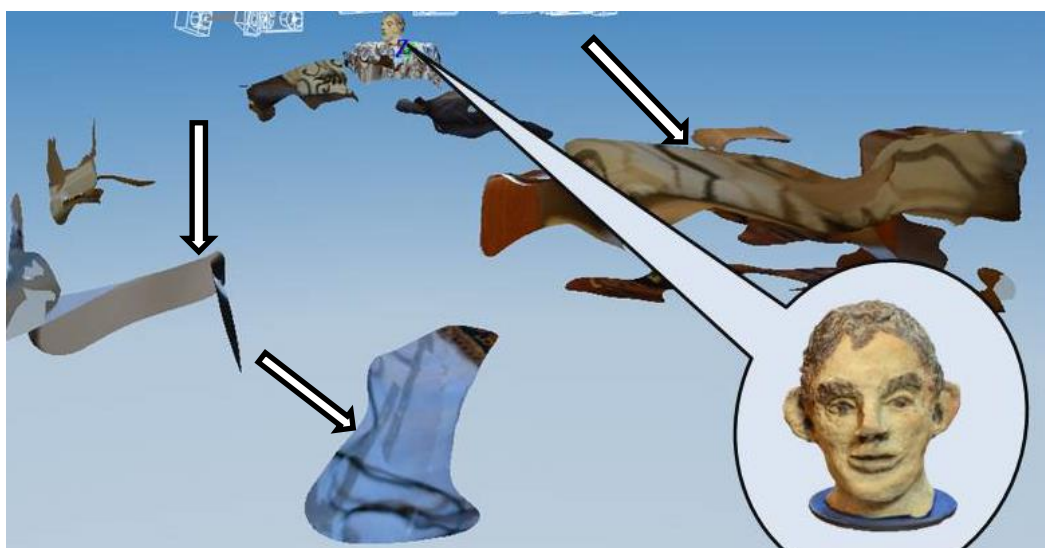


Figure 6.1: Processed digital image ready to be cleaned.

The resulting processed textured 3D mesh might also show minor flaws or distortions, which were then corrected using the methods described in Chapter 6.1.2 and 6.1.3. The processed photo-textured 3D mesh image head could have been repaired using software, but by adding and increasing the number of images, with more angled shots and greater image overlap, complex repairs to the point cloud and textured mesh were eliminated. The additional photographic digital images, once added to the original data set of images, were reprocessed

and sent by the internet to be cloud processed and returned ready to be recleaned. By selecting the appropriate control in the editing section, a wire frame, wire frame and texture, or texture only model could be obtained. This would facilitate a limited amount of repair if required on the model.

### 6.1.2 Incomplete data

The main objective of the two primary software programs used in this research, was to convert 2D images, in both cases, digital photographs, into 3D virtual point cloud or textured images. In both instances the software programs contained limited repair tools and were not designed to recreate parts of the image that were missing.

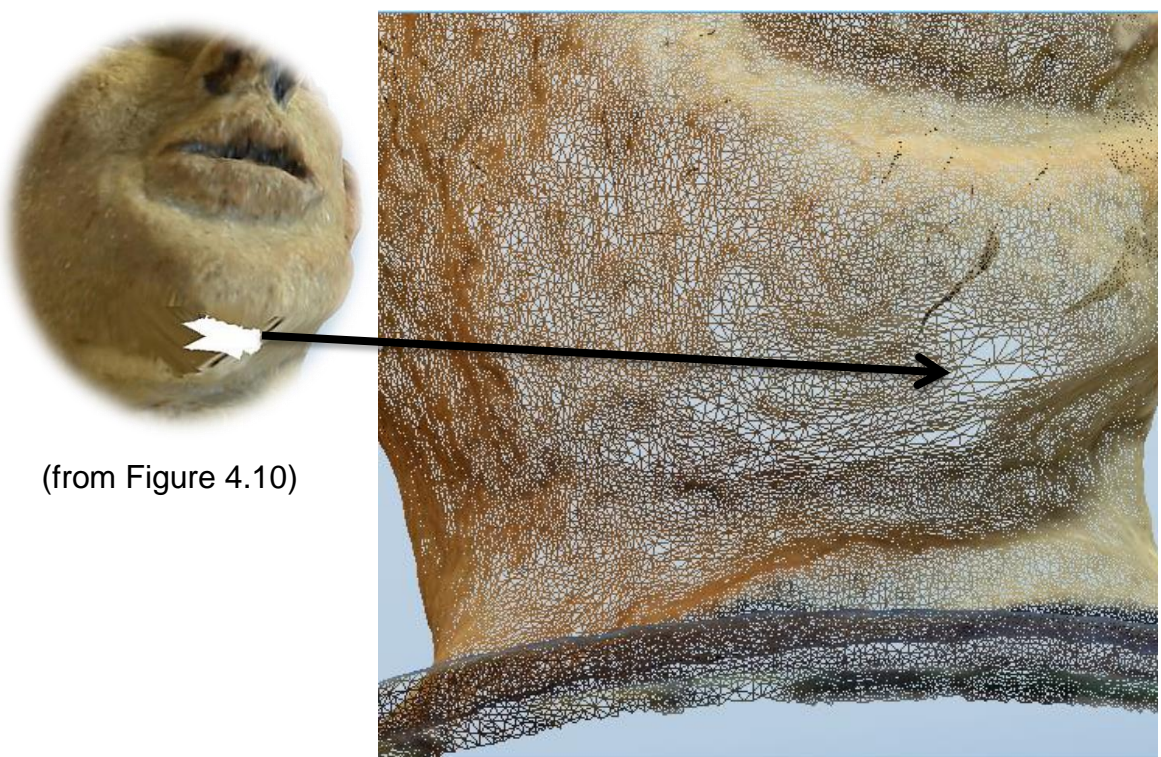


Figure 6.2: Hole under chin - automatic mesh repaired.

If, in the initial data collection, part of the artifact was missing and showed up in the processed data image as a large hole, the software could fill in that hole as a flat surface. If an object with a flat base was being photographed with the object on a plinth, the bottom of the object could obviously not be seen by the camera lens and that data would be missing from the data set. The software repair commands allowed for this hole to be “filled in” but the polygons formed would join the edges that were found into a flat plane. In the example of the flat

base object, this was acceptable, as a flat surface was needed to be replicated for the base of the object.

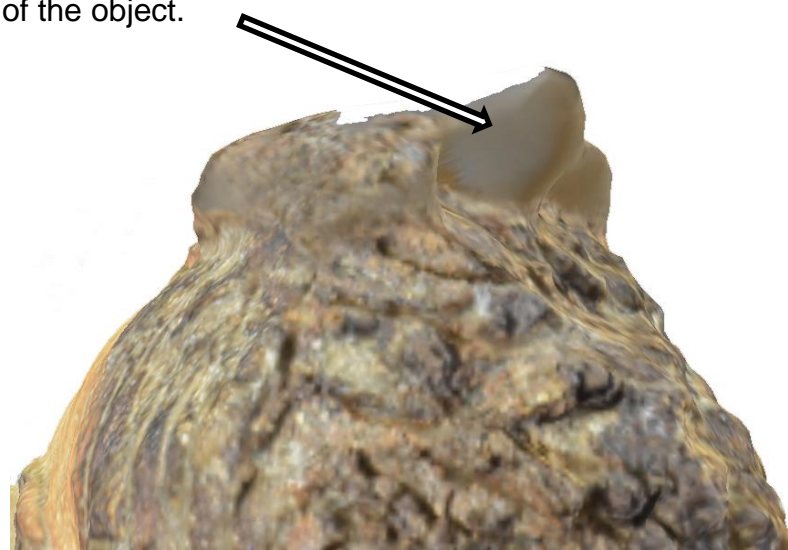


Figure 6.3: Distortion on top of head.

However, if for example, the top part of a head was missing, this might show up as a hole or as a bulge. In Figures 6.2 and 6.3 both problems occur, the first hole, due to lack of data, and the second fault, a bulge (indicated), due to a small amount of light reflection or flare. The hole under the chin (from Chapter 4.2.1: Figure 4.10) was relatively small, (it was enlarged by the author so as to be seen clearly in the screen shot), and the flat surface automatic repair merged with its surroundings as seen in Figure 6.2.

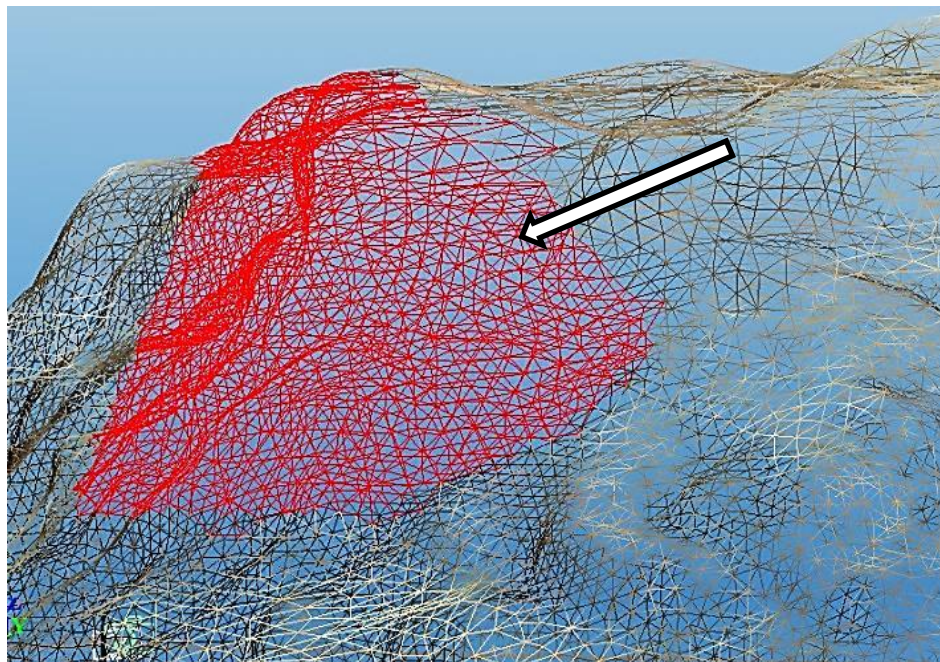


Figure 6.4: Red polygons ready to be removed.

The bulge however, was not ideal to repair: although it was a simple matter to remove the polygons that formed the bulge, thereby turning the image into a mesh and deleting the rogue triangles (shown as light red in Figure 6.4 and arrowed), this would have left too large a hole to repair without complicated reconstruction of the mesh.

The option in this case was far more straightforward – more digital images were taken and added to the original data set. Having “stitched” these new images in to the data set (see Chapter 6.1.3), the whole set was then reprocessed. As this was originally processed by *123D Catch®* it was sent via the internet back to AutoDes.

### 6.1.3 Unglazed Ceramic Vase – a lesson in sewing

This example of an unglazed Ceramic Vase is very similar to the above problem, in that after processing the original 52 images a large hole was seen to exist in the returned data. Here was another case of not enough data having been captured of the inner part of the vase. Another 17 images were taken with greater emphasis on the inside of the vase.

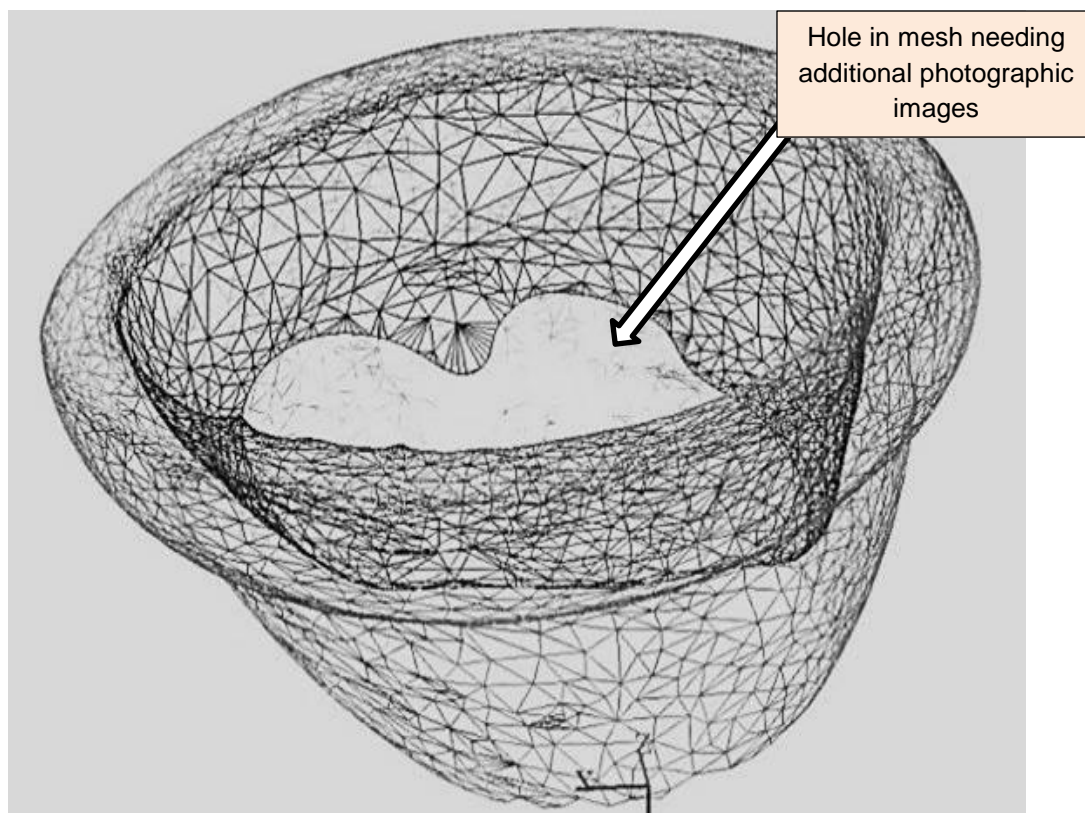


Figure 6.5: Hole in Vase mesh due to lack of digital data.

It was found by experience that the chances for successfully matching additional images were greatly enhanced if the “scene” was not disturbed, i.e. the position of the vase in relation to the surrounding furniture or cloth on which it stood. If the scene had changed then it was more difficult to match points. Of the 17 images taken, two were rejected as they were unable to identify the required three points on the images. This meant that while the initial photoshoot data was being processed, which could take more than an hour, the scene was not disturbed. The data file returned was then examined for flaws, and, if all was satisfactory, the “studio” was taken down or dismantled, unless more images were required to be taken.

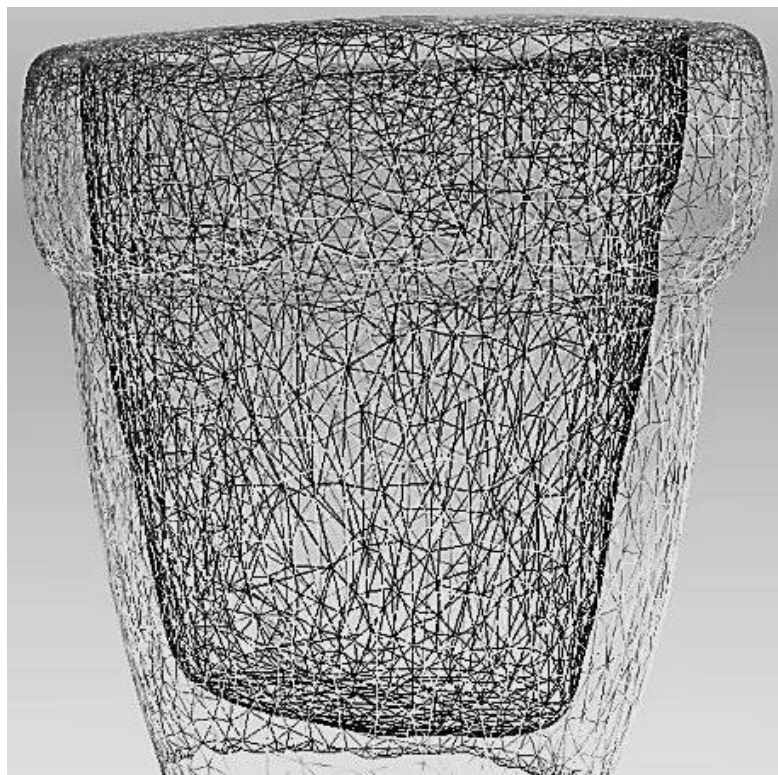


Figure 6.6: Inner Vase mesh now complete.

By turning the textured images into meshes, the fault and its repair were clearer to identify (Figures 6.5 and 6.6). Figure 6.5 shows the result of processing the original 52 images: a hole in the inside of the vase. Figure 6.6 clearly shows that 15 extra digital images were needed to fill in the hole. The data image file had now been completed, again without any complex software repairs being necessary, and could be processed using the same procedure as with the Clay Head. The outside and inside of the original vase was quite smooth and therefore

there was no loss of definition in the model made by the FDM machine. Although this model was made to one quarter scale, a full size replication would no doubt result in a true likeness.

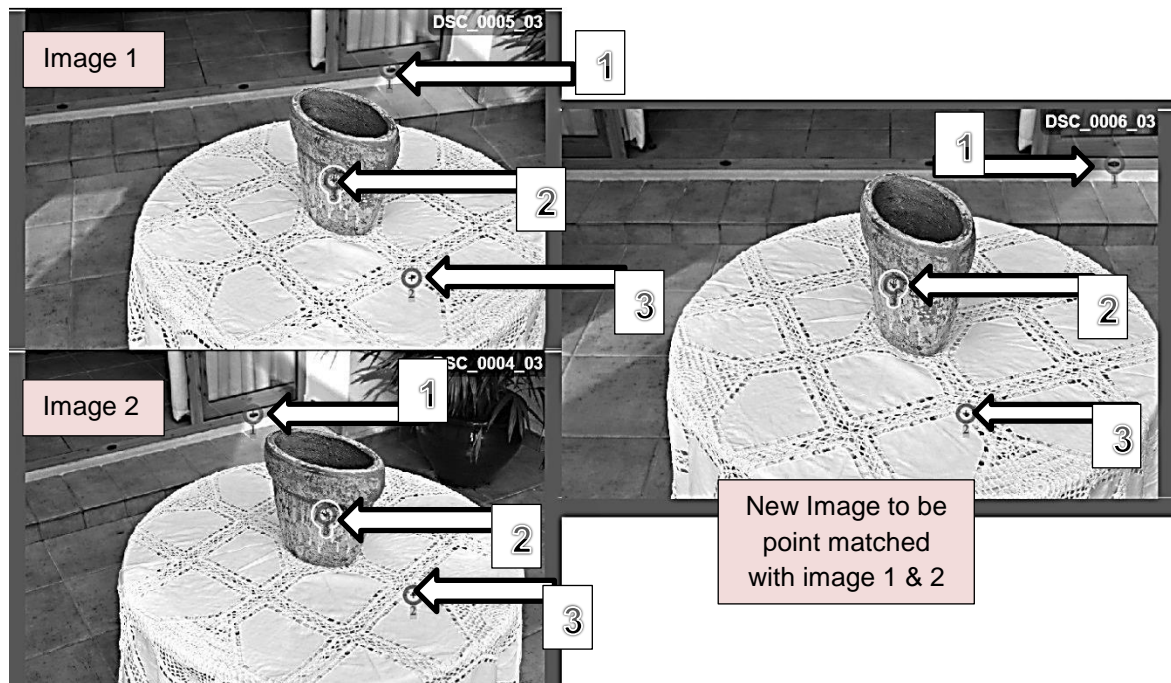


Figure 6.7: Identifying and manually stitching/matching three points to integrate additional digital images.

In Figure 6.7, three separate data images are seen with the subject, the Vase, in sharp focus, but the large area surrounding the main subject is also in very sharp focus. Three identifiable points were needed to match each image. Point 1 was down on the floor by the door; point 2 was on the vase, and the third identification, point 3, on the tablecloth on which the vase stood. This made the identification of the reference points in each photograph easy to see and match, either by the human eye or by the computer recognition software. It can also be seen, that of the three identification points selected, only one is on the main object. The other two are positioned on the surrounding background.

#### 6.1.4 Repair using the Mesh

In the case of the Egyptian Vase, discussed in Chapter 4.9, although the images produced a good result for the outside of the vase, there was an amount of cleaning required in and around the neck opening (see Figure 6.8). As this was only a small area to be cleaned, it was decided to repair the vase by cleaning the

affected part using the mesh. The textured image was transformed back into a mesh (Figure 6.9). The inside of the neck is seen in Figure 6.8 in its textured form.

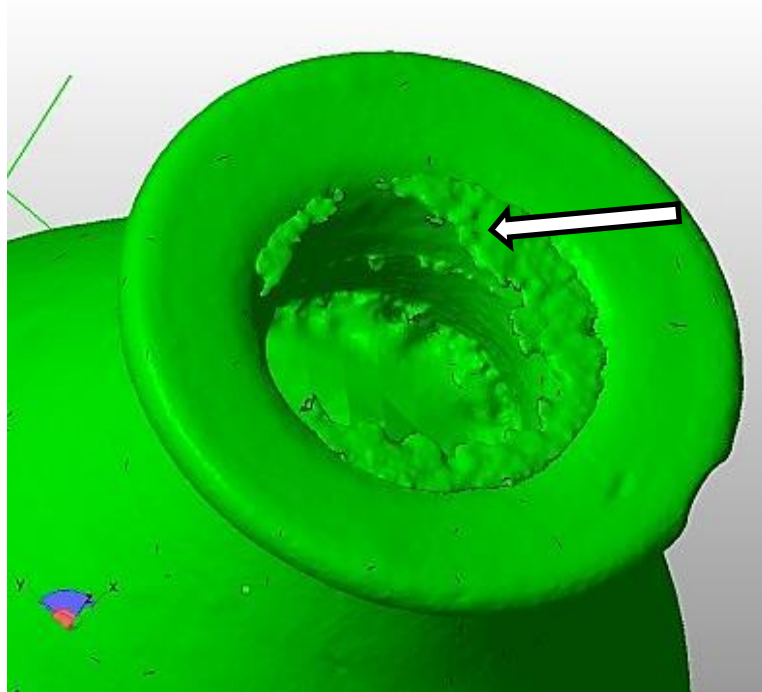


Figure 6.8: Area needing to be cleaned at mouth of Egyptian Vase.

Deleting the small triangulated polygons as seen in the enlarged screen shot, (Figure 6.9) was a simple but tedious task well within the capabilities of *StudioPro®* and an operator.

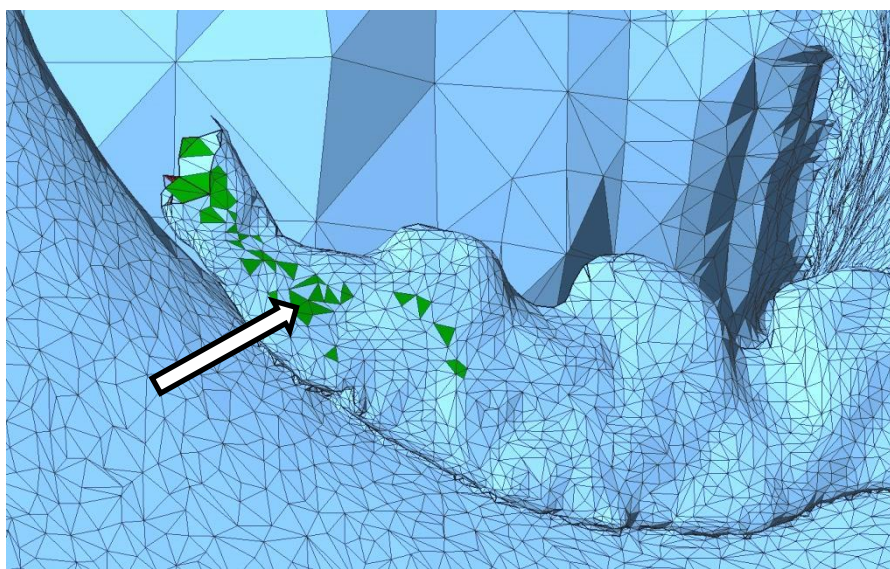


Figure 6.9: Working with a large scale mesh – Egyptian Vase.

At an enlarged scale each polygon or group of polygons was easily identified, highlighted (indicated in Figure 6.9) and deleted. The holes in the side

of the neck of the vase, which were caused by deleting some of the triangles, were so small that the repair blended in with the original sides without any additional problems being created. Having removed the “noise” from the neck, the next process was to hollow out or shell the vase, so as to use less material and reduce the weight.

Finally, having made a very accurate measurement of the neck diameter of the vase, a cylinder was created to this exact size. Using the Boolean tool, as described in Chapter 5.7, the cylinder was placed in the neck opening and subtracted from the whole. This took several attempts at placing the cylinder in exactly the correct location, but when finally achieved, a clean opening through to the hollowed body of the vase was created, ready for 3D fabrication.

## 6.2 Damaged Digital Images Beyond Repair

Of the many objects that were processed in the course of this research, there were a few items which proved impossible to capture satisfactorily and simply, using the digital methods employed, without further research into the problems which affected these items. Koutsoudis *et al.* lists a selection of “friendly materials” which are good for photogrammetric purposes and a list of “non-friendly” materials such as water, glass, varnish, steel and many more [164]. The main cause of these problems was light reflection off the surface of the artifacts. These flares could not be processed by the software and caused distortion in the digitally processed image. Even lowering the light levels as discussed in Chapter 4.2.3 did not produce the required result (i.e. this did not produce images which could be processed).

This problem occurred on surfaces such as glass, glazed china or porcelain, or any surface which had been polished, varnished or had a light reflective surface. The problem could possibly be overcome, as suggested by Porter [165], by coating the surface with fine powder chalk or talcum powder. The powder was suspended in alcohol or acetone and sprayed on any of the artifacts which were translucent or had a shiny surface, producing readable features, especially if then processed using the High resolution setting in *PhotoScan Pro*®.

However, this method was still invasive, whilst this research used only non-invasive methods. If invasive methods had been used, talcum powder would no doubt have led to all types of non-reflective water soluble coatings being used,

but it was not how this research intended to photograph the artifacts. It could then be argued that what was being photographed was a fine layer covering the artifact and not the artifact itself. Although the coating was removable with water, it was not felt that the curator of the Kendal Museum, or any other reputable curator, would have taken kindly to giving Sobekhotep or any other c.3,500-year-old artifact a wash under the tap.

Shown below (Figures 6.10 to 6.19) are the results of some of the failures (fortunately there were not many), the original images having been placed alongside the point cloud or textured digital image for comparison. Table 6.1 lists the ten items and has identified the problems encountered, with some explanations as to the cause. It also shows how each artifact was processed.

Table 6.1: Reference table for original and failed artifact point cloud images.

Processed with		<i>123D Catch</i> ®	<i>PhotoScan Pro</i> ®
Figure K.01	Serenity	Item – G.03	Item – J.32
Figure K.02	Dolphins	Item – G.04	Item – J.33
Figure K.03	Glazed Vase	Item – G.06	
Figure K.04	Mollusc	Item – G.08	
Figure K.05	Frosted Bottle	Item – G.11	Item – J.34
Figure K.06	Ceramic Vase	Item – G.17	
Figure K.07	China Dish		Item – J.39
Figure K.08	Batwing Sea Shell		Item – J.54
Figure K.09	Lincrusta - Acanthus	Item – G.18	
Figure K.10	Lincrusta - Aphrodite	Item – G.19	

By way of explanation of Table 6.1, the Figure numbers on the left refer to the photographic images within the table. Each named item may have one or two Item numbers which would refer to the numerical order in which they were processed (Item – Appendix J - J.03). The first Item number (e.g. Appendix G - G.03) refers to the artifact being processed by *123D Catch*®. If there is a second Item number (e.g. Appendix J - J.03), the same artifact would have been reprocessed using *PhotoScan Pro*®.

- The full numerical Item sequence of all 58 photographic images can be seen in Appendices G and J.

- Table K.1:- “*Capture data Log – Failed Artifacts*” - Appendix K. This table records the full numerical Item sequence of all 12 failed photographic artifacts, day to day record and evaluation.
- Table K.2:- “*Photographic images of Failed Artifacts*” - Appendix K.

### 6.2.1 Figure K.01 - Serenity – Items G.03 and J.32

Three attempts using *123D Catch*<sup>®</sup> were made using Serenity and another five attempts using *PhotoScan Pro*<sup>®</sup> (Appendix K - Table K.2: Figure K.01). Some of the problems that occurred using this software have already been discussed in Chapter 4.4.3.



Figure 6.10:

Figurine - textured point cloud image -  
rough, spiky surface.

At a later date, the first two data sets that had been shot for *123D Catch*<sup>®</sup> processing, were processed by *PhotoScan Pro*<sup>®</sup>. The first attempt had been shot at f/14, had 71 images and produced a better result than the original, whilst the

second attempt, shot at f/8 with a few more images added, did not give a good result, as the shallow DoF only helped the image to merge with the background (Appendix K - Table K.2: Figure K.01a).

Reshooting a further three digital sets, increasing from 92 images to 145 images, stopping down from f/18 to f32, and pre-process masking produced a “good” result. However, on careful examination of the screen shot of the digital image of the \*.obj file (see Figure 6.10), the surface had a rough, spiky finish (highlighted by the arrows), which would have needed sanding down in post-processing to achieve a smooth finish. This *High* resolution digital image (Figure 6.11) could possibly have been improved by careful manipulation and cleaning of a reprocessed *Ultra High* resolution point cloud image, as seen from the *PhotScanPro4<sup>®</sup>* screen shot.



Figure 6.11: Figurine - High resolution point cloud image.

However, this would have added a couple of hours to the processing time and would have required some very careful deleting of the highlighted point cloud. So the result was “good” but perhaps not good enough.

#### **6.2.2 Figure K.02 – Dolphins – Items G.04 and H.33**

Four attempts were made to capture the Dolphins; two using *123D Catch*<sup>®</sup> and the other attempts with *PhotoScan Pro*<sup>®</sup>. Good sharp images were produced (Appendix K - Table K.2: Figure K.02), but the reflective light from the semi polished wood surface of the statuette produced the distortions as seen in Appendix K - Table K.2: Figure K.02a. These two sessions were all shot at f/18, initially with 64 images, then adding by stitching into the data set another eight, to make it 72. Although the camera was set on automatic for the shutter timing, on inspecting the camera log data this returned an average time of 2 seconds per frame. The results were not greatly improved with a green Chroma Key backdrop, although masking was not employed before the *PhotoScan Pro*<sup>®</sup> process began. Reducing the f/stop even further would have increased the time per frame even more than 2 seconds. Adding the masking frame before processing might have been beneficial, but the time factor would certainly have been increased, both in pre-processing and in digital capture.

#### **6.2.3 Figure K.03 – Glazed Vase – Item G.06**

This vase was semi glazed (polished) on the outside but the inner surface had been given a high gloss white glaze (Appendix K - Table K.2: Figure K.03). Three attempts were made, including photographic stitching, which produced 61 images. A further attempt to stitch additional images to the data set failed. It can be seen from Appendix K - Table K.2: Figure K.03a, the final images were badly distorted including holes in the side. No further trials were possible as this item was not amongst the author’s permanent collection, nor was it possible to regain access to the item.

#### **6.2.4 Figure K.04 – Mollusc - Item G.08**

This item was one of the most difficult to process, *123D Catch*<sup>®</sup> was the only software to be used and was unfortunately not at all suitable for the job in hand. The mollusc (Appendix K - Table K.2: Figure K.04), was a very complex shape

which twisted and spiralled. Seven attempts were made, increasing the number of images from 43 to 73 images at each session, including alteration to the f/stop between f/4.8 to f/11 and adding additional photographs to the data sets by stitching. The image, which is a mesh and textured mix, shown in Figure 6.13, was the best result available from the series, but the arrows show the white mesh areas which would need repairing. As this item was only in the author's possession for a short time, it was not possible to re-process it. If more photographic images could have been added to the original 123D *Catch*® data set, which might have helped; as might using *PhotoScan Pro*® with a turntable, and photographing it from much closer positions with smaller f/stops, perhaps as small as f/22, to give greater DoF and therefore sharper images. Also by applying masks to the pre-processed data the background "noise" would have been eliminated helping the overall processing.



Figure 6.12: Mollusc - High resolution textured point cloud image.

It would have been possible to repair the mesh automatically by allowing the software to fill in the gaps, but this would have produced smooth flat areas. The complex surface texture as seen in Figure 6.13, which is an enlargement of the

original surface texture, would not have been replicated in these repaired areas and the integrity of the artifact would have been compromised. To repair the mesh by hand would have been impractical with the software being used, because, as stated previously, this was not the intended use of this particular software and it did not possess the tools which would be required to be used.



Figure 6.13: Enlarged surface texture of original Mollusc – note the ridged surface.

#### 6.2.5 Figure K.05 – Frosted Bottle - Items G.10 and H.32

Three data sets were photographed and processed with *123D Catch*<sup>®</sup> and four sets with *PhotoScan Pro*<sup>®</sup>. The first attempts tried indoor and outdoor natural lighting, using both newsprint and spotted cloth for the background in order to help with the computer stitching of the images. Between 34 and 61 images were shot per session but all processed data sets were equally distorted. The results were slightly better with *PhotoScan Pro*<sup>®</sup>. The f/stop was lowered to f/22 and rotated 15° on the turntable to obtain 89 images. Two masked and two unmasked data sets were processed. The final masked set showed the best results (see Appendix K - Table K.2: Figure K.05a), where the screw top and label on one side of the bottle are relatively clear.

### **6.2.6      Figure K.06 – Ceramic Vase - Item G.15**

The Ceramic Vase was one of the first artifacts to be processed using *123D Catch*<sup>®</sup>. This vase was photographed in a low level of natural light in the outdoor walk-in light tent. In hindsight, the DoF was too shallow, hence the top double image; also there was reflection off the top glazed band causing some distortion to the images (Appendix K - Table K.2: Figure K.06a). 72 images were taken, of which six were restitched back into the original data set. The artifact is no longer in the author's possession or a smaller aperture and half neutral filter might have been tried, using the turntable and pre-processing masking.

### **6.2.7      Figure K.07 – China Dish - Item H.37**

Apart from the black square and white elephant, there were no discernible patterns or markings on the dish, which was white with a gold edge. Two attempts using *PhotoScan Pro*<sup>®</sup> were made, but the first data set did not build at all. The aperture was stopped down to f/29 and pre-processing masks were used. The result is seen in Appendix K - Table K.2: Figure K.07a. The centre black square with the elephant has emerged as a whole section. Apart from the high gloss, which can be seen to have cause an orange peel type surface, there were very few points on the original images which the computer software could identify and match. Ground markers placed around the dish might have helped this matching process. Green Chroma Key was used with 15° rotation on the turntable and 73 images were taken.

### **6.2.8      Figure K.08 – Batwing Sea Shell - Item H.50**

In this example, the Batwing shell, two very different surfaces existed on the shell, the front being mother-of-pearl, smooth, silvery and quite shiny, giving off a lot of reflected light, whilst the rear of the shell was very rough, and a matt surface. This shell amassed 160 photographic shots using a wooden stick to support it on the rotating turntable.

Using a fixed focus of f/22 allowed for less light to enter the camera and a greater DoF to be obtained. The shutter speed was set to automatic but this did not help to eliminate the light reflecting from the front of the shell. On examination of the Metadata from the digital image, the speed of the shutter increased from between 3 and 2.5 seconds for the darker side of the shell to between 0.25 and

0.5 seconds for the shiny side. In the Appendix K - Table K.2: Figure K.08a and also Figure 6.14, the smaller photograph shows highlighted areas picked up by the camera lens, whilst on the enlarged screen shot of the point cloud image, indicated by the dotted line, can be seen an orange peel effect (indicated) which the reflective surface has caused to the computer generated processed image.

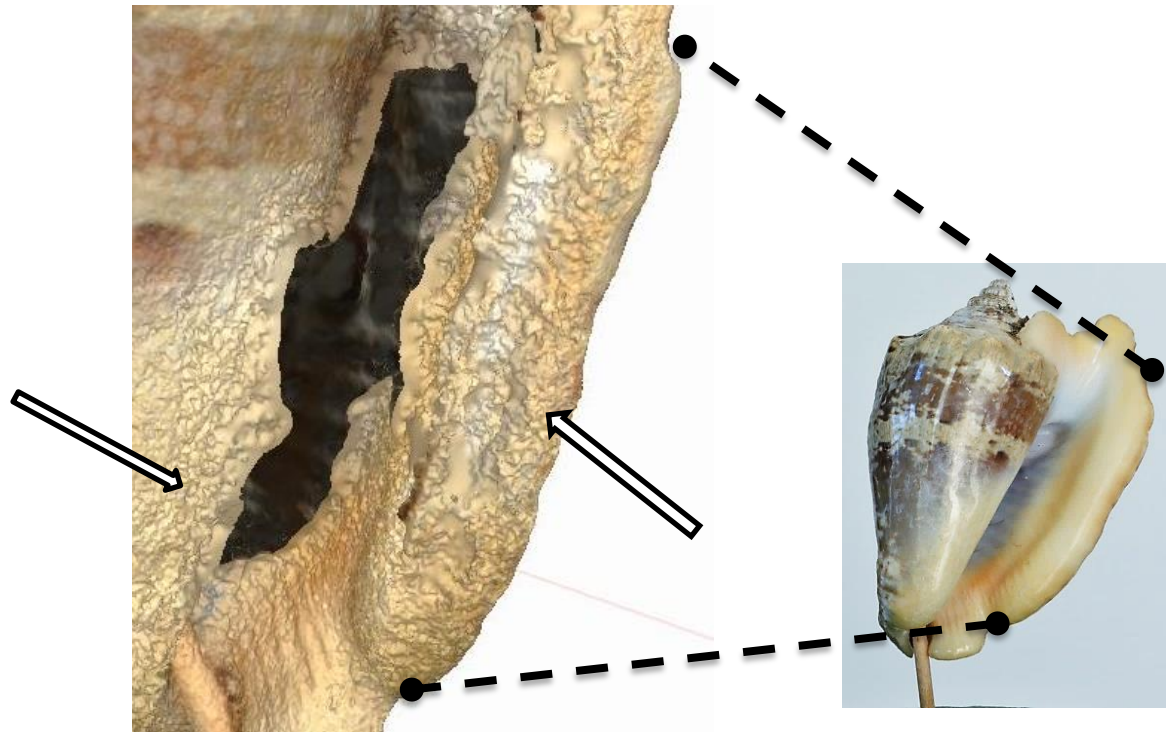


Figure 6.14: Smooth shell surface of original to orange peel effect on digital image.

#### 6.2.9      **Figure K.09 - Lincrusta - Acanthus - Item - G.16** **Figure K.10 - Lincrusta - Aphrodite - Item - G.17**

In 2014 the Engineering Department at Lancaster University were involved in a project with a local company in Morecambe, believed to be the only company left that still made this original Victorian wall covering. Invented by Frederick Walton as a development of the floor covering *Linoleum*, it became one of the many Victorian success stories that is still used in the 21<sup>st</sup> century.

*"Lincrusta was launched in 1877 to instant success in a host of applications from royal homes to railway carriages. Heralded as the first washable wallcovering, it appealed to Victorians because of its sanitary properties as well as its durability and ornate*

effects.....Originally launched as "Linoleum Muralis", it was subsequently re-named "Lincrusta-Walton" - Lin for Linum (flax, from which linseed oil is made) and Crusta (Relief), with the inventor's name being added to prevent other firms using the same title." [198]

Having digitised the Relief painting (Figure 2.23 and 3.27), these two *Lincrusta* samples presented a challenge. The difference in surface texture was different in that the painted relief was far more pronounced than the *Lincrusta*. The ridges that had been crafted on the painted canvas surface were over 10mm deep in places; whereas the raised relief on the *Lincrusta* was from 0 to 1.5mm high off the flat surface with no negative relief at all. Both pieces of *Lincrusta* were photographically processed in exactly the same way and both measured 550mm x 460mm x 3mm thick. The items were hung on the wall, suspended by spring clips, and a string was run through the clips to form a triangular hanger.

The same method was employed to digitally capture the images in the Relief canvas, Figure 3.27 as described in Chapter 3.9. The camera was moved in an arc, at approximately 130mm away from the centre of the *Lincrusta*. On average, good results were obtained taking between 60 and 65 images at f/14 or f/16 on both items. If the f/stop was opened to f/8, either blurring occurred or only half the image was captured. Both were processed using *PhotoScan Pro*<sup>®</sup> at a *high* resolution setting. Good \*.obj resolution screen shots were obtained but these degraded when the file was saved and converted to an \*.stl file.

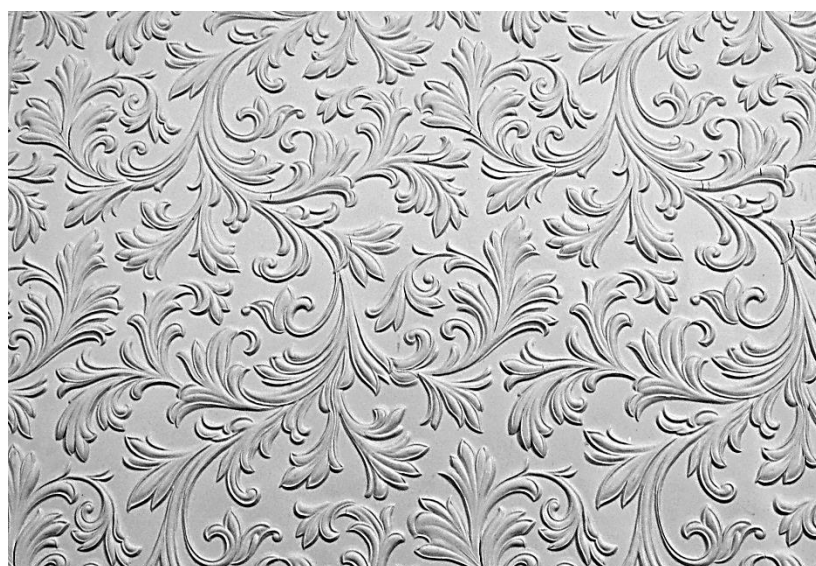


Figure 6.15: Part of a roll of *Lincrusta* – Design "Acanthus".

The dark areas on the screen shot of the \*.stl file image (Appendix K - Table K.2: Figure K.09a), processed in *StudioPro*<sup>®</sup> show a negative layer below the surface. The author would not recommend printing the *Lincrusta* as seen in Appendix K – Table K.2: Figures K.9 or K.10 unless a fine micron printer were used in the order of 16µm or less.

In a recent project, in October 2015, set up by the British Ceramics Biennial [199], artists and potters were invited to create new designs using CAD. It was hoped that by submitting the final design in the form of an \*.stl. file, and by using a ceramics 3D Systems printer, modern technology in the form of AM fabrication would lead the way, away from the tradition of water, clay and potter's wheel. It was hoped that whilst the exhibition was in progress several items would be created in front of the viewing public. One of the stipulations or suggestions that was made about any relief work on the surface of the artifacts that were created was that a height/depth of 3mm was the minimum that was needed to be successfully fabricated and be seen on the artifact. So, in the light of this recommendation, 1.5mm was perhaps too fine a relief on the *Lincrusta* to be printed successfully.

### **6.3 Summary of Repaired Data Images**

In many of the artifacts that were photographed, common problems occurred, for example, as shown in Figures 6.2, 6.3, and 6.5. Some of these problems were identified and were resolved as examples discussed in Chapters 6.1 to 6.4, but several recurring themes regarding very complex shapes, glazed surface objects, and highlights caused by light reflection are still to be resolved, which are discussed in Chapter 9. Several of the items that were used in this research were unfortunately not in the author's possession long enough to be re-examined and reprocessed, for example, the 'Mollusc' was only processed with *123D Catch*<sup>®</sup> and not *PhotoScan Pro*<sup>®</sup>, which might have proved a better method of data capture. Although the results with the item 'Serenity' were not perfect, improvements were achieved and this might have also been true of the 'Dolphins' had longer time been spent, with more data images captured and lower lighting levels used. The author would be most interested in investigating a method suggested by Nicolae *et al.* [200] of using cold lamps and circular polaroid (CP)

filters on both lamps and camera, this cross polarisation reducing the amount of (speculative) light hitting the camera sensor.

However, AutoDesk [6] in its very good and well-presented beginners' tutorial guide to the art and tricks of producing 3D images, warns that:

*"plain, reflective or transparent surfaces or objects will not work."*

The answer remains to be found, using artifacts such as the high glazed 'China' dish and the glass bottle, with more advanced programs and hardware than were the aim of this research.

## **6.4 Removing Flare/Glare and Reflection**

It was noted in Chapters 6.2.1, 6.2.2 and 6.2.8 that excessive reflection caused problems with the processing of the digital files of several artifacts. In this sub-chapter, two methods are investigated which greatly help in solving the problem of flare and light refection.

### **6.4.1 Polarising Filters**

There are two types of polarising filters which can cut down direct reflections and increase colour saturation of an image. The CP filter screws onto the front lens of the digital camera in the same way as most other filters. It is different from the linear polarising filter in that it has been designed to function with the digital metering and autofocus system of the DSLR camera and linear filters are also cheaper than the circular filters. Many manufacturers identify their circular polarising filters with the CPL or PL-Cir letters on the rim of the filter. The polarising filter works on the principle of filtering light, usually from the sun or sky, coming from a direction perpendicular to the reflected light. Rotation of the lens will cut the light or glare from a reflective surface such as water, glass, vegetation, or indeed most surfaces except metal or others that are highly glazed, which will reflect light. Usually this rotation is about 45-50°. The filtered light allows the 'natural' colour to show through from the surface, intensifying the colours.



Figure 6.16: Without CPL filter - Focal length 36mm @ f/11 @ 1/1.6s.



Figure 6.17: With CPL filter - Focal length 36mm @ f/11 @ 1/1.3s.

However, outdoors under very cloudy skies, as in Chapter 3.8.1, a CPL filter may not work at reducing glare, as there may be very little light reflection, and it may only perhaps intensify the colours by increasing the contrast. As shown in Figures 6.16 and 6.17, the photographs were taken under partly cloudy skies with the sun trying to break through; when turning the CPL lens until the best result was obtained, the wet flag stones and the glass roof of the conservatory showed the greatest changes, removing the reflection from both glass and wet stones.

Unfortunately, CPL filters do not work under artificial light conditions which are normally used within the studio environment, except perhaps as a neutral density filter (see Chapter 3.3.), so these would only be of limited use, unless the artifacts were outdoors under natural light.

#### 6.4.2 Testing CPL Filters - Artificial Lighting

A test was conducted to see if a CPL lens made any difference to glare or reflections, on the highly polished wooden base of the figurine 'Serenity', under artificial lighting conditions. In Figures 6.18 to 6.20 the focal length (fl) of 48mm was the same in all three images, as well as the aperture setting of f/11; only the shutter speed changed, automatically by the camera.



Figure 6.18:  
CPL filter not rotated  
fl/48mm @ f/11 @ 2.5sec.

Figure 6.19:  
CPL filter rotated  
fl/48mm @ f/11 @ 3sec.

Figure 6.20:  
No filter  
fl/48mm @ f/11 @ 1sec.

In Figures 6.16 and 6.17, a Polaroid filter was used, whilst in Figure 6.18, the lens was not rotated from the perpendicular. In Figure 6.19, the lens was rotated approximately  $50^{\circ}$  from the original position and in Figure 6.20, the CPL lens was removed. As can be seen by comparing the three photographs, Figures 6.18 to Figure 6.20, the highlights on the polished base have not significantly changed. Figure 6.18a to 6.20a are enlarged images of the original for clarity.



Figure 6.18a: Enlarged image - CPL filter not rotated - fl/48mm  
@ f/11 @ 2.5sec - artificial lighting.



Figure 6.19a: Enlarged image - CPL filter rotated - fl/48mm  
@ f/11 @ 3sec - artificial lighting.



Figure 6.20a: Enlarged image - No filter - fl/48mm  
@ f/11 @ 1sec – artificial lighting.

#### 6.4.2 Testing CPL Filters - Natural Lighting

In Figures 6.21 to 6.23 the same test was conducted but this time in natural daylight, with cloudy but bright skies. The settings for both the focal length and aperture were set and fixed, leaving the camera to automatically compensate for the changes in light by shutter speed alteration. The reflection on the top side of the wooden plinth and highlights on the lower front rim (as indicated by the black arrows on Figure 6.21), can be seen in both Figures 6.21 and 6.23. As indicated in Figure 6.21, are features being almost identical in both images, but in Figure 6.22 the reflection on the top side has disappeared and the highlight on the lower rim greatly diminished.



Figure 6.21: CPL filter not rotated  
f/48mm @ f/11 @ 2.5sec.

Figure 6.22: CPL filter rotated  
f/48mm @ f/11 @ 3sec.

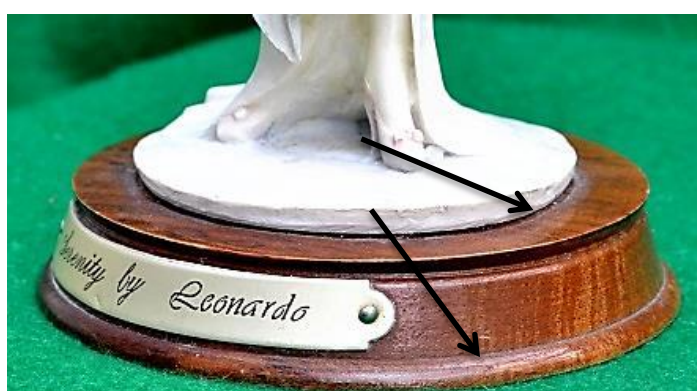


Figure 6.23: No filter f/48mm @ f/11 @ 1sec.

This simple experiment demonstrates that the CPL filters are far more effective in reducing highlights, flare and glare, in natural daylight than in artificial light. Figure 6.21a to 6.23a are enlarged images of the original for clarity.

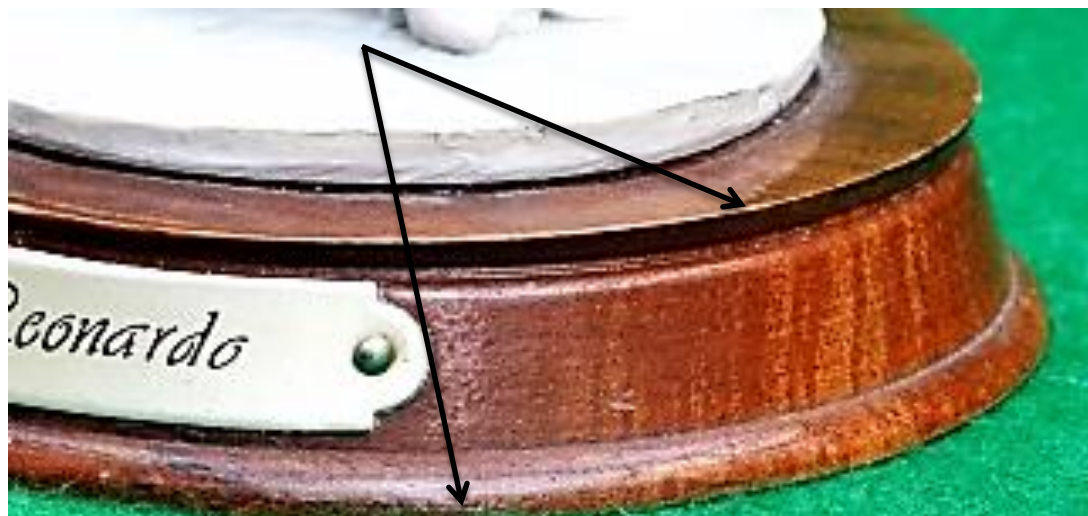


Figure 6.21a:

Enlarged image - CPL filter not rotated –  
f1/48mm @ f/11 @ 2.5sec - Natural Lighting.



Figure 6.22a

Enlarged image - CPL filter rotated –  
f1/48mm @ f/11 @ 3sec - Natural Lighting

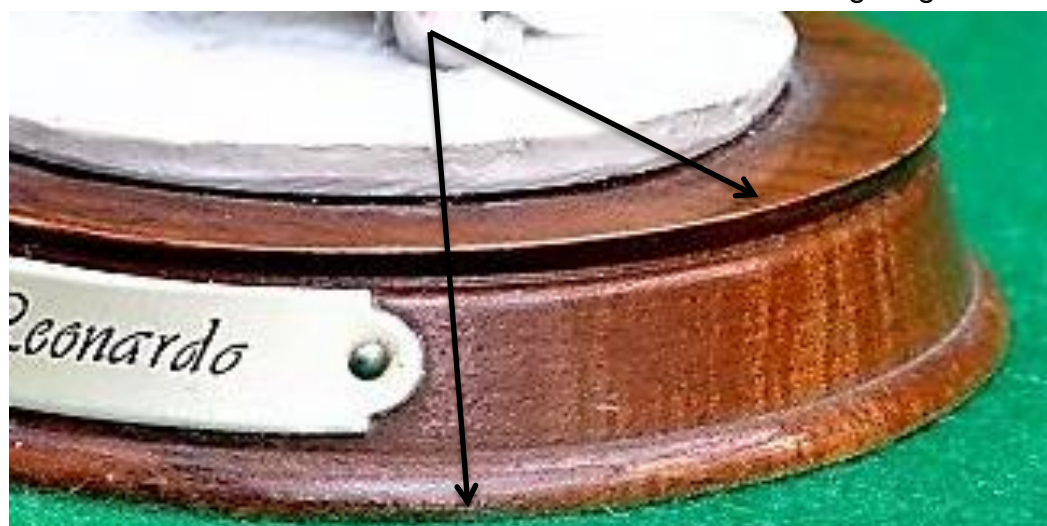


Figure 6.23a

Enlarged image - No filter - f1/48mm  
@ f/11 @ 1sec - Natural Lighting.

## 6.5. Digital Negative Editing Software

To understand how editing software can be useful in post-processing the dataset that has been captured by the camera, an appreciation of the differences between the types of files, RAW, Jpeg and Tiff, is required. For a greater in-depth understanding and explanation of file formats and the differences between them, reference books such as by Murry *et al.*, *Encyclopaedia of Graphics File Formats*, are a valuable source of information [201].

### 6.5.1 File Format

The imaging sensor of the standard Nikon D3100 camera (the camera as used for this research) captured two types of file: NEF and Jpeg. The NEF (Nikon Electronic Format) is Nikon's version of the RAW data file format. In addition to capturing all the digital image data, it provides additional information about the lens and camera identification, including the settings, time and date, and in more advanced camera models, GPS references. Both types of file format are written to the memory card. For hereon the RAW format acronym will be used as being a universal format, as opposed to NEF, which is camera specific [142].

All the images which came directly from the camera as "camera ready" images were Jpeg files. The Jpeg file can be directly read by the most basic digital photographic software, which turns the captured data into the pixels that are shown on computer monitors. These files can be directly processed by digital printers straight from the memory card to produce a 'hard' copy photograph. Conversely, RAW files are unprocessed data, which must be read and converted by more specialist software, which transforms the data into files that can be read by a host of other software, such as Gif, Eps, Pdf, Psd, Bmp, Jpeg or Tiff [202] [203]. The two file formats most relevant to this research are Jpeg and Tiff and unlike some of the other formats, they are not program specific, but rather universally imported to most photo-editing software.

Apart from cropping the images (Figures 6.18 to 6.23), the contrast was slightly enhanced so as to show the effect more clearly of the CPL filter under two sets of lighting conditions. The prime cause of manipulation was the filtering of light before the images were recorded by the camera's processor. But as seen from the images taken under artificial light, the CPL had very little, if any, effect

on the highlights and reflections seen in the finished images. There is, however, another tool which can be used to pre-process the digital images before the data set is processed by the point cloud converting software.

As discussed in Chapter 4.11.3, the imaging sensor of the digital camera records information on many aspects of the digital image. This unprocessed data is called “RAW data”, and is commonly referred to as ‘RAW image’ or ‘Camera RAW’ files. The term ‘Digital Negative’ an expression arguable coined by Thomas Knoll, the developer of Adobe *Photoshop*, and is often used to mean an unprocessed RAW image similar to that of an analogue film. It goes back to the original concept of the non-digital ‘Roll film’ camera in which a negative image was exposed but unprocessed, prior to the chemical development stage, which would finally produce a positive photographic print. Both type of images share in the similarity that neither unprocessed image can be used or evaluated until further processing.

Many standard DSLR cameras can export the data in its unprocessed RAW form, or compress the data to another format, such as a Jpeg file. The Jpeg format will have some of the data compressed, which cannot be manipulated, whilst other sections of the data are accessible by post-processing editing software programs such as Photoshop *Elements 11<sup>®</sup>* (PSE) [204], *Photoshop CS5/6<sup>®</sup>*, *Lightroom<sup>®</sup>* [145] and *Camera Raw<sup>®</sup>*, to name but a few. The compressed Jpeg file is processed in the camera and written to the memory card as a file, which can be used immediately and downloaded directly to a printer without further processing by a computer. RAW files differ in that all the data is written to memory and none of the details are compressed but do require further processing before an image can be obtained. Both forms can be post-processed by the preferred editing software, but with the RAW files, there is more information contained in the file which is accessible to be edited [171] [205].

There are five formats that the D3100 can process and the operator can choose any one of them by selecting the “Image Quality” menu on the camera and opting the desired format. These options are laid out in Table 6.2.

Table: 6.2 Image Quality Options [142].

RAW	12-bit NEF (RAW) files	Best quality and creative flexibility
Fine <sup>#</sup>	8-bit files compression ratio 1:4	Suitable for prints of Tabloid/A3 Size 4608x3072 pixels
Normal <sup>#</sup>	8-bit files compression ratio 1:8	Suitable for prints of A4 Size 3456x2304 pixels
Basic <sup>#</sup>	8-bit files compression ratio 1:16	Suitable for email or website use not for printing - 2304 x 1536 pixels
RAW & F	Two copies of same image are recorded: one RAW one Fine <sup>#</sup>	

<sup>#</sup>Denotes Jpeg image

### 6.5.2 Editing the Data, Post-processing

If a potential problem in point cloud processing of the photographic data set of the artifacts is envisaged, then the decision must be taken as to what post-processing work is to be carried out on the dataset of images. The best option for the digital set is the RAW format. Although this editing is not intended to produce printed images, the point cloud processing still requires high quality images and as seen in Chapter 6.2, the problems encountered of high reflection and flare can cause serious deformity to the finished virtual 3D model. The dataset will be checked by the point cloud processing software for quality (as already discussed in Chapter 4.8). If the majority of photographic images fall below 0.5 when scanned by the 'Quality tool', then the point cloud process is likely to produce deformed results.

The list of options that exist within the post-processing editing software programs depends on the complexity of the selected software and are beyond the remit of this discussion; some of the manuals that have been written dealing with these issues are referenced within this chapter. To dwell on a few that are directly relevant to this chapter will give a flavour of what is possible to achieve by an experienced operator using editing software. One of the basic recommendations from Agisoft is not to crop or geometrically transform the images, so although one might be tempted to crop the dataset to get a larger magnification, such action will totally confuse the processing software when trying to stitch the 2D photographic data together. If it is felt that better results will be achieved with larger images, then the camera must be moved closer to the subject, or the focus length must be adjusted.

The following editing software programs were used throughout this research to enable post-processing: PhotoShop Elements 11, which is a simpler version of Adobe *Photoshop CS6®* and *Lightroom®*. These programs are considered Industrial standards, in their own right; AP CS6 is Adobe's "flagship" and PSE is aimed at the hobbyist and domestic markets. PSE can achieve some degree of editing and many of the features such as Contrast, Colour correction, Image Sharpness and Light Adjustment can be achieved automatically by PSE, as well as a certain amount of operator control. The white balance of a RAW image (not Jpeg or Tiff) can be altered in PSE as well as Shadows, Brightness, Contrast, Highlights together with many more tools which are relevant to editing the digital images before post-processing to remove or lessen the effects of flare and reflection. However, one of the main differences between the programs, which would affect the time taken in editing, say, 130 images in a typical dataset, is the ability in CS6 and *Lightroom* to synchronise and copy automatically any edited alterations made to one image, across the whole of the dataset images. At the same time as saving the new altered images to a new directory in a new format, usually Tiff or Jpeg, the original RAW images are preserved in the original unaltered format [205] [171]. If PSE was used, the settings of each editing enhancement would have to be recorded manually, and transferred to the next image, one by one. This would be a long and tedious operation. Each image file would then have to be resaved with a different name and in a new format (Tiff or Jpeg) so as to ensure the integrity of the original RAW data files.

If in photographing the artifact, none of the problems that have been discussed seem to be present, then by shooting the dataset in Jpeg Normal or Fine format, elimination of the additional post-processing stage will be achieved. If on the other hand potential problems are envisaged RAW format should be used.

## **6.6 Overview of other uses and benefits**

In this chapter, several items were examined which required the processed data image to be repaired for a variety of reasons where there had been a shortfall in the original digital data that had been collected and processed. The following examples discussed in this chapter, show how it is possible to repair artifacts

where the original item had been damaged, as in the photo frame (Figure 6.15) or where part of the object had been lost, as in the missing crown on the statuette of Horus, in Chapter 6.7, Figure 6.28. The starting point for both objects was the same: digital collection and input of the collected data into the primary software, *PhotoScan Pro*<sup>®</sup>. The secondary software, *StudioPro*<sup>®</sup>, was used to repair the photo frame, whilst a third software, SolidWorks was used to recreate from researched drawings, two versions of Horus's crown.

## 6.7 Repair of broken Photographic Frame

The original Photo frame had been painted in gold, which presented two problems, the first being that light would be reflected off the gold and would degrade the quality of the digital images captured due to issues as discussed in other chapters. To overcome this problem, the solution would have been to spray the whole frame a neutral matt colour such as rust red, which itself caused the second problem: this action might have caused the purists to strongly object as this was a very invasive method of preparing the artifact for the photographic digital data capture.

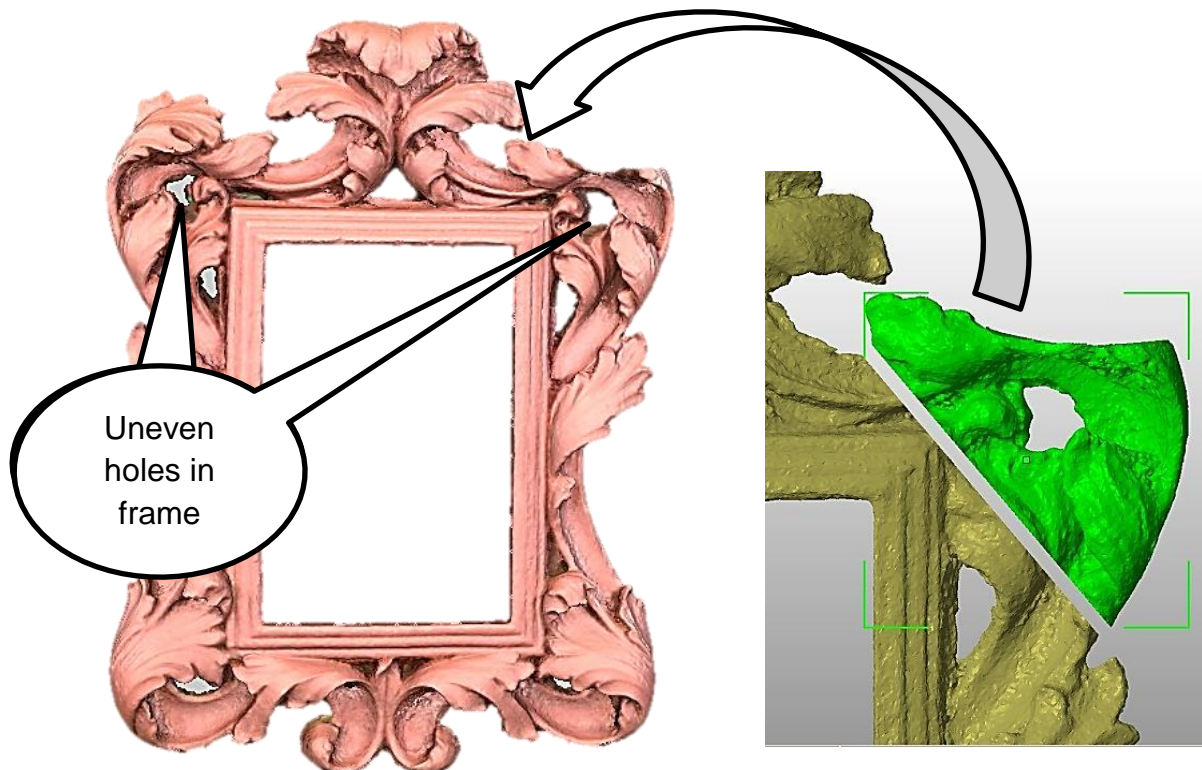


Figure 6.24: Photo frame missing corner.

Figure 6.25: Damaged corner of frame removed.

This problem has been discussed in this Chapter 6.2, and in that instance, such a method was rejected. The overriding factor in the current situation, was that the frame was broken as seen in Figures 6.24 and 6.25. If a renewed section was to be grafted onto the original, in this case an AM fabricated white nylon material, the new part would need to be painted by hand or spray gun and blended in with the rest of the picture frame to complete the repair.

The obvious course of action was to repair the frame, attach the newly made part in place, smoothing the joint and covering the whole repaired frame with undercoat paint, then repainting entirely in gold. Due of the complex nature of the frame, 112 images were digitally captured and processed to produce an \*.obj file, which in turn was imported into *StudioPro*<sup>®</sup> so as to repair the frame. In addition, a thin prop was used to support the frame on the turntable. This positioned the frame at an angle from the horizontal plane of the turntable with the possibility of distorting the images.



Figure 6.26: Digital image of frame.

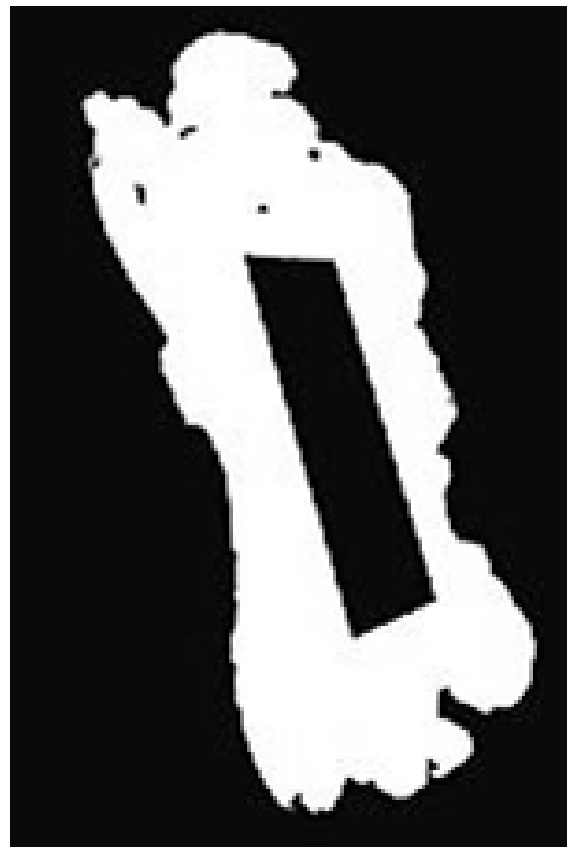


Figure 6.27: Frame mask.

When positioning the camera for the first rotation of the turntable, this had to be compensated for so as to maintain a 90° angle with the revolving frame. A dark grey card was also inserted into the picture aperture, as shown in Figure 6.26, to stop the background from showing through. By using a mask (Figure 6.27), the support and centre grey card were eliminated from the digital image.

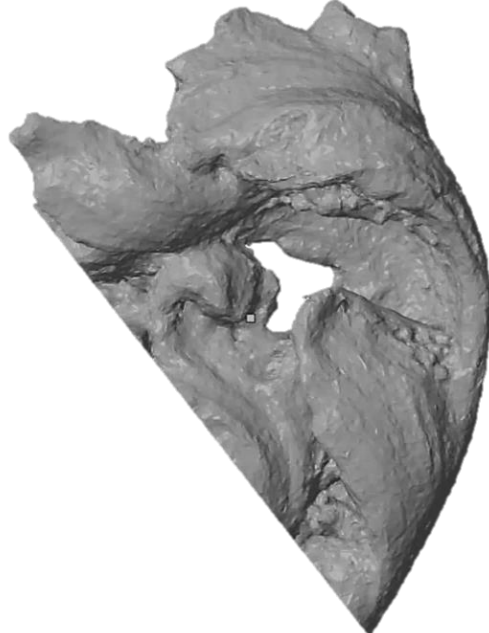


Figure 6.28: Mirrored corner of frame.

Processing the digital set with the inclusion of a wooden prop, presented similar problems and solutions, as were used and discussed in Chapter 4.10.1, but in this case the prop was much thicker (see Figures 4.44 and 4.45). By close observation, it was noted that the illuminations and carvings on the frame were not symmetrical, nor mirrored. Being hand crafted, this was not a surprise (note the variation in hole size as indicated on Figure 6.24). In a similar slicing process as used with the Warrior (see Figure 5.12) the damaged corner of the frame was removed (Figure 6.24). The undamaged corner was then copied and mirrored (Figure 6.28). In Figure 6.29 the white line also indicates the join between the frame and corner.

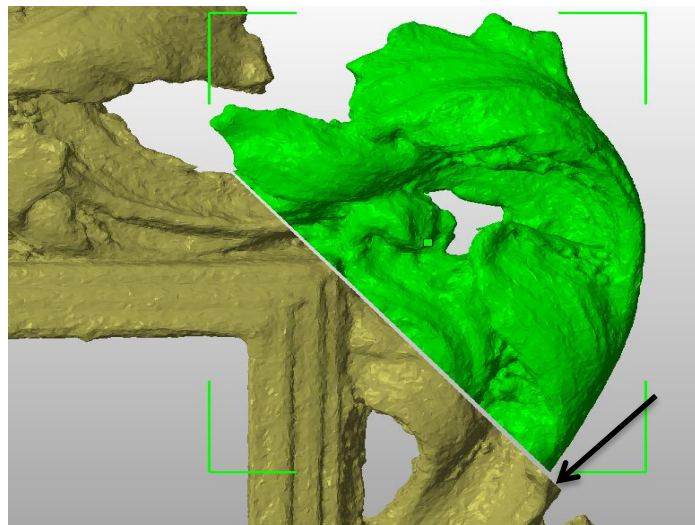


Figure 6.29: Small discrepancy on the frame to be rectified.

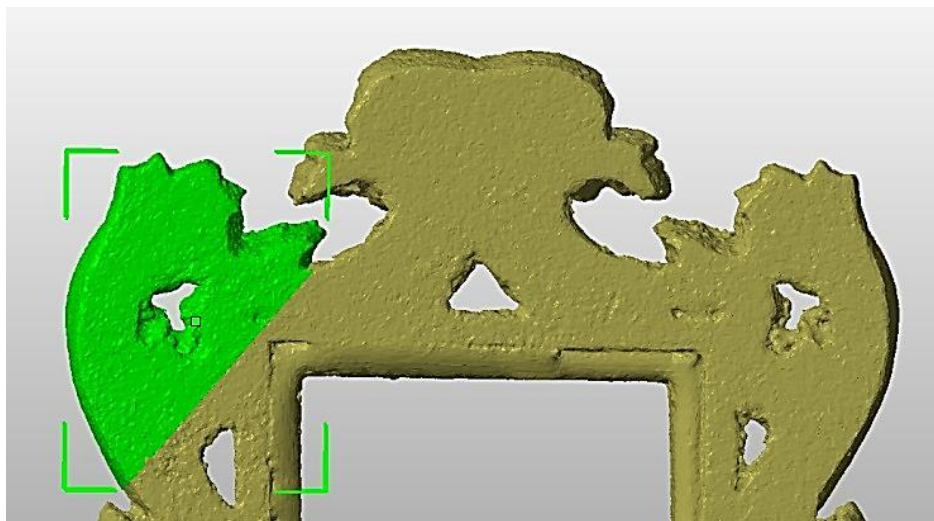


Figure 6.30: Reverse of the repaired frame.

The black arrow indicates the small under-sizing of the copied mirrored corner, which needed to be corrected, this being due to the fact that the two corners, being hand carved, were not symmetrical. In Figure 6.30 the join as seen from the reverse; being relatively flat and smooth, the join is hardly noticeable. To give added strength and reinforce the joint, small strips of plastic would have been glued across the join. However by scaling the new corner piece in one of the three directional planes and with slight repositioning, the mirrored corner piece was made to fit and the damaged corner was replaced. As these two corners were not identically symmetrical, it did mean, however, that the repair would need hand-finishing to smooth out any imperfections where the new corner piece had been joined to the main frame, which was most prominent on the

carved face side. It should be noted that the two top holes in Figure 6.31 are now identical and the top corner motifs are identical, being mirrored.

In the final stage of this repair there were two options:-

1. To fabricate the revised corner piece using AM and attaching it to the original frame. This would have entailed cutting away the damaged corner of the frame at exactly the correct angle, gluing on the new AM corner and as mentioned, reinforcing the joint, then hand-finishing by filling and blending an epoxy resin if required (this material being better than plaster of Paris as it has a better thermal expansion, and the contraction of the plaster could lead to it falling away from the frame) finally undercoating and respraying with gold paint.



Figure 6.31: Repaired Frame.

2. As the original frame had been digitised, it would now have been possible to digitally join the corner piece to the frame using the Boolean option in the software. The file would then have been converted to an \*.stl file ready for the AM machine. As the original size of the photo frame was only small, approximately 205mm x 280mm, this was a possibility; however, for large portrait or landscape frames whose size may go into two or three metres, option 1 might be preferred as these large sizes may have proved too expensive to print, apart from the difficulty of finding a machine with a platform size that could accommodate such a large frame.

### 6.7.1 The Stair Stepping effect

A third problem that could occur, which is applicable to any repaired artifact as well as “new” build, is the “stair stepping” effect (see Figure 8.2 – FDM dog and Figures 8.5 and 8.6 – Mcor paper bonded cat). If an FDM or sheet lamination type of AM machine is used, a more distinctive stepping effect will occur than with the use of SLS or SL machines. If the surface is quite intricate, FDM or sheet lamination may not be suitable either for a repair or new build of a model without post-processing of the surface.

### 6.8 The Egyptian Bowl

In the above example, a section of the original artifact was removed, mirrored and then grafted on to replace the missing section of the original artifact. Using the same software as above, a repair to the Egyptian bowl was possible. As long as the damaged artifact was reasonably symmetrical and uniform in its design, it was possible to merge a complete copy of the original artifact and combine the original and the copy into one item. In the case of the bowl, the copy was rotated between 90° and 135° (by trial and error), until the damage as seen around the rim were offset from each other and when combined into one, disappeared.

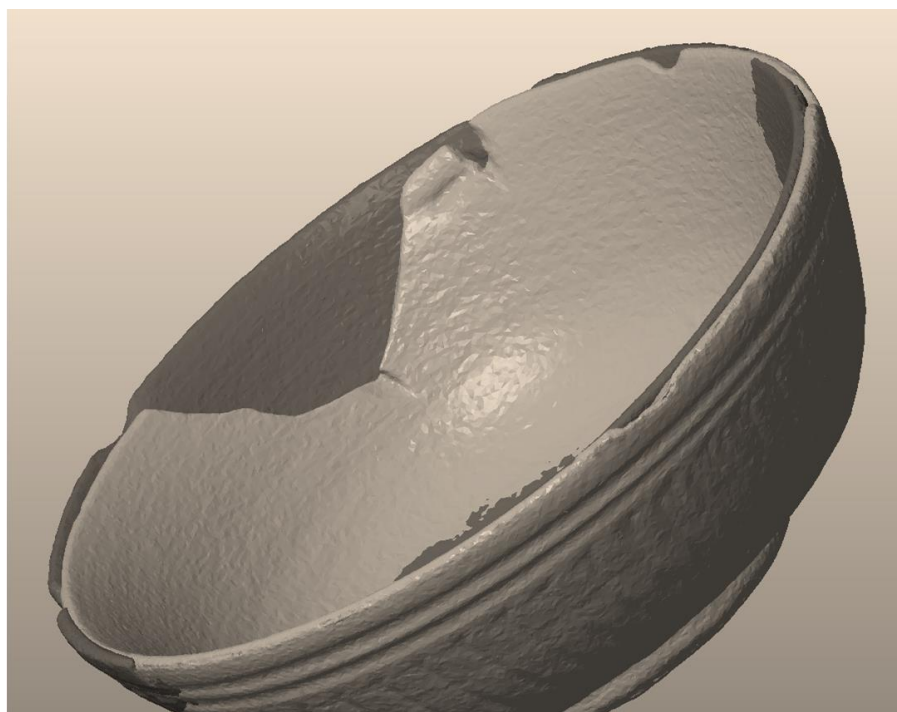


Figure 6.32: Copy and original bowl, combined and then off-set to facilitate repair.

In Figure 6.32, the dark and light shaded parts of the image are the two whole 3D images merging. It was the same with the large V shaped piece that was missing from one side (Figure 6.32). When the copy and original bowl were combined, this missing V-piece also merged into one. The merge was performed by using a Boolean function, in this instance to add two pieces together, as opposed to subtracting.

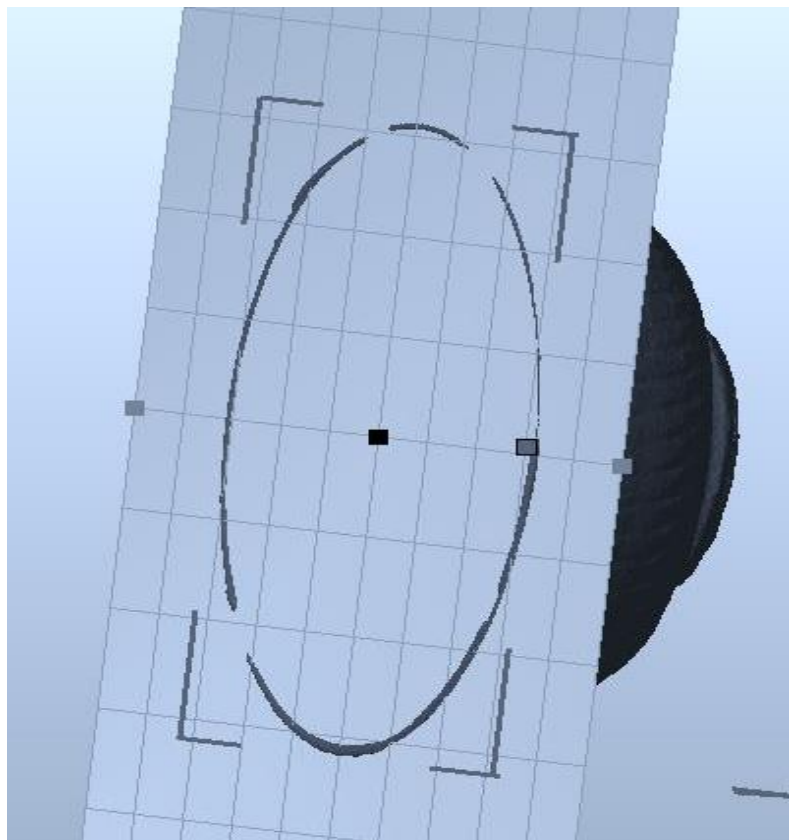


Figure 6.33: Trimming the rim of the repaired bowl.

The original ancient Egyptian bowl was not perfectly symmetrical and the copy did not superimpose 100% over the original. Therefore, very minor cleaning was carried out by way of using the cutting function to slice off less than 1 mm from the rim and the base. In Figure 6.33 the outer top rim was trimmed by using the cutting plane in the software.

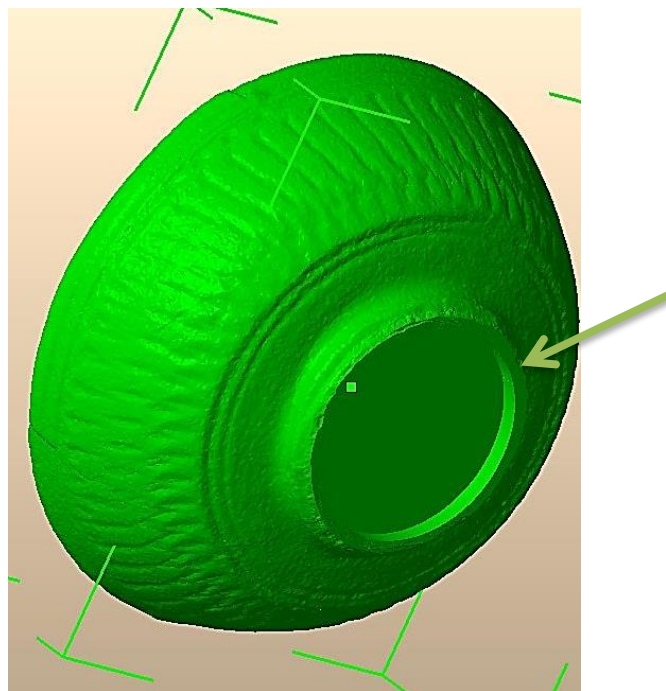


Figure 6.34: Underside of bowl.

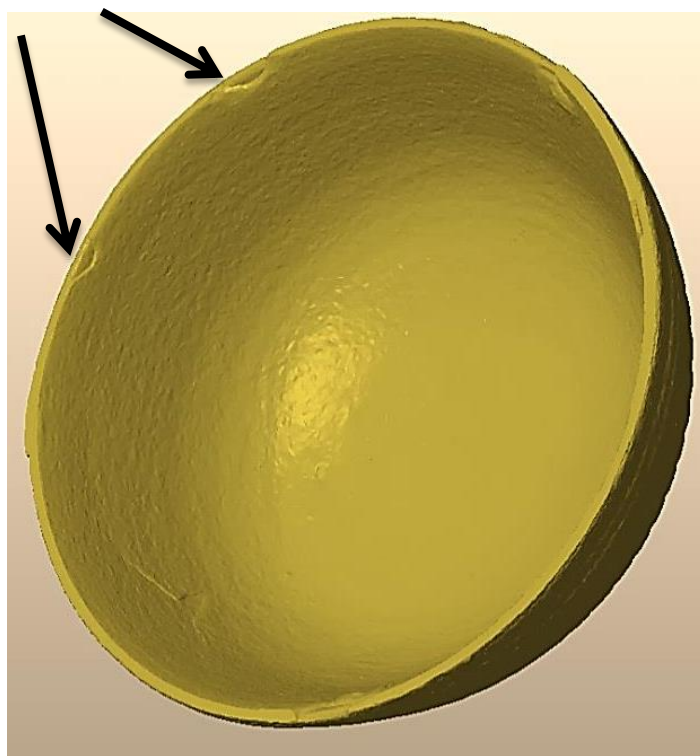


Figure 6.35: Inside of *new* bowl.

On close examination this new bowl still had some imperfections and blemishes on the inside and around the rim and these can be seen as indicated in Figure 6.35, which under the circumstances was not such a bad thing, as the replica bowl was supposed to appear to be 3,500 years old. The final action using

the software was to convert the file to an \*.stl format ready to be fabricated using additive manufacturing. When manufactured, fine grain sandpaper was used to put a very small bevel around the top rim and to smooth off the edge of the bottom stand.

### 6.9 The lost Crown of Horus

It was during the “Egyptian period” of the author’s research, and whilst processing the three Egyptian artifacts from The Kendal Museum collection, with Egyptology in mind and whilst rummaging in a flea market, that the modern statuette of Horus was found. Presumably it had been produced as a memento or souvenir for tourists on the Egyptian tourist trail, a statuette made for the tourist in the Valley of the Kings discovering the mysteries of the Pyramids and Nile.



Figure 6.36: Horus minus his Crown.

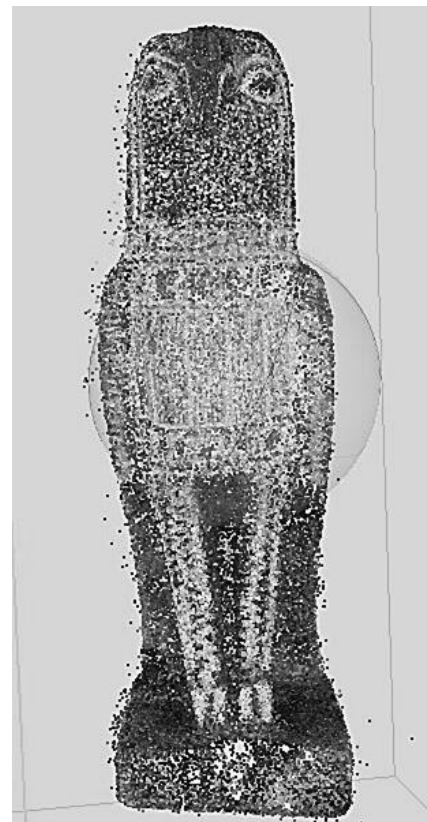


Figure 6.37: Point cloud image of Horus.

Unfortunately time had not been good to Horus, for he was crownless (Figure 6.36). Upon examination, one could see the flattened skull where the crown had once been attached. The question was whether RE and AM

techniques could be used to reinstate his majestic status. Using the same techniques as those employed to replicate Sobekhotep, a model of Horus could be created - that was not a problem, except that this technique could not be used on negative space. As the crown was missing, it could not be copied. Figure 6.37 is a screen shot showing the 3D point cloud image after having processed 145 digital 2D images. A 3D graphics drawing program would have to be used to create a crown for the statuette. The selected program to be used was by Dassault Systems called *SolidWorks*<sup>®</sup>.



Figure 6.38: Four styles of crown as worn by Horus.  
 Bronze [206]    Reproduction Resin [207]    Hard stone [208]    Sandstone [209]

Research found that there was no definitive crown that was worn by Horus. Over the centuries that the Ancient Egyptian dynasties existed, several versions of Horus wearing different crowns exist.

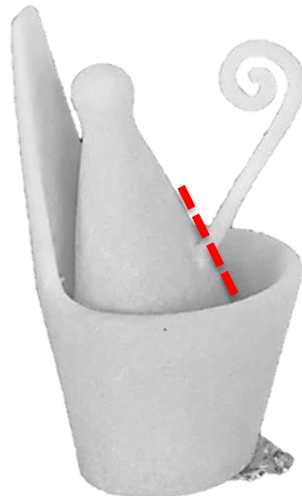


Figure 6.39: FDM printed model - version 1 – without support bar – unpainted.

The first crown was fabricated using a FDM machine and made in plastic; the curled extrusion at the front of the crown, being only 2.5mm thick, soon broke off at the base (as indicated by the dotted line on the Figure 6.39). This may have

been caused because it was made of a polymer, or equally the “grain”, if going across the curled extension, may have created a weakness at this point. This is due to the anisotropic properties inherent within layer manufacturing going across the curled extension. If fabricated in a stronger material such as steel or bronze, this damage might not have happened and the added bar could have been omitted.

Figure 6.39 is the fabricated FDM printed model - version 1 (before the curled extension broke off). The crown was redesigned and in the final version (Figure 6.40), the curled extension was thickened to 3mm and the horizontal bar was added for strength. It will be seen that the original AM model does not have a support bar and is un-painted.

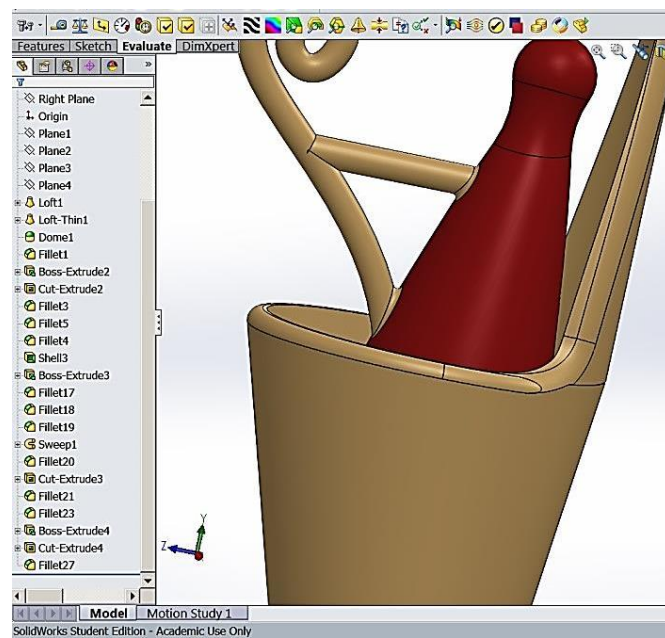


Figure 6.40: Crown being constructed within SolidWorks®.

This constructional stage can be seen within the CAD screen shot with the extension bar in place (Figure 6.40). This is a typical manufacturing problem and would have to be resolved if any type of quantity were to be envisaged, for example fabrication using a SLS machine. Using the same method that was used to build the first crown, a second design was created referencing the original Egyptian research data, the result of which can be seen in Figures 6.41 and 6.42.



Figure 6.41: *SolidWorks*<sup>®</sup> screen shot  
Crown - version 2.



Figure 6.42: 3D printed model -  
Final version 2 – hand painted.

Figure 6.41 is a CAD screen shot, whilst Figure 6.42 is a photograph of the model crown, hand-painted with a matt purple paint for the inner crown and a semi-gloss 'old gold' paint for the lower outer crown.

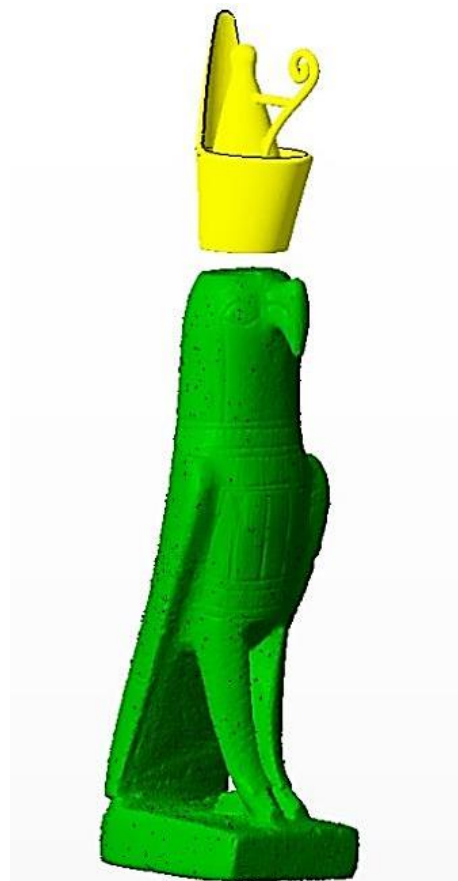


Fig.6.43: *SolidWorks*<sup>®</sup> screen-shot Horus and unattached crown.



Fig.6.44: Finished unpainted SLS model.



Figure 6.45: Hand painted finished model.

Having already produced a 3D image of Horus, as described above, and having converted the image to an \*.stl file, all that was left to do was to assemble

the crown and body together (Figure 6.43). Importing both parts into *StudioPro*® computer software, and joining the two parts together, was a straightforward process, adjusting the size of the crown slightly by using the ‘scale-up’ command so as to fit the head exactly. Once assembled and joined together, the single artifact was hollowed out with an outer shell of 3mm.

This procedure reduced manufacturing time and used less material, thus reducing the cost of the whole process. Finally all that was left to do was the fabrication on a SLS machine (Figure 6.44) and then paint the white plastic (Figure 6.45). Sections from this chapter were published in the specialist publication *Ancient Egypt* (see Appendix D) [210].

## 6.10 Educational use

It has been shown in earlier chapters how museums and schools have introduced, or are trying to introduce, cultural artifacts into the educational curriculum, whether it has been the local history of the area, such as the Crosby Garrett Helmet (Chapter 2.9.1) or a collection of less valuable artifacts from distant lands, as found in the School Loan (Chapter 2.5). But such rare figurines as Sobekhotep, the small Egyptian model excavated in Garstang in 1903, will by nature of their uniqueness and fragility have to remain in glass cabinets.



Figure 6.46: The SL2 model of *XYZRGB*® structured light scanner.

As demonstrated by this dissertation, replication using photogrammetry for the general benefit of the wider community has been possible at a modest cost. Modest cost and simplicity is the key factor throughout this dissertation, as is seen in contrast with Soile *et al.* [211], who enhanced the museum/school room experience of visitors and school children, by drawing on the adventures of Greek hero Odysseus, as depicted on two famous *lekythos* (small perfume vessels).

These *lekythos* were housed by the National Archaeological Museum of Athens in Greece. By digitising and creating 3D models they hoped to inspire the recipients with the ancient myths and stories of this famous adventurer. The project was a great success but, unlike the procedures described in this research, it was very complex in execution. Their equipment was impressive, see Figure 6.46; for the data collection they used the SL2 model of XYZRGB structured light scanner which consisted of a *Canon 450D HD* camera, two *uEye* machine vision cameras, an *Infocus IN35W projector*, a calibration board as well as the use of specialist software such as *3D Studio Max* and *Photoshop CS5*. In their conclusion they felt that the procedures carried out were the most appropriate for the excellent results that had been achieved:

*“However the low degree of automation of the process may create problems as the final product depends on the experience and the knowledge of the user.”*

But of great importance was.....

*“... an attractive solution to the presentation of archaeological findings in an effort to create an attractive educational tool, which may help kids and students to participate actively during their visit to an archaeological museum. .... Children are encouraged to observe, to think, to express themselves and act.”*

Being the national museum, there were many more resources available to them than to a local county museum, such as at Kendal. However, whether the data capture is achieved with very modest means, or with more complex equipment as cited, it is important that having obtained the digital data captured for model replication further use can be made of this data, perhaps to widen the

educational horizons and interests in educational fields. The following sections of this chapter present some suggestions for this expansion and five different examples are presented here, all digital data having been captured using only a single DSLR camera.

#### 6.10.1 Further use of Horus's Crown

Chapter 6.9, Horus has two crowns designed and created using CAD software and referencing several books dealing with the Ancient Egyptian dynasties. Here was seen the possibility of using the research to build the crowns in educational environments. Although, in this instance *SolidWorks*<sup>®</sup> was used, there are many other CAD software programs which could have been used to teach pupils in schools how to design and fabricate such artifacts.



Figure 6.47:  
The first loft of the inner crown.

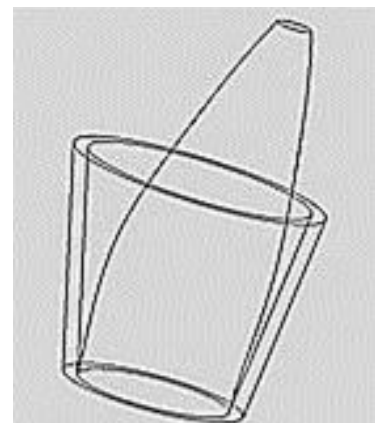


Figure 6.48:  
Second outer crown added.



Figure 6.49:  
Top Dome & fillet added to inner crown.

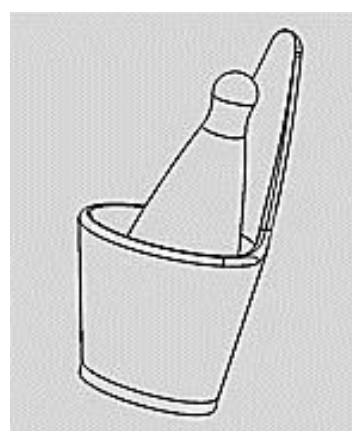


Figure 6.50:  
Top of outer crown added and edges smoothed.



Figure 6.51:  
Curled front swept extrusion added.

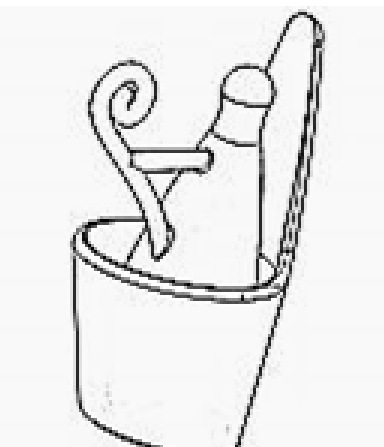


Figure 6.52:  
Secondary support bar added.

Figure 6.47 to Figure 6.52 show the stages in creating the crown within this CAD software program. Each diagram is a 2D sketch of the lofted 3D image as it is built up using a selection of commands within the software. The CAD drawing in Figure 6.47 was the first part of the crown model to be replicated. The other shapes were then added in stages, Figures 6.47 to 6.52. Once the model CAD file had been created it was converted into an \*.stl file ready for AM fabrication.

### 6.10.2 Morphing Models

In Chapters 2.5, 2.14.2 and 2.14.3, the role of museums and educational institutions was discussed, together with the benefits of a 'hands-on' experience not only for children at school but also by the museum visitor. As the price of entry level AM machines falls, increasing numbers of schools and even private homes are being tempted to acquire these low cost "3D printing" machines.

These budget machines include the RepRap *Prusa I3*<sup>®</sup> 3D Printer Machine (Figure 6.53) and the Aurora Z605<sup>®</sup> Replicator Machine, printing in PLA or ABS materials. These particular machines are intended for DIY assembly by the purchaser and in October 2015 were selling on UK E-Bay websites for between £250.00 and £300.00. With a little imagination, these machines could fabricate far more than the Hobgoblins and Bunny Rabbits which are so often shown in the publicity material for their manufacturing platforms. The white fabricating material, ABS or nylon, which could be used to replicate the artifacts discussed in this research, could be hand painted by schoolchildren, encouraging further research and interpretation, by participating in creating their own historic or cultural

artifacts. The two further examples that are discussed here, show the versatility of the software that had been used, and how it could be further used in the classroom or in the home.

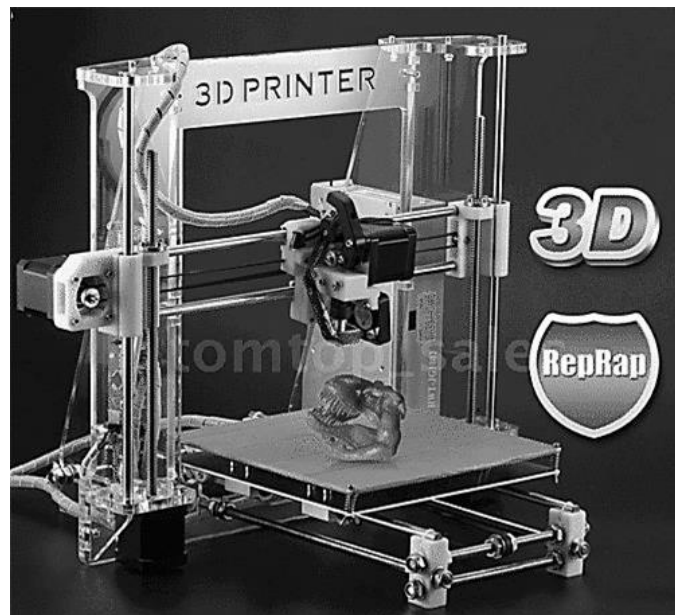


Figure 6.53: *RepRap*<sup>®</sup> machine as sold on e-Bay for £250.

The main secondary software program used to convert the digital data files captured by either *Catch123D*<sup>®</sup> or *PhotoScan Pro*<sup>®</sup> into \*.obj or \*.stl files, was *StudioPro*<sup>®</sup>. This program had three very simple features which were employed to manipulate or morph the original object into another shape.



Figure 6.54: Original Roman jug.



Figure 6.55: Screen shot of \*.stl image.

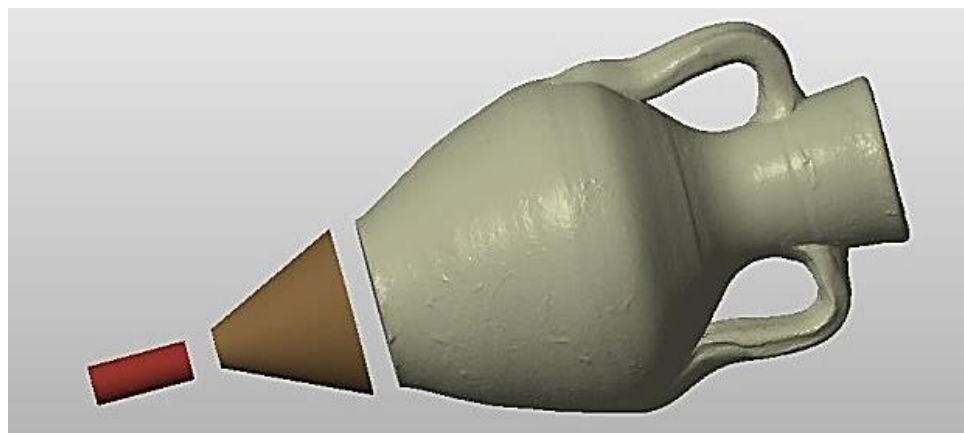


Figure 6.56: Screen shots of addition parts made for jug.

In the example shown, a modern copy of a Roman jug (Figure 6.54) was digitally captured and processed using PhotoScan Pro® software, as discussed in Chapter 4.9, and a 3D CAD \*.stl file created (Figure 6.55). Importing the \*.stl file into StudioPro®, two simple shapes were created using the 'create primitives' function and then, using the 'Boolean function', these were joined together. Figure 6.56 shows the two new shapes, a cylinder and a frustum of pyramid ready to be joined to the main jug. This resulted in the formation of the amphora jug as seen in Figure 6.57. The first Jug "A" is the original as digitised and processed.

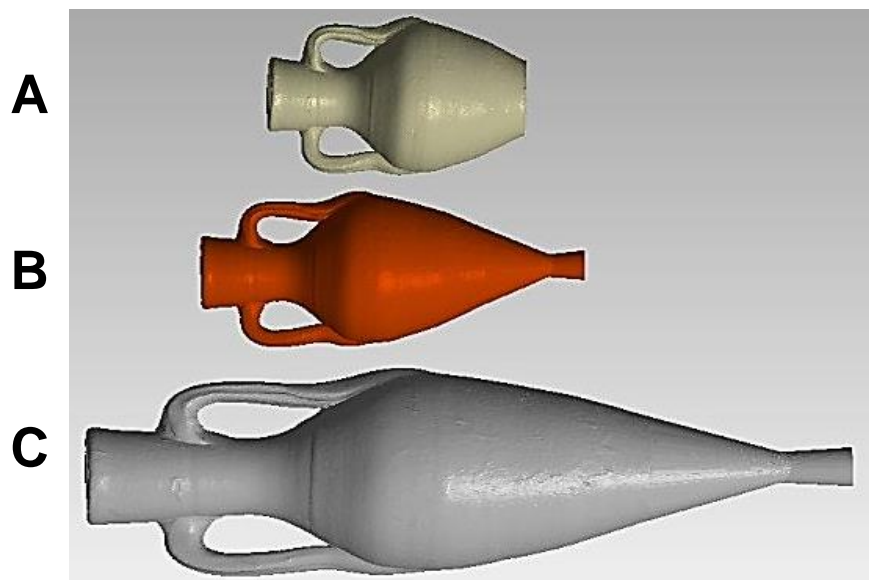


Figure 6.57: The three stages of transformation.



Figure 6.58:<sup>11</sup> “Dressel” Wine amphora.



Figure 6.59: Screen shot of amphora \*.stl image.

The second jug “B” shows the intermediate version after the additional parts were added. Using the ‘scaling’ function, the jug was stretched in the x axis, producing the long wine amphora “C”, a shape seen amongst the Dressel amphora [212] (Figure 6.58). The \*.stl file was now ready to fabricate on an AM machine and be hand-painted as required by the student (Figure 6.59).

#### 6.10.3 A stand for the Amphora

These shaped vases were designed to store or carry wine or olive oil and would have been positioned standing up, dug into the earth of a warehouse or pushed into sand in the hold of a ship. Stands have been made of metal [213] such as in Figure 6.60 so that these vases could be used indoors on tiled or mosaic floors. With the use of CAD software, such a stand can be designed and fabricated on an AM machine (Figure 6.61), perhaps more retro than Roman. Figure 6.62 shows the photograph of the finished AM fabricated models, amphora supported by the three legged AM stand.

---

<sup>11</sup> c100 BC wine amphora – Museo Archeological Nazionale, Florence



Figure 6.60:  
Greco Roman amphora and stand.



Figure 6.61:  
*SolidWorks*® amphora stand.



Figure 6.62: Unpainted white AM fabricated amphora and black stand.

#### 6.10.4 Flat Bottom Grain Jar

A further shape was recreated using the original jug as a model, inspired by a modern glass type of jar in which dry goods or grain might have been kept (Figure 6.63). The circumference of the original jar was enlarged in relation to the jar's height. A simple operation was performed increasing the X and Y plane until the shape was visually acceptable, then just a small amount of increase was added in the Z direction. Turning the jar to face sideways, the cutting tool was used to slice off part of the bottom of the jar at an angle of 25° to 30°.

Finally a stopper was created to fit the jar mouth opening; this was done using the “*create primitives*” option. To make the cork for the jar opening, the “*Frustum of Pyramid*” was selected and resized to fit the opening of the jar. In Figure 6.64, the morphed jug and cork are seen together with the original jug on the same scale.



Figure 6.63: Modern flat bottom jar [214].



Figure 6.64: Morphed jar together with original.

#### 6.10.5 Making Technical Drawings of the Models

A further aid to the classroom was the ability to use the computer software to create 2D drawings of the artifacts so as to record accurate information about the objects under study. SolidWorks® CAD software has an engineering 2D technical drawing facility as has the DeskArts' 3data Expert® program; both facilities could then be printed out to the standard paper sizes of A1 to A4 or to a custom designed sheet size.

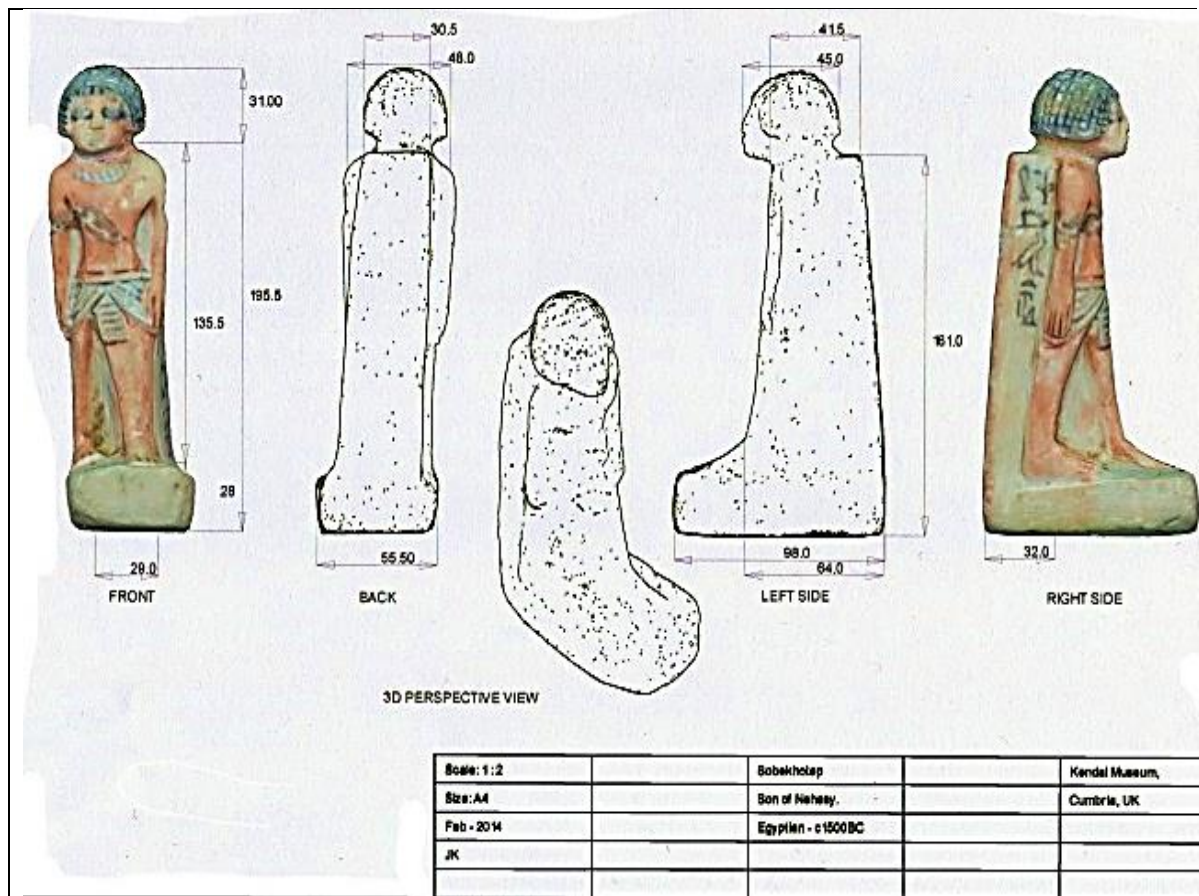


Figure 6.65: 2D Drawing of figurine Sobekhotep with information extracted from DeskArts' 3data Expert®.

Figure 6.65, a printout from this CAD software, shows four views, front, back, left side and the right side as 2D drawing of the figurine Sobekhotep, whilst the middle drawing is shown as an isometric view. Information could be recorded by the students about the size, colour, materials etc., on such drawing sheets, further engaging in the cultural learning experience.

Using these drawings as a basis, the students, if so inclined, could then move into an art studio in order to attempt a reproduction of the artifacts themselves by hand in materials such as clay, or to try their hand at carving in wood or stone, adding yet another dimension to the learning process.

## 6.11 Well Protected for the Journey

A great amount of effort, expertise and in many cases cost has gone into the replication of both large and small historic artifacts. Both original artifacts and replicas need to be transported from one gallery or museum to another; yet there is limited published material about the possibility of using RE, 3D scanning and

high resolution Photogrammetry to produce containers to transport original artifacts around the world. One of the uses of the application of 3D digitisation that Zhao and Loy reported [215], regarding a Chinese programme of Cultural Heritage preservation, was the use of a CNC machine to cut out shapes that the artifacts fit into perfectly. Considering the photographic illustrations in the report, it appears materials such as foam or polystyrene sheeting were used, although this information was not given.

This presents a further good opportunity: instead of using another form of replication, a CNC machine, it might have been possible to use an AM machine for the whole process. The replication model and the transportation bed could be fabricated in one session, even perhaps an outer layer in the form of a box. Such machines as the Stratasys Triple-jetting 3D printer [216] from the Connex3 range are able to produce rubber-like materials [217].

*“With Rubber-like PolyJet photopolymers, you can simulate rubber with different levels of hardness, elongation and tear resistance. Grey, black, white and translucent, Rubber-like material enables you to simulate a very wide variety of finished products, from soft-grip handles to footwear. With Connex3 systems, you can add colour to the mix for exceptional final-product realism.”* [217]

These materials which have soft, non-slip surfaces, together with many other materials including *Digital ABS™* [218], could be used for the replicated model at the same time as fabricating transporting cases. Using the same software, *StudioPro®*, an attempt was made to combine all of these items into one printable file. Sobekhotep was used as the artifact to be housed in the finished container.

Figure 6.66 is a screen shot from the software showing how the complete five piece nested Transporter would look. The following are the listed parts:

- i. Outer top lid of Transporter box.
- ii. Top lid of Rubberised block
- iii. Sobekhotep
- iv. Lower Rubberised block
- v. Lower outer casing

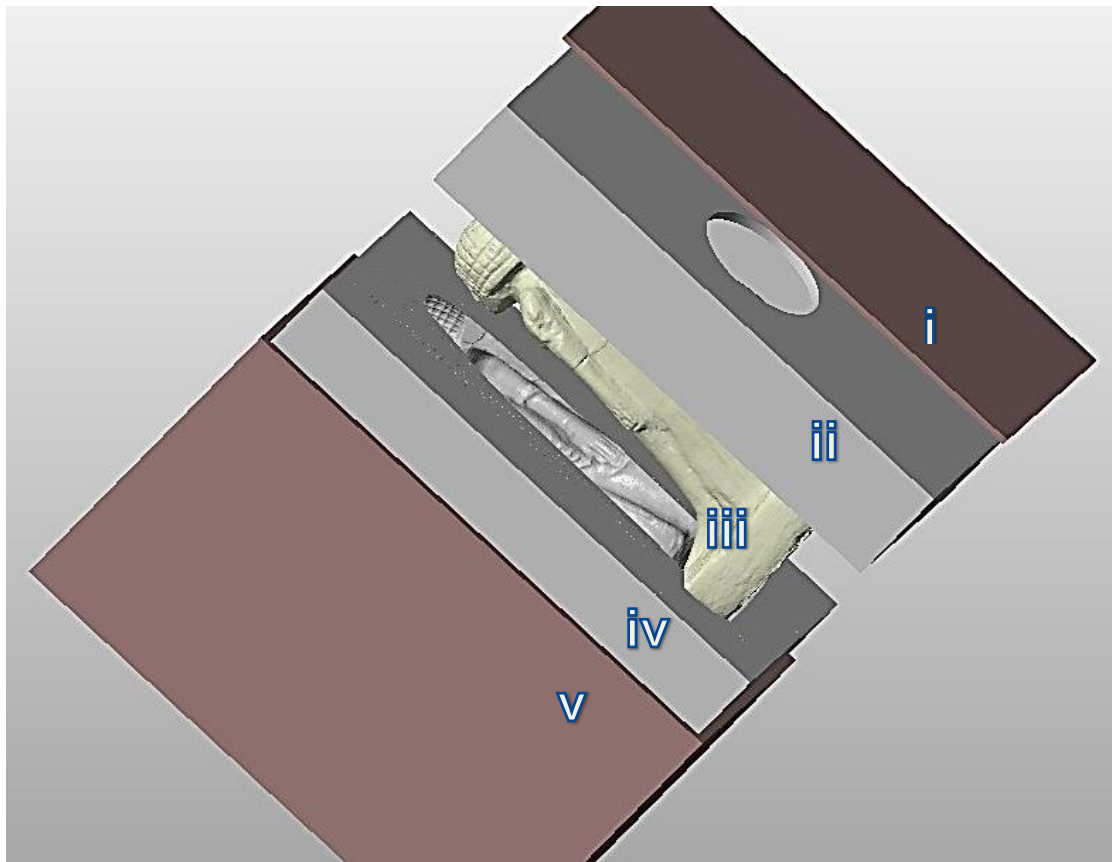


Figure 6.66: Five parts of the Boxed Set.

The practicalities of this proposal are unknown as a machine from the Connex3 range, (such as the PolyJet J750), was not available to test print the \*.stl file that had been created. This file by any standards was very large: 281,085kb, because it combines all the components, (of which there are five) into one executable \*.stl file.

Another way would have been to individually fabricate the parts of the transporter; thereby reducing the overall size of the file to a more manageable size which the AM machines could handle, but still using the capabilities of AM technology to fabricate all parts of the packaging. Of course the cost of manufacturing the outer box compared to using an off the shelf cardboard box and adjusting the size of the rubberised inner blocks to fit the cardboard box would also have to be considered.

## Chapter 7: Compact Camera v DSLR

### 7.1 Compact camera as an alternative

In Chapter 3.4.1, the subject of the multi-camera test rig that was built to hold and test the digital output of compact cameras was discussed. The point was to establish whether there was any substantial advantage to be gained by using a much larger and heavier DSLR camera. The outcome, unfortunately, was that the rig that had been built and fabricated on the AM machine in nylon, was not rigid enough to support the cameras. It was felt that further work on its design and the materials used was needed and as this did not feature in the main plan of the dissertation and because of a limited time schedule, further work on the rig was abandoned. To continue with the test, as stated previously, a Canon *IXUS 100IS*® was used which came with a capacity for 12.1 megapixels. The resolution was downgraded progressively for each of the tests, and as the camera was a basic “Point and Shoot”, there were no other parameters that could be changed. Table 7.1 shows the main data: number of images, image size in pixels, and image of file size in kilobytes, aperture, speed and focal length, and the last three items being totally automatic.

Table 7.1: Basic Camera Data Comparison.

	Camera	No. Images	Aperture f/-	S/Speed second	F/Length	Image size pix	Image File* size - kb
Roman Jug	Nikon <i>D3100</i>	130	22	1/2 - 1/5	52 - 48	4608 x 3072	3477 - 3903
Roman Jug	Canon <i>IXUS</i>	95	5 - 5.8	1/60 - 1/80	14.8 - 17.9	3264 x 2448	1518 - 2003
Botijo	Nikon <i>D3100</i>	118	18 - 22	1/2 - 1/5	26 - 40	4608 x 3072	3143 - 3955
Botijo	Canon <i>IXUS</i>	75	2.8 - 3.5	1/60	5.4 - 9.3	1024 x 768	194 - 205
Dog	Nikon <i>D3100</i>	88	14	1/2 - 1/4	40 - 48	4608 x 3072	3440 - 4064
Dog	Canon <i>IXUS</i>	75	3.5	1/40	7.2	640 x 480	81 - 101

\*File data is for the set of images captured

Table L.1 – “*Compact camera v DSLR Data comparison*” - Appendix L. contains greater detail of digital data comparisons between Compact and DSLR camera as well as mesh and image details.

## 7.2 Basic Trial

Three artifacts were chosen: the Dog, the Roman jug and the Spanish Botijo, and which compared with previously collected and processed data from the Nikon *D3100*<sup>®</sup>.



Figure 7.1: Roman Jug  
Resolution: 4608 x 3072 (Nikon).



Figure 7.2: Spanish Botijo  
Resolution: 4608 x 3072 (Nikon).



Figure 7.3: Dog  
Resolution: 4608 x 3072 (Nikon).

The compact camera did not come with the facility to attach a shutter release and reference to the table shows that the speeds were much faster: 1/60<sup>th</sup> of a second as compared to the Nikon leisurely half or a quarter of a second, with a corresponding smaller aperture, resulting in sharper images. As the turntable method was used (see Chapter 4), a tripod for the camera was employed to maintain a steady position throughout the data capture sessions. Before each artifact was digitally processed, the resolution on the Canon was reduced:

- the Roman Jug - 3264 x 2448 pixels;
- Spanish Botijo - 1024 x 768 pixels;
- Dog - 640 x 480 pixels.

This was conducted in order to see the lowest digital camera resolution that would produce a good 3D virtual image using *PhotoScan Pro*®.

Each artifact had already been photographed and processed using the Nikon camera and *PhotoScan Pro*® in the normal way with the standard resolution (as used in this dissertation) of 4608 x 3072 pixels. Figures 7.1 to 7.3 show the screen shots of the Nikon images acting as the bench mark for each artifact, a comparison could be drawn with those screen shots from the Canon camera, Figures 7.4 to 7.6. All Figures 7.1 to 7.6 are dense cloud images.



Figure 7.4: Roman Jug  
Resolution: 3264 x 2448 (Canon).



Figure 7.5: Spanish Botijo  
Resolution: 1024 x 768 (Canon).

It can be seen that all of the Canon-processed artifacts have produced digital images, and although the printed images have been degraded, the Jug and Botijo have still produced quite acceptable prints. However, the Dog was very degraded and a screen shot of the 'sparse cloud' image was hardly visible on the monitor screen.



Figure 7.6: Dog - Resolution: 640 x 480 (Canon).

By reference to the Table M.1 in Appendix M, it can be seen that the 'Sparse Cloud' count for the Dog is a mere 5,540 points and, as a 'Dense Cloud' (DC) image, contains only 225,501 points. In the belief that a low resolution of 640 x 480 was not going to produce a very good 3D digital image, the 'Build Dense Cloud' function in *PhotoScan Pro*<sup>®</sup> was set to the maximum of 'ultra-high', and in the case of the Dog, if there was not enough detail captured in the original photographs, the software could not create what it could not 'see'.

The photographs of the Botijo, taken by the Canon, were able to produce a usable image but at the lower end of the scale producing 813,059 as a DC point image. The Roman jug, however, produced a good result, with a resolution of 3264 x 2448, equating to just under 8 mega pixels, well within the AgiSoft's guide-lines; the DC count was 4,247,853 points as compared to the Nikon DC count of 6,894,939 points.

Appendix L also shows, apart from the numerical data, the comparison of the screen shot images such as the Mesh, Sparse point and Dense cloud images. Also included are the "Orthophotos" which represent a digital image produced by the software, from the original digital captured photographs. For

reference, the original photographic images of the artifacts can also be seen in Appendix L.

### 7.3 The Griffin

At a very early stage of this research, The Griffin was photographed using the Canon *IXUS*. At this point in time, no experiments had been carried out with any software, as the actual software that was to eventually be used had not even been decided. In the event, only 35 images were taken, without the use of a tripod or the acquired knowledge of image overlap and what was required for digital data capturing for the creation of 3D virtual images. It was in effect, the first digital set taken.

Stored, but not processed on the computer, the set of Griffin images lay dormant until the three sets of artifacts above (Chapter 7.2) had been processed. At this stage the one set of Griffin images was processed using both AutoCad's *123D Catch®* and AgiSoft's *PhotoScan Pro®*.



Figure 7.7: The Griffin.



Figure 7.8: Dense Cloud image of Griffin.

This would be a good test to see how the data compared to other artifact data sets, and how the two software programs compared to each other using the

minimum amount of data. It was not even certain whether a 3D image could be obtained using a data set of 35 images.



Figure 7.9: section from Shield from *123D Catch*®.



Figure 7.10: section from Shield from *PhotoScan Pro*®.

The original Griffin stood over one metre high, on a plinth which was raised off the ground, standing on a stone balustrade wall, the wall being about 900mm high (Figure 7.7). Although not known at the time, the height was the reason for not being able to capture the top part of the Griffin's head, as the average height of the camera off the ground was in the region of 170cm (Figure 7.8).



Figure 7.11: section from Shield from original photograph.

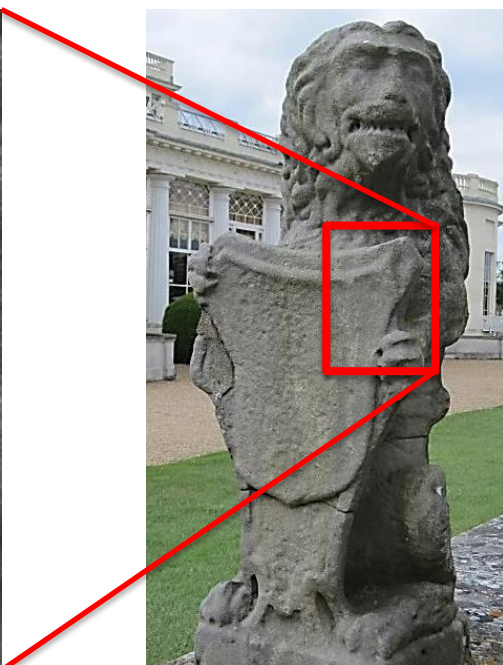


Figure 7.12: original digital image and section used for comparison.

Apart from the missing top part of the Griffin's head and the plinth that the Griffin stood on, the detail obtained from both software programs was good. By using *PhotoScan Pro*®, the operator had more control over the setting and therefore was able to set the functions to the highest values.

In doing so, the detail obtained was better using the Agisoft software. In Figures 7.9 and 7.10, a section of the shield, from the same part of each statue has been enlarged to the same size, to show the comparative detail of that section (Figure 7.9 being from *123D Catch*® and Figure 7.10. from *PhotoScan Pro*®), whilst Figure 7.11 was from the original digital photographic image and although is enlarged from the original photograph, is reasonably sharp. Figure 7.12 shows the area selected from the original photograph.

On viewing the images, it can be seen that Figure 7.9 has begun to pixelate (the black and white dots and jagged edges), whilst in the image in Figure 7.10 the detail is still visible. Having been processed into \*.obj files they were then imported into *StudioPro*® to transform into \*.stl files. By referencing Table L.1 in Appendix L, it can be seen that the imported sizes of the \*.obj files are quite different, although using the same digital data set of images. As discussed previously in Chapter 5, as no ground markers or coded targets were used, the resulting sizes of the 3D images are arbitrary. When entering into correspondence with Agisoft about this arbitrary size, the following reply was received:

*"In this case PhotoScan cannot estimate the real dimensions of the object. There's no formula for this arbitrary scale unit definition, but in the general case it is selected as a distance between two overlapping images with the high number of matching points, but that are not too close with each other, to avoid small parallax effect." [170]*

Using the source data, Table L.1 and Table 7.2 show the comparison of the two software programs and how each program converted this source data (a set of digital images), together with the differences when exported as two distinct \*.obj data files. These in turn were imported into the secondary processing software to produce the final \*.stl file.

Table 7.2: Dimensional comparison between same digital image data set.

	Length mm	Width mm	Height mm	Triangles	*.obj file size kb	*.stl file size kb
<i>PhotoScan Pro<sup>®</sup></i>	2.36	3.1	4.8	2,742,798	307,006	132,933
<i>123D Catch<sup>®</sup></i>	18.34	25.90	37.74	700,618	50,289	167,143

On examining the screen shot of the two imported images side by side (Figure 7.13), the one on the left, from *123D Catch<sup>®</sup>*, has lost surface texture and the roughness that one would have expected to see in a statue made of stone.



Figure 7.13: Screen shot from *StudioPro<sup>®</sup>*  
Imported from: Left – *123D Catch<sup>®</sup>* Right – *PhotoScan Pro<sup>®</sup>*.

As the mesh (the number of triangles) of the digital image was degraded, the surface appeared to have a smooth liquid covering over the whole area, which was the result of a loss of surface definition.

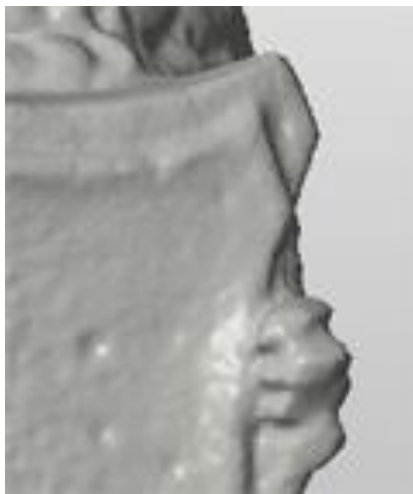


Figure 7.14: detail from shield  
– *123D Catch*<sup>®</sup>.



Figure 7.15: detail from shield  
– *PhotoScan Pro*<sup>®</sup>.

However, the figure on the right, from *PhotoScan Pro*<sup>®</sup> still retains the gritty surface texture and has not lost any detail. Figures 7.14 and 7.15 show the details from the main Figure 7.13.

#### 7.4 Summary

The conclusion which can be drawn from the information presented is that a small digital compact camera such as the Canon *IXUS*, can be used with varying degrees of success. In this case the resolution, although lower than the Nikon, when used at the higher resolution of 3264 x 2448, which is the standard format for this camera, produced results in 3D image quality as good as the Nikon. Even at the lower range of 1024 x 768 a usable amount of data was obtained so as to produce a 3D model which could be used in a virtual presentation. It may, however, have lost too much definition to obtain a good AM part, although this was not tested. At the lowest level of resolution which the camera can be set to, 640 x 480, as seen from the screen shots of the dense cloud image, this was far short of the benchmark of the Nikon camera which is required before being processed for an \*.stl file to be created. By introducing the Griffin images at a later stage in this discussion, it was shown that even with the lack of data (i.e. only 35 images), the resolution and data collection from the Canon was good enough to process images and to take this through to the \*.stl stage with the intention of AM replication.

However, without the systematic planning of data capture, a less haphazard approach would not result in an object or artifact's complete data

capture, leading to loss of detail, in this case the scalp of the Griffin. To reinstate the lost part of the 3D model would have involved complex building of the mesh, which none of the software used was designed to do. A tripod and small step ladder would have been very useful additions to the camera, allowing a much higher viewpoint to be reached when photographing the statue and this would have produced a complete data set even with the lower photograph count. A more versatile cameraman would have jumped up and stood on the balustrade wall, on which the Griffin was perched, and taken a few more back of head shots: on this occasion, however, the camera shoot was unplanned as the author was attending a wedding reception and thought the opportunity too good to miss, as the Griffin stood watch over the guests and proceedings, in the grounds of a minor stately home. But it does emphasise the fact, that for good results, careful planning was required and thought needed as to what equipment should be available.

The final conclusion must be that the compact camera was very useful (as illustrated by the example of the Griffin), in that the camera just slipped into a small pocket, and if used with all the rules of data capture being taken, it produced good 3D images, when used with software which could produce good quality, high count, point cloud images. A downside was that the Canon did not have a controllable speed or f/ stop, and the lens was much wider focus. Small artifacts, where the image capture was at close range, might require greater DoF for sharp images, which this camera could not accommodate.

## **Chapter 8: The Finished AM Replicated Models**

### **8.1 Introduction to the AM models**

The main focus preceding this chapter has been the method of data capture using only a single camera, processing this information to obtain good digital virtual 3D images, the problems encountered on this journey, repairing bad data and comparing the image with the real object including the photographic image. Many artifacts have been digitally replicated, in all 54, some very successfully, whilst others were not so successful. The model may have gone from being a virtual 3D replication, stored in a digital file within the computer's memory, to a fabricated additive manufactured replica of the original artifact. Apart from the "Bench Test" Warrior head trial (see Chapter 4.12), no mention has been made of how its physical features compared to the original. Nor of how one AM processed model compared to another, for example, a FDM item to the same item but fabricated using an SLS machine. This chapter deals with these issues.

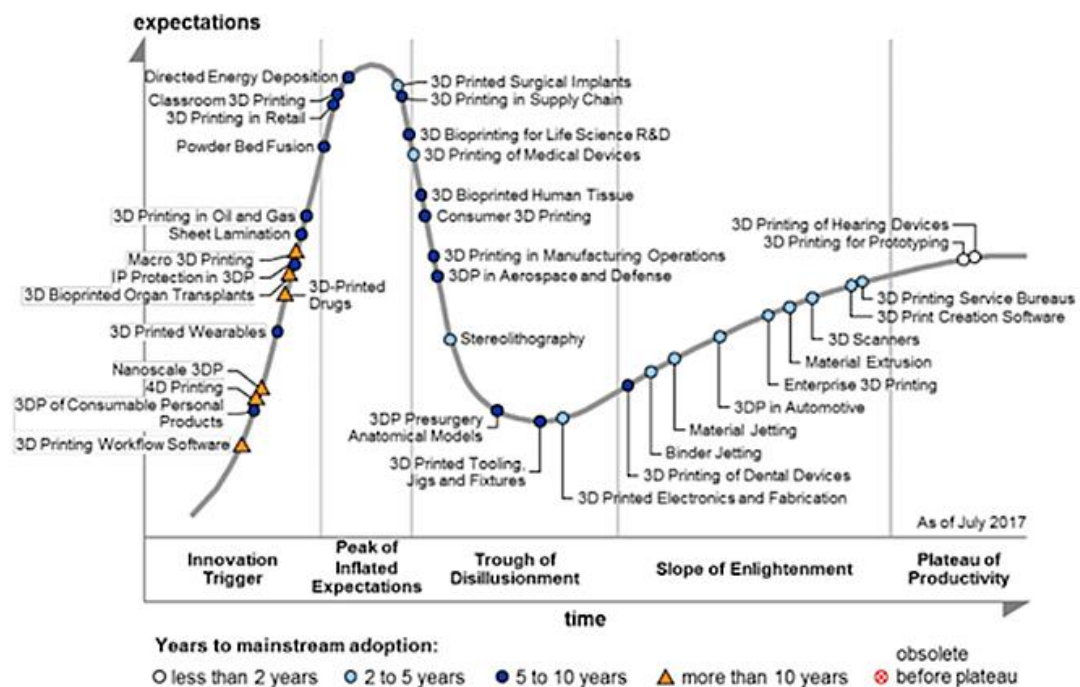
### **8.2 Current Diversity**

Over the course of this research, the development of AM machines and materials has continued to improve at a very fast pace, and as mentioned in previous chapters the cost of entry level machines has continued to fall. As recently as Summer 2015, a Kickstart company, *Peachy 3D printers*, through "cloud funding," promised a photolithographic technology replicator for \$100 [219]. However, by the spring of the following year there were reports that the company had collapsed. (Buyer/Investor Beware! [220]). At the other end of the scale, a Dutch company, *Rohaco Industrial Handling*, specialising in articulated, gantry robotic arms, has been building a printer capable of building in concrete for Eindhoven University of Technology [221]. Although the concept of "Contour Crafting" was first discussed and a model built by Khoshnevis in 2004 [222], the concept and project is now so important to the building industry, that €650,000 has been spent on this robotic AM printer, which has a build area of 11 x 5 metres with a 4 metre high gantry. In his original paper, Khoshnevis also suggested that his method of construction would be ideally suited to the 3D printing of buildings for habitation on the Moon or on Mars. With the renewed public interest in the international

Space Station and interplanetary exploration, this method now looks even more likely to be achieved as a by-product of the space exploration industry.

In any developing market there are always rumours, claims and counter-claims about new products that become available to service the core market, in this case the production of new materials for use by the core markets of AM machines, and by the users and manufacturers of these machines. Many of these companies are testing the (new to them) 3D technology and buying into the entry level 3D fabricators, originally aimed at the domestic markets. As seen in Chapter 6.11.2 with replicators being sold on e-Bay for around £250, the demand for more and more materials that can be used by both the domestic industrial markets is growing.

The AM market is now divided between industrial and domestic use according to Gartner's Hype Cycle for Emerging Technologies [223], with many businesses looking to become digital but cautious of a large investment.



Source: *The Gartner Hype Curve on 3D Printing 2017*

Figure: 8.1: Gartner's 3D Printing Hype Cycle 2017

Gartner must consider that the AM industry has expanded enough for a dedicated 2017 Hype Cycle report just for 3D printing to be released (see Figure 8.1). Commentators [223-225] [226] seem to be mixed on their views as to what is rising to or slipping from the "Peak of Inflated Expectation" into the "Trough of Disillusionment", or visa-versa, all indications of fluctuating, confusing, volatile

and fast moving markets. In the Hype Cycle for Emerging Technologies 2017, the focus was on three emerging technologies (Figure 8.2), Artificial intelligence (AI), transparently immersive experiences and digital platforms.

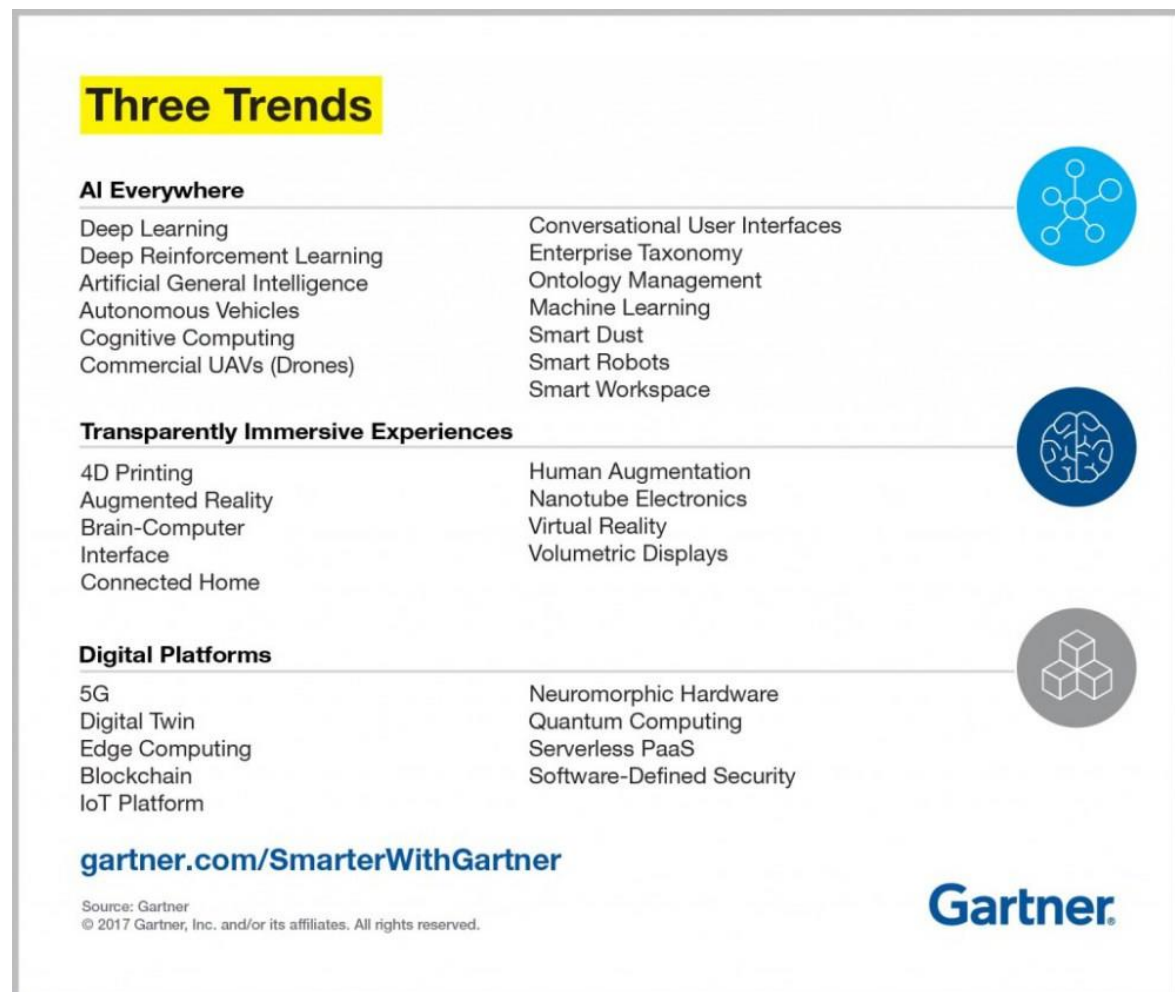


Figure 8.2: Gartner's 2017 Trends [223].

In two years the focus has shifted; in 2015, Conner *et al.* [227] in an assessment of the entry-level 3D printers from the perspective of small businesses, there was interest in these entry level machines by smaller companies and the larger 3D printer manufacturers such as Stratasys, who acquired the entry level manufacturer of *MakerBot*® and 3D Systems, the manufacturers of the *Cube*® family of printers. This presumably indicated that both domestic and industrial markets were of importance to the main 3D AM machine manufacturers so as to maintain their market dominance. But market strategies and business plans change in this fast moving, cutting edge technological industry. By spring 2016, 3D Systems' web site [126] stated that "*Cube3*® printers are discontinued and out of stock at 3D Systems". The sale of

these machines had now moved from the on-line manufacturers direct sales, onto the high street and into Staples, a retailer with a national presence in the USA.

There are many companies such as *Emerging Objects*™ [228], which have already developed a range of non-mainstream materials for the AM markets. These materials include chocolate, paper, reinforced cement polymer, salt and wood. By 2015 [229] another Dutch company, *colorFabb* [230] was producing not only a wood-like filament, ‘*woodFill*’, but a soft flexible material with the characteristics of cork – ‘*corkFill*’ - all aimed at the entry level AM hobbyist market, using such machines as *Makerbot Replicator2*. If the AM machine is not available to the hobbyist or start-up/designer business, then internet third party fabricators give a choice of 54 [231] materials to fabricate the original or replicated model. At the other end of the spectrum, researchers such as Gunasekera *et al* [232]. have been using compounds such as 1-ethyl-3-methylimidazolium acetate [233] in trying to manufacture materials from bio-renewable sources, these waste materials first having to be turned into soluble products that can be fed to the ink-jet printing heads of the AM machines [227].

These few diverse examples are a small part of what has been happening in the continually developing AM industry within the recent period in which this research has taken place, both in hardware machinery and the materials markets which go together hand-in-hand with the hardware. It would have been very easy to have been distracted by such an array of activities and to start investigating which AM machine using which material and by which process, produced the nearest equivalent to the original artifact that was being reverse engineered. These objectives were better left for future investigation and research, concentrating instead on the main criterion for now: the ability to produce an \*.stl (or equivalent) file, which resembled the original artifact, ready for the AM printer.

### **8.3 General Observation on Replicated Artifacts**

Of the 54 artifacts which were processed, the data capture of several using both primary methods, i.e. *123D Catch*® and *PhotoScan Pro*®, only 15 artifacts were finally fabricated using the limited range of fabrication printing processes which were available to the author. These were the Stratasys *Dimension 2000*® FDM machine and DTM *Sinterstation* SLS machine at Lancaster University, the

services of two AM machine manufacturers, Mcor Technologies Ltd., using a *IRIS HD 3D* colour printer, and EMCO using a 3DSystems *ProJet 660<sup>®</sup>* colour printer, plus two commercial internet based 3D print fabricators, ShapeWays and Sculpteo. Later objects were fabricated on an Ultimaker 2 and a *ProJet J750<sup>®</sup>*



Figure 8.3: Miniature FDM black dog – 50mm long x 20mm high seen alongside original clay dog.

In all cases, the author had no input in the fabrication process, having sent the appropriate type of digital file, which was processed and the model returned to the author for inspection. Five artifacts were processed to yield coloured digital files as well as non-colour digital files. These digital files were intended to be fabricated in a monochromatic material, normally white. However, the miniature black FDM dog (Figure 8.3) and roman amphora stand (Figure 6.52) were both fabricated in a black ABS.

### 8.3.1 Defect or Enhancement

In the enlarged image of the FDM dog (Figure 8.4) the contoured layers of the FDM process can be seen on its top back and side, where the neat layers or contours of the black filament can be identified. This had the effect of creating interesting patterns on the back of the dog, shown even more clearly in Figure 8.5.



Figure 8.4: Enlarged detail of miniature FDM dog.

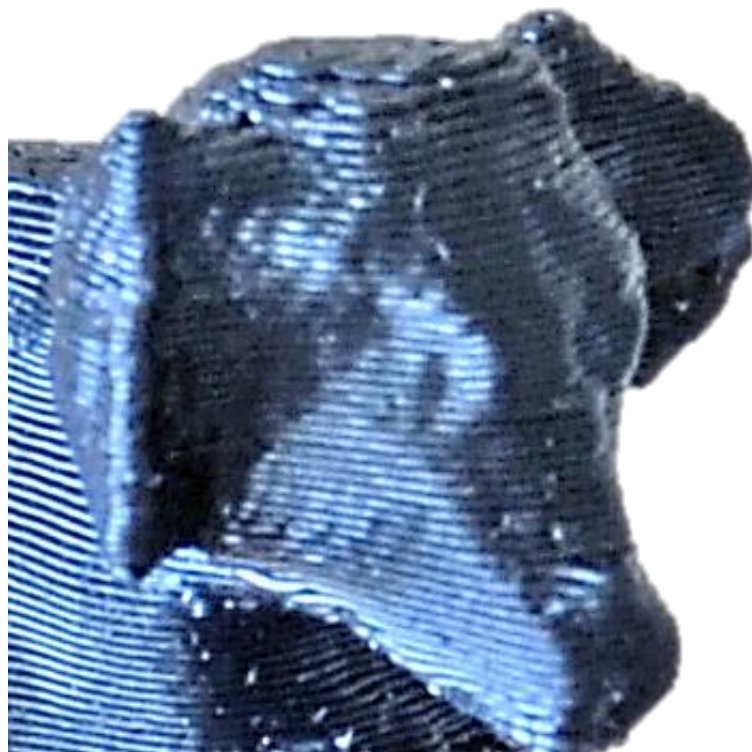


Figure 8.5 Dog's head further enlarged to show layer-wise effect.

In Chapter 6.5, the stair stepping effect can be seen as a defect, and as such, the remedy would be to use another form of AM machine such as SLS, SL or DLP or eliminate the effect by post-processing finishing. But this stepping effect is not seen by all as a defect. Using a similar technique, having converted a *Fanuc* robot machine, Dutch designer Dirk Vander Kooij [234], produced chairs made of ground up recycled plastic, extruded through a heated nozzle, much like an FDM machine. In the finished product, each layer of extruded plastic was fused to the previous, giving the structure a layered or ribbed effect with enough strength to seat a person (Figures 8.6 and 8.7).



Figure 8.6:  
The back of Dirk Vander Kooij's chair.



Figure 8.7: Author tries the chair.

In 2007, using his *D-Shape 3D printer* process (Figure 8.8), Enrico Dini, an Italian designer [235], patented a method of construction using sandstone and an inorganic binder to build a nine metre structure famously called the Radiolarian. The machine could build sections of two metres high which were then fixed together [236]. Although each layer of the build was 10mm thick, the final structure was post-processed to achieve a smooth appearance instead of a layered look.



Figure 8.8:  
Enrico Dini of Monolite UK with *Radiolaria* - the biggest structure ever built by the D-Shape 3D printer [237].

Ten years later this concept was in full flight. So important was this technology, that Kidwell had already thought of the building implications and how the construction industry might benefit from a new set of guidelines and the “*Best Practices and Applications*” which were needed [238]. Additionally, one of the foremost design, construction and engineering companies, ARUP, in collaboration with architectural studio CLS Architetti, were constructing a 3D concrete house for the 2018 Milan Design Week [239].

In 2014, Lisa Ertel, a German furniture designer, produced a collection of wood furniture which had been sand-blasted. “*Through the dialogue between naturally grown wood and the input of industrial process*” [240], this enhanced the 16th Century inspired collection of chunky stools and benches, with the annual tree ring exposed. By using a larger diameter nozzle on an FDM machine so as to increase the layer thickness, this would emphasise the stepped effect, producing a wood grain texture. This process mimicked the creations of Ertel, whose work was highlighted at the 2017 Milan Design Fair (Figures 8.9 and 8.10).



Figure 8.9: Sand blasted enhanced tree ring wood.



Figure 8.10: Ertel’s chair.

Although a process may at first seem to have failed or be deemed a defect to be post-processed and corrected, for some, such defects can benefit from the serendipity effect and be utilised to enhance a design, or to create an interesting tactile, surface texture and therefore must not be dismissed “out of hand”.

## 8.4 Colour Printing

The digital files that were produced for colour AM fabrication were not \*.stl files but \*.wri files, which unlike \*.stl files, retain the colour information. The overall process was very similar but another software program was used to produce the required colour-data-retaining files. In this case DeskArtes Oy [8] [241], a Finnish company, allowed the author free use of their software program *3Data Export*<sup>®</sup>. Two artifacts were replicated by Mcor Technologies Ltd, the Eureka cat (Figure 8.11) and the Eureka man (Figure 8.14), which were fabricated on a *IRIS HD 3D*<sup>®</sup> [242] colour AM machine. Three items printed on the *ProJet 660*<sup>®</sup> colour printer: the Egyptian bowl, Egyptian figurine Sobekhotep, and the clay head, unfortunately came out of the machine a mid-grey colour. A Eureka Cat was later successfully fabricated in colour on the *ProJet J750*<sup>®</sup>.

### 8.4.1 Eureka Cat and Man

Both these artifacts were processed on the *IRIS HD3D*<sup>®</sup> printer. This machine was different from all the other machines used in this research, in that it used standard office A4 80gsm paper as the basic material to form the replicated models, laser cutting each sheet of paper and then binding the sheets of paper together with a glue-like bonding agent.



Figure 8.11: Original Eureka Cat.



Figure 8.12: Unvarnished Mcor Cat.

A high colour resolution was printed on all the outside edges as appropriate. The original clay Eureka Cat, measured 180mm long by 35mm high and 16mm in depth (Figure 8.11).

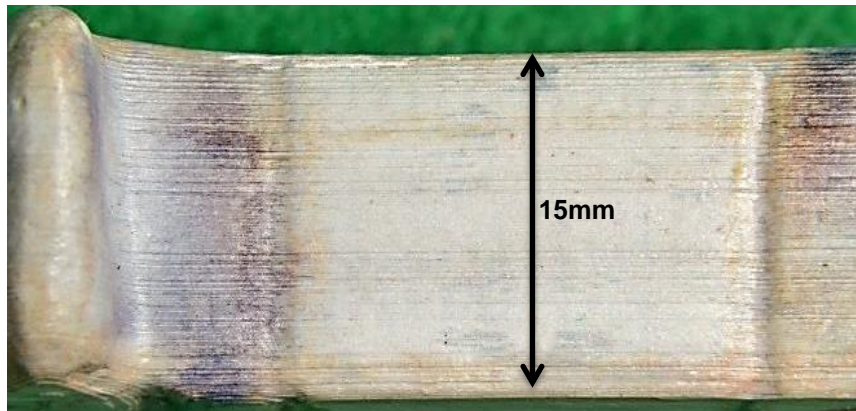


Figure 8.13:

Enlarged top view of Eureka Cat  
to show vertical paper layers.

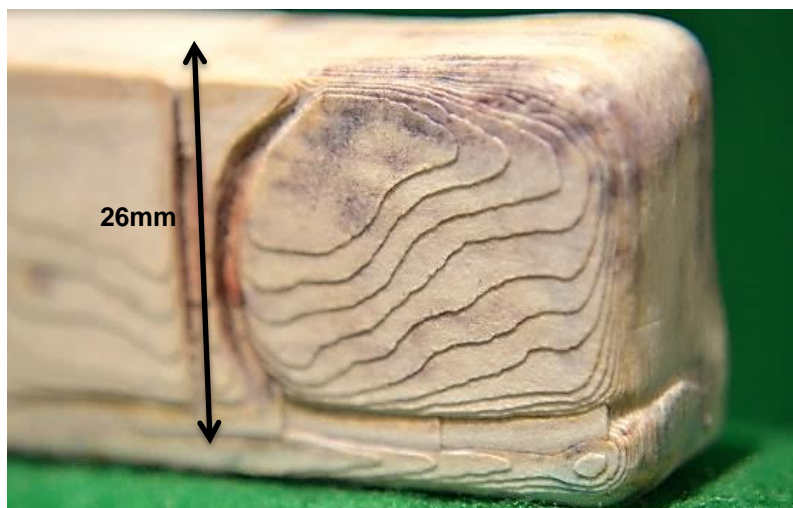


Figure 8.14:

Enlarged back hindquarters of Eureka Cat  
to show paper contours.

Although the original was a darker shade of brown and glazed, the replicated model nevertheless maintained a lot of the detail and replicated very well as seen in Figure 8.12. In Figures 8.13 and 8.14 the paper grain, or individual layers of paper can be seen, but the image of Figure 8.14 has been magnified using a CU x10 dioptre lens just to show the vertical layered effect (the horizontal lines) which were not really discernible with the naked eye.

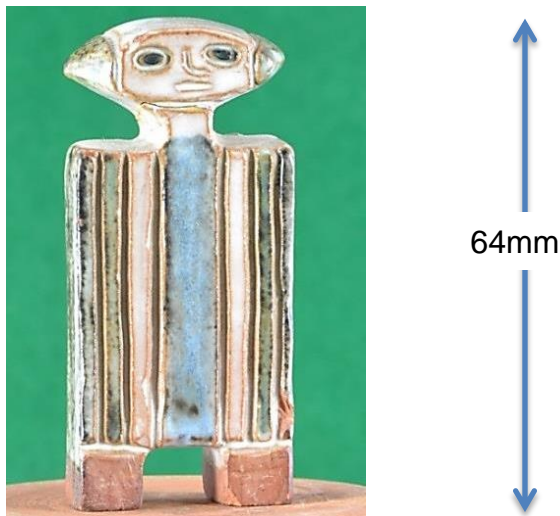


Figure 8.15: Original Eureka clay man.

However, the paper layers or contours on the front are quite clear without any enlargement (although the image Figure 8.14 has been enlarged for clarity). The same can be said for the Eureka Man, with regard to colour and size (64mm high x 29mm wide x 11mm deep and also made of glazed clay), but perhaps because he was longer and narrower, the contour effect was not so noticeable (Figure 8.16).



Figure 8.16: Enlarged section of replicated unvarnished Eureka clay man.

Two interesting little items of fine detail showed up on the backs of both artifacts. The first was on the Eureka man (Figure 8.17): the original figure had been repaired and a crack across the neck was visible on the right hand figurine as seen in Figure 8.17. On close examination of the left hand replica, this crack could just be seen as a hair line mark, as indicated.



Figure 8.17: Left hand figurine with hair line printed crack visible.

The second fine detail to be replicated was on the back of the Eureka cat (Figure 8.18). The original glazed cat had a partly faded label on which the detail of the artist's company name appeared together with information stating that the artifact was "Handmade", now quite faded (Figure 8.18).



Figure 8.18: Enlarged image of faded label on back of original cat.



Figure 8.19: Enlarged image of faded printed label visible amongst contoured paper layers on fabricated cat.

Although very faint and lacking colour, this label (13mm wide) was also replicated and could just be seen on the model; also the layers were quite visible as seen in Figure 8.19. The finished Mcor models were very true to the original likeness both in size and in the fine detail that was captured and printed from the

original photo shoot, although the colour was perhaps rather faded. This could very well have been to do with the colour saturation of the original digital photographs and any degrading during the virtual image processing stage to obtain either the \*.obj file or \*.wri file. The original digital images of these Eureka objects and the other three artifacts, which follow in Chapter 8.4.2, were taken before any investigations into the possibility of coloured replications being made. True colour matching and how colour would transpose across to the colour AM machines and the ink printing process were not considered, but it is something that users should be more aware of, if contemplating full colour replications. Both these original models were also fabricated using FDM and SLS machines, and although the fine detail such as the label on the cat and the hair crack on the man were lost, the physical grooved details such as faces on both, vertical ribs on the man in Figure 8.20, front, back legs and paws on the cat in Figure 8.21, have been reproduced in both other forms of AM fabrication.



Figure 8.20: The Eureka Man

Top row – Paper bonded, FDM and SLS.  
Bottom row – Original.

The cream coloured models in Figures 8.20 and 8.21 were both made on the SLS machine, and then the models were coated with a “clear” satin varnish (see Chapter 8.14).



Figure 8.21: The Eureka Cats

Top row – SLS and FDM  
 Bottom row – Original and Paper bonded (unvarnished).

This was done to give additional strength and binding as they seemed on handling to be rather fragile and possibly prone to disintegrating. In Figure 8.15, the FDM cat is seen sitting on the raft which was formed as part of the model's support structure. This would normally have been removed in the cleaning process but was left to show the raft.

#### 8.4.2 Greyed out

Three models were selected and processed so as to be fabricated on a 3DSystems *ProJet 660* colour printer. This process involved preparing the file as with the models in Chapter 8.4.1 to produce the \*.wri file. These were sent to the fabricator for processing but unfortunately all three, which were processed together, were returned as grey coloured models. The models had traces of colour printed on them but in the main looked as though they had a washed-out look (see Figure 8.22). The clay head in Figure 8.23 can be seen to have a darker colouring to the hair and eyebrows and the face has a yellowing jaundiced look, whilst the left ear has a faint pink tone. The SLS model was about 80% of the original size and although the main features were good, the model had lost the spiky rough tactile handle that the original clay head had.

However, the tactile feel of the other two models, regardless of colour or lack of it, was more in keeping with the original Egyptian Sobekhotep sandstone figurine and the slightly rough, reddish brown Egyptian clay bowl.



Figure 8.22: The three items in the ProJet660®.



Figure 8.23: Tinted but not coloured clay head.

Both the original Egyptian models were much smoother than that of the clay head and the detail was also well replicated on both these models. It was relatively easy to follow the grooves in Sobekhotep and using a light water-based paint, to tint the body. For the rest of the highlighting, a pencil was used to follow the grooves and copy the hieroglyphics on the sides and back. A light dusting with a hair spray was enough to seal the paint and pencil graphite. The result can be seen in Chapter 8.6.1 (Figure 8.28).

## 8.5 Monochrome Models

All of the remaining models that were fabricated were produced in a white material with the exception of two which were printed in black.

### 8.5.1 Clay Head

Apart from the clay head model that was discussed in Chapter 8.4.2, another was reproduced using an FDM machine and this can be seen on the right hand side, in the collection of heads (Figure 8.24). Of the two replicas, this was the smoother, possibly to be expected since the filament size and extrusion head in the FDM machine would account for the loss of detail, as well as the reduction to 80% of its size, as discussed in Chapter 4.2.1.



Figure 8.24: The collection of heads.  
The Original – SLS – Hand painted FDM.

The head can be seen to be still attached to the grey support material and in Figure 8.25, some of the main structure supports are seen still in position. The material that it was made from was quite bright, which caused the image, when photographed, to lose its interesting features and resolution, becoming quite lifeless (Figure 8.26). It was thus decided to hand paint the reproduction, in order to bring back some of its character and life as seen in Figure 8.24, the model on the right hand side.



Figure 8.25: The FDM model head with structure supports.



Figure 8.26: Unpainted FDM replicated model head.

## 8.6 The Egyptians – Ancient

### 8.6.1 Sobekhotep

In Figure 8.27 all the fabricated models from the Kendal Museum collection that were digitally copied are seen, surrounding Sobekhotep, the original coloured 3500 year old Egyptian figurine, at the centre of the display.

In this collection of models, ten were made in total:

- six using a SLS machine:
  1. large vase
  2. miniature vase – unpainted
  3. miniature vase – hand painted
  4. limestone effect Sobekhotep
  5. rust coloured bowl
  6. miniature Sobekhotep
- two using a FDM machine:
  1. small Sobekhotep – not shown (as damaged in fabrication process)
  2. large vase - not shown (as damaged in fabrication process)
- two using a *ProJet 660<sup>®</sup>* machine:
  1. grey coloured Sobekhotep
  2. grey coloured bowl



Figure 8.27: The Kendal museum replicas with the original Sobekhotep in the centre and the greyed coloured models indicated.

The grey coloured models (indicated) in Figure 8.27 are the *ProJet 660<sup>®</sup>* models, and a faint colour tint can be seen trying to surface through the grey top coat of Sobekhotep, as is the colour tint in the grey bowl though to a lesser extent. In the family group of the Egyptian figurines (Figure 8.28), it will be seen that the hand painted model on the right, Sobekhotep, was in fact originally the grey colour model, whilst the other larger model (on the left) was covered with a white emulsion paint and when dry, the surface was distressed by lightly rubbing with a used piece of sandpaper; this process helped to produce an ageing effect, as well as creating the effect of its having been made from limestone material. The model at the centre back (Figure 8.28) was the height of the original artifact (200mm) and has been left in its natural SLS state.



Figure 8.28: Clones of Sobekhotep.

The two small figurines in the front (Figure 8.28) have been fabricated (indicated) on a FDM machine and the other on a SLS machine and then varnished, hence its discolouration (see Chapter 8.14).

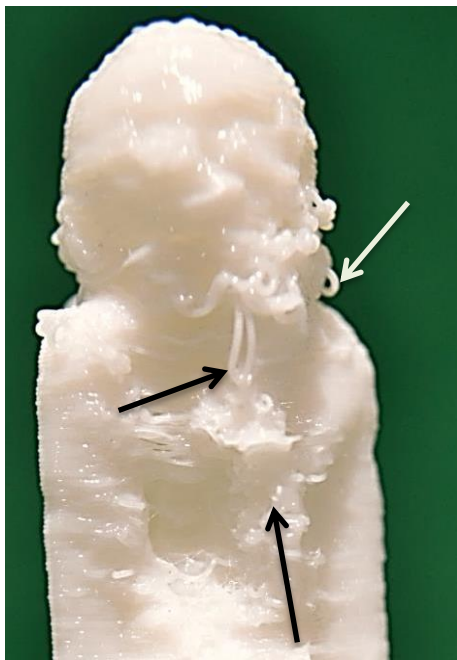


Figure 8.29:

Distorted FDM model – loops and incorrect placement of extruded filament.

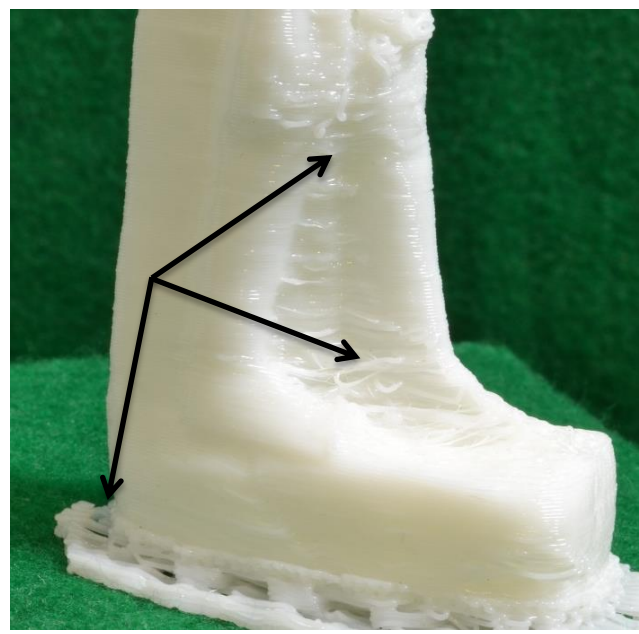


Figure 8.30:

The enlarged images of the miniature FDM model (Figure 8.29 and Figure 8.30) show what can go wrong. There are several possible causes; external influences such as a cold draught of air, the machine extrusion temperature might have been set too high or the extrusion rate might be too fast pushing out the filament at excessive rate. The model in Figure 8.29 is facing slightly to the right, and apart from the missing features of the head and face, loops of extruded filament can be seen hanging down (as indicated).

### 8.6.2 The Egyptian Bowl

The bowl which was discussed in Chapter 8.4.2, was in fact the second attempt at fabrication, and is seen in greater detail in Figure 8.31.



Figure 8.31: Full size replicated Egyptian bowl.

The first bowl (as seen in Chapter 4.7, Figure 4.28) was fabricated at an earlier date and reproduced at 80% of its full size (110mm diameter), using a SLS machine. The problems that were encountered at that time related to DoF, which caused part of the image to become out of focus; the results are documented in Chapter 4.7. The original is seen in Figure 8.32.



Figure 8.32: Original 3,500 year old bowl.

This problem was overcome and the new digital file was sent to be fabricated. Although the colour failed, the physical detail of the chips and grooves on the sides of the bowl can be clearly seen in Figure 8.31.

The discrepancy between the two sides of the bowl can be seen more clearly in the hand painted version in Figure 8.33, than in the non-painted version (Chapter 4.7, Figure 4.26).

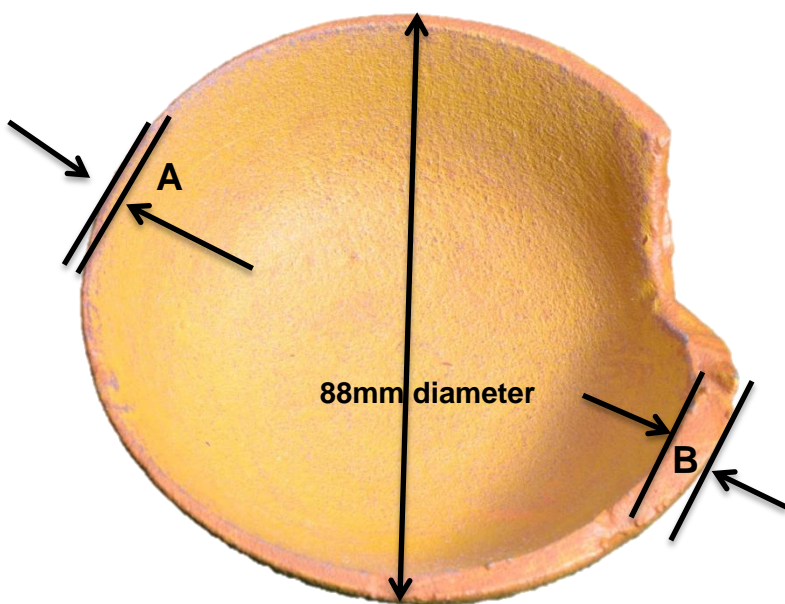


Figure 8.33: First attempt at bowl – discrepancy between sides of bowl.

Notice the distance between the arrow heads; at point A the thickness is approximately 2mm, whilst at point B the thickness is approximately 6mm. Points A and B are both on the rim of the bowl.

Finally, having digitally repaired this Egyptian antiquity, as shown in Chapter 6.9, it was fabricated on the SLS machine as seen in Figure 8.34.

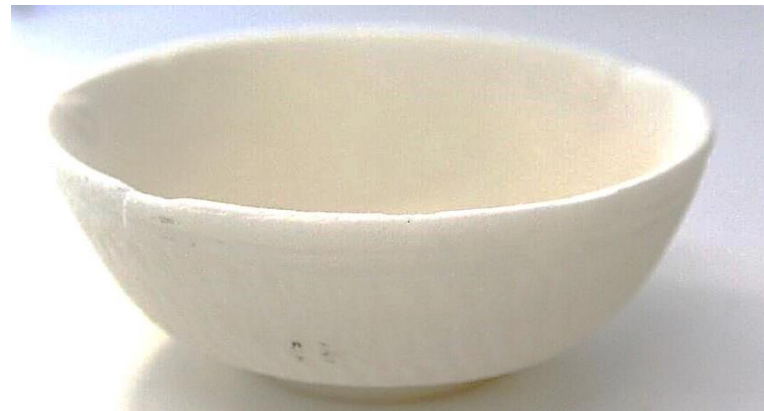


Figure 8.34: The digitally repaired and SLS fabricated Egyptian Bowl.

### 8.6.3 The Vase

The third Egyptian item which was reverse engineered from Kendal Museum can be seen in Figure 8.35. This was a 120mm high x 100mm diameter vase made from rust coloured clay, which had been painted with contrasting brown bands of colour.



Figure 8.35: Original Egyptian Vase.

The four replicas are seen in Figure 8.36; three were made on a SLS machine and the fourth on a FDM machine. The largest of the models, the one on

the left in Figure 8.37, was very true to life, even to the lopsided stance that it had.

The shell thickness was kept the same as the original, which was 6mm, which also helped to make the model more realistic, in that it felt reasonably heavy to handle, as did the original clay vase. When the first miniature was made and the virtual model scaled down to about a third of the original size, the fact that this scaling down would also affect the thickness of the walls was overlooked; at its thinnest point, the vase wall was just under 2mm thick. The model, when finished, started to disintegrate around the neck area and the pieces had to be glued back into place.

As well as gluing, a small hole also needed to be filled using *Polyfilla* (indicated in Figure 8.38), and it was at this stage that the miniature models were also given a coat of varnish to strengthen the structures. The third model, another miniature, was scaled down to the same size as the first miniature, but the wall size was then increased to a thickness of 3.5mm. This also gave the model more weight, in turn improving the physical tactile feel. After the model was fabricated on the SLS machine it was then painted by hand (centre in Figure 8.36).



Figure 8.36: Four replicas of the Egyptian Vase.

The largest of the group and the two small models were made on the SLS machine whilst the “pure” white model, still sitting on its’ mesh support, was made on the FDM machine.

The fourth model was made by FDM to 80% of the full scale. On this sample model, there were two areas of concern: the first was under the rim, where the supporting mesh framework, which normally supported the upper part of the rim whilst the filament was extruded and solidified (indicated in Figure 8.38), failed to peel away as it should have done, without causing any distortion or damage.

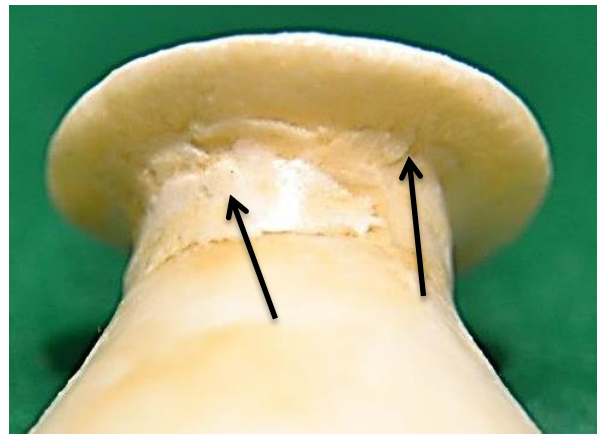


Figure 8.37: Repaired neck of Vase.

However, in this instance the supporting structure was fused to the under surface of the rim and it was not possible to remove this part without damaging the main body of the vase. The second problem was found at the bottom of the vase, where again, similar to the FDM model of Sobekhotep (Figures 8:29 and 8:30), leaving loops and coils, as indicated in Figure 8.38.



Figure 8.38: Incomplete FDM model showing detached filaments.

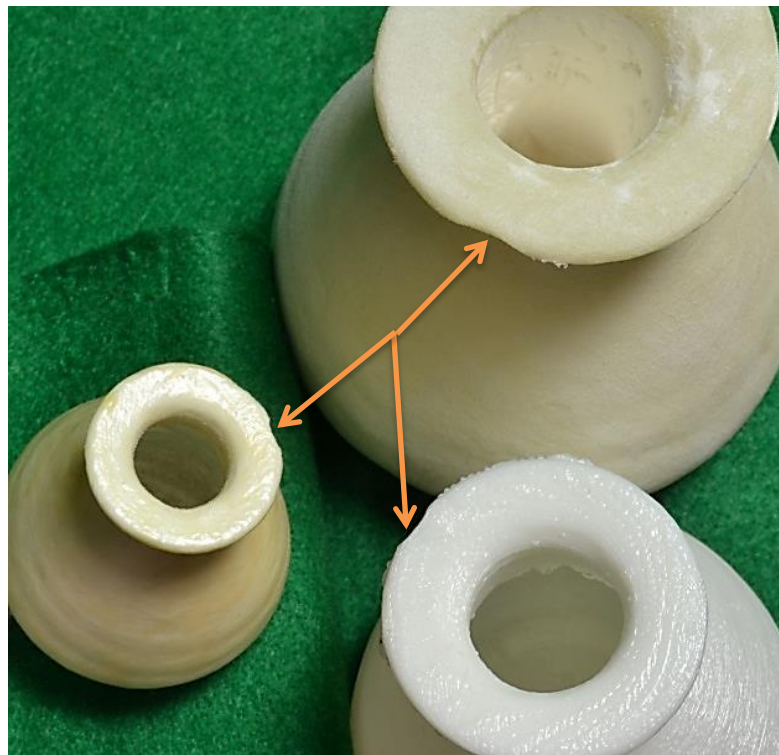


Figure 8.39: Minor detail of 'chip' in rim replicated across models.

The replication was, however, true to the original Egyptian vase, in that all models had the same lopsided stance and had the same 'chip' in the rim (indicated in Figure 8.39).

The process employed in the digital capture and replication of these artifacts from the Kendal Museum's Egyptian collection was featured in the *American Scholar* specialist publication [243] (see Appendix E).

## 8.7 The Egyptians – Modern

### 8.7.1 Painted Fish Vase

This vase was a modern Egyptian artifact, made in 2002 and found in a local UK jumble sale. It had nothing to commend it, other than that it was found at the time the ancient Egyptian artifacts from Kendal Museum were being processed. As can be seen in Figure 8.40, it was a round painted clay vase 130mm high and with a diameter of 120mm. However, it did have a few features which would prove interesting to discover how they replicated. The main body of the vase had penetrating small holes, both round and triangular, as well as a base relief of painted pictures of fish and other ornamentation.



Figure 8.40: Egyptian Fish Vases – Original and SLS miniature.



Figure 8.41: Enlarged image of hand painted SLS vase to show detail.

The miniature model that was produced on the SLS machine still retained enough detail (lower image Figure 8.41) to be able to hand paint the relief features of the fish and other detail. Although the holes did not penetrate the body of the miniature vase, they were clearly defined so it was possible with a fine drill and file, to complete this detail.

### 8.7.2 Horus

The final Egyptian artifact that was replicated was Horus, for which two new crowns were designed and fabricated using the SLS machine (Figure 8.42). Without crown (as found), the original Horus is 180mm high by 54mm wide and 70mm deep.

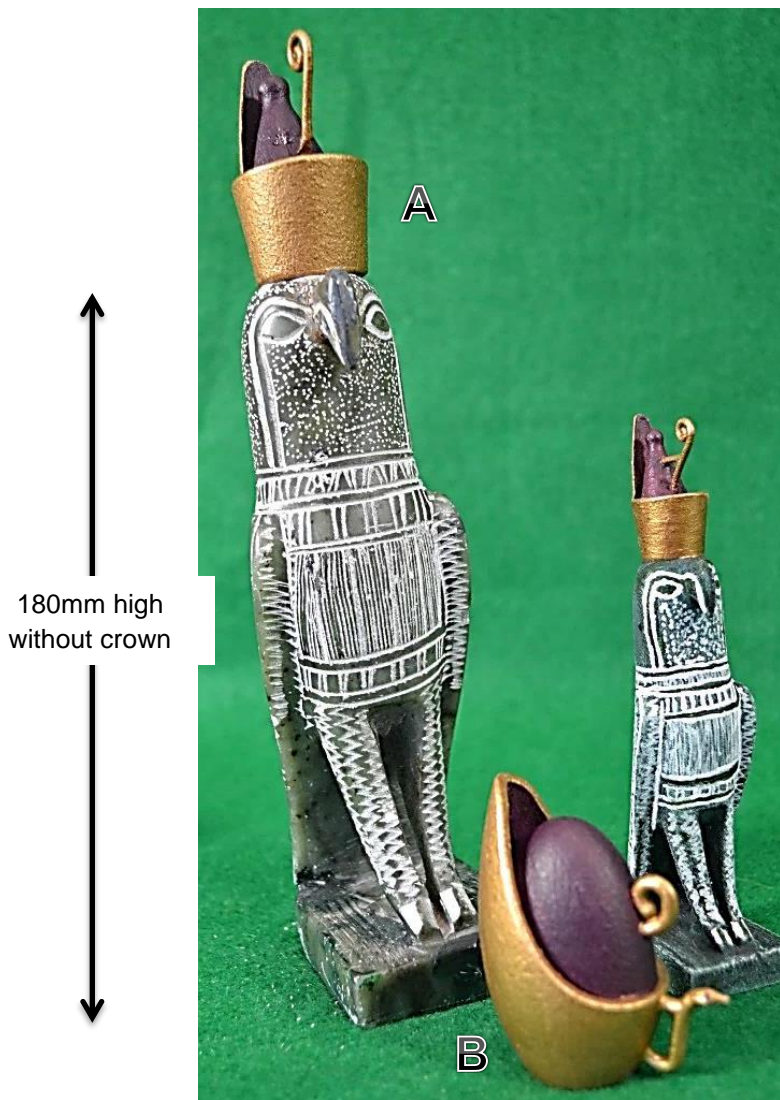


Figure 8.42: Original Horus and SLS model on right Alternative crowns indicated **A** and **B**.

The lost crown of Horus is discussed in Chapter 6.10 with additional information about the CAD design in *SolidWorks*<sup>®</sup> in Chapter 6.11.1. The hollow model of Horus was made using a nylon powder. The finished model was then sanded with very fine sandpaper before being painted so as to create a very smooth finish to the body – just like the original. The original was carved from marble or a similar stone, and was quite heavy for its size, whereas the model of Horus was very light to handle, which could detract from some of the attractiveness when physically handled. The two larger crowns seen in Figure 8.42, indicated **A** and **B**, are interchangeable, whereas the smaller version of Horus with crown, is one single, hand painted, hollow SLS model.

## 8.8 The Dog

The dog was made from coarse modelling clay (shown on the left in Figure 8.43) which was quite dense and gritty. This item was one of the first to be processed using *123D Catch*<sup>®</sup> and a very small FDM replica was originally made in black. This small version is seen sitting between the original and the SLS copy (Figure 8.43), and although maintaining the posture and pose of the original, lost all of the fine detailed features that the artist had crafted into this coarse clay model animal. When the full size model was manufactured on the SLS machine, the resulting model (shown on right in Figure 8.43) still did not seem to have all the detail, and looked as though the digital file had been degraded.



Figure 8.43: Family of Dogs  
Original – FDM miniature – SLS duplicate.

Examination of the digital files revealed file sizes which were not as high as one would have expected for such a complex subject. All the artifacts shown for comparison in Table 8.1 were processed using the “High” setting in *PhotoScan Pro*<sup>®</sup> and the \*.psz files which were then produced were imported into Netfabb’s *StudioPro*<sup>®</sup> for processing. Column 7 of Table 8.1 shows the number of triangles per cm<sup>2</sup>; this gives an indication as to the amount of surface detail that had been retained by the software and was available to be replicated by the AM machines.

Column 6 shows the percentage of available triangles (the detail) per cm<sup>2</sup>, and although the Dog does appear at first glance in Column 4 to have a large number of captured triangles compared with some of the other artifacts, on close

examination of the figures in Column 6, it is seen that percentage-wise it is the lowest number per  $\text{cm}^2$  of all the artifacts.

Table 8.1: Data comparison chart of 11 artifacts.

Artifact Name		1	2	3	4	5	6	7	8
		Shell mm	Vol cm <sup>3</sup>	Surface Area cm <sup>2</sup>	NettFab Studio Pro Triangles	KB stl file	% of triangles available per cm <sup>2</sup>	Number triangles per cm <sup>2</sup>	Images
J.30	Dog	2.5	141.47	1115.75	1,117,012	57,472	0.090	1001.13	109
J.47	Spanish Botijo	5.0	305.01	1019.81	834,372	40,741	0.098	818.16	128
J.50	Concrete Mix	2.5	91.11	710.79	881,548	43,045	0.141	1240.24	135
J.31	Head	3.0	85.30	611.49	1,752,380	85,566	0.164	2865.75	126
J.53	Horus	2.5	76.59	607.51	749,524	36,598	0.165	1233.76	148
J.43	Roman Jug	5.0	155.89	545.29	512,000	25,001	0.183	938.95	133
J.51	Ammonite	2.5	67.81	537.95	1,475,388	72,041	0.186	2742.61	134
J.42	Sobekotep	3.0	62.10	505.90	320,824	15,666	0.198	634.16	125
J.52	Trilobite	3.0	24.21	196.36	879,818	42,960	0.509	4480.64	149
J.38	Warrior	3.0	21.52	171.12	323,510	15,797	0.584	1890.54	109
J.55	Sea Shell	3.0	13.62	97.95	548,510	26,783	1.021	5599.90	119

Hence the loss of detail in the replica for an artifact that had so much detail in the original. On the other hand the Spanish Botijo, which is much larger than the Dog ( $305.01\text{cm}^3$  to  $141.47\text{cm}^3$ ), had only a slightly higher percentage triangle to surface area ratio than the Dog because it had a very smooth surface with hardly any detail except the blemishes as seen in Chapter 8.11, Figure 8.59.



Figure 8.44: Enlargement of original Dog's face.

Figure 8.45: Enlargement of SLS model of Dog's face.

The dog was processed using *PhotoScan Pro*<sup>®</sup> at a time when the computer being used could not process this software above its Build Density setting of 'High', as the amount of available RAM was only 12GB; had more RAM been available at that time, an 'Ultra High' setting could have been used, which would have produced a more detailed point cloud image. This in turn would have increased the number of triangles that would have been produced by *StudioPro*<sup>®</sup>.

It might be possible for future work to calculate the optimum number of digital images which might be required for the highest number of triangles, which would equate to the greatest amount of detail by including the size or volume of the artifact, the surface area, and the number of triangles needed per cm<sup>2</sup> to produce an \*.stl file that would produce a high grade detailed fabricated model.

Ultimately the detail on the finished AM model will still depend on the limitations of the AM machine used to fabricate the model.



Figure 8.46: Enhanced features of dog's face due to painting.

The initial reaction on seeing and holding the replicated nylon fabricated dog and the original coarse modelling clay dog (Figure 8.44), was that detail had been lost due to the reasons stated above.

However, on reflection and after looking at the enlarged image of the dogs (Figure 8.45), many features have been replicated and although there is some degeneration in the copy, by virtue of the fact that the materials that the two dogs are made from are quite different, it is almost impossible for them to be identical. Two other factors may also play an important part in how the models are perceived, the physical weight and the colour of the copy dog; the weight of the replica was 136grams, representing 16.79% of the original weight.

By examining the hand painted version of the nylon replica (Figure 8.46), features began to appear by virtue of the light and shade of the coloured model, which were there in the white bright state but had been lost in the monochromatic whiteout. So perhaps to truly say that a replica has been made of an artifact, we must look to the weight, colour and one of *ShapeWays*® [231] or *Sculpteo*®'s [244] many materials that can be used to fabricate a true replica.

### 8.9 The Warrior

This ancient Warrior (90mm x 35mm) was replicated by both FDM and SLS at the full scale as well as a miniature by SLS.



Figure 8.47: Warrior - Original, miniature SLS and FDM models.

As with the other miniatures, a coat of varnish was applied to it (turning it yellow), this strengthens the model as the shell was very thin. With the other miniatures, the fine detail was lost but the overall stance and pose of the original artifact was captured. The *Dimension 1200*® FDM machine, in this instance, completed the white model on the left of the photograph without any defects in the fabricated part. The FDM model can be seen standing on the bottom section of the raft that supported the model during fabrication (Figure 8.47). The grey Warrior, on the right was created on the *Ultimaker 2*®, but reversing the image before fabrication.

The SLS model was a good likeness but the powder which was left after supporting the model during the fabrication process was very difficult to remove. Perhaps this was due to an elevated machine temperature, such as the bed

temperature being too high. Because of this problem some damage was caused to the detail on the model in trying to remove the powder. The model's colour after being fabricated, as with the other SLS models, was an ivory, as opposed to the bright white as supplied from an internet based third party fabricator.



Figure 8.48: Full size Warrior SLS model with residual powder.

However, the bright white powder from which the model was fabricated still clung to the surface and could not be easily removed without further damage. Where the powder brushed away easily, for example around the face, the detail of the eyes, nose, and mouth etc., were faint but clearly visible (Figure 8.48). The SLS model was left in its natural state so as to show these blemishes.

### 8.10 Ceramic Vessels

This series of miniature models was processed using *123D Catch*<sup>®</sup> and was the first to be photographed whilst in Spain. The digital photographic capture is described in Chapters 3.8 to 3.10 and 4.2 and the repair of artifacts in Chapter 6.

The miniature Urn seen at the back of Figure 8.49, along with the miniature dog (Figure 8.3), as already stated, were both too small to be of real use as all fine detail had been lost. Both miniatures were made on the FDM machine, and both were 20mm high. When compared with the original large floor standing Urn

(Figure 8.50), which measured 1 metre high, or with the original Dog measuring 95mm long, the excessively small size of the replicas precluded any useful comparison. The *bas-relief* on the Urn, as seen in Figure 8.49 is completely lost on such a small model.

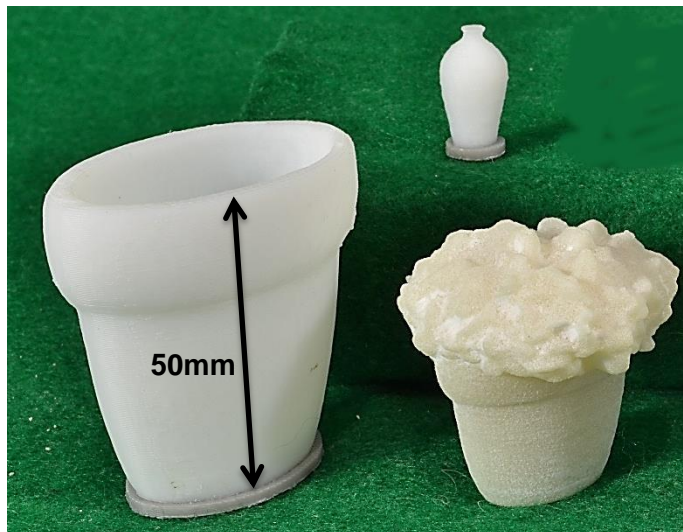


Figure 8.49: Miniature Urn (rear), Vase and Vase with silk flowers.



Figure 8.50: Full size Urn.

The two items in the front of the photograph (Figure 8.49) are from the same original item, the ceramic flower vase (Chapter 4.2.2, Figure 4.14). The larger of the two models was made 50mm high, and was fabricated on the FDM machine, the original vase being 200mm high. The smaller model next to it, was originally processed containing a bunch of silk flowers (Figure 8.51) and was scaled down even more when fabricated on an SLS machine.

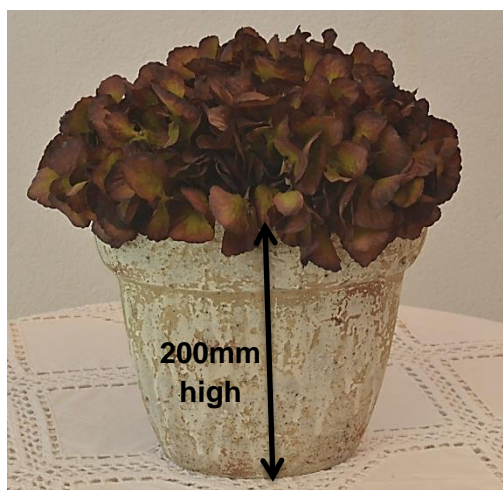


Figure 8.51: Original Vase and silk flowers.



Figure 8.52: Repaired FDM model of Vase.

Both items were processed completely separately and whereas the first vase's digital files had to be repaired (see Chapter 6.3, because of the hole on the inside skin of the vase, seen in Figure 6.5, which had been caused through insufficient digital data) the vase with the flowers needed no such repair. Although the individual silk petals have not been replicated (Figure 8.49) as seen in the original Figure 8.51, the replicated model still has the "look" of a bunch of flowers. Figure 8.52 is the FDM repaired vase and the completed interior of the repaired ceramic vase can now be seen.

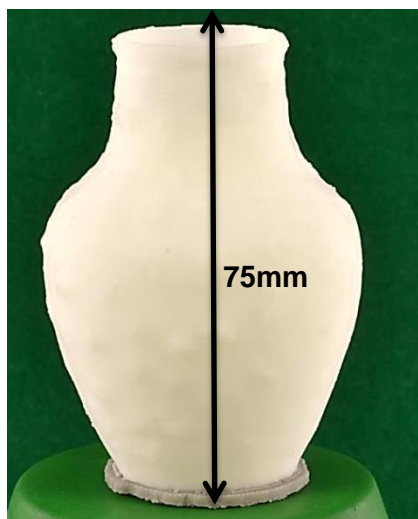


Figure 8.53: FDM model vase.



Figure 8.54: Original vase with raised whirls and patterns.

The model of the white clay vase in the photograph (Figure 8.53), was fabricated on the FDM machine and made 75mm high, representing 20% of the original vase height, which was 460mm high; a section of the original vase can be seen in Figure 8.54. Although small bumps can be seen (and felt) on the model, the raised relief of these features was lost. When compared to the original photograph, it can be seen that they are not bumps but whirls, patterns and sharp points oscillating in different directions around the surface of the vase (Figure 8.54).

However, an interesting insight into how the fabrication process worked could be seen in this miniature vase. By looking down at the top, so as to see the inside, the supporting mesh, which held the outer skin in place while the vase was being fabricated, could be observed (Figure 8.55). This mesh structure

would normally be removed unless it was thought that the outer skin was too thin, in which case the mesh could be left (as in this case).



Figure 8.55: Inside mesh as seen from top of vase.

### 8.11 Handled Vessels

Under this heading there are three items which were fabricated, all using a SLS machine. The distinguishing feature on two of these items was that they both had protrusions in the form of spouts and carrying handles. The following comments, which at first glance may seem trivial or petty, demonstrate the visual accuracy that the camera has captured and the digital process has been able to reproduce blemishes and features in both model artifacts.

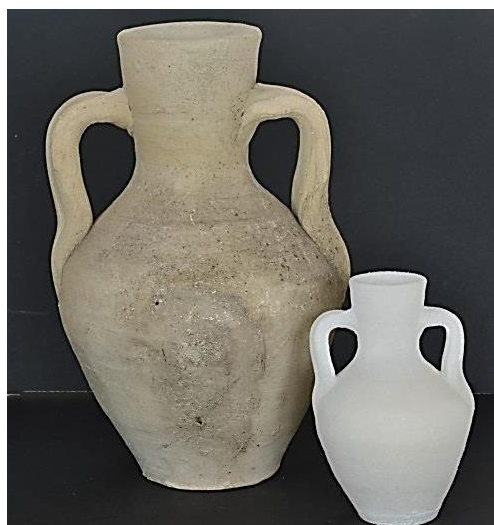


Figure 8.56: Front view of Roman vase and miniature copy.



Figure 8.57: Side view of Roman vase and miniature copy.

The first two were the Spanish and Roman vessels, whilst the third item was the morphed amphora (being formed from the Roman Jug) and its stand. Both the Botijo and the Roman jug were smooth, non-reflective, unglazed surfaces, handmade in white clay. Being handmade, both were non-symmetrical, having irregular or lopsided appendages and shapes; the interest was in how these protrusions and irregular shapes would replicate.



Figure 8.58: Lopsided off set loop handle replicated.

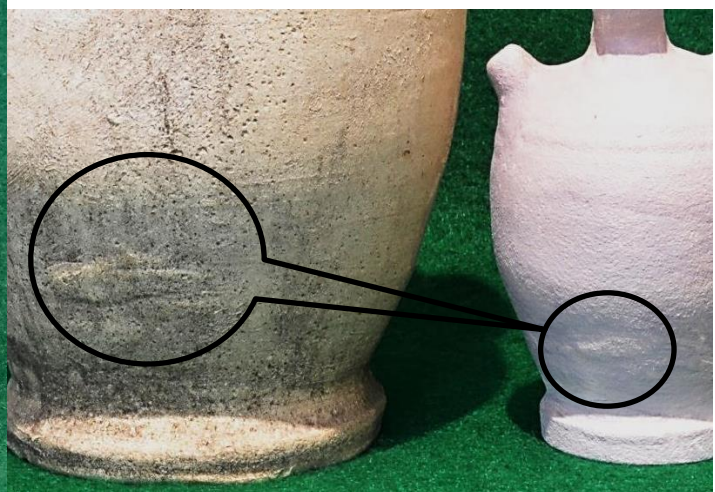


Figure 8.59: Surface flaws and blemishes replicated.

It can be seen in Figures 8.56 and 8.57 how closely the contour of the miniature Roman jug model follows the larger original, even to the small irregular curve of the neck as indicated in Figure 8.57.

The Spanish Botijo<sup>12</sup> (Figure 8.58), was much more regular in shape but it can be noted how the large loop when viewed from the side view is very slightly off centre. The replicated model shows the same irregularity (the short black dash lines being perpendicular at 90° to the base). The minor flaw on the surface, on the lower left side of the bottle, has a blemish on the surface (indicated), which can be seen on the miniature in Figure 8.59. The last item in this trio was the morphed amphora (Figure 6.49) and its stand which had been constructed using

---

<sup>12</sup> A water bottle made of unglazed earthenware that cools the water it contains by evaporation

*SolidWorks*<sup>®</sup>. Full details and images can be found in Chapters 6.8.3 (see Figures 6.52 to 6.54).

### 8.12 Concrete Mix

The digital capture of the Concrete Mix has been discussed in Chapter 4.10.1 and how the wooden props that supported it whilst it was being photographed were removed.



Figure 8.60: Topside of Concrete Mix.

Original - left              and              SLS duplicate - right

The images in Chapter 4.10.1 (Figures 4.43 and 4.44) show the underside of the concrete mix. In Figure 8.59 several of the small stones can be identified from the original concrete mix and seen in the SLS copy (right hand side) as indicated. The original piece of concrete was 155mm high by 110mm wide, and apart from the rough gritty handle, the most obvious difference between the original concrete mix and the SLS replica is the weight. This is not really a surprise when the underside of the replica is exposed (Figure 8.61), as being hollow. The original weight of the solid concrete block was 567gm, whereas the hollow replica was only 52gm having a shell wall thickness of 2mm. This concrete replica was fabricated on the DTM Sinterstation 2000.



Figure 8.61: Hollow underside of SLS concrete mix replica.

### 8.13 Items from the Natural World

All the items that have been described up to this point have been man-made, at some point in the last four millennia. As explained in Chapter 4.12.1, an article by the British Geological Survey about the creation, and the use of 3D scanners, to generate an online database of 3D virtual fossils inspired an additional exploration of this research into processing a small selection of rocks, fossils and shells. The challenge again was whether a single DSLR camera performed as well as a 3D scanner. Some of the image data capture for these highly detailed, small, irregular shaped objects was conducted in natural daylight, in the open with only a backdrop and turntable (see Figure 4.55). If good results were obtained, the photogrammetry process might inspire a mineralogist or fossil hunter, both professional and amateur, to digitise their collection and display them on a museum or school website giving access to the wider community. If successful, the scope and applications of this research would be widened.

Apart from the concrete mix SLS replication (part natural, part man made), shown in Figure 8.58, three other organic objects were reversed engineered and fabricated using SLS, with some degree of success: the Trilobite, the Ammonite and a Sea Shell.

### 8.13.1 Sea Shell

The sea shell (Figure 8.62), was perhaps the most complex to replicate as it was quite small, being just over 80mm in length, with a large amount of fine detail. Photographing the shell was quite a challenge, as described in Chapter 4.9.1.



Figure 8.62:

Sea Shells – side view.

Original shell.

Copy shell.



Figure 8.63:

Sea Shells – head-on view.

Left-hand side – original.

Right-hand side - copy.

Although some detail was lost, the bumps and nodules along the body replicated well (see Figure 8.62), but as seen in Figure 8.63, some of the small nodules from the front of the original shell (right-hand), had degraded and were therefore not so prominent.

### 8.13.2 Fossils - Ammonite

The final two artifacts were both the fossils which were fabricated using SLS technology. The ammonite (112mm wide x 82mm high) was used as the example to illustrate the differences in high and low resolution (see Chapter 4.11).



Figure 8.64: Ammonite fossil family.

The effect this had on the size of the files produced, which had a consequential effect when submitting the final \*.stl file to the AM machines. In Figure 8.64, the original fossil is seen on the right hand side of the picture. The hollow miniature was printed in one piece, but because of the size and hence price, it was cheaper to split the full size replica in half to be printed.

An enquiry was made to ShapeWays, the company who fabricated the two halves, as to why it was cheaper to cut the model in half. The explanation from them was that it was not to do with the amount of material that was used, which was more or less the same for two halves as for a whole model. Rather it was the fact that the two halves of the model could be nested within the fabrication platform and would take up less room. This allowed room for other projects from other clients to be printed, hence the cheaper price. The only drawback being that, if the finished model is scrutinised very carefully, a faint seam can be observed where the two halves were joined together by using adhesive glue.



Figure 8.65: Enlarge image of the front of the Ammonite showing the join.

This can just be seen as indicated in the enlarged segment of the replicated fossil as seen in Figure 8.65. Interestingly, what are noticeably missing from the copies are the very small silver grains of natural materials such as sand and the minerals from which the fossil is formed and which sparkle, glint and reflect light. The original weight of the solid Ammonite fossil was 729gm, whereas the hollow replica was only 130gm having a shell wall thickness of 3mm.

### 8.13.3 Fossils - Trilobite

With the Trilobite, although 150 photographs were used in the data capture process, the SLS model which was painted lacks the original gritty handle. Again, this might have been improved if fabricated on a colour printer such as a *ProJet 660<sup>®</sup>*, using a more gritty sandstone material. The replica was a few millimetres longer and wider than the original, (original 87mm x 57mm) although this did not detract from the finished model.

The original trilobite is seen on the left hand side of Figure 8.65, next to the hand painted replica. Apart from the weight of the original artifact (the original fossils weighs 142gm, and the hollowed copy only 50gm) the only significant difference between the two is that the replicated model has lost the sharp gritty tactile surface texture, and the sharp features of the shell are not as pronounced and more muted on the replica.



Figure 8.66: Original Trilobite next to replicated model.

#### 8.14. Varnished models

When the original white models were varnished they turned cream on drying, possibly due to the varnish used. In this instance the varnish used was from a part-used tin of 'clear' satin wood vanish, itself having a yellowish hue or tinge. Having seen this yellowing effect, it was thought that a high quality clear artists' varnish (as used on oil or acrylic paintings) might give a clearer non-yellowing result. Several months after the Eureka Cat and Man models had been fabricated, it was noticed that the colours had begun to fade. It was then decided to varnish both models as considered in the months previously with a *Daler and Rowney*® gloss varnish (Figures 8.67 and 8.68). The artists' varnish, made specifically for acrylic paints, was crystal clear and cost £6.50 for 75ml. as opposed to c£10.00 for a 750ml tin of varnish from the local DIY shop.



Figure: 8.67 Eureka Cat.

Unvarnished

Varnished



Figure: 8.68 Eureka Man.  
Unvarnished



Varnished

As well as the two Eureka models, part of the Concrete Mix model was varnished to see how it affected the painted sections and whether it turned the white base material yellow, as had happened to previously varnished models using the 'clear' satin wood varnish.

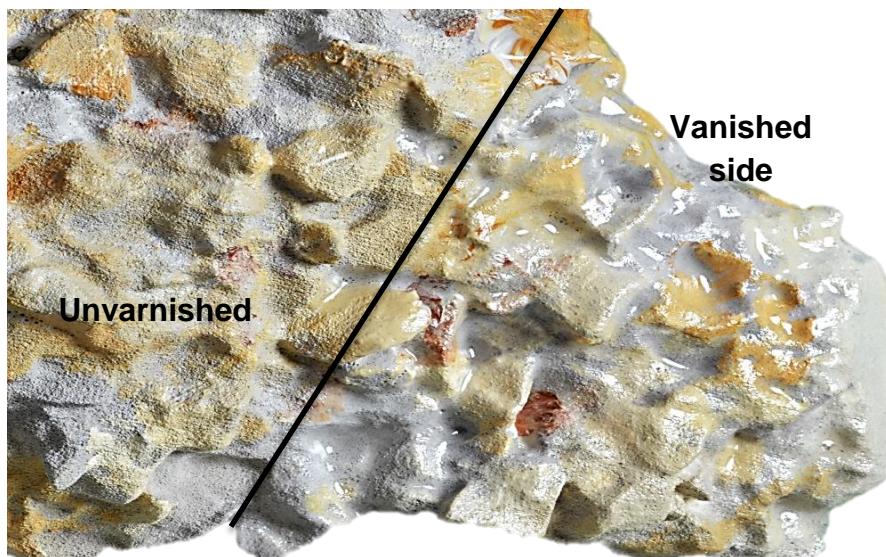


Figure: 8.69 Concrete Mix.



Figure: 8.70 Concrete Mix Side view.

Left – unvarnished  
Right - varnished - showing brighter colours.

Varnished underside  
showing bright white base  
material.

Figures 8.69 to 8.70 show the results. The colours have been enhanced a little but unfortunately had faded before being varnished although the white nylon base material has not turned yellow (Figure 8.69). It was therefore concluded that if the models were to be varnished, then it should be done soon after the models

have been printed or painted. Only the best crystal clear varnishes must be used so as not to degrade the colours, or change the monochromatic base materials. Cheaper wood or decorating varnishes should not be used.

### **8.15 Summary**

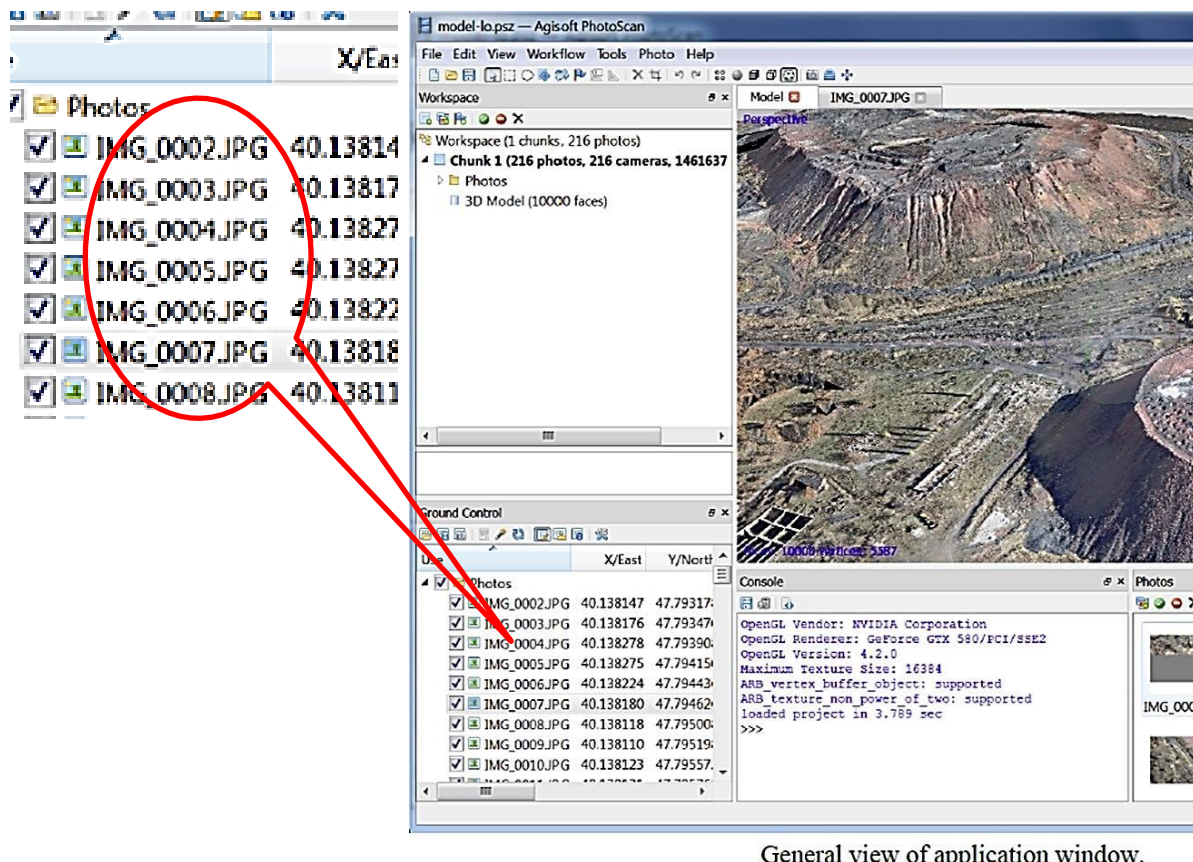
In the collection of 15 replicated models, there was a good cross-section of the AM processes used. There can be no doubt that all the models, with the exception of the deformed miniature FDM model of Sobekhotep, were clearly recognisable as replications of the originals. Two themes, however, seemed to have run through all the models: that of the degrading of the detail from the initial \*.obj file through to the \*.stl file, but more noticeably the further degradation once the model was fabricated on the AM machines. The second was the severe degradation of very detailed artifacts when a replica was made which was too small, the result being of little use except perhaps to see outline, shape and form.

The limitation of an AM machine printing at 100 $\mu\text{m}$  compared with one printing at 60 $\mu\text{m}$  had a negative effect on the amount of detail achieved in this research. As AM equipment development continues and machines such as the PolyJet J750 fabricating at a resolution of 14 $\mu\text{m}$  become more main-stream, so the physical detail in models will improve. In addition, techniques in the fabrication process, such as discussed by Laput *et al.* [245], using an FDM soft strand, fibres and bristle process, inspired by the 'stringing' effect of a hot glue gun. Other experimental work like this by Ou *et.al.* [246], will result in very fine detail, which is difficult to achieve at present but is essential for a true replicated likeness.

## Chapter 9: Shooting in RAW – The Digital Negative

### 9.1 Historical Background

When the concept of this research/thesis was first discussed, the two software packages that were investigated and subsequently used to process the digital images, were *123D Catch®* and *PhotoScan Pro®*. In the documentation that was available for the beta version of *123D Catch®* that was available at the time, the author of an online tutorial spoke about “Snaps” and photographs [247], the key concept being “*Know how to take photos using your camera to generate the best resulting 3D model.*” An online article in “Business Wire” proposed using your iPad camera to “*transform the images into a 3D model*”, again only the taking of photographs, not what digital format they took [248].



General view of application window.

Figure 9.1: Screen shot of application window showing use of Jpeg images.

The Professional Edition, v0.9.0 of the Agisoft *PhotoScan* [249] user manual noted that several image formats could be processed and would be accepted by the software. In setting out several basic rules “*for taking and selecting pictures*

*that provide the most appropriate data for 3D model generation” a “digital camera with reasonably high resolution (5 MPix or more)” was required.*

In an explanation of the graphical interface used within the software, a screen shot was displayed showing the use of Jpeg images, enlarged on the left of the figure for clarity, highlighted and ringed in red (Figure 9.1), clearly showing that in the early days of the software usage, RAW or NEF images had not been used and the quality of Jpeg images were considered sufficient for processing. In a personal email from an Agisoft senior executive [250], the recommendation for computer hardware configuration at that time was an i7 CPU with a minimum 8GB RAM and NVidia GeForce GTX 580® or similar GPU. Under the backdrop of this level of technology, the project was started with the aim as previously stated - to have simplicity of execution. Camera ready Jpeg digital images were thus used for the research.

## **9.2 The Search for Solutions**

By 2015, hardware and software had the capability of processing large quantities of high quality resolution images and the minimum specification of processing computers had risen significantly as discussed in Chapter 4.10.2.

After reviewing and analysing some of the problems encountered in Chapter 6, it was decided to test whether the use of “other means” could improve the quality of the original images that had caused the aforementioned problems. The main problem that recurred in photographing the artifacts was that the processing software could not cope with light reflection or glare. This was a universal problem and all point cloud data (PCD) processing software pointed to this as an issue.

A circular Polaroid lens was tried as demonstrated in Chapter 6.4.2 and found to be successful in overcoming some of the issues. Another method was of post processing the image by manipulation of the digital negative, a method used by 2D digital photographers for many years [172] [171]. By the 1990s, the digital camera was beginning to take over from the roll film camera. The dark room/wet room had given way to electronic processing and desktop publishing. The computer, monitor and colour printer had replaced the traditional developing and printing (D&P) process of the local photographic high-street shop; electronic

imaging for photographers had come of age [202]. By importing the digital image into third party software, special effects could be created, colour editing, image cropping, and adjusting both the brightness and contrast being a few of the tools available.

### **9.3 The Digital Negative**

The digital camera used a sensor which was a grid or matrix that was made up of a series of small light receptors. These tiny sensors could not record the colour, only the intensity of the light falling on the sensor. A small filter was attached to each sensor site in what is called a “Bayer” pattern. For more detailed information such reference books as *RAW Workflow* [205] or *Graphics File Formats* [251] [252] should be consulted. It is not within the scope of this research to explain or to examine this process in great detail, but the result was that the camera had a processor that saved this digital information into a RAW file, containing information with regard to brightness and colour about the scene or object that had been photographed. This RAW file could not be edited or enhanced in this format but had to be converted into a format that could be read by standard photo editing software. Each camera manufacturer had a file format of their own, in the case of the Nikon *D3100*<sup>®</sup> camera, as was used in this research, a NEF file, commonly known as a Digital Negative or a camera RAW file. The camera also had the option to download the RAW data as it was (as a NEF file) [253] or convert the file in the camera to a Tiff or Jpeg, both these types of file being able to be read by photo-editing software. In the case of the compact camera, also used in this research, the Canon *IXUS 100*<sup>®</sup>, it converted the file to a Jpeg image file in camera, though it did not support the downloading of the raw digital information in any other way.

### **9.4 Tiff and Jpeg**

Historically, with the old type of roll film, a negative would be used to produce the final photographic image which was then developed into a positive image (the photograph) on separate media. The negative itself would remain unaltered and if stored correctly could be used many times without loss of quality. The concept of the RAW data file is the same, hence it is widely known as a digital negative. Some of the high-end “professional” cameras do not have the capability of

shooting in anything but RAW mode, whilst on the other hand most compact cameras only shoot in Jpeg mode.

The RAW file could be converted to different types of files that could be read by photo-editing software to produce a “positive” image. The RAW data could be converted automatically by the proprietary camera-editing software or using third party photo-editing software. The most commonly used file types were Tiff and Jpeg but they differed in two basic ways; when a RAW data file was converted to a Jpeg, the data was compressed and in doing so some data was permanently lost. The data held in the Jpeg image file, after conversion from a RAW file, was irreversibly lost and is known as *lossy* file. Unlike other photographic data files, the Jpeg file was also prone to degrading every time it was opened or manipulated, since when the file was then re-saved, even if only opened, viewed and then closed and “saved as”, it was again compressed, with further loss of data, resulting in further loss of quality. An on-line article by P. Taylor, describes this process with photographic examples [254], in addition to the literature quoted in this chapter. When converting the RAW data to a Tiff file, although compressed, this data was not lost (hence commonly called a *lossless* file) and as long as the Tiff file was not overwritten it did not degrade with constant use.

There is a lot of discussion as to whether the Jpeg file loses enough data when processing to make any real difference when creating a 3D PCD image see Table M.1 In Appendix M (and also from the Agisoft website) [255] [256] [257] and the photographic reference literature contains a great deal covering the subject but not necessarily with reference to PCD conversion. Even for 2D photography, there are many pro’s and con’s as to whether setting the camera mode quality to take a “fine or normal” grade Jpeg image is sufficient for all but the best quality, large commercial photographers.

## 9.5 Size Matters

On a very basic and practical issue, the difference in size in digital storage terms was quite considerable. Table 9.1 shows, for the same image, the size in Kilobytes plus number of pixels, in RAW (NEF) format, converted to a Tiff file or a Jpeg file, or straight from the camera as a camera ready file; fine, normal or basic Jpeg files. The camera ready Jpeg files could also be pre-set for image size,

equating to the image size in pixels; large (4608 x 3072 pixels = 14.1Mpix), medium (3456 x 2304 pixels = 7.9Mpix) or small (2304 x 1536 pixels = 3.5Mpix).

The different types of digital file (RAW, NEF, Tiff or Jpeg) of the Warrior artifact were used for the data presented in Table 9.1.

Table 9.1: Image file size comparison.

Nikon large size image 4608 x 3072 pixels = 14.1Mpix			
	Image Quality (File type)	Image File size in Kb	Data File size to be processed (135 images)
1	RAW - NEF	12,350 kb	
2	RAW to a Tiff	82,969kb	11,200,815kb
3	RAW to a Jpeg	8,708kb	1,175,580kb
4	CR Jpeg - Fine	6,441kb	869,535kb
5	CR Jpeg - Normal	3,603kb	486,405kb
6	CR Jpeg -Basic	1,611kb	217,485kb

The same lighting and camera settings were used on all images, except that the image quality mode was altered each time to produce either a RAW image, (which was then converted to a Tiff or Jpeg in photo-editing software) or a CR image in which the mode was changed for each image from fine, normal or basic.

In Table 9.1 the large image size was selected for all image qualities. In camera terms, this reflected the number of images that could be stored in either the camera's built in memory or on the removable data storage card if applicable. As well as camera storage capacity, if say on average 135 images were processed by the Agisoft software, the processing time taken and the power of both CPU and GPU would have had to be taken into consideration.

Table N.1 - Appendix N, The Photographic Image data log:

*“Capture log – RAW & Jpeg – Photographic Image Data”.*

Table N.2 - Appendix N, *PhotoScan Pro<sup>®</sup>* processing data log:

*“RAW & Jpeg image Processing log – PhotoScan Data  
processing Information”.*

## 9.6 Case Studies

Three of the original artifacts (Figures 9.2 to 9.4) that had been problematic, as discussed in Chapter 6: China Dish (Chapter 6.2.7), Serenity (Chapter 6.2.1),

and the Dolphins (Chapter 6.2.2) as well as one artifact that had been replicated successfully, the Warrior (Figure 3.4), were selected to be re-photographed in RAW format. The original data-sets were all camera ready Jpegs, and processed in *PhotoScan Pro*<sup>®</sup> without any editing.



Figure 9.2: China Dish.



Figure 9.3: Serenity.



Figure 9.4: Dolphins.

As the former three items had shown problems with flare/glare in the original trials, a CP lens was used (see Chapter 6.4.2). The RAW data was then pre-processed using Adobe *PhotoShop CS6*<sup>®</sup> to convert the files to either Tiff or Jpeg

format. If required, using this photo-editing software, the digital file was altered to enhance the images. Adobe *PhotoShop Elements 11<sup>®</sup>* (a cheaper version of CS6) could have done the same editing but lacked the facility to “batch” process the digital set of up to 140 images needed to convert the 2D image into a 3D point cloud image.

Of the four artifacts, three were successfully converted to PCD images and saved as \*.obj files using *PhotoScan Pro<sup>®</sup>*, then converted to \*.stl files ready to be fabricated, but one, the China dish, was still problematic. The details of the processing log of all four artifacts can be seen in Appendices Q and R. It was during this RAW data processing of the newly acquired set of images, that the original computer’s GPU was found inadequate to process the Ultra High resolution Tiff images. Two of the artifacts’ digital data-sets were checked and processed by Agisoft on their computers in their head office, which verified that the data sets were not corrupted. The original GPU was then upgraded to a NVidia *GEForce<sup>®</sup> GTX 1060 6GB* card, as discussed in the latter part of Chapter 4.10.2 and Chapter 4.11, and all four data sets, both in Tiff and Jpeg format, were processed without further problems.

### 9.6.1. Warrior

It was decided that a benchmark model should be made from one of the new data sets and fabricated on a *PolyJet J750<sup>®</sup>*, so as to have “hard-copy” models to compare. The Warrior model was chosen and a data set of 138 images was used. The head section of each model was isolated from the main body in order to reduce the unnecessary amount of material used. Each resolution, UH to UL, in both Tiff and Jpeg were processed and then AM models fabricated. The model heads were then compared with each other and at the same time the original CR Jpeg data set was processed and also fabricated on the same *J750<sup>®</sup>* machine. These models were used as a comparison, and fully described in Chapter 4.12 and with full details in Appendix M.

Although both the Tiff and Jpeg files were processed in the editing software, so as to convert the NEF file, no other digital manipulation was carried out on the RAW data. In Appendix P, Image Sheet (IS).1, “*Warrior – Pre-processing RAW images v Camera ready Jpeg images*”, details can be found of the point cloud data and screen shot images of the resulting “shaded” PCD

image. Also a section of the model was enlarged, as indicated in the IS.1, so as to show the wire frame variation between the resolutions processed.

### 9.6.2. Serenity

As a result the glare/flare problem as described previously (Chapter 6.2.1), a CP filter was used to try and eliminate the original problem as shown in Figure 6.10 and Figure 6.11. In this new data-set 140 digital images were used and then the original RAW file was edited in the photo-software before saving as a Tiff or Jpeg file. The highlights were darkened and the mid-tone contrast was slightly increased.

Screen Shots of Cloud Point “Shaded” Serenity Images

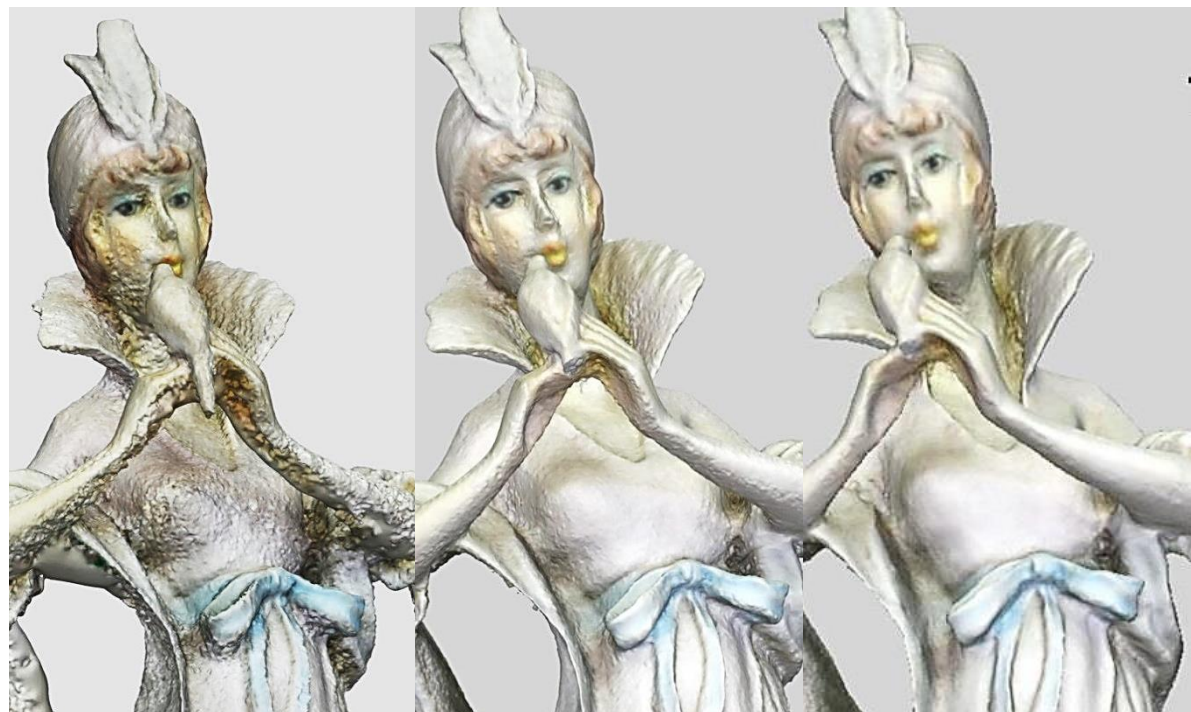


Figure 9.5:  
Original **CR Jpeg** process  
to an \*.obj file.

Figure 9.6:  
Processed **Jpeg** file to  
an \*.obj file.

Figure 9.7:  
Processed **Tiff** file to  
an \*.obj file.

As can be seen from Figure 9.5, the original CR Jpeg processed model, the “orange peel” effect (see Chapter 6.2.8) is quite noticeable on most of the surface of the model but has been reduced considerably using the Jpeg converted image as in Figure 9.6. However, Figure 9.7 was clearly a great improvement over both other models and could very well be further improved by smoothing the surface in secondary software, such as *StudioPro®*, which would be required to convert the

\*.obj file into an \*.stl file, ready for AM fabrication. Detailed screen shots as seen in Figure 9.6 and Figure 9.7 as well as PCD data information are available for inspection in Appendix P, IS.2, “*Serenity – Pre-processing RAW images v Camera ready Jpeg images*”.

### 9.6.3. Dolphins

Similar problems to those encountered with Serenity also existed with the original Dolphin model when the CR Jpeg data-set was processed (see Chapter 6.2.2). A very similar pre-processing procedure took place with 141 images. The RAW Dolphin file, as before, was saved as Tiff and Jpeg files from the original NEF file. As with Serenity, by using the CP filter and manipulation of the RAW file, great improvements were achieved.

Screen Shots of Cloud Point “Shaded” Dolphine Images

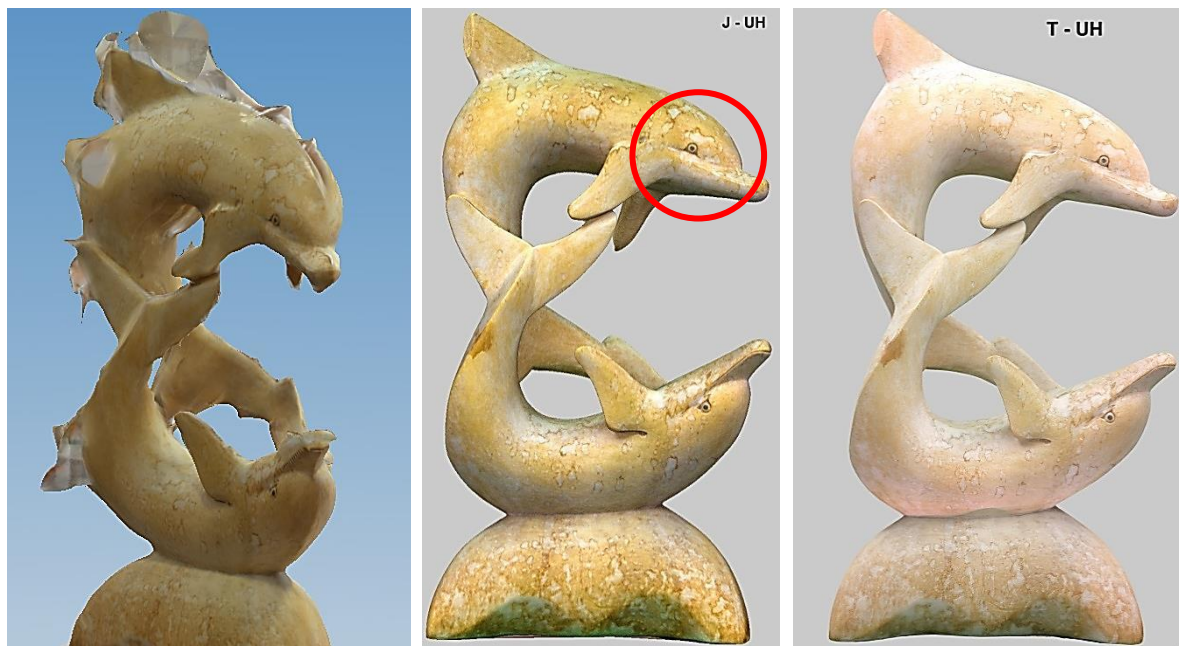


Figure 9.8:  
Original **CR Jpeg** process  
to an \*.obj file.

Figure 9.9  
Processed **Jpeg** file to  
an \*.obj file.

Figure 9.10:  
Processed **Tiff** file to  
an \*.obj file.

The main difference between the Serenity and the Dolphin data-sets was that the Dolphin Jpeg file was as good as the Tiff file; either could have been used to convert to an AM ready fabrication file. The whole range of CPD images are seen in Appendix P, IS.3 together with the processing data.

### Selection of Screen Shots from the Dolphin Jpeg images

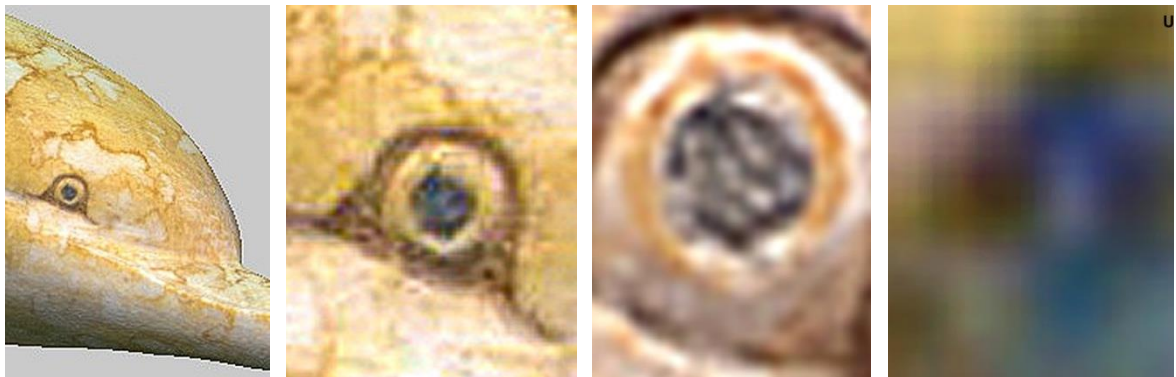


Figure 9.11:  
Head.

Figure 9.12:  
Eye.

Figure 9.13:  
Pupil.

Figure 9.14:  
Quarter Iris.

To further compare the Tiff resolution against the Jpeg resolution, the upper Dolphin's eye was used as a focal point, ringed in red on Figure 9.9. Through four stages, the head was enlarged to the point that only a quarter of the eye's iris was visible and the pixels could be seen through the range of UH to UL resolution.

However, this experiment must be seen as 2D printing/pixelation as opposed to an AM fabrication exercise though it has shown the increase/decrease in quality of file available to be converted into an \*.stl file. Figures 9.11 to 9.14 show examples of images that were taken from the full photographic data set, as seen in Appendix P1.3, “*Dolphin – Pre-processing RAW images v Camera ready Jpeg images*”.

#### 9.6.4. China Dish

Of all the 59 artifacts that had been photographed, the China Dish, Figure 9.4, was perhaps the most difficult to digitise (see Chapter 6.2.7). A further attempt was made using the same method as with Serenity and the Dolphins but unfortunately to no avail. The high gloss surface of the glazed porcelain together with the featureless surface both inside and outside of the bowl, gave very few reference points for the *PhotoScanPro*® to be able to identify marker points so as to stitch the images together (Figure 9.15).

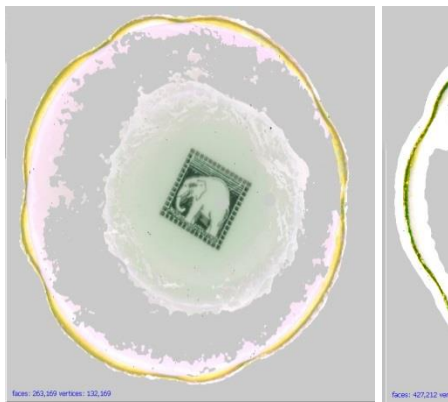


Figure 9.15:  
Unsuccessful results in processed \*.obj files.

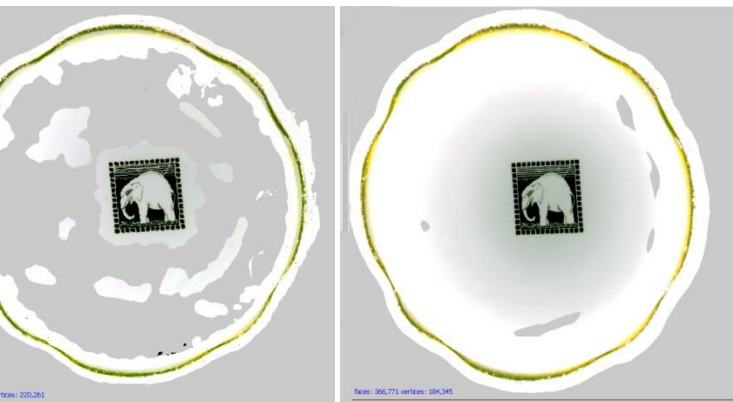


Figure 9.16:  
UH Tiff file – the best  
achieved.

It will be noted that the elephant motif in the centres of the bowls and the gold rim were processed and replicated. There was some success when the data set was processed at Ultra High resolution (Figure 9.16), but not good enough to take forward and produce an \*.stl file. Another attempt was made using the technique described in Chapter 5.2 but without placing any targets onto the surface of the dish. A non-invasive method was the most important part of this exercise. This was a modern dish and could easily have been washed, but had it been a priceless museum piece, sticky-back paper or other such markers on the surface would not have been sanctioned by any curator!

A background disk was created as seen in Figure 9.17, with coded-target symbols printed so as to give some reference points that the processing software could have identified and used to stitch the images together.

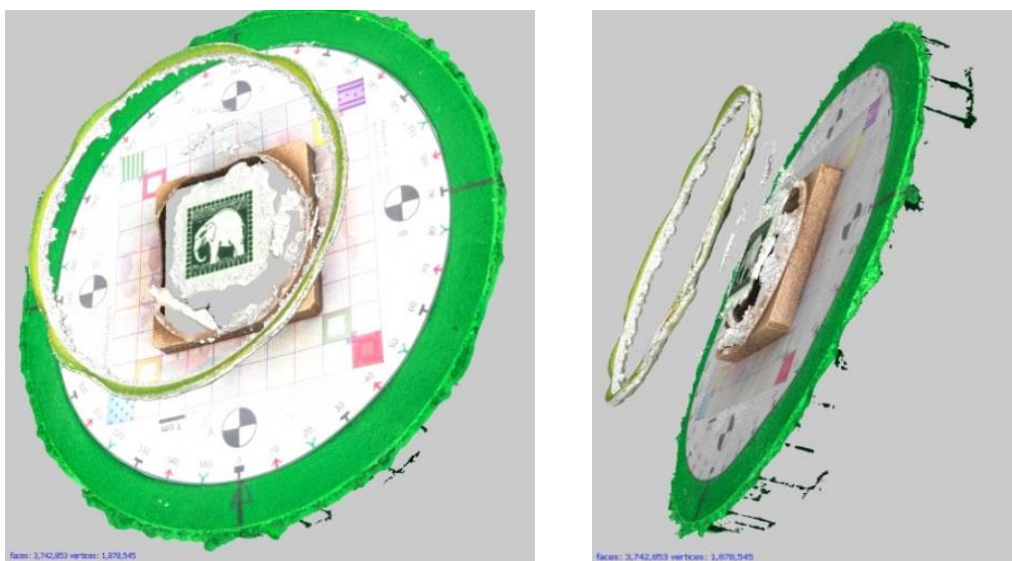


Figure 9.17: Further attempts using coded targets.

As can be seen in all the Figures 9.15 to 9.17, only the elephant and gold rim (plus the background disk and turntable in Figure 9.17) were created into a point cloud image.

## 9.7 RAW v Jpeg - For and Against

From this small experimental trial, it must be concluded that there can be no definitive rules as to which file format to use. Two of the artifacts showed no conclusive difference between the use of Tiff or Jpeg files. The RAW converted Tiff and Jpeg files of the Warrior CPD screenshot show little advantage over the original CR images. Examination of the AM fabricated heads as shown in Figure 4.71 showed very little difference between UH, H or M resolution models and the original CR model could not be distinguished from the rest without inspection of its side identification marking. The Dolphin images as shown in Appendix P, IS.3 are nearly identical to each other. The polarising filter definitely made a big difference by being used with both the Dolphin and Serenity models, with some help from pre-processing photo-editing software. Although not perfect, the RAW converted Tiff version of the Serenity model was clearly better than the RAW converted Jpeg and certainly both RAW versions were infinitely better than the original CR Jpeg version.

There are three other considerations that must be taken into account:

- size of the digital files that are created;
- processing time to create point cloud data;
- computing power and cost of processors.

As seen from Table 9.1 (Chapter 9.5), the size of the different file formats is considerable and the immediate impact of this was on the size of the camera memory. The approximate size of a NEF file (at say 11,500kb) was four times larger than a normal CR Jpeg (at say 3,250kb) and in the region of 135 to 145 images were taken in one session. Although the cost of memory cards was relatively low, not all cameras had the capacity to install removable cards and therefore might be limited as to their storage capacity. Table 9.2 is a ready reckoner, as supplied by SanDisk®, which helped to put this problem into context.

Table 9.2: Number of digital images that can be stored on a card



The following assumptions were made to calculate the number of images per card:

MP = 1,000,000 pixels

1MB = 1,000,000 bytes, 1GB = 1,000MB

TIFF image has 24 bit color depth, one of 16,777,216 colors per pixel

JPEG 100% Quality = Visually lossless JPEG compression with 1:10 ratio of RAW image

Photos - Compressed (JPEG 100% quality) Images per card.

NOTE: JPEG is the most common file format for consumer cameras.

Megapixels	File size (MB)	1GB	2GB	4GB	8GB	16GB	32GB	64GB	128GB
4MP	1.2	715	1430	2861	5722	11444	22888	45776	91552
5MP	1.5	572	1144	2288	4577	9155	18310	36620	73240
6MP	1.8	476	953	1907	3814	7629	15258	30516	61032
7MP	2.1	408	817	1634	3269	6539	13078	26156	52312
8MP	2.4	357	715	1430	2861	5722	11444	22888	45776
10MP	3.0	286	572	1144	2288	4577	9155	18310	36620
12MP	3.6	238	476	953	1907	3814	7629	15258	30516
14MP	4.2	204	408	817	1634	3269	6539	13078	26156
16MP	4.8	178	357	715	1430	2861	5722	11444	22888
22MP	6.6	130	260	520	1040	2080	4161	8322	16644

Photos - Uncompressed RAW (24 bits per pixel) Images per card

Megapixels	File size (MB)	1GB	2GB	4GB	8GB	16GB	32GB	64GB	128GB
4MP	12.0	71	143	286	572	1144	2288	4576	9152
5MP	15.0	57	114	228	457	915	1831	3662	7324
6MP	18.0	47	95	190	381	762	1525	3050	6100
7MP	21.0	40	81	163	326	653	1307	2614	5228
8MP	24.0	35	71	143	286	572	1144	2288	4576
10MP	30.0	28	57	114	228	457	915	1830	3660
12MP	36.0	23	47	95	190	381	762	1524	3048
14MP	42.0	20	40	81	163	326	653	1306	2612
16MP	48.0	17	35	71	143	286	572	1144	2288
22MP	66.0	13	26	52	104	208	416	832	1664

[https://kb.sandisk.com/app/answers/detail/a\\_id/69/~/number-of-pictures-that-can-be-stored-on-a-memory-device](https://kb.sandisk.com/app/answers/detail/a_id/69/~/number-of-pictures-that-can-be-stored-on-a-memory-device)

## 9.8 Conclusion

Appendix N contains the data regarding the time it took to process and build the point cloud images, and the time build can be seen by examination of the lines of the Warrior details, as seen in Figure 9.18 and highlighted in red. All details of time data were recorded in minutes.

Appendix Q - All times in minutes											
Building Dense Cloud											
Depth Filter:- Aggressive, Moderate, Mild, Disable											
Time to build photos	Quality	Depth Filter	Dense Cloud Count	Build Mesh Tile size 4096		Face Count	Time to Building Dense Cloud		Texture mapping		
				Faces	Triangles		Mapping - Generic	Blending - Mosaic			
3 21.6	UH	A	Out of Memory - 3 attempts old GPU				2,875.0	X	X X X		
	UH	A	Filtering Depth Map error				1,108.6	X	X X X		
	UH	A	20,800,670	4,161,290	2,080,665	H	2,026.5	G Mo n/k	✓ ✓ 459,		
	H	A	4,563,594	912,717	456,601	H	145.0	G Mo	2.1 ✓ ✓ 96,		
	M	Mo	1,092,005	218,401	109,286		39.3	G Mo	5.1 ✓ ✓ 21,6		
	L	Mo	257,873	180,000	90,002		14.5	G Mo	4.9 ✓ ✓ 17,6		
	UL	M	59,545	118,690	59,347		8.6	G Mo	4.8 ✓ ✓ 11,5		
5 29.9	UH	A	18,928,476	3,786,846	1,893,461	H	952.2	G Mo	6.9 ✓ ✓ 420,5		
	H	A	4,628,238	925,066	462,550		163.7	G Mo	1.5 ✓ ✓ 97,5		
	M	Mo	1,111,324	222,426	111,217		40.4	G Mo	1.0 ✓ ✓ 21,9		
	L	Mo	257,873	180,000	90,018		16.3	G Mo	0.8 ✓ ✓ 17,		
	UL	M	59,939	119,842	59,923		3.0	G Mo	0.8 ✓ ✓ 11,		
	H	A	196,498		98,239		280.0	G Mo	4.0 ✓ ✓ 1		
H A	Out of memory - two attempts - old GPU				2,854,427	570,885	285,609	H	72.4 G Mo 3.5 ✓ ✓		
	A	16,961,556				3,392,310	1,696,773	H	438.4 G Mo 3.4 ✓ ✓		
	A	1,664				881,466	440,729	H	83.9 G Mo 2.0 ✓ ✓		

Figure 9.18: Section from Appendix N Table N.2 showing building time of Point Cloud images.

As discussed in Chapter 9.6, after nearly two days and then a further 18 hours, the first two attempts failed (indicated in red in Figure 9.18). Only after a new GPU card was installed with its own 6GB RAM were the ultra-high Tiff resolution images successfully processed, but it still took over 33 hours to process. This dropped down to a more manageable level when the high resolution images were processed. If compared to the CR Jpeg images

(highlighted orange) the time difference is considerable. Using the old GPU, the data-set was processed in just over four and a half hours and, the same data with the new GPU card installed, one hour and twelve minutes.

The processing times would have been much faster if more RAM had been available for both the i7 CPU and an even faster GPU card had been installed, but unlike the camera memory card, this new level of technology had not reduced in cost and therefore if images of high quality are to be regularly processed, the cost and time implications must be considered. Within the concept of this research, the results of the fabricated Warrior model heads (Chapter 4.12) and Dolphin models (Chapter 9.6.3) do not seem to justify additional hardware costs in the use of the RAW format, although if more problematic models such as Serenity (Chapter 9.6.2) are to be undertaken, then the use of the RAW format is perhaps justifiable.

## Chapter 10: Conclusions and Future Research

### 10.1 Introduction

In an article written in February 2016, Biz Stone, co-founder of Twitter, writing for *Fast Company* [258], an on line design magazine, described why designing something easy was so exceedingly difficult.

*“Keeping things simple is difficult. I like making simple things because I’m frustrated easily by overly complicated products. When I review a product, I think like an editor—what can we take out? Too many options just make me confused and I’ll just delete it rather than try unless I have to”.*

This research into reverse engineering using single camera photogrammetry has in many ways tried to emulate Stones sentiment. The following section is used to remind the reader of the sequence of events in this thesis beginning with the research objectives which have focussed on an ever-growing, developing and complex technology. Chapter 1.3 not only asked the questions pertaining to the main title, but followed through with the plans and their execution in Chapters 1.4 and 1.5, and in Chapter 3, considered the issues of hardware and software use. The three main empirical methodologies were discussed in Chapters 4 and 5 under their own subheadings including the detailed use of the hardware and software. Chapter 6 then considered the problems encountered as the research progressed, identifying some that were beyond the realms of this project which are discussed in the 'Future Research' (Chapter 10.7). There were many benefits found which were additional to the original objectives, and these were elaborated upon towards the end of Chapter 6.

The research then investigated how a basic (non-DSLR) compact camera could be used, with regard to its lowest digital pixel rating, before the 2D digital image was degraded to such an extent that it was not usable for the overall process to fabricate AM models. The results of this investigation into the use of a Compact versus DSLR camera were documented in Chapter 7.

In Chapter 8, a close look was taken at the final collection of fabricated Jpeg format AM models that were made. These consisted mainly of FDM and SLS models, some of which were left in their natural post-fabrication state, whilst

others were hand painted. Both miniature and full size models were produced by the different types of AM machines which were available at that time for this research.

The industries of 3D animation and AM fabrication was a fast developing environment into which this research delved, and it was decided to revisit some of the methods of photogrammetry and use a more complex format for the image capture. In part this was due to the upgrading of software programmes that were available as well as some of the hardware which had also been upgraded.

For example, the GPU card was upgraded from an AMD HD7850 card with no RAM (considered to be a medium to high end at the time of the start of the research in late 2012) to a mid-entry level NVidia GTX 1060 card with 6GM RAM. Agisoft, the prime processing software used, was also upgraded and new versions became available. Their recommendation also changed for the hardware to be used. The GPU cards, from GTX 280 to GTX 560 in 2013, to a starting minimum card of GTX560 to the GeForce Titan X card with 12GB RAM on board by 2016. This research used an i7's CPU originally with 8GB of RAM this was upgraded to 32GB of RAM (now considered the minimum requirement). Chapter 9 deals with the implementation of using the photographic RAW format and the results this format produced. It ended with a discussion on the merits of a more complex and expensive system over the simpler camera ready Jpeg format, originally proposed in this research.

## **10.2 Core Research Questions**

The initial research investigated whether it was possible by using a relatively simple-to-operate, low-cost, mid-range DSLR camera, as opposed to, in the main, expensive complex 3D scanners, in conjunction with other optical equipment, to convert 2D images into 3D replications of the artifacts that were digitally captured by the camera.

It went on to consider whether a competent computer-literate person, would have been able to utilise user-friendly software and with the minimum of software manipulation, produce a digital file readable by an AM machine so as to produce fabricated models.

Furthermore, it considered whether the system and methodological process could be used by local communities, educational institutes, museums, galleries and commercial businesses both large and small. It also considered if the methods used were within the capabilities of these communities to replicate fine and rare *objets d'art*, modern sculptures and other items usually kept behind glass. Such objects may be too fragile for ordinary members of the public, or school children to touch and handle. Or perhaps the system could record and replicate objects of historical heritage, which would later be shipped off to national museums for "safe keeping". In Chapter 2.9 two case studies are contrasted illustrating this point of "safe keeping", of how a missed opportunity slipped through the hands of one community but was successfully achieved by another.

The research considered whether the complexities of the systems employed were simple enough for the business communities, both large and small, to capitalise on these new technologies to promote their design, research and development projects to World-wide markets. It asked if they would be able to produce workable facsimiles, using a single DSLR camera or even a compact camera, by their own computer literate staff, and if necessary using third party bureaux for the actual fabrication of the AM models.

Having obtained CR digital images of artifacts, the research further investigated how far this technology could be employed in their repair and renovation in a non-invasive way.

### **10.3 Methodological Reconstructions**

This research was undertaken to explore the possibilities of how to achieve a simpler, more accessible, less expensive means of data capture than with the use of 3D scanners; instead an alternative method was used with a single DSLR camera and standard software programs, each requiring a different method of data capture, but producing a virtual model of the artifact. These two primary programs, AutoDesks's *123D Catch*<sup>®</sup> and AgiSoft's *PhotoScan Pro*<sup>®</sup>, both required secondary software, *StudioPro*<sup>®</sup>, to convert the virtual files produced into an AM readable format, so that a 3D fabricated replica of the selected artifact could then be produced on an AM machine.

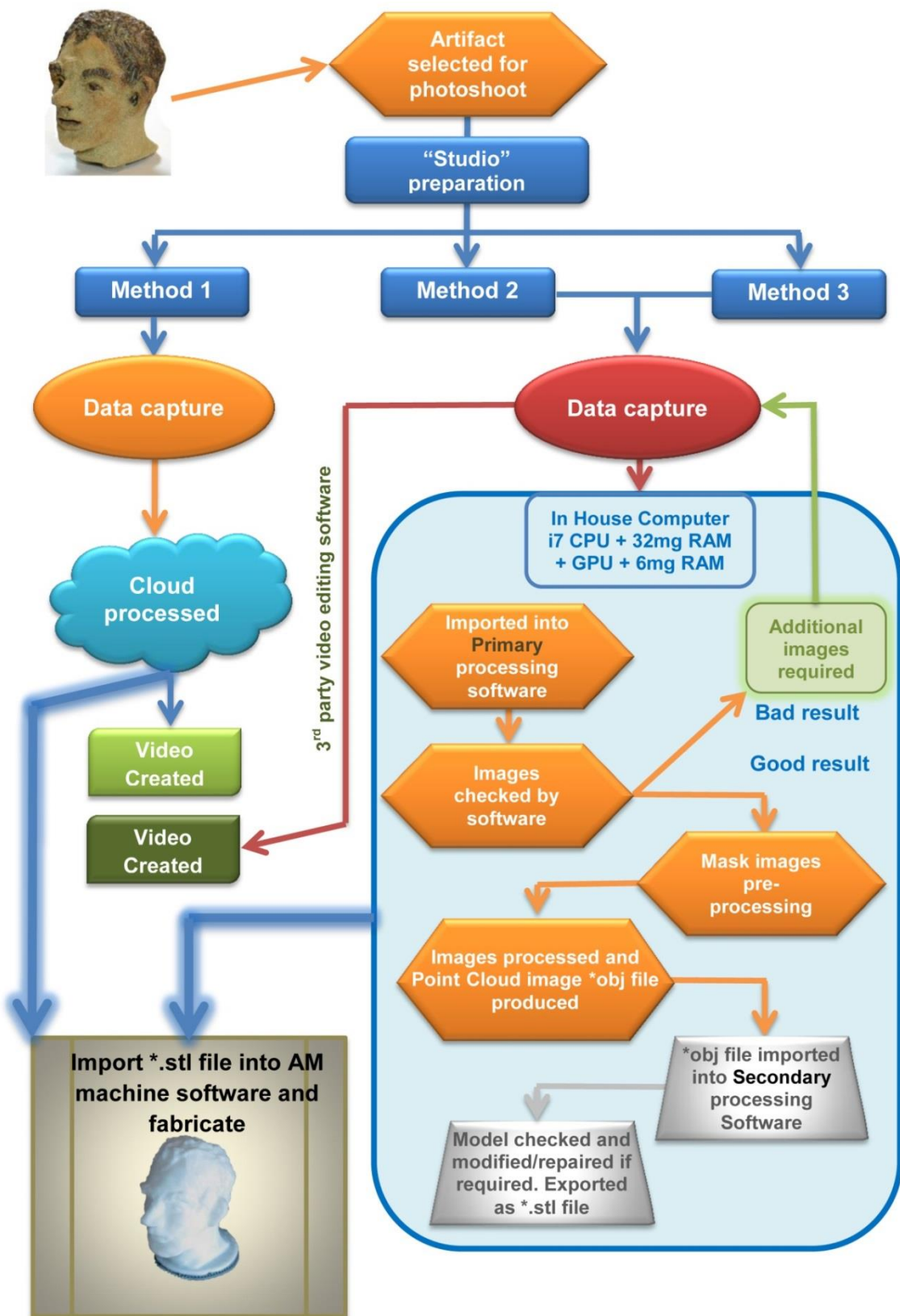


Figure 10.1: Flow Chart of Methodology for Monochromatic Replication.

By the end of the research, all three programs had had significant modification to them. At the time of writing, *123D Catch®* no longer exists in its

previous form, *PhotoScan Pro*<sup>®</sup> has had several upgrades and *StudioPro*<sup>®</sup> has been acquired by AutoDesk and although an original updated version still is in use, AutoDesk have rebranded and transformed this program to encompassed many totally new functions. Figure 10.1 illustrates the processes, in the form of a Flow Chart, which can be consulted whilst following the explanation in the remainder of the chapter.

The two primary programs required quite different methods of data capture: the first method used *123D Catch*<sup>®</sup> to process the captured data. The camera for stability reasons had been mounted on a tripod and was moved around the artifact in a 360° circle. The camera was moved on the completion of each revolution by between 30° and 40° (depending on the complexity of the artifact and the number of images required) from the horizontal plane up and down and if required from directly overhead, capturing between 75 and 90 digital images.

The second method required the artifact to be positioned on a turntable and the camera was set up close to the object in a fixed position. The turntable was rotated by 10° or 15° per frame shot and the camera moved up or down from the horizontal on each completed circle of the turntable as per method one. In this method, between 100 and 150 images were taken, depending on the physical complexity of the artifact. In this method the captured data was processed using *PhotoScan Pro*<sup>®</sup>.

Both sets of digital data were then processed in individual ways. The first method was automatic, by uploading the data to a website with the operator only being left to clean data so as to obtain the virtual image on the returned download. This “cleaning” function removed unwanted “noise” left by this method of data capture. This required the operator to have a “live” internet connection for both the upload and download, which could be several hours later.

The second method was semi-automatic as the operator had more control over the processing of the data, which was undertaken on the authors own computer. However, the downside was that for the best results, a standard 2012 off the shelf computer with an i5 CPU and standard GPC was not powerful enough and an i7 CPU was ideally required with 32GB of RAM. For the best results, the subject image in each frame required masking, a somewhat tedious but straightforward process using a built-in tool in the software.

Once masked, the image data was automatically processed but depending on the processing power of the computer, this could take between one to five hours. In this method, the artifacts were placed in a light tent, by which the amount of light falling on the artifact was controlled, the light tent removing any background “noise” from the subject. A third method was employed using all the same techniques but without the light tent. In this method a backdrop was used to eliminate background noise.

Each method produced its own type of data file, method one having the extension \*.3dp, whilst methods two and three had the extension \*.obj. The data files were then imported as virtual 3D mesh images ready to be processed in the secondary software, StudioPro®. In this secondary software, simple repairs were carried out to the imported mesh, if required, ready to produce the required \*.stl files. Using the tools provided in this secondary software, fine tuning of the data file of the artifacts was possible as well as being able to carry out necessary minor repairs on the mesh of several of the items.

Figure 10.2 indicated the concerns and problems that the user should be aware of if successful results were to be obtained, but also mindful, as referred to previously, that some objects such as glass and other highly reflective materials which the artifacts might be made from, were extremely difficult, if not impossible, to replicate by non-invasive methods. Also it should be remembered that the higher the resolution of the point cloud image data, the greater the computing power of both CPU and GPU required. The questions then had to be asked whether the AM machinery that would fabricate the models was capable of processing the very large files that would be produced and whether the AM machine’s resolution was high enough to warrant the additional cost of the computer processing equipment. If all was satisfactory, the finalised digital files were then converted to \*.stl files, which were readable by the AM software, now enabling the AM machines to produce the fabricated replicas.

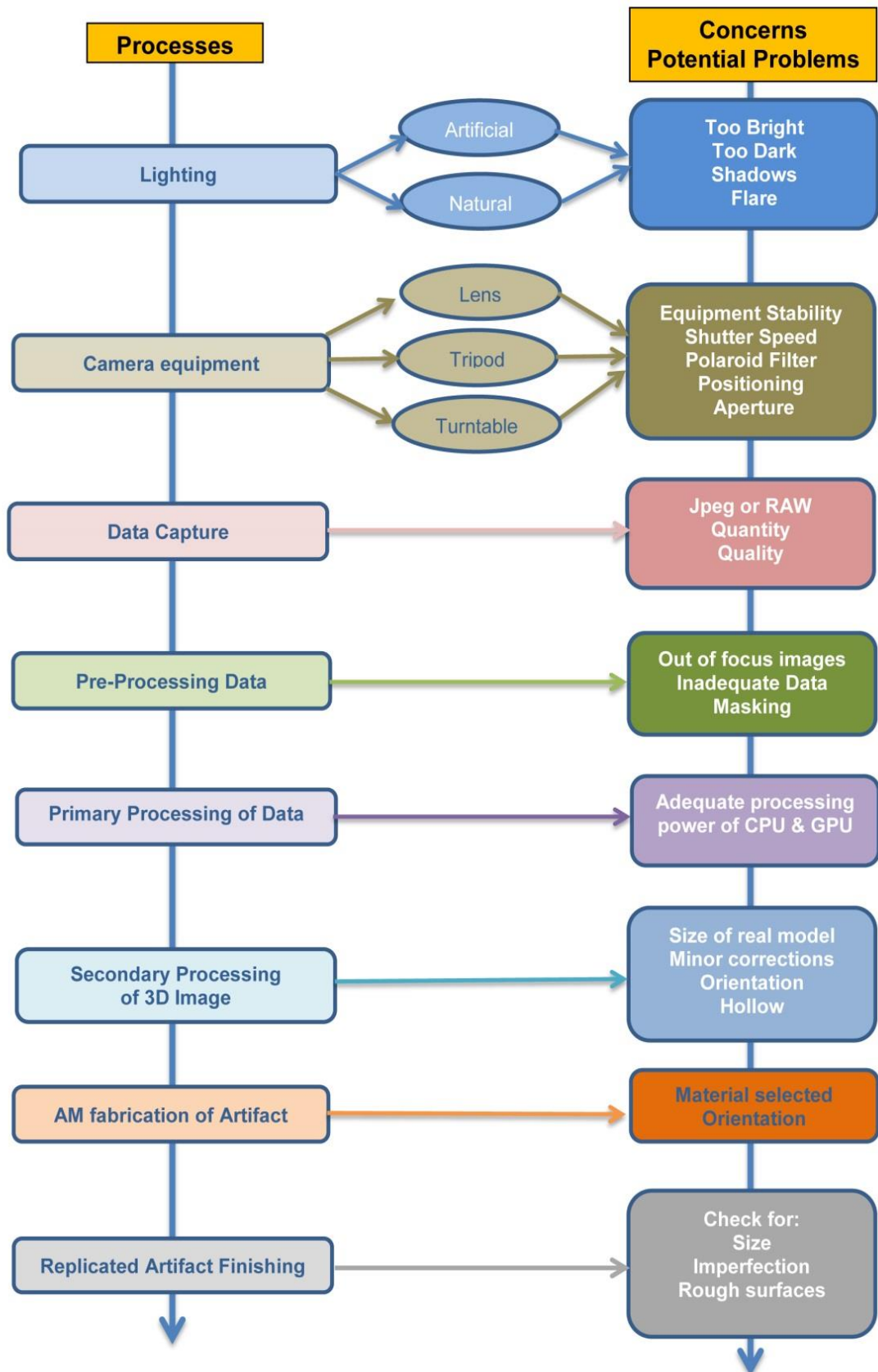


Figure 10.2: Schematic diagram of Concerns and Problems.

Table 10.1: Results of Models Processed and Fabricated.

	Method 1	Method 2&3	CAD	Total	% of Total	Total %
AM models made	6	16	4	26	44.07%	71.19%
Awaiting fabrication	7	6	1	14	23.73%	
Repaired	-	1	1	2	3.39%	
Non-manufacturable	7	6	-	13		
Detail too small	2	-	-	2		
Objects too large	2	-	-	2		
Total processed	24	29	6	59		

Table 10.1 summarises the results for all 59 objects which were processed using a combination of the three methods described above. From the digital files processed or created in CAD (*SolidWorks*<sup>®</sup>) a further six artifacts were produced. This produced 59 artifacts of which 13 items were deemed as total failures or required re-photographing and re-processing. The geometric detail produced in two items was deemed too small for the AM machines to replicate. Two items were also too large for the AM machines to handle and therefore left uncompleted. Two damaged items were digitally captured using method 2 and repaired using CAD, of which one item was replicated using AM.

In the latter research (Chapter 9), four of the original Camera Ready Jpeg models were revisited and the new RAW format that was used showed a mixed result. The question was addressed of whether the additional cost in both time and equipment would justify the results unless very complex artifacts were to be replicated on a regular basis.

#### 10.4 Empirical Findings

Throughout this research, references have been made to a series of alternative, complex, multi-equipment methods using selection of 3D scanning operated equipment, either singly or with other optical combinations and complex software to synchronise and unite the different methods of data capture. There are of course, multi-camera installations with remote sensors firing simultaneously costing many thousands of pounds (as referred to in Chapter 3.10). All these budgets far exceeded that of the single DSLR or compact camera approach used in this research and many of the methods quoted required hardware and software engineers to operate the equipment and process the results.

Photogrammetry by reverse engineering using a single camera has shown that none of the above complexities existed in the methods employed and advocated in this research. Furthermore, in the initial research, the Jpeg format models that have emerged and were recreated using AM technology, showed a very high success rate, at just over 44% (see Table 9.1). With the use of AM machines with greater capacity for printing finer layers than 60µm and less, greater detail has been shown to be able to be present on the fabricated models (as shown in Chapter 4.12 using a *PolyJet J750<sup>®</sup>*). When the fabricated model total was added to the \*.stl files waiting to be fabricated, plus the repaired models, this total increased to just over 71% of the artifacts processed. Also as the operatives improve in their techniques of data capture, and with a higher level of attention and planning in the pre-data capture stage, a better quality of data to be processed will be ensured, in turn producing better quality fabricated models.

The various complex and precise methods used in this research have led to the establishment of guidelines which can now be followed by computer literate professionals employed in museums, galleries or areas involving cultural heritage. The methods recommended for future use by others needed no complex formulae to calculate or manipulate the software that was used. All the software used was user friendly, although some training with the tools used in the software might be required, but this would be expected of any user introduced to new software.

The computer software used in this research was not Shareware, Freeware or under development, but commercially available on a variety of licensing terms, although Autodesk had promoted their software by not charging for the licensing or the downloading of the program. Both Netfabb and AgiSoft licensing fees depended on the status of the organisation using the software and whether they were educational or commercial, but in general would have to be purchased by organisations which would want to pursue the techniques employed in this thesis for commercial gain. AgiSoft's Professional commercial licence cost was \$3,499.00/£2510.00 (the basic stand-alone edition \$179.00) and Netfabb \$355.00/£252.00 for a yearly licence (both quoted at 2018 prices). Although it was commercial software, it was no more expensive than other graphic, CAD or photographic programs. Employing a mid-range DSLR camera or even, as

shown, a compact camera, further reduced the budget to manageable proportions, even when including lighting and props, to under £5,000 (at 2018 prices). When compared to some of the laser and optical equipment as used by others, budgets of several thousand pounds would be needed per piece of equipment. But as can be seen from the examples quoted in Chapter 1.18, the cost and quality of 3D scanners had come down to affordable levels, and is now within the scope of many budgets, though still not as versatile as a compact or DSLR camera and not a piece of equipment that could be used for daily photographic use.

It can be seen that AM fabricators at all prices existed in the market place, but anything at entry level would not produce the quality needed for serious replication. Whilst we all might like to own the latest colour AM printer, there are many third party companies who are happy to invest in this machinery and fabricate models with a few days turnaround, charging on “a pay as you go” basis. A list of such machines and the names of the manufacturers has been produced and included in Appendix V. This list includes such details as; model name, the resolution, build platform and layer thickness, and should help the reader in identification, but as stated, in a very fast moving and competitive industry, with such a list many of the names and models soon become outdated and obsolete.

Large artifacts presented their own set of problems in capturing all the data but most of the artifacts in this research were under 300mm in height. One of the bulkier items was successfully digitised and the virtual 3D textured mesh replica cut in half and the two fabricated halves glued together, showing that apart from the saving in cost, large objects can be sectioned and re-joined if the platform of the AM machine is too small.

## **10.5 Implications in RE using SC Digital Photogrammetry**

It has been shown through the examples cited in this research that there are many organisations pursuing the preservation and restoration of National Heritage or State Collections housed in the principal city museums or galleries throughout the world. Teams of researchers are supported by large financial grants that are available to many of these institutions to pursue this important work and in one or two instances, the high cost in equipment and the manpower

to operate and evaluate the results has been questioned, given the limited results obtained. The larger the team collecting the initial data, the greater the disruption caused to the galleries where these artifacts are housed, often to the detriment of the public who are excluded whilst the gallery may be closed for the duration of the data collection period.

The proposed methods advocated in this research are shown to be viable with most, but not all types of artifacts. Small sea shells and fossils, ancient and modern statuettes, figurines, and assorted bowls and pots were reproduced using a single camera, with a sole operator and processed using a single computer. Even with the use of a digital compact camera it has been shown that replication of artifacts was possible if used with the camera's higher resolution, which means that a compact camera can be carried in a bag or pocket ready for the unexpected field encounter on an archaeological dig or shore line walk, away from the studio, office or home. These facts indicate that it would be possible for these methods to be employed by low budget, small town institutions, and country museums to replicate their collections of artifacts with the use of the minimum number of operators, causing minimum disruption to the public or even inviting members of the public to participate in such projects.

What better way to entice potential art buyers to attend the sale room than to send them, along with the catalogue, one or two miniature replicas, from the collections which are for sale? Who would not be tempted to bid for a famous sculpture if one was clutching a miniature sent by special courier from the auction house? The added cost of such projects in relation to the object's value would be insignificant compared with the publicity or intrinsic value added. What could be simpler than sending a digital file to a local AM fabricator, where the miniature models could be made and delivered locally to your client, be it in New York, Beijing, Paris or Sydney? All of this is achievable with the single camera method.

## **10.6 Limitations of the Study and Challenges**

Although the literature review considered a number of examples of data collection including both CT and MRI scanners, photogrammetry has its limitations and therefore cannot compete with these types of geometry data collection. With photogrammetry, whether using 100 synchronised digital cameras or just one solitary camera, the sensor in the camera can only collect and record the

reflected surface light. It is not currently possible to delve below the layers of bandage of an ancient mummy, nor beneath the shattered and splintered remains of damaged bone that may lie under the skin with a DLSR or compact camera.

If this reflective light is too speculative or too reflective, ways of elimination had to be found, otherwise the digital image was distorted and the final results did not reflect the true image or artifact which was the subject of replication. Through the operator's experience that is gained in the data collection process, together with the suggestions of others, many of the obstacles encountered were overcome. The later use of Polaroid filters greatly helped, but there is still much more work needed in overcoming glare produced by glass, polished metals, stone or glazed surfaces.

Unfortunately, coloured replication of artifacts was only just touched on due to the lack of easy access to Multi-colour printers/fabricators, but this should also be considered for the future. The fabricated artifacts that had been hand painted gave a good representation of the originals and brought life to the otherwise monochromatic models, although a professional colourist or artist's hand would no doubt have been a greater improvement. However, the research had set out to show that replication was possible (and to this extent it did), and not to make fake reproductions.

With the use of the selected software, it was possible by the addition of computer power and the number of digital data images collected to improve the quality of the virtual 3D image to the point where a textured mesh point cloud image was indistinguishable from an original photograph of the artifact. However, in the final fabricated AM artifacts, where the surface was quite flat and smooth such as the Egyptian figurine Sobekhotep (H.42), Horus (H.53), the Egyptian bowl (H.28) or the Eureka cat (H.40) and Man (H.41), these artifacts lost very little, if any, detail. Unlike the Clay Head (H.31), the Clay Dog (H.30), the Sea Shell (H.55), the Ammonite (H.51) or the Concrete Mix (H.50), all instantly recognisable as "good" representations of the originals, but on closer examination these AM models had lost the very fine, granular, gritty complex detail of their original counterparts.

It has also been shown that the more complex digital RAW format used to record the original artifacts can improve and overcome certain problems that are encountered within the photogrammetry process though at a cost both in time and

money. But surprisingly, using this more complex format and advanced pre-processing software, did not always produce better results than the original, instantly available camera-ready Jpeg format.

Hopefully with developments in AM technology in the near future, it is anticipated that fine resolution layers will become more readily available and affordable and the quality of fine detail on models will improve.

## 10.7 Recommendations for Further Research

Warning was given very early on in the research by AutoDesk [6] that:

*“plain, reflective or transparent surfaces or objects will not work,”*

and it has been seen in this research and that carried out by others, that this light flare and reflection is still problematic. This is therefore a major issue that needs to be addressed. As bright light causes the problem, lower light (or no light) might be a solution.

As discussed, one or two alternative methods of lighting have been suggested, but nothing about the use of an infrared camera. There is the near infrared (IR), which is just beyond what the human eye can detect. At the other end of this spectrum is thermal imaging technology, popularised in its use by the military, emergency services and surveillance agencies, but it is not this end of the spectrum that is of interest. Digital cameras can be adapted for the capture of IR by the use of circular filters or by adaptation of the camera itself, a more expensive alternative, but one that gives good results. There have been many uses of IR cameras being flown in UAVs to study crops, tree crowns and archaeological sites, to name but a few. Agisoft have stated that with the use of *PhotoScan Pro*<sup>®</sup>, the IR data can be converted to produce very good point cloud images. There does not seem to be any academic literature regarding artifacts being processed as in this research. Whether the same techniques and methods that have been used in this thesis, could apply, would form the basis for further research.

The two other methods that have been used in this research, were RAW negatives (Chapter 9) and the use of a Polaroid lens (Chapter 6.4.1) which showed limited results. With the RAW negative and the use of specialist editing software, it was possible to correct defects of a set of digital images; having corrected one image, the corrections were transferred to the whole set of images

(batch processing). This worked well, if for instance the images had been over or under-exposed, and with other corrections of a similar generic nature, but correcting flare involved single manipulation of each digital negative, since the position of the flare in each image was in a different position as the target object was revolved around on the turn table. Equally, some of the digital images did not have any flare coming off the artifact in that particular camera shot.

For the addition of a polaroid lens, the limitations were shown in Chapter 6.4.1; CP worked best under natural outdoor lighting, eliminating reflections from objects such as plate glass and water and excellent results were obtained, but metallic objects and transparent glass objects were still problematic, as was shooting images indoors under studio lighting. These would provide the opportunity for further research.

### **10.7.2      Colour Fabrication**

Little was done with colour fabricated models for the reasons already discussed and more research is therefore required into this area. Perhaps a series of experimental trials could be set up using different sets of digital data and processed using a selection of different coloured images, in which the colour intensity of the images would change, to find a “best” match with the original. Ideally, this research would need access to a range of dedicated colour fabricating machine so as to test the consistency in the finished printed objects comparing one manufacturer to another as well as to the original artifact. It would also be interesting to compare the consistency of colour and permanency (as in a BS, RAL or Pantone standard) in printing AM models, using a selection of manufacturers’ AM machines and consistency with the same range of machine, both at the delivery print-head and the source ink mixture used.

### **10.7.3      Questionnaires**

At the outset of this research, there were several areas with which the author was unfamiliar, however, was able to master a good working knowledge of each topic under review through perseverance. The author came to the conclusion that the research as a whole, if explained in the manner of this thesis, was not beyond the capability of many potential users or adopters of the approach as presented in this thesis (i.e. those who are computer literate and social or work groups of

people, with a collective interest in the variety of topics discussed in this thesis, to come to grips with the techniques and procedures documented. This assumption was based purely on the author's experience and remained an assumption without any firm basis to refer to except casual conversations with interested parties.

Questionnaires are now an integral component in many areas of research, in order to gather useful data, or for the validation of a particular development. To validate the author's untested assumptions, a questionnaire and demonstration exercise, involving photogrammetry and the preparation of virtual 3D models, could be prepared and shown to interested groups of people as suggested previously: museums, local history groups, colleges etc. As demonstrated by Novak and Wisdom [259], a questionnaire before and after engaging preservice teachers, introducing them to the emerging technology of 3D printing and the integration of its use with the elementary science curriculum which the preservice teachers would be required to teach in schools, gave insight into the apprehension and anxieties as well as the positive outcomes of the participants. The paper also demonstrated the complex system of designing a questionnaire and the ethics processes that must be satisfied in order to meet academic standards. Kamp *et al*, in *Applied Nursing Research* [260], states :-

*"Questionnaires are a standard component of quantitative research, but seldom do researchers consider the importance of item clarity and participant comprehension."*

Volpatto *et al* [261], reviews Brazilian auditory questionnaires and checklists for medical screening as used in Brazil; both identifying the problems and possible solutions of designing and identifying factors for specific target clients. The method of analysis of results is obviously of great importance so as to achieve reliable and useful data.

These papers clearly show that designing a questionnaire is not to be taken lightly and time and consequently funding is required to achieve any meaningful evaluation of the author's assumptions which can be seen as a future valued project.

## 10.8 Conclusion

The initial research undertook to investigate the claims of others, that a “happy snap” approach and no prior knowledge of photogrammetry, was a viable alternative to other methods of reverse engineering which employed the use of complex photogrammetry and/or 3D scanning. The research objectives achieved results demonstrating that artifacts could be replicated by a computer literate person without using expensive, complex software and hardware, showing that it was more cost effective and cheaper than most 3D scanning systems. However, by using both a mid-range DSLR camera and a “point and shoot” compact camera, it was found that a laissez faire “happy snaps” approach did not achieve good results, but with careful planning, limits were established for acceptable image resolution which could be used in the process of converting 2D images into 3D replicated AM objects. The research further investigated with the use of commercially available, user friendly software, the process of reverse engineering artifacts and converting the resulting digital files into an AM printable format.

With the collaboration of the Kendal Museum, three Egyptian artifacts were selected to be the focus of the research. This initial selection was expanded to include some 50 other artifacts: a mixture of hand-crafted, mass produced and naturally occurring objects. With these it was proven effectively that planned systematic simplicity did work, within certain limitations and conditions, and that there were also other useful applications that could be utilised from an expansion of the basic system employed. This collaboration showed that the development of this system could potentially be utilised by a variety of users including community projects, educational institutions, and museums and galleries.

The research also examined the justification and consequences of processing high and ultra-high resolution point cloud digital images, and their use with AM technology. It was shown that longer times were required to process high and ultra-high resolution digital images, and a greater, more expensive specification of processing computer hardware was required. The investigation also demonstrated that unless the AM technology output was of a high enough resolution, the artifacts produced would not match the high specification of the digital images, and both time and therefore money would be wasted. Within this section of the research, comparisons were made using RAW (NEF) and Jpeg

digital image format. Through the use of bench-mark AM models and a series of 2D printed image examples, which were all processed within the same software, evaluation of the benefits of one format over the other were made. It was subsequently shown that the preconception of the use of RAW images as superior to Jpeg was not always merited.

The popular view was that 3D scanners were the only reliable (although mostly expensive) pieces of equipment that could reverse engineer artifacts, be they new, old, large or small objects, with any degree of success. In this research, acceptable results were achieved in the use of photogrammetry, through the development of a procedure which was more cost effective and cheaper than most 3D scanning systems. Given training in its techniques, the use of single digital camera technology (both DSLR and compact) should be within the achievable reach of many, if not all, computer literate operators. The procedure was non-invasive and therefore capable of replicating hand-crafted original artifacts, and as such might prove to be a more economically viable method to be used by small businesses (SME's) for the promotion of their designs.

This system should potentially make it an ideal operating method for organisations working with modest budgets who wish to replicate and fabricate artifacts by non-invasive RE with the use of photogrammetry, contributing to the development of techniques and methods which can be used by computer-literate, but not necessarily expert, computer software operatives.

## References

- [1] Laser Design. (2017). *3D Scanning Technology — Hard Work That Looks Like “Magic”*. Available: <https://www.laserdesign.com/what-is-3d-scanning> [Accessed January 2017].
- [2] Thomas Tong. (2011). *3D Scanners: Laser Versus White Light*. Available: <http://go.lmi3d.com/3d-scanners-laser-versus-white-light> [Accessed Jan 2013].
- [3] F. Bernardini and H. Rushmeier, "The 3D model acquisition pipeline," in *Computer graphics forum*, 2002, pp. 149-172.
- [4] H. Rubinsztein-Dunlop, A. Forbes, M. Berry, M. Dennis, D. L. Andrews, M. Mansuripur, C. Denz, C. Alpmann, P. Banzer and T. Bauer, "Roadmap on structured light," *Journal of Optics*, vol. 19, p. 51, 2016.
- [5] V. Viswanatha, N. B. Patil and S. Pandey, "Computation of Object Parameter Values based on Reference Object Embedded in Captured Image," *Research Journal of Computer Systems Engineering - RJCSE*, vol. 02 pp. 183-191, 2011.
- [6] AutoDesk, "123D Catch," ed. California, USA: AutoDesk Inc, 2012, p. a suite of hobbyist CAD and 3D modelling tools
- [7] AgiSoft, "PhotoScan Pro," ed. St Petersburg, Russia: Agisoft LLC, 2006.
- [8] AutodesSys, "form-Z pro ", 8 ed. Columbus, OH. USA: AutoDesSys, Inc., 2005, pp. a general-purpose solid and surface modeler with an extensive set of 2D/3D form manipulating and sculpting capabilities.
- [9] netfabb, "Studio Professional 5 ", ed. Parsberg, Germany: netfabb GmbH, 2012, p. Provider of Additive Manufacturing software solutions.
- [10] S. Foster and D. Halbstein, "Adapting curriculum to explore new 3D modeling technologies and work-flows," in *ACM SIGGRAPH 2012 Posters*, Los Angeles CA, USA, 2012, p. 1.
- [11] M. Holewinski, "Sculpting Objects with Images in form-Z," in *AutoDesSys*, ed. Columbus, OH. USA, 2014.
- [12] R. Ball. (2008) Oldest Animation Discovered in Iran. *Animation Magazine Inc*. Available: <http://www.animationmagazine.net/features/oldest-animation-discovered-in-iran/> [Accessed 17/10/2012].
- [13] D. Joyce, "Euclid's Elements," in *Clark University*, D. o. M. a. C. S. C. University, Ed., ed. Worcester, MA. USA, 1996.
- [14] J. O'Connor and E. Robertson, "Euclid of Alexandria," in *History of Mathematics*, ed: MacTutor, 1999.
- [15] F. Gemma, "Eclipse of the Sun - 24th January, 1544," in *De Radio Astronomica et Geometrico'*, ed. London: © Science Museum / Science & Society Picture Library, 2014.
- [16] J. Zahn, "The Reflex Camera Obscura, 1685 ", ed: Courtesy of the Gernsheim Collection, Harry Ransom Humanities Research Center, University of Texas at Austin., 2013.
- [17] Film National Media. (2012) Camera Obscura. Available: [www.nationalmediamuseum.org.uk](http://www.nationalmediamuseum.org.uk) [Accessed 07/09/2015].
- [18] M. Slatoff-Burke. (2005) The Legacy of Camera Obscura. *Discoveries*. 29-34. Available: [http://www.arts.cornell.edu/knight\\_institute/publicationsprizes/discoveries/publist2005.htm](http://www.arts.cornell.edu/knight_institute/publicationsprizes/discoveries/publist2005.htm) [Accessed 01/12/2014].

[19] J. Nicéphore Niépce, "View from the Window at Le Gras," ed. Le Gras, France. : © 1996-2014 National Geographic Society, 1826, p. World's First Photograph.

[20] M. Daniel, "Daguerre (1787–1851) and the Invention of Photography," vol. Heilbrunn Timeline of Art History, ed. New York, USA: The Metropolitan Museum of Art, 2000.

[21] R. Watson, "Lacock Abbey, Fox Talbot Museum & Village," ed. Swindon SN2 2NA: National Trust, 2014.

[22] R. Lenman. (2005). Stereoscopic Photography - Oxford Companion. *Oxford Companion to the Photograph Photography Encyclopedia*. Available: <http://www.oxfordreference.com/view/10.1093/acref/9780198662716.001.0001/acref-9780198662716-e-1474?rskey=DihIWy&result=1> [Accessed 3/11/2012].

[23] D. Brewster, "Lenticular stereoscope," ed. National Museums Scotland: National Museums Scotland, Scottish Charity No. SC011130, 1860.

[24] Ignomini. (2012). Kaiser Panorama. Available: <http://ignomini.com/photographica/stereophotovintage/kaiserpanorama/kaiserpanorama.html> [Accessed 3/11/2012].

[25] New York Public Library. *Stereogrammator*. Available: [www.nypl.org](http://www.nypl.org) [Accessed January 2013].

[26] J. Heineman. (2011). *Stereoscopic photography*. Available: <http://stereo.nypl.org/about/stereoscopy> [Accessed 01/12/2014].

[27] C. Zeiss, "Pocket Stereoscope," ed. Germany, c1950.

[28] ASPRS, "American Society for Photogrammetry and Remote Sensing" in *The International Society for Photogrammetry and Remote Sensing (isprs)*, ed. Maryland, USA.: The Imaging & Geospatial Information Society, 1934.

[29] C. Charles. (2014) Why did Germany's WWI Airforce outperform the Luftwaffe? *Armchair General*. Available: <http://www.armchairgeneral.com/forums/showthread.php?t=98374&page=5> [Accessed 01/12/2014].

[30] E. Dainese, "Le Corbusier, Marcel Griaule, and the Modern Movement: exploring the habitat from the airplane," presented at the 11th EAEA Envisioning Architecture: Design, Evaluation, Communication Conference in 2013, Milan, Italy, 2013.

[31] M. Nagai, T. Chen, R. Shibasaki, H. Kumagai and A. Ahmed, "UAV-borne 3-D mapping system by multisensor integration," *Geoscience and Remote Sensing, IEEE Transactions on*, vol. 47, pp. 701-708, 2009.

[32] A. Jaakkola, J. Hyypä, A. Kukko, X. Yu, H. Kaartinen, M. Lehtomäki and Y. Lin, "A low-cost multi-sensoral mobile mapping system and its feasibility for tree measurements," *ISPRS Journal of Photogrammetry and Remote Sensing*, vol. 65, pp. 514-522, 2010.

[33] U. Niethammer, M. James, S. Rothmund, J. Travelletti and M. Joswig, "UAV-based remote sensing of the Super-Sauze landslide: Evaluation and results," *Engineering Geology*, vol. 128, pp. 2-11, 2012.

[34] M. Zhang, "The World's first Digital Camera," vol. 2012, D. Cade, Ed., ed. Davis, San Francisco, USA.: PetaPixel, 2010.

[35] C. H. Townes, "The First Laser," in *A Century of Nature: Twenty-One Discoveries that Changed Science and the World*, L. Garwin and T. Lincoln, Eds., ed Chicago, USA: University of Chicago Press, 2003, pp. 107-120.

[36] R. Highfield, "Happy 50th birthday to the laser, the 'death ray' at every supermarket till " in *The Telegraph*, ed. London. UK: Copyright of Telegraph Media Group Limited 2010.

[37] C. H. Townes, N. G. Basov and A. M. Prohorov. (2006). Charles H. Townes - Biographical. *Nobelprize.org*. Available: [http://www.nobelprize.org/nobel\\_prizes/physics/laureates/1964/townes-bio.html](http://www.nobelprize.org/nobel_prizes/physics/laureates/1964/townes-bio.html) [Accessed 01/09/2016].

[38] I. Fleming, "Goldfinger," G. Hamilton, Ed., ed. UK: United Artists, 1964, p. 110 minutes.

[39] P. Hardy and P. Woodsford, "Laser-Scan History," Cambridge, UK 2007.

[40] I. Matthews. (2003) Commodore PET. *The Amazing Commodore PET*. Commodore Business Machines,. Available: [http://www.commodore.ca/products/pet/commodore\\_pet.htm](http://www.commodore.ca/products/pet/commodore_pet.htm)  
[http://www.commodore.ca/history/company/chronology\\_portcommodore.htm](http://www.commodore.ca/history/company/chronology_portcommodore.htm) [Accessed 12/12/2014].

[41] Statista. (2014). *Percentage of households with home computers in the United Kingdom (UK) from 1985 to 2014*. Available: <http://www.statista.com/statistics/289285/household-desktop-computers-in-the-uk-by-income-group/> [Accessed October 2014].

[42] D. Semyonov, "Algorithms used in PhotoScan - Point Cloud Data," J. Kaufman, Ed., ed. Manchester: AgiSoft LLC, 2012.

[43] T. Lemmon and P. Biddiscombe. (2005). TRIMBLE® 3D Scanning for Surveyors. Available:  
[http://tr1.trimble.com/docushare/dsweb/Get/Document-262881/022543-177\\_3DScanningforSurveyors\\_WP\\_1005\\_Ir.pdf](http://tr1.trimble.com/docushare/dsweb/Get/Document-262881/022543-177_3DScanningforSurveyors_WP_1005_Ir.pdf),  
[http://www.trimble.com/corporate/about\\_history.aspx](http://www.trimble.com/corporate/about_history.aspx) [Accessed 08/11/2012].

[44] K. Hanke, P. Grussenmeyer, A. Grimm-Pitzinger and T. Weinold, "First experiences with the Trimble GX scanner," *Arch. of Photogrammetry and Remote Sensing and Spatial Information Sciences*, vol. 36, pp. 1-6, 2006.

[45] T. Kersten, H. Sternberg, K. Mechelke and C. A. Pardo, "Terrestrial Laserscanning System Mensi GS100/GS200—Accuracy tests, Experiences and Projects at the Hamburg University of Applied Sciences," presented at the Panoramin Photogrammetry Workshop 2004, Stuttgart, Germany, 2004.

[46] D. Southam. (2010). Documenting Byland Abbey in 3D for English Heritage. *Faro user Story*. Available: <http://www.faro.com/content.aspx?ct=uk&content=news&item=2821&tab=3> [Accessed 8/11/2012].

[47] SurvTech Solutions, "Tampa Florida 3-D Laser Scanning - History of LS," ed. Tampa, Florida. USA SurvTech Solutions 2012.

[48] LinDarUSA, "ScanLook 2.0," ed. Somervill Alabama. USA 2014.

[49] DAVID Vision Systems GmbH, "DAVID Structured Light Scanner SLS-2," ed. Koblenz, Germany, 2009.

[50] S. Holmes. (2014) Apple files patents for 3D laser scanning technology in its handsets. *DEVELOP3D*. Available: <http://www.develop3d.com/blog/2014/12/apple-file-patents-for-3d-laser-scanning-technology-in-its-handsets> [Accessed 13/12/2014].

[51] J. Brecko, A. Mathys and P. Semal, "Cost Analyse of 3D Digitisation Techniques," *Digital Presentation and Preservation of Cultural and Scientific Heritage*, vol. IV, pp. 206-212, 2014.

[52] S. Crawford. (2013). How Microsoft Kinect Works - The Kinect Sensor. *howstuffworks*. Available: <http://electronics.howstuffworks.com/microsoft-kinect2.htm> [Accessed].

[53] A. Das, J. , D. C. Murmann, K. Cohn and R. Raskar, "A method for rapid 3D scanning and replication of large paleontological specimens," *PLoS one*, vol. 12, p. e0179264, 2017.

[54] R. Redwood. (2005) PhotoShop Elements History. [www.easylelements.com/photoshop-history.html](http://www.easylelements.com/photoshop-history.html). Available: <http://www.easylelements.com/photoshop-history.html> [Accessed 01/01/2015].

[55] Agisoft, *PhotoScan Professional Edition*. St Petersberg, Russia: Agisoft LLC, 2012.

[56] S. Pfeifle. (2012). Will photogrammetry make laser scanning obsolete? *Spar point Group*. Available: <http://www.sparpointgroup.com/Print.aspx?id=3136&lang> [Accessed 11/11/2012].

[57] M. Wang, J. Chang, J. Kerber and J. J. Zhang, "A framework for digital sunken relief generation based on 3D geometric models," *The Visual Computer*, vol. 28, pp. 1127-1137, 2012.

[58] Y.-W. Zhang, Y.-Q. Zhou, X.-L. Li and L.-L. Zhang, "Line-based sunken relief generation from a 3D mesh," *Graphical Models*, vol. 75, pp. 297-304, 2013.

[59] T. Weyrich, J. Deng, C. Barnes, S. Rusinkiewicz and A. Finkelstein, "Digital bas-relief from 3D scenes," in *ACM transactions on graphics (TOG)*, San Diego, USA, 2007, p. 32.

[60] Y. Peng, C. Chen, L. He and H. Chen, "3D Reproduction of Oil Painting Based on UV Ink-Jet Technology," *ICECTT 2015*, 2015.

[61] K. Steele and R. Williams, "Reverse engineering the Greek comic mask using photographic three-dimensional scanning and three dimensional printing techniques and related seepage control. ,," *Rapid and Virtual Prototyping and Applications : 4th National Conference*, pp. 73-81, 2003.

[62] P. Failing. (2011) Unraveling the Mysteries of Degas's Sculpture. *Art news*. Available: <http://www.thomaskinkadebirmingham.com/pdfs/UnravelingMysteriesDegas0611.pdf> [Accessed October 2015].

[63] A. Sugar, R. Bibb, C. Morris and J. Parkhouse, "The development of a collaborative medical modelling service: organisational and technical considerations," *British Journal of Oral and Maxillofacial Surgery*, vol. 42, pp. 323-330, 2004.

[64] F. Stockmans, K. Leuven and T. Husby. (2008). 3D deformity of the Radius. About Materialise - SurigCase Orthopaedics. Available: <http://www.materialise.com/cases/striking-the-right-note-with-a-well-planned-radius-reconstruction> [Accessed 14/06/2011].

[65] N. L. Leong, G. A. Buijze, E. C. Fu, F. Stockmans and J. B. Jupiter, "Computer-assisted versus non-computer-assisted preoperative planning of corrective osteotomy for extra-articular distal radius malunions: a randomized controlled trial," *BMC musculoskeletal disorders*, vol. 11, p. 282, 2010.

[66] D. Popescu, D. Laptoiu, A. Hadar, C. Ilie and C. Pârvu, "Workflow for Additive Manufacturing of an Individual Surgical Template," *Proceedings in Manufacturing Systems*, vol. 10, p. 131, 2015.

[67] D. D. Popescu, "POIGO," J. Kaufman, Ed., ed. Manchester, 2018.

[68] A. Guarnieri, F. Pirotti and A. Vettore, "Cultural heritage interactive 3D models on the web: An approach using open source and free software," *Journal of Cultural Heritage*, vol. 11, pp. 350-353, 2010.

[69] P. Salonia, S. Scolastico, A. Marcolongo and T. L. Messina, "Survey and 3D reconstruction of the St. Orso capitals in Aosta, through three-focal photogrammetry," in *15th International Conference Virtual Systems and Multimedia, VSMM'09.* , Vienna, Austria, 2009, pp. 35-40.

[70] G. Verhoeven, "Taking Computer Vision aloft – Archaeological 3D Reconstructions from Aerial Photographs with PhotoScan," *Archaeological Prospection*, vol. 18, pp. 67-73, 20 January 2011.

[71] B. Kreimer and M. Waite, "The Feasibility of Using Small Unmanned Aerial Vehicles for Mapping News Events," presented at the Computation + Journalism Symposium, Columbia University, New York, USA, 2014.

[72] M. Waite and B. Kreimer, "Using Drones to make 3D Models on deadline," *American Journalism Review*, 2014.

[73] H. M. Nguyen, B. Wünsche, P. Delmas and C. Lutteroth, "3D Models from the Black Box: Investigating the Current State of Image-Based Modeling," in *Proceedings of the 20<sup>th</sup> international conference on computer graphics, visualisation and computer vision (WSCG 2012)*, , Pilsen, Czech Republic, 2012, pp. 249-258.

[74] S. G. Barsantia, F. Remondino and D. Visintini, "3D Surveying and Modelling of Archaeological Sites - some critical issues," in *ISPRS Photogrammetry, Remote Sensing and Spatial Information Sciences*, Strasbourg, France, 2013.

[75] Kendal Museum. (2012). *History of Museum - From Egypt's Sands to Northan Hills*. Available: <http://www.kendalmuseum.org.uk/the-collections/history-of-the-museum/> [Accessed January 2013].

[76] T. Caulton, *Hands-on exhibitions: managing interactive museums and science centres*: Psychology Press, 1998.

[77] Y.-x. Zheng, D.-f. Yu, J.-g. Zhao, Y.-l. Wu and B. Zheng, "3D Printout Models vs. 3D-Rendered Images: Which Is Better for Preoperative Planning?," *Journal of surgical education*, 2016.

[78] V. Georgiev, "Tools for Presenting 3D Objects and Virtual Collections Online," *Digital Presentation and Preservation of Cultural and Scientific Heritage*, pp. 285-292, 2015.

[79] Khronos Group. *WebGL – OpenGL ES 2.0 for the web*. Available: , <http://www.khronos.org/webgl/> [Accessed September 2015 ].

[80] J. P. Gee, "What video games have to teach us about learning and literacy," *Computers in Entertainment (CIE)*, vol. 1, pp. 20-20, 2003.

[81] G. M. Friberger, J. Togelius, C. A. Borg, M. Ermacora, A. Mousten, M. Møller Jensen, V.-A. Tanase and U. Brøndsted, "Data Games," presented at the Proceedings of the Workshop on Procedural Content Generation. 2013. , Chania, Crete, Greece, 2013.

[82] GitHub. (2007). *MuseumVille*. Available: <https://github.com/bogusjourney/museumville/blob/master/README.mkd> [Accessed September 2015].

[83] Europeana Foundation. *Europeana collections*. Available: <http://www.europeana.eu/portal/en> [Accessed September 2015].

[84] M. P. Long and R. C. Schonfeld, "Supporting the Changing Research Practices of Art Historians," *Ithaka S+R's Research Support Services Program*, 2014.

[85] B. Bontchev, "Serious Games for and as Cultural Heritage," *Digital Presentation and Preservation of Cultural and Scientific Heritage*, pp. 43-58, 2015.

[86] W. Schuhra and J. Leeb, "Filling Gaps in cultural Heritage Documentation by 3D Photography," *ISPRS-International Archives of the Photogrammetry, Remote Sensing and Spatial Information Sciences*, vol. 1, pp. 365-369, 2015.

[87] M. R. E. Pantalony, "Managing Intellectual Property for Museums," *WIPO. World Intellectual Property Organization*, 2013.

[88] M. Weinberg, "What's the Deal with Copyright and 3D Printing?," in *Public Knowledge's Institute for Emerging Innovation*, ed. Washington DC. USA: Public Knowledge, 2013.

[89] Sinclair Research Ltd, "Zx Spectrum," ed. London, 1982 - 1992.

[90] Commodore Bussiness Machines, "Vic 20," ed. USA, 1980 - 1985.

[91] H. Maier, "Games as Cultural Heritage:Copyright Challenges for Preserving (Orphan) Video Games in the EU," Humboldt Universitat zu Berlin .2015.

[92] G. Fangi, "Documentation of some Cultural Heritage Emergencies in Syria by Spherical Photogrammetry," presented at the 25th International CIPA Symposium - ISPRS Annals of the Photogrammetry, Remote Sensing and Spatial Information Sciences, Taipei, Taiwan, 2015.

[93] E. Stathopoulou, A. Georgopoulous, G. Panagiotopoulos and D. Kaliampakosb, "Crowdsourcing Lost Cultural Heritage," *ISPRS Annals of Photogrammetry, Remote Sensing and Spatial Information Sciences*, vol. 11-5/W3, pp. 295-300, 2015.

[94] G. Grenzdörffer, A. Engel and B. Teichert, "The photogrammetric potential of low-cost UAVs in forestry and agriculture," *The International Archives of the Photogrammetry, Remote Sensing and Spatial Information Sciences*, vol. 31, pp. 1207-1214, 2008.

[95] J. Torres-Sánchez, J. Peña, A. De Castro and F. López-Granados, "Multi-temporal mapping of the vegetation fraction in early-season wheat fields using images from UAV," *Computers and Electronics in Agriculture*, vol. 103, pp. 104-113, 2014.

[96] K. Stereńczak, "Factors influencing individual tree crowns detection based on airborne laser scanning data," *Forest Research Papers*, vol. 74, pp. 323-333, 2013.

[97] P. Dvořák, J. Müllerová, T. Bartaloš and J. Brůna, "Unmanned Aerial Vehicles for Alien Plant Species Detection and Monitoring," *International Archives of the Photogrammetry, Remote Sensing & Spatial Information Sciences*, vol. 40, 2015.

[98] A. Mozas-Calvache, J. Pérez-García, F. Cardenal-Escarcena, E. Mata-Castro and J. Delgado-García, "Method for photogrammetric surveying of archaeological sites with light aerial platforms," *Journal of Archaeological Science*, vol. 39, pp. 521-530, 2012.

[99] I. Colomina and P. Molina, "Unmanned aerial systems for photogrammetry and remote sensing: A review," *ISPRS Journal of Photogrammetry and Remote Sensing*, vol. 92, pp. 79-97, 2014.

[100] K. J. Neumann, "Digital Aerial Cameras," *Intergraph Z/I Deutschland GMBH*, pp. 1-5, 2005.

- [101] T. Ashmore, "Drones in Archeology: professional and avocational," Concho Valley Archeological Society, San Angelo, Texas. July 2015.
- [102] DJI Enterprise. (2006). *DJI Phantom 2 Vision plus Manual*. Available: <http://www.dji.com/company> [Accessed February 2015 ].
- [103] DJI DroneUAV.co.uk. (2001). *The Future of Possible*. Available: <http://droneuav.co.uk/civilian-drones/dji-phantom-2-vision-plus-manual/> [Accessed February 2015].
- [104] M. J. Bennett, "Presentation on Evaluating the Creation and Preservation Challenges of Photogrammetry-based 3D Models," in *DigitalCommons@UConn*, ed: University of Connecticut Libraries Published Works, 2015.
- [105] The Westmorland Gazette, "Youngsters Demi and Luke Mason get close up to the Crosby Garrett helmet in its new home in Carlisle ", ed. Kendal, Cumbria, 2013.
- [106] M. Addison, "Rare £2m Roman helmet goes on show in Cumbria," in *The Westmoreland Gazette*, ed. Kendal, Cumbria: Newsquest (North West) Ltd, 2013.
- [107] R. Jackson, "Roman Cavalry Sports helmet from Crosby Garrett, Cumbria," British Museum, London 2010.
- [108] S. Worrell, R. Jackson, A. Mackay, R. Bland, M. Pitts and D. Bradbury, "The Crosby Garrett Roman Helmet," *British Archaeology*, Jan/Feb 2011 2011.
- [109] G. Mann, "Shine," ed. Edinburgh: Hamilton & Inches, 2008, p. Victorian Candelabra.
- [110] J. Kaufman, "Concept to Customer using Additive Manufacturing - A review of current Craft Designers' and Digital Artists' AM use and how design-led SME's could benefit by their example," MSc Engineering, Lancaster University, Lancaster, 2011.
- [111] R. E. Hollinger, E. John Jr, H. Jacobs, L. Moran-Collins, C. Thome, J. Zastrow, A. Metallo, G. Waibel and V. Rossi, "Tlingit-Smithsonian Collaborations with 3D Digitization of Cultural Objects," *Museum Anthropology Review*, vol. 7, pp. 201-253, 2013.
- [112] European Commission's ICT Policy Support Programme, "3D-ICONS," 3D-ICONS is co-ordinated by the Università degli Studi di Napoli L'Orientale, Ed., ed, 2012.
- [113] G. Guidi, P. R. Navarro, S. G. Barsantia, L. L. Micoli and M. Russo, "Quick textured mesh generation in Cultural Heritage digitization. , presented at the Proceedings of the International Conference on Built Heritage 2013 (BH2013), , Milan, Italy, 2013.
- [114] G. Barsantia, L. Micoli and G. Guidi, "Quick textured mesh generation for massive 3D digitization of museum artifacts," in *Digital Heritage International Congress*, Marseille, 2013, pp. 197-200.
- [115] D. Akca, F. Remondino, D. Novák, T. Hanusch, G. Schrotter and A. Gruen, "Recording and modeling of cultural heritage objects with coded structured light projection systems," presented at the Institute of Geodesy and Photogrammetry,, Zurich, Switzerland, 2006.
- [116] Anon. (2016). *Photogrammetry - Current Suites of Software*. Available: <http://en.wikipedia.org/wiki/Photogrammetry> [Accessed 01/01/2016].
- [117] D. L. Milgram, "Computer methods for creating photomosaics," *Computers, IEEE Transactions on*, vol. 100, pp. 1113-1119, 1975.

[118] A. West. (2010). *20 years of Adobe Photoshop*. Available: <http://www.webdesignerdepot.com/2010/02/20-years-of-adobe-photoshop/> [Accessed].

[119] R. Szeliski, "Image Alignment and Stitching: A Tutorial1," Microsoft Corporation, Redmond, Washington, USA2006.

[120] M. James and S. Robson, "Straightforward reconstruction of 3D surfaces and topography with a camera," *Journal of Geophysical Research*, vol. vol. 117, 11 Aug 2012 2012.

[121] F. Remondino, L. Barazzetti, F. Nex, M. Scaioni and D. Sarazzi, "UAV photogrammetry for mapping and 3d modeling—current status and future perspectives," *International Archives of the Photogrammetry, Remote Sensing and Spatial Information Sciences*, vol. 38, p. C22, 2011.

[122] R. Knowles, "UK's first drone conviction will bankrupt me, says Cumbrian man," in *The Guardian*, ed. London, UK: Guardian News and Media Limited 2014.

[123] J. Straub, B. Kading, A. Mohammad and S. Kerlin, "Characterization of a Large, Low-Cost 3D Scanner," *Technologies*, vol. 3, pp. 19-36, 2015.

[124] *Hazard Classification for Lasers & Laser Registration Form* E. D. Lancaster University 5.0, 2015.

[125] N. Snavely, S. M. Seitz and R. Szeliski, "Photo tourism: exploring photo collections in 3D," *ACM transactions on graphics (TOG)*, vol. 25, pp. 835-846, 3rd July 2006.

[126] 3D Systems. (2008). *Support: 3D printers*. Available: <http://www.3dsystems.com/shop/support/cube/videos> [Accessed].

[127] L. Tiertime Technology Co., "UP!3DPP," ed. Beijing, China, 2003.

[128] RepRap Ltd and eMAKER Ltd., "RepRap," ed. Bristol, UK, 2011.

[129] MakerBot® Industries LLC. Stratasys, "Makerbot Replicator," ed. Brooklyn, NY. USA.

[130] J. Kaufman. (2014) Touching History: 3D Replica Artifacts. *Ancient Egypt*. 32-33. Available: [www.ancientegyptmagazine.com](http://www.ancientegyptmagazine.com) [Accessed Dec/Jan 2014].

[131] L. Rie, "Bottle," in *Craft Council Collections Online* vol. 13.5 x 17 x 23cm, ed. London: courtesy of the Craft Council 1967.

[132] K. Thompson, "Goveshy," in *Craft Council Collections Online*, ed. London: courtesy of the Craft Council, 2013, p. ceramic Bust.

[133] Katharine Morling, "Morling and the Hoard," in *Crafts Council Collections Online* vol. 37 x 57 x 59.9 cm, ed. London: courtesy of the Craft Council - Photo: Todd-White Art Photography, 2012, p. Ceramic figureine.

[134] The National Gallery. (2015). *Art through Words*. Available: <http://www.nationalgallery.org.uk/whats-on/art-through-words/> [Accessed].

[135] L. da Vinci, "The Mona Lisa," ed. Florence, Italy.: The Louvre, Paris, c1503.

[136] software.informer. (2016). *ArtCAM Insignia*. Available: <http://artcam-insignia.software.informer.com/> [Accessed].

[137] AutoDes Inc., "Autodesk ArtCAM®," ed, 2018.

[138] A. Stangl, C.-L. Hsu and T. Yeh, "Transcribing Across the Senses: Community Efforts to Create 3D Printable Accessible Tactile Pictures for Young Children with Visual Impairments," in *Proceedings of the 17th International ACM SIGACCESS Conference on Computers & Accessibility*, 2015, pp. 127-137.

[139] Budds Dian. (2016). *Anyone can 3D print these beautiful storybooks for VI kids*. Available: [www.fastcodedesign.com/3056557/wanted/anyone-can-3-d-print-these-beautiful-storybooks-for-vi-kids/](http://www.fastcodedesign.com/3056557/wanted/anyone-can-3-d-print-these-beautiful-storybooks-for-vi-kids/) [Accessed Feburary 2016].

[140] mediacollege.com. (2010). *Colour Temperatures in the Kelvin Scale*. Available: <http://www.mediocollege.com/lighting/colour/colour-temperature.html> [Accessed October 2015].

[141] Narsuitus. (2004). *Kelvin Scale*. Available: <http://forums.popphoto.com/showthread.php?284625-Kelvin-Scale> [Accessed January 2016].

[142] J. Sparks, *Nikon D3100, The Expanded Guide*. Lewes, UK: Ammonite Press, 2011.

[143] Nikon Corporation, "Nikon - Digital Camera D3100. User's Manual," vol. SB0H02(11) - 6MB09311-02, ed. Japan: ©2010 Nikon Corporation - 2010.

[144] Pixelz. (2014). Need Accurate Colour? Let Grey Cards and White Balancing Come to Your Rescue! *Pixelz Blog*. Available: <https://www.pixelz.com/> [Accessed April 2017].

[145] Adobe Systems Inc., "PhotoShop CS5, Adobe Lightroom, ,," ed. San Jose, California USA: Adobe Creative Cloud, c 2012.

[146] BSi, "Consistent colour, consistently happy clients," in *BSi Customer Services*, B. S. I. Group, Ed., ed. London UK, 2016.

[147] Pantone Colours. (2014). *The Pantone Colour Matching System*. Available: <http://www.pantone-colours.com/> [Accessed 01.01.2017].

[148] Rapid Tables, "Online Scientific and Engineering Resource," in <a href="<http://www.rapidtables.com>">RapidTables.com - Engineering Resources</a>, Color Wheel Chart and Color Conversion, Eds., ed: © 2017 RapidTables.com, 2017.

[149] ASTM International, "Standard Practice for Calculating Yellowness and Whiteness Indices from Instrumentally Measured Color Coordinates," in *ASTM E313-15e1*, ed. West Conshohocken, PA, USA: ASTM International, 2015.

[150] x-rite, "A Guide to Understanding Color Communication," X-rite, Ed., ed. Michigan USA, 2007, p. 27.

[151] Visual Workplace Inc., "Workplace Color Coding Standards," vol. 616-583-9400, Visual Workplace Inc., Ed., ed. Michigan USA, 2017.

[152] BSi, "British Standard 2660 Colour Chart - Fan Deck ", B. S. Institute, Ed., ed. London UK: Color Harzen Europe - BritishStandardColour.com, 2017.

[153] International Commission on Illumination, "Advancing knowledge and providing standardization to improve the lighted environment," ed. Vienna, Austria, 2000 - 2017.

[154] J. Reece, "Mcor IRIS becomes first 3D printer to embrace International Colour Standard for Unprecedented 3D Printing Colour Accuracy," Mcor Technologies Ltd.,, Dunleer, Ireland2014.

[155] E. Chalcraft. (2012). Cadbury wins court battle over trademark Pantone 2658C purple wrappers. *Dezeen Magazine* (October 2012). Available: [https://www.dezeen.com/2012/10/03/cadbury-wins-court-battle-over-trademark-purple-wrapper/#disqus\\_thread](https://www.dezeen.com/2012/10/03/cadbury-wins-court-battle-over-trademark-purple-wrapper/#disqus_thread) [Accessed May 2017].

[156] ASTM International. (2017). *Additive Manufacturing Technology Standards*. Available: <https://www.astm.org/Standards/additive-manufacturing-technology-standards.html> [Accessed 01/05/2017].

[157] Alex Price. (2013). *BSi - Additive Manufacturing – Standards*. Available: <https://www.nottingham.ac.uk/research/groups/advanced-manufacturing-technology-research-group/documents/manufacturing-metrology-team/qcam-17/bsi.pdf> [Accessed 2017].

[158] J. Titlow. (2012) What you need to know about colour 3D printing. *Make Parts Fast*. Available: <http://www.Makepartsfast.com/what-you-need-to-know-about-colour-3D-printing/> [Accessed May 2017].

[159] Stratasys Inc, "PolyJet J750 & GrabCAD," ed. Rehovot, Israel, 1992.

[160] B. Wilde. (2013). *Green Screen, a Guide to Chroma Key Photography*. Available: <https://www.udemy.com/blog/how-to-use-a-green-screen/> [Accessed September 2014].

[161] J. Kaufman, M. Clement and A. E. Rennie, "Reverse Engineering Using Close Range Photogrammetry for Additive Manufactured Reproduction of Egyptian Artifacts and Other Objets d'art," *Journal of Computing and Information Science in Engineering*, vol. 15, p. 011006, 2015.

[162] IR-Entertainments Ltd, "Infinite-Realities multi camera studio," ed. Suffolk, UK, 2014.

[163] H. Brooks, A. Rennie, T. Abram, J. McGovern and F. Caron, "Variable fused deposition modelling: analysis of benefits, concept design and tool path generation," in *5th International Conference on Advanced Research in Virtual and Rapid Prototyping.*, Leiria, Portugal, 2011, pp. 511-517.

[164] A. Koutsoudis, F. Arnaoutoglou and G. Pavlidis, "Structure from Motion–Multiple View Stereovision (SFM/MVS) An Introduction on how to perform SFM/MVS," University of the Aegean Summer Schools, Delphi, Greece 2015.

[165] S. T. Porter. (2014). A Portable Photogrammetry Rig for the Reliable Creation of High-Quality 3D Artifact Models in the Field. *University of Minnesota: Dept. of Anthropology*. [Accessed June 2015].

[166] T. Luhmann, S. Robson, S. Kyle and J. Boehm, *Close-Range Photogrammetry and 3D Imaging*, 2nd ed. Berlin/Boston: De Gruyter, 2014.

[167] J. Schewe, *The Digital Negative*, 2nd ed. San Francisco, CA: Pearson/Peachpit Press, 2016.

[168] S. Cox. (2017). *What is Lens Diffraction*. Available: <https://photographylife.com/what-is-diffraction-in-photography/> [Accessed 01/10/2017].

[169] S. McHugh. (2005-2017). *Lens Diffraction & Photography*. Available: <http://www.cambridgeincolour.com/tutorials/diffraction-photography.htm> [Accessed 01/01/2017].

[170] Agisoft Technical Team, "Arbitrary Size of Image," J. Kaufman, Ed., Email correspondence. ed. Manchester, 2015.

[171] J. Schewe, *The Digital Negative, Raw Image Processing in Lightroom, Camera Raw and Photoshop*, 2nd ed.: Peachpit Press, 2016.

[172] Nick Vandome, *Photoshop Elements 11*. Leamington Spa: Easy Steps Ltd., 2013.

[173] Agisoft Technical Team, "Log File," J. Kaufman, Ed., ed. St Perserberg: G-mail, 2017.

[174] M. Bach, "Agisoft PhotoScan GPU Acceleration,

Agisoft PhotoScan Multi Core Performance," Puget Systems, Auburn, Washington State, USASeptember 11, 2015 2015.

[175] W. C. Smith and R. W. Dean, "Structural characteristics of fused deposition modeling polycarbonate material," *Polymer testing*, vol. 32, pp. 1306-1312, 2013.

[176] UltiMaker B.V., "UltiMaker & Cura," ed. 4191 PN Geldermalsen, The Netherlands, 2011.

[177] CGTech., "Vericut," ed. California, USA, 1988.

[178] T. R. Kramer, F. M. Proctor and E. Messina, *The NIST RS274NGC Interpreter - v3* vol. 5416. Gaithersburg, Maryland 20899. USA: National Institute of Standards and Technology, 2000.

[179] D. Chakravorty. (2017). *G-Code Tutorial: 3D Printer Commands Simply Explained*. Available: <https://all3dp.com/g-code-tutorial-3d-printer-gcode-commands/> [Accessed 14/08/2017].

[180] Nikon Corporation, "ViewNX 2," Ver 2.0.1 ed. Japan: Nikon Corporation, 2010.

[181] J. Kaufman, A. E. W. Rennie and M. Clement, "Single Camera Photogrammetry for Reverse Engineering and Fabrication of Ancient and Modern Artifacts," *Procedia CIRP*, vol. 36, pp. 223-229, 2015.

[182] British Geological Survey. Available: <http://www.bgs.ac.uk/about/home.htm> [Accessed March 2015].

[183] Joint Information Systems Committee (Jisc), "JISC:GB/3D type fossils online," M. Howe, Ed., ed, 2014.

[184] Scanning Cars LLC. (2017). *Coded Targets PDFs (#1001-1186*. Available: <http://scanningcars.com/free-coded-target-pdfs-1001-1186/> [Accessed 01/05/2017].

[185] L. Galantucci, G. Percoco and U. Dal Maso, "Coded targets and hybrid grids for photogrammetric 3D digitisation of human faces," *Virtual and Physical Prototyping*, vol. 3, pp. 167-176, 2008.

[186] P. Drap, J. Royera, M. Nawaf, M. Saccone, D. Merad, Lo'pez-Sanz, J. Ledoux and J. Garrabou, "Underwater Photogrammetry, Coded Targets and Plenoptic Technology:," *The International Archives of the Photogrammetry, Remote Sensing and Spatial Information Sciences*, vol. Volume XLII-2/W3, 2017.

[187] A. Tscharf, M. Rumpler, F. Fraundorfer, G. Mayer and H. Bischof, "On the use of uavs in mining and archaeology-geo-accurate 3d reconstructions using various platforms and terrestrial views," *ISPRS Annals of the Photogrammetry, Remote Sensing and Spatial Information Sciences*, vol. 2, p. 15, 2015.

[188] M. R. Shortis and J. W. Seager, "A practical target recognition system for close range photogrammetry," *The Photogrammetric Record*, vol. 29, pp. 337-355, 2014.

[189] Netfabb. (2015). *3DModel Repair*, . Available: <https://service.netfabb.com/login.php> [Accessed September 2015].

[190] S. Huang, Z. Zhang, T. Ke, M. Tang and X. Xu, "Scanning Photogrammetry for Measuring Large Targets in Close Range," *Remote Sensing*, vol. 7, pp. 10042-10077, 2015.

[191] Agisoft.com. (2015). *On line Tutorial*. Available: <http://www.agisoft.com/forum> [Accessed January 2015].

[192] J. G. Fryer and J. Chandler, "Accuracy of Autodesk 123D Catch," *Geomatics World*, 2013.

[193] P. Brindley, R. Goodridge, M. East and R. Hague, "Preliminary Investigation into the Mechanical Properties of Stratasys Polycarbonate & M30 ABS materials," Rapid Manufacturing Research Group, Loughborough, UK. 2008.

[194] R. Striling, "EOS - Material Data Sheet - PA 2200," EOS GmbH, Munchen .2013.

[195] 'NIAR' Test Results Pending, 2009 NIAR Testing and S. I. Testing, "Preliminary ASTM Test Data Results," ed: Stratasys Mechanical Test Reports, 2009.

[196] A. Sherif El-Gizawy, S. Corl and B. Graybill, "Process-induced Properties of FDM Products," Mechanical and Aerospace Engineering Department, University of Missouri., Columbia, MO, USA .2010.

[197] W. E. Frazier, "Metal additive manufacturing: A review," *Journal of Materials Engineering and Performance*, vol. 23, pp. 1917-1928, 2014.

[198] Lincruster. (1877). Available: <http://lincrusta.com/AboutUs.Asp> [Accessed Feburary 2016].

[199] British Ceramics Biennial. (2009). Available: <http://www.britishceramicsbiennial.com/> [Accessed October 2015].

[200] C. Nicolae, E. Nocerino, F. Menna and F. Remondino, "Photogrammetry applied to Problematic artefacts," presented at the ISPRS-International Archives of the Photogrammetry, Remote Sensing and Spatial Information Sciences, Riva del Garda, Italy, 2014.

[201] J. Murry and W. Van Ryper, *Encyclopedia of Graphics File Formats*, Second ed.: O'Reilly & Associates, 1996.

[202] A. Davies and P. Fennessy, *Electronic Imaging for Photographers*, Second ed. Oxford: Focal Press/Reed Educational and Professional Publishing Ltd., 1996.

[203] D. Harman and D. Jones, *The Digital Photography Handbook*. London: Smith-Davies Publishing Ltd., 2005.

[204] N. Vandome, *Photoshop Elements* Warwickshire, UK: Easy Steps Ltd, 2013.

[205] P. Andrews, Y. Butler and J. Farace, *RAW Workflow from Capture to Archives*. Oxford: Elsevier/Focal Press, 2006.

[206] Williams College of Art. (1793). *Horus - bronze*. Available: [http://web.williams.edu/wcma/modules/ancient/60\\_36\\_4.shtml](http://web.williams.edu/wcma/modules/ancient/60_36_4.shtml) [Accessed May 2014].

[207] ArtQuid. (2006). *Horus - Reproduction Resin*. Available: <http://www.artqid.com/artwork/5868/2826/horus-as-a-falcon.html> [Accessed May 2014].

[208] Metropolitan Museum. *Horus - Hard stone*. Available: <http://www.ancient-egypt.co.uk/metropolitan/pages/horus.htm> [Accessed May 2014].

[209] The Global Egyptian Museum. (2006). *Horus - sandstone*. Available: <http://www.globalegyptianmuseum.org/glossary.aspx?id=192> [Accessed May 2014].

[210] J. Kaufman. (2015) Touching History: The Lost Crown of Horus. *Ancient Egypt*. 22 - 23. Available: [www.ancientegyptmagazine.com](http://www.ancientegyptmagazine.com) [Accessed Apl/May 2015].

[211] S. Soile, K. Adam, C. Ioannidis and A. Georgopoulos, "Accurate 3d Textured Models of Vessels for the Improvement of the Educational Tools of a Museum," *ISPRS-International Archives of the Photogrammetry, Remote Sensing and Spatial Information Sciences*, vol. 1, pp. 211-217, 2013.

[212] P. Akesson, "Amphora Types According to Dressel," in *Corpus Inscriptionum Latinarum, band XV*, H. Dressel, Ed., ed. Berlin 1899, 1999.

[213] Ancient Artifax Galleries. (2003). *Custom metal stand*. Available: <http://www.ancientartifax.com/classic.htm> [Accessed June 2015].

[214] Etsy/Globalfindings. (2015). *Spanish Handmade Storage Jars*. Available: <https://www.etsy.com/listing/214732517/glass-storage-jars-with-cork-lid-made-in> [Accessed September 2015].

[215] S. C. Loy and F. Zhao, "Application of 3D Digitization in Cultural Heritage Preservation," *Digital Presentation and Preservation of Cultural and Scientific Heritage*, pp. 227-241, 2015.

[216] Stratasys Ltd, "Triple-Jetting Object 500 Connex3," ed. Maine. USA: Rehovot. Israel, 2014.

[217] Stratasys Ltd, "Tango family," ed. Rehovot, Israel, 2014.

[218] Stratasys Ltd - PolyJet Systems & Materials, "Digital ABS & Digital ABS2", ed. Maine. USA: Rehovot. Israel, 2014.

[219] S. Cosimo. (2015) \$100 Peachy 3D printers available for pre-order. ([www.peachyprinter.com](http://www.peachyprinter.com)). Available: <http://www.3ders.org/articles/20150529-peachy-printer-3d-printers-now-shipping-and-available-to-purchase.html> [Accessed 15/12/2015].

[220] S. J. Grunewald. (2016). Peachy Printer Collapses After Embezzlement of \$320K. *3DPrint.com*. Available: <https://3dprint.com/133842/peachy-printer-embezzlement/> [Accessed 06/04/2018].

[221] A. Buren. (2015) Technical University Eindhoven takes massive 11x5x4m concrete 3D printer into production. Available: <http://www.3ders.org/articles/20151023-technical-university-eindhoven-takes-massive-concrete-3d-printer-into-pr> [Accessed 17/12/2015].

[222] B. Khoshnevis, "Automated construction by contour crafting—related robotics and information technologies," *Automation in construction*, vol. 13, pp. 5-19, 2004.

[223] Gartner. (2017). Hype Cycle for Emerging Technologies. *Gartner Hype Cycle*. Available: [www.gartner.com/newsroom/id/](http://www.gartner.com/newsroom/id/) [Accessed].

[224] F. Robinson. (2015) 3D Printing Trends 2015: Gartner's Hype Cycle. *Disruptive*. Available: <http://www.disruptivemagazine.com/opinion/3d-printing-trends-2015-gartner%E2%80%99s-hype-cycle> [Accessed April 2016].

[225] L. Barber. (2017). Gartner Hype Cycle 2017: Artificial intelligence at peak hype, blockchain heads for disillusionment, but say hello to 5G. *CityA.M*. Available: <http://www.cityam.com/270451/gartner-hype-cycle-2017-artificial-intelligence-peak-hype> [Accessed July 2018].

[226] L. Columbus. (2017). Gartner's Hype Cycle for Emerging Technologies, 2017 Adds 5G And Deep Learning For First Time. *Forbes*. Available: <https://www.forbes.com/sites/louiscolombus/2017/08/15/gartners-hype-cycle-for-emerging-technologies-2017-adds-5g-and-deep-learning-for-first-time/#6c008f255043> [Accessed July 2018].

[227] B. P. Conner, G. P. Manogharan and K. L. Meyers, "An assessment of implementation of entry-level 3D printers from the perspective of small businesses," *Rapid Prototyping Journal*, vol. 21, pp. 582-597, 2015.

[228] Emerging Objects. (2015). Available: <http://www.emergingobjects.com/> [Accessed Jan 2016].

[229] A. Buren, "ColorFabb unveils sturdy cork Fill wood-like 3D printer filament," in [www.3ders.org](http://www.3ders.org), ed. Katwijk, Holland, 2015.

[230] colorFabb. (2013). Learn colorfabb. Available: <http://learn.colorfabb.com/> [Accessed Jan 2016].

[231] Shapeways. (2007). Material Available: <http://www.shapeways.com/materials/> <http://www.shapeways.com/materials/material-status> [Accessed 01/01/2014].

[232] D. H. Gunasekera, S. Kuek, D. Hasanaj, Y. He, C. Tuck, A. K. Croft and R. D. Wildman, "Three dimensional ink-jet printing of biomaterials using ionic liquids and co-solvents," *Faraday discussions*, vol. 190, pp. 509-523, 2016.

[233] a. A. H. Volker Lesch, a Christian Holmb, Jens Smiatek,, "Solvent effects of 1-ethyl-3-methylimidazolium acetate: solvation and dynamic behavior of polar and apolar solutes†," *Physical Chemistry Chemical Physics PCCP*, pp. 8480--8490, 14/07/2016 2015.

[234] N. Schmidt. (2010). Automated but flexible processing: 'Endless' by Dirk van der Kooij (NL). *Daily Tonic (FRI 12.11.)*. Available: <http://www.dailytonic.com/automated-but-flexible-processing-endless-by-dirk-van-der-kooij-nl/> [Accessed 10/02/2014].

[235] E. Dini. (2017). D-Shape. Available: <https://d-shape.com/> [Accessed May 2017].

[236] T. Abrahams, "The World's First Printed Building," *Blueprint Magazine*, 2010.

[237] Jan Belezina. (2012). D-Shape 3D printer can print full-sized houses. *New Atlas/ Source:Monolite UK via The Verge*. Available: <http://newatlas.com/d-shape-3d-printer/21594/#gallery> [Accessed 20/05/2017].

[238] J. Kidwell, "Best Practices and Applications of 3D Printing in the Construction Industry," 2017.

[239] T. Ravenscroft. (2018). "Europe's first 3D-printed house" at Milan design week. *Dezeen Magazine*. Available: <https://www.dezeen.com/2018/03/29/arup-cls-architetti-3d-printed-house-milan-design-week/> [Accessed 29/03/2018].

[240] E. Tucker. (2017). Lisa Ertel - Sandblasted Dune Furniture. *Dezeen Magazine*. Available: <https://www.dezeen.com/2017/04/23/lisa-ertel-sandblasts-dune-furniture-highlight-underlying-patterns-wood-growth-milan-design-week-2017/> [Accessed May 2017].

[241] DeskArtes Oy, "3Data Expert," 10.1.0.17 ed. Olarinluoma 7,Finland, 1998-2015.

[242] Mcor Technologies Ltd, "IRIS HD," ed. Dunleer, Ireland, 2005.

[243] J. Glausiusz. (2014) Ode on a Grecian Replica. *The American Scholar*. Available: [www.theamericanscholar.org/ode-to-be-a-grecian-replica/](http://www.theamericanscholar.org/ode-to-be-a-grecian-replica/) [Accessed October 2014].

[244] Sculpteo, "Sculpteo 3D Printing," ed. Villejuif Paris, France, 2009.

[245] G. Laput, X. A. Chen and C. Harrison, "3D Printed Hair: Fused Deposition Modeling of Soft Strands, Fibers, and Bristles," in *Proceedings of the 28th Annual ACM Symposium on User Interface Software & Technology*, 2015, pp. 593-597.

[246] J. Ou, C.-Y. Cheng, L. Zhou, G. Dublon and H. Ishii, "Methods of 3D Printing Micro-pillar Structures on Surfaces," in *Proceedings of the 28th Annual ACM Symposium on User Interface Software & Technology*, 2015, pp. 59-60.

[247] Pouliquen D, "It's a Snap! Take a photograph and create a 3D Model," in *Autodesk University 2011 LEARN.CONNECT.EXPLORE* vol. 2012, ed. California, USA: AutoDesk Inc., 2011.

[248] J. Gentrup. (2012) Autodesk 123D Catch for iPad Turns Your Photos Into 3D Models. Converting Physical to Digital on Mobile, Making 3D More Accessible to Everyone *Business Wire*. Available: <http://search.proquest.com/docview/1011648878?accountid=11979> [Accessed 19.10.2012].

[249] AgiSoft LLC, *Agisoft PhotoScan User Manual: Professional Edition, Version 0.9.0*. St. Petersberg, Russia.: AgiSoft LLC, 2012.

[250] Alexey Pasumansky, "Hardware Configuration," J. Kaufman, Ed., e-mail ed. St Petersberg, Russia: Agisoft, 2012.

[251] D. C. Kay and J. R. Levine, *Graphics file formats:2nd edition*: McGraw-Hill, Inc., 1994.

[252] J. D. Murray and W. VanRyper, *Encyclopedia of graphics file formats: 2nd edition*. Sebastopol, CA, USA: O'Reilly & Assoc., Inc., 1996.

[253] Nikon Inc. (2017). *Nikon Electronic Format (NEF)*. Available: <http://www.nikonusa.com/en/learn-and-explore/a/products-and-innovation/nikon-electronic-format-nef.html> [Accessed 26/02/2017].

[254] Taylor P. (2010). JPEG Image Compression Degradation. Available: [www.patricktaylor.com/](http://www.patricktaylor.com/) © Patrick Taylor 2005-2017 [Accessed September 2010].

[255] C. Stamatopoulos, C. Fraser and S. Cronk, "Accuracy aspects of utilizing RAW imagery in photogrammetric measurement," in *International Archives of the Photogrammetry, Remote Sensing and Spatial Information Sciences. XXII ISPRS Congress*, Melbourne Australia, 2012, pp. 387-392.

[256] Ö. Akçay, R. Erenoglu and E. Avsar, "The Effects of JPEG Compression in Close Range Photogrammetry," *International Journal of Engineering and Geosciences (IJEG)*, vol. Vol;2, pp. 35 - 40, 2017.

[257] K. W. Lam, Z. Li and X. Yuan, "Effects of JPEG compression on the accuracy of digital terrain models automatically derived from digital aerial images," *The Photogrammetric Record*, vol. 17, pp. 331-342, 2001.

[258] Biz Stone, "On How To Design Simple Solutions For Complex Problems," in *Fast Company* vol. 02.03.2016, ed. World Trade Center, NY USA: fastcompany dot.com, 2016.

[259] E. Novak and S. Wisdom, "Effects of 3D Printing Project-based Learning on Preservice Elementary Teachers' Science Attitudes, Science Content Knowledge, and Anxiety About Teaching Science," *Journal of Science Education and Technology*, pp. 1-21, 2018.

[260] K. Kampa, G. Wyatta, S. Dudley-Brown, K. Brittaina and B. Givena, "Using cognitive interviewing to improve questionnaires: An exemplar

study focusing on individual and condition-specific factors," *Applied Nursing Research*, 2015.

[261] F. L. Volpatto, I. C. Rechia, A. H. Lessa, C. L. C. Soldera, M. I. D. da Costa Ferreira and M. S. Machado, "Questionnaires and checklists for central auditory processing screening used in Brazil: a systematic review," *Brazilian Journal of Otorhinolaryngology*, 2018.

---